



Small-Signal Stability Techniques for Power System Modal Analysis, Control, and Numerical Integration

Georgios Tzounas

17203122

A thesis submitted to University College Dublin
in fulfilment of the requirements for the degree of

Doctor of Philosophy

College of Engineering and Architecture
School of Electrical & Electronic Engineering

Head of School: Prof. Peter Kennedy

Supervisor: Prof. Federico Milano

February 2021

I hereby certify that the submitted work is my own work, was completed while registered as a candidate for the degree stated on the Title Page, and I have not obtained a degree elsewhere on the basis of the research presented in this submitted work. ‘

© Georgios Tzounas, 2020. All Rights Reserved.

Acknowledgements

The content of this thesis is the result of my three-year long research in Dublin, Ireland, working under the supervision of Prof. Federico Milano and within the AMPSAS (Advanced Modelling for Power System Analysis and Simulation) project. Therefore, on completion of writing this thesis, I wish to thank my mentor, Federico, for the constant support, motivation, and feedback he provided throughout my PhD. Working with him has been a great experience, mainly for two reasons: first, his immense knowledge and passion about power systems worked as a source of inspiration and made me always try to give my best; and second, he always encouraged me to explore different directions and implement my ideas, which made the PhD an enjoyable adventure.

In addition, I would like to thank all the members of the group for their invaluable help, our interesting discussions, and mostly, for sharing everyday life on and off campus. Special thanks to Dr. Ioannis Dassios, first for his friendship and then for the continuous assistance and collaboration, which have definitely influenced my path toward the PhD and, in turn, the content of this thesis. Special thanks also to my pals and colleagues Dr. Mohammed Ahsan Adib Murad and Dr. Muiyang Liu, with whom I had extended collaboration within the group.

Many thanks to Prof. Rifat Sipahi, for his guidance and pleasant collaboration during my stay at Northeastern University in Boston, MA.

Finally, I am very grateful to some people who have supported me along this way in my PhD but most importantly, in my life in general. These are my parents and siblings, my friends in Greece, and Avgi. To all of you, thanks for your love and for putting up with me being far from home for such a long period.

Georgios Tzounas
Dublin, October 2020

Στους γονείς μου, Σοφία και Γιώργο.

Abstract

This thesis proposes novel Small-Signal Stability Analysis (SSSA)-based techniques that contribute to electric power system modal analysis, automatic control, and numerical integration.

Modal analysis is a fundamental tool for power system stability analysis and control. The thesis proposes a SSSA approach to determine the Participation Factors (PFs) of algebraic variables in power system dynamic modes. The approach is based on a new interpretation of the classical modal PFs as eigen-sensitivities, as well as on the definition of adequate inputs and outputs of the system's state-space representation. Both linear and generalized eigenvalue problems are considered for the calculation of PFs and a theorem to cope with eigenvalue multiplicities is presented.

SSSA is also ubiquitous in the synthesis of controllers for power systems. The thesis explores SSSA techniques for the design of power system controllers. The contributions on this topic are twofold, as follows:

(i) Investigate a promising control approach, that is to synthesize automatic regulators for power systems based on the theory of fractional calculus. In particular, using eigenvalue analysis, a comprehensive theory on the stability of power systems with inclusion of Fractional Order Controllers (FOCs) is provided. Moreover, the software implementation of FOCs based on Oustaloup's Recursive Approximation (ORA) method is discussed. A variety of FOC applications are illustrated, namely, automatic generation control of synchronous machines; frequency control of a converter-interfaced energy storage system; and voltage control through a static synchronous compensator.

(ii) Propose a novel perspective on the potential impact of time delays on power system stability. In general, measurement and communication of control signals in electric energy networks introduces significant time delays that are known to be a threat for the dynamic performance of power systems. However, research in control theory has shown that, by nature, delays are neutral and, if properly introduced, can also stabilize a dynamical system. Through SSSA, the thesis systematically identifies the control parameter settings for which delays in Power System Stabilizers (PSSs) improve the damping of a power system. Both analytical and simulation-based results are presented.

Finally, SSSA is utilized in the thesis to systematically propose a delay-based method to reduce the coupling of the equations of power system models for transient stability

analysis. The method consists in identifying the variables that, when subjected to a delay equal to the time step of the numerical integration, leave practically unchanged the system trajectories. Automatic selection of the variables and estimation of the maximum admissible delay are carried out by SSSA-based techniques. Such an one-step-delay approximation increases the sparsity of the system Jacobian matrices and can be used in conjunction with state-of-the-art techniques for the integration of Differential-Algebraic Equations (DAEs). The proposed approach is evaluated in terms of accuracy, convergence and computational burden.

Throughout the thesis, the proposed techniques are duly validated through numerical tests based on real-world network models.

Contents

List of Figures	x
List of Tables	xii
Acronyms	xiv
1 Introduction	1
1.1 Research Motivation	1
1.2 Thesis Overview	3
1.2.1 Contributions	3
1.2.2 Organization	6
1.2.3 Publications	8
2 Small-Signal Stability Analysis	11
2.1 Introduction	11
2.2 Power System Model	11
2.3 Linearized Power System Model	12
2.3.1 DAE Formulation	12
2.3.2 ODE Formulation	13
2.4 Linear System of Differential Equations	14
2.4.1 Formulation	14
2.4.2 Matrix Pencil	15
2.4.3 Solutions	16
2.4.4 Eigenvalue Problem	16
2.4.4.1 Formulation	16
2.4.4.2 Properties	17

2.4.5	Stability	19
2.5	Numerical Methods	20
2.5.1	Eigenvalue Algorithms	20
2.5.2	Open-Source Libraries	21
2.5.3	Spectral Transforms	24
2.5.4	Computational Complexity	25
2.6	Case Studies	26
2.6.1	All-Island Irish Transmission System	27
2.6.2	21,177-bus ENTSO-E	33
2.7	Concluding Remarks	36
3	Participation Factors	37
3.1	Introduction	37
3.2	Classical Participation Factors	38
3.2.1	Definition	38
3.2.2	Residues	39
3.3	Generalized Participation Factors	40
3.3.1	Formulation	40
3.3.2	Illustrative Example	44
3.4	Participation Factors of Algebraic Variables	46
3.5	Case Studies	50
3.5.1	Two-Area System	50
3.5.2	All-Island Irish Transmission System	53
3.6	Conclusions	56
4	Fractional Order Control	57
4.1	Introduction	57
4.2	Essentials of Fractional Calculus	59
4.3	Power System with Fractional Order Control	60
4.3.1	Modeling	61
4.3.2	Stability	62
4.3.3	Properties of Fractional Order Controllers	65
4.3.4	Examples	66

4.3.4.1	Illustrative Example	67
4.3.4.2	WSCC 9-bus System	70
4.4	Oustaloup's Recursive Approximation	71
4.4.1	Formulation	71
4.4.2	DAE Model	73
4.4.3	Steady State Error	76
4.4.4	Parameters Selection	76
4.5	Case Studies	77
4.5.1	WSCC 9-bus System	77
4.5.2	All-Island Irish Transmission System	84
4.6	Conclusions	86
5	Time-Delay-based Control	87
5.1	Introduction	87
5.2	Spectral Analysis of Time-Delay Systems	89
5.2.1	Preliminaries	89
5.2.2	Analytical Study of Second-Order LTI Systems	90
5.2.2.1	System Description	91
5.2.2.2	Stability Analysis	91
5.2.2.3	Delay-Independent Stability	92
5.2.3	Linear Large-Scale Time-Delay Systems	94
5.2.4	Non-Linear Large-Scale Time-Delay Systems	95
5.3	One-Machine Infinite-Bus System	97
5.3.1	Classical Model	97
5.3.2	Power System Stabilizer with PR Control	99
5.3.3	Illustrative Example	100
5.4	Case Study: IEEE 14-bus System	104
5.5	Remarks	108
5.6	Conclusions	110
6	One-Step Delay Approximation	111
6.1	Introduction	111
6.2	Implicit Integration of Power Systems	113

6.3	One-Step-Delay Approximation	115
6.4	Selection of Variables to be Delayed	116
6.4.1	Systematic Selection of Variables	117
6.4.2	Illustrative Examples	119
6.4.2.1	Center of Inertia	119
6.4.2.2	Turbine Governor	120
6.4.2.3	Automatic Generation Control	120
6.4.2.4	Secondary Voltage Regulation	120
6.5	Maximum Delay / Time Step	121
6.6	Case Studies	124
6.6.1	IEEE 39-bus System	124
6.6.2	21,177-bus ENTSO-E	129
6.7	Conclusions	134
7	Conclusions and Future Work	135
	Appendices	139
A	Proofs	140
A.1	Proof of Theorem 2.1	140
A.2	Proof of Theorem 3.1	141
A.3	Proof of Theorem 4.1	143
B	Map of the All-Island Irish Transmission System	145
	Bibliography	146

List of Figures

2.1	AIITS: root loci computed with LAPACK	29
2.2	AIITS: shift & invert transform image of the spectrum	30
2.3	AIITS: Cayley transform image of the spectrum	30
2.4	AIITS: root loci obtained with z-PARES	34
3.1	Two-area four-machine system: single-line diagram	50
3.2	AIITS: participation of bus active power injections to Mode 1	55
3.3	AIITS: participation of bus active power injections to Mode 2	55
4.1	PID vs FOPID: from point to plane	58
4.2	FOPI block diagram	68
4.3	Numerical example 1: root loci	70
4.4	WSCC system with FOPSS: most critical eigenvalues	72
4.5	Oustaloup's recursive approximation block diagram	73
4.6	Bode plot of the ORA	74
4.7	ORA frequency response	78
4.8	WSCC system with AGC: CoI frequency	79
4.9	Active power flow of simplified ESS model	80
4.10	WSCC system with ESS frequency control	81
4.11	WSCC system with ESS frequency control	82
4.12	VSC outer and inner control in dq-frame	83
4.13	WSCC system with STATCOM: voltage at bus 8	84
4.14	AIITS: frequency response following the loss of EWIC	85
4.15	AIITS: impact of FO-AGC on frequency response	85
5.1	OMIB system: single-line diagram	97
5.2	PR control based PSS diagram	99

5.3	Closed-loop linearized OMIB system: stability map	101
5.4	Closed-loop non-linear OMIB system with noisy rotor speed measurement	102
5.5	Closed-loop linearized OMIB system: stability map	103
5.6	Closed-loop linearized OMIB system: stability map	103
5.7	Closed-loop non-linear OMIB system with noisy rotor speed measurement	104
5.8	IEEE 14-bus system: single-line diagram	105
5.9	Power system stabilizer block diagram	106
5.10	IEEE 14-bus system: stability map	107
5.11	Dual-channel PSS configuration	107
5.12	IEEE 14-bus system: stability map	109
6.1	Types of Jacobian matrices	112
6.2	IEEE 39-bus system: density of Jacobians	125
6.3	IEEE 39-bus system: transient following a three-phase fault	128
6.4	ENTSO-E system: transient following a three-phase fault	131
6.5	ENTSO-E system: number of Newton iterations	132
B.1	AIITS: transmission system map	145

List of Tables

2.1	Methods of open-source libraries	23
2.2	Relevant features of open-source libraries	23
2.3	Common linear spectral transforms	25
2.4	Coefficients of special Möbius transformations	25
2.5	Versions and dependencies of open-source libraries	27
2.6	AIITS: dimensions of the LEP and GEP	28
2.7	AIITS: Schur decomposition methods	28
2.8	AIITS: subspace iteration method	31
2.9	AIITS: Krylov subspace methods, LEP	32
2.10	AIITS: Krylov subspace methods, GEP	32
2.11	AIITS: contour integration method	33
2.12	ENTSO-E: statistics	34
2.13	ENTSO-E: impact of the search region of the CIRR method	35
2.14	ENTSO-E: impact of spectral transforms of the CIRR method	35
3.1	Illustrative example: PFs associated to finite modes	46
3.2	Two-area system: critical modes	51
3.3	Sensitivity test for the inter-area mode	51
3.4	Two-area system: PFs	52
3.5	Impact of SVC-POD installation in the critical mode	53
3.6	AIITS: examined modes	54
4.1	Parameters of the ESS lead-lag frequency controllers	81
4.2	Parameters of the STATCOM controllers	84
5.1	IEEE 14-bus system: PSS parameters	106
5.2	Analogy between the dual-channel PSS and the PR controller	108

6.1	IEEE 39-bus system: NNZ Jacobian elements of the original DAE system	124
6.2	IEEE 39-bus system without delays: rightmost eigenvalues	125
6.3	IEEE 39-bus system with one-step delay: rightmost eigenvalues	126
6.4	IEEE 39-bus system with one-step-delay: relative errors of rightmost eigenvalues	126
6.5	IEEE 39-bus system: Maximum absolute rotor speed trajectory mis- matches induced by the proposed method	130
6.6	ENTSO-E system: NNZ Jacobian elements	130

List of Acronyms and Abbreviations

AGC	Automatic Generation Control
AIITS	All-Island Irish Transmission System
AVR	Automatic Voltage Regulator
BBD	Bordered-Block Diagonal
CIH	Contour Integration with Hankel matrices
CIRR	Contour Integration with Rayleigh-Ritz
CoI	Center of Inertia
CSR	Compressed Sparse Row
DAE	Differential-Algebraic Equation
DDAE	Delay Differential-Algebraic Equation
DDE	Delay Differential Equation
EMT	Electro-Magnetic Transient
ENTSO-E	European Network of Transmission System Operators for Electricity
ERD	Explicitly Restarted and Deflated
ESS	Energy Storage System
EWIC	East-West Inter-Connector
FACTS	Flexible AC Transmission System
FO	Fractional Order

FOC	Fractional-Order Controller
FOI	Fractional-Order Integral
FOPI	Fractional-Order Proportional Integral
FOPID	Fractional-Order Proportional Integral Derivative
FOPSS	Fractional-Order Power System Stabilizer
GD	Generalized Davidson
GEP	Generalized Eigenvalue Problem
GRPR	Generator Reactive Power Regulator
HVDC	High Voltage Direct Current
IO	Integer Order
ITM	Implicit Trapezoidal Method
JD	Jacobi-Davidson
LEP	Linear Eigenvalue Problem
LM	Largest Magnitude
LRP	Largest Real Part
LTI	Linear Time-Invariant
MPI	Message Passing Interface
NNZ	Number of Non-Zero
ODE	Ordinary Differential Equation
OMIB	One-Machine Infinite-Bus
ORA	Oustaloup's Recursive Approximation
PDE	Partial Differential Equation
PF	Participation Factor

PI	Proportional Integral
PID	Proportional Integral Derivative
POD	Power Oscillation Damper
PR	Proportional Retarded
PSS	Power System Stabilizer
RCI	Reverse Communication Interface
RL	Riemann-Liouville
RoCoF	Rate of Change of Frequency
SM	Smallest Magnitude
SSSA	Small-Signal Stability Analysis
STATCOM	STATic synchronous COMPensator
SVC	Static Var Compensator
SVR	Secondary Voltage Regulation
TDI	Time Domain Integration
TG	Turbine Governor
VSC	Voltage Source Converter
WADC	Wide-Area Damping Controller
WAMS	Wide-Area Measurement System
WSCC	Western Systems Coordinating Council

Notation

This section states the notation adopted throughout the thesis.

Vectors and Matrices

a, A	scalar
\mathbf{a}, \mathbf{a}	vector
\mathbf{A}, \mathbf{A}	matrix
\mathbf{A}^T	matrix transpose
\mathbf{A}^H	matrix conjugate transpose (Hermitian)
\mathbf{I}_r	identity matrix of dimensions $r \times r$
$\mathbf{0}_{r,m}$	zero matrix of dimensions $r \times m$

Sets and Units

\mathcal{C}^n	n time continuously differentiable functions
\mathbb{C}	complex numbers
j	unit imaginary number
\mathbb{I}	imaginary numbers
\mathbb{N}	natural numbers
\mathbb{R}	real numbers
\mathbb{Z}	integer numbers

Time and Frequency Domain

$a(t)$	time domain quantity
$\dot{a}(t)$	first order derivative
$\ddot{a}(t)$	second order derivative
$a^{(n)}(t)$	n -th order derivative (of fractional order or of integer order ≥ 3)
$a(s)$	frequency domain quantity

\mathcal{L}	Laplace transform
s	complex Laplace variable
z	spectral transform

Eigenvalues and Eigenvectors

f_n	natural frequency of eigenvalue
v	element of right eigenvector
\mathbf{v}	right eigenvector
\mathbf{V}	right modal matrix
w	element of left eigenvector
\mathbf{w}	left eigenvector
\mathbf{W}	left modal matrix
ζ	damping ratio of eigenvalue
λ	eigenvalue
$\text{Im}(\lambda)$	imaginary part of eigenvalue λ
$\text{Re}(\lambda)$	real part of eigenvalue λ
μ	multiplicity of infinite eigenvalue
ν	number of finite eigenvalues
π	participation factor
$\mathbf{\Pi}_{\text{PF}}$	participation matrix

Parameters

B	susceptance
c	constant
D	damping coefficient
G	conductance
h	time step size
K	control gain
M	mechanical starting time
R	resistance
\mathcal{R}	droop constant of primary frequency control
T	time constant
X	reactance
τ	time delay

Variables and Functions

e	electromotive force
P	active power
Q	reactive power
t	time
u	input signal
v	voltage magnitude
\mathcal{V}	Lyapunov function
w	output signal
x	state variable
y	algebraic variable
δ	angular position
θ	voltage phase angle
τ	torque
ω	angular speed

Superscripts and Subscripts

d	direct axis of the dqo transform
d	delayed quantity
m	mechanical
min	minimum
max	maximum
o	initial condition
q	quadrature axis of the dqo transform
r	rotor
ref	reference
s	stator

Chapter 1

Introduction

1.1 Research Motivation

Electric power systems around the world are currently undergoing a deep structural transformation. Arguably the most important change is the gradual replacement of conventional synchronous generator-based fossil fuel power plants – that have been dominating the dynamic response of power systems for more than a century now – by converter-based, intermittent renewable energy resources, such as wind and solar photovoltaic generation. Other significant changes are the increasing flexibility of energy consumption – partially due to the electrification of transportation and heating systems –, as well as the integration of power networks along with digital technologies and communication systems. Meanwhile, there is a continuous expansion of national distribution and transmission networks, as well as of international interconnections and power exchanges, especially by means of High Voltage Direct Current (HVDC) connections.

As dynamical systems, power systems are large-scale, highly non-linear systems which include continuous, discrete and stochastic variables. Moreover, following from the aforementioned changes, the size, uncertainty and dynamic complexity of power systems are further increasing. Therefore, stability assessment, optimal control synthesis, and accurate and efficient computer-based simulation of power systems are challenging tasks which, in order to be adequately addressed, require the development of ad hoc analytical and numerical tools.

Undoubtedly, the most successful method for assessing the dynamic behavior of a power system model after a disturbance is to carry out a numerical time domain simulation. On the other hand, assessing the overall performance of a power system by means of time domain simulations requires considering a large number of disturbances and scenarios. Even so, and despite some efforts that have been made, see e.g. [40], time domain analysis typically does not answer crucial quantitative questions such as: What is the stability margin of the system? What are the properties, e.g. natural frequency and damping, of the most critical for the stability dynamic modes? What are the couplings between the critical modes and the variables of the power system? These questions are typically addressed by means of stability analysis.

Power system stability is defined as *the ability of an electric power system, for a given initial operating condition, to regain a state of operating equilibrium after being subjected to a physical disturbance, with most system variables bounded so that practically the entire system remains intact* [72]. There are various mechanisms that may lead a power system to instability. For this reason, power system stability has been classified in categories, which helps identify the causes of instability and simplify the analysis by using appropriate models and tools. Following from [72], the ability of a power system, following a disturbance, to maintain (i) synchronism, defines *rotor angle stability*; (ii) steady voltages at all buses, defines *voltage stability*; and (iii) steady frequency, i.e. balanced generation and load, defines *frequency stability*. Due to the the increasing penetration of power electronic converter interfaced technologies, this classification has been recently revisited in [59], to include two new types of stability, namely, (iv) *resonance stability*, which is concerned with resonances of electromechanical and electrical nature; and (v) *converter-driven stability*, which is concerned with fast and slow interactions caused by the operation of power electronic converters. Finally, from a system-theoretic point of view, the conditions that may lead a dynamical system and hence also a power system to collapse after a disturbance are, ultimately, three, as follows: (i) a post-disturbance operating equilibrium does not exist; (ii) a post-disturbance equilibrium exists but it can not be reached, because the trajectory that the system follows is unstable; and (iii) a post-disturbance equilibrium exists but it is unstable.

Among the various stability analysis techniques available for power systems, this thesis focuses in particular on Small-Signal Stability Analysis (SSSA), which studies

the third condition, i.e. the stability of equilibria. SSSA has been mostly used for the analysis of rotor angle stability of small-disturbances. However, the definition and most importantly the tools of SSSA also apply to other types of power system stability. In particular, resonance stability, both torsional and electrical, as well as the fast-interaction converter-driven stability, can be studied and addressed using SSSA. The main advantage of SSSA is that, provided that a stationary condition exists, it can be always applied to a system, as opposed to other stability analysis techniques, such as Lyapunov’s energy function, which cannot be defined for all systems. On the other hand, SSSA is valid only in the neighborhood of an examined stationary point and thus it is not suitable for assessing the stability following a large disturbance. Despite this limitation, SSSA provides valuable insights on a power system model by capturing its structural characteristics and hence, it is a fundamental component of power system dynamic analysis. Among other applications, SSSA has been employed in power systems as a tool for modal analysis, see e.g. [52, 119, 123], control design, see e.g. [25, 50, 180], and numerical analysis, see e.g. [94, 182]. The objective of this thesis is to explore all three above directions. In particular, the thesis employs SSSA techniques to feature novel aspects in modal participation analysis, automatic control design, and time domain integration.

1.2 Thesis Overview

1.2.1 Contributions

The main goal of this thesis is to contribute to the stability analysis and control of power systems by developing a handful of novel analytical and computational tools, based on SSSA. In particular, the main contributions of the thesis are in three directions, namely, modal participation analysis, automatic control design, and time domain integration.

Modal Participation Analysis

Modal analysis studies the properties of a dynamical system in the frequency domain. An important component of power system modal analysis is *participation analysis*, which is an approach to efficiently determine the sensitivities of the dynamic modes of a power system model to variations of its variables. In its classical formulation, modal

participation analysis quantifies the coupling of the states of a linear system of Ordinary Differential Equations (ODEs) with its dynamic modes (eigenvalues of the state matrix), and is considered a standard tool of power system SSSA [123]. The non-linear power system model for angle and voltage stability analysis, however, is typically formulated as a set of Differential-Algebraic Equations (DAEs). That is, it also includes a variety of algebraic equations and variables, e.g. power and/or current flows in network branches, that constrain the system and define its dynamics. To study the impact of algebraic variables on the system dynamic response through participation factors is one of the scopes of this thesis. Such a study is relevant since, very often, the measurements taken on the transmission network and used by local and wide area controllers are modeled as algebraic variables.

This thesis proposes a measure for the modal participation of the algebraic variables of a power system model in its dynamic modes, through the definition of appropriate input-output vectors of the system's state-space representation. To this aim, an alternative interpretation of the classical participation factors as eigen-sensitivities is also proposed. The new interpretation removes the basic assumptions of classical participation analysis, since it assumes that the power system is modeled as singular system of differential equations with eigenvalue multiplicities.

Control Design

Proper control design is crucial to ensure a stable operation of a power system. This thesis employs SSSA techniques for the purpose of control design in two ways: (i) by studying an extension of classical control theory which stems from the theory of fractional order differential equations; (ii) by exploring the impact of delay-based controllers on power system stability.

1. Fractional Order Control:

The selection of a proper control scheme is a critical decision during a control design. With this regard, despite the recent developments in the theory of robust and advanced control, see [22, 184], the vast majority of controllers employed in industrial applications are still based on classical schemes, such as the Proportional Integral Derivative (PID) controller. This is mostly due to the fact that classical control schemes combine simple structure, easy tuning, and overall good

performance. With this in mind, the thesis investigates a promising extension of classical controllers, which stems from the theory of fractional calculus. Fractional calculus is the mathematical analysis that studies differentials and integrals of non-integer order. Control schemes based on fractional calculus have gained momentum in power system applications due to their ability to enhance performance and increase the stability margin, under the presence of topological changes, parameter uncertainty and noise.

In this thesis, a theory on how to carry out SSSA of power systems with *exact* fractional dynamics is developed. In addition, a step-by-step analytical study on the modeling and parameters selection of Oustaloup's Recursive Approximation (ORA)-based Fractional-Order Controllers (FOCs) is provided. Finally, the thesis carries out a systematic analysis of FOC applications to power system controllers. These include automatic generation control of synchronous machines; frequency control of a converter-interfaced energy storage system; and voltage control through a static synchronous compensator.

2. *Delay-based Control:*

Measurement and communication delays in local Power System Stabilizers (PSSs) and Wide-Area Damping Controllers (WADCs) are known to be a potential threat for the overall dynamic performance of power systems [86, 97, 148, 179]. How to properly study the impact of delays through accurate yet robust numerical techniques is still an open and active field of research. In spite of their bad reputation, delays are not always detrimental, but can also have unexpectedly beneficial effects on the stability of dynamical systems [2, 129, 143, 144, 149]. It has been shown, for example, that intentionally inserting a certain amount of delay in a feedback control system can enhance disturbance rejection capabilities, improve response time, and add the required damping to avoid undesired oscillations in a closed-loop system, see, e.g. [113]. More recently, analytical tuning techniques have been proposed to adjust time delays and controller gains to achieve fast response [131, 132, 134]. These new results motivate the use of intentional time delays as part of controllers, e.g. to effectively suppress poorly damped synchronous machine electromechanical oscillations.

In this thesis, the structure of stability crossing boundaries and the damping characteristics in the delay-controller gain parameter space of power systems with delay-based control are featured using two complementary approaches. First, through an analytical proof-of concept, by using the one-machine infinite-bus system. Second, through a numerical analysis on a larger, more realistic system. The main novel result of these studies is that proper design of a two-channel PSS allows unifying disconnected stability regions.

Time Domain Integration

The power system model for rotor-angle and voltage stability analysis is conventionally formulated as a set of non-linear DAEs. These equations are mutually dependent due to the meshed topology of transmission networks and the action of secondary controllers.

This thesis proposes a technique to decouple the power system DAEs by introducing a delay that is equal to the time step of the numerical integration. Such delay, while not altering the overall dynamic response of the system, allows reducing the coupling of the DAEs by removing off-diagonal elements of the system Jacobian matrix. The impact of the proposed *one-step-delay* approximation on the accuracy, convergence and computational burden of the time domain integration routine are rigorously and systematically discussed. In addition, a method to identify the elements of a power system DAE model that can be delayed by one time step, as well as a technique to estimate the maximum admissible delay, so that the approximation is within a given tolerance are provided.

* * *

Simulations in this thesis are carried out using the Python-based power system analysis software tool Dome [93]. These include solution of power flow problems, SSSA, and time domain simulations. In addition, the models and techniques developed in the course of this thesis are implemented and included in Dome.

1.2.2 Organization

The remainder of the thesis is organized as follows.

Chapter 2 provides the fundamentals of SSSA, which are then utilized throughout the thesis. The formulation, eigenvalue analysis and stability condition of linearized

power systems are presented. In addition, the chapter provides an overview of existing algorithms, and a comprehensive comparison of available open-source libraries, that are suitable for the solution of non-Hermitian eigenvalue problems.

Chapter 3 focuses on modal participation analysis as a measure of the coupling between the variables and dynamic modes of a power system. Classical definitions of participation factors are provided first. The modal participation analysis of a power system modeled as a singular system of differential equations with eigenvalue multiplicities, as well as a new interpretation of participation factors as eigensensitivities, are presented next. Then, the chapter proposes an approach to determine the participation of algebraic variables in power system dynamic modes, which considers adequate input/output variables of the system's state-space representation. Both the linear and generalized eigenvalue problems are considered for the calculation of the participation factors. An illustrative example on the two-area system, as well as a study on the 1,479-bus All-Island Irish Transmission System (AIITS) model are carried out to support the theory and illustrate the features of the proposed approach.

Chapter 4 presents the theoretical foundation and practical implementation aspects of FOCs for power system applications. First, essential definitions and concepts from fractional calculus are described. Second, mathematical theory on the stability analysis of power systems with inclusion of FOCs is presented. Next, Chapter 4 discusses the software implementation of FOCs based on the ORA method. A variety of examples of ORA-based FOCs are illustrated, namely, integral FOC for Automatic Generation Control (AGC); lead-lag FOC for frequency regulation of an Energy Storage System (ESS); and multiple Proportional Integral (PI) FOCs for voltage regulation provided by a STATic synchronous COMPensator (STATCOM). The Western Systems Coordinating Council (WSCC) 9-bus test system and the 1,479-bus AIITS model are employed to test and compare the examined FOCs with their integer-order versions.

Chapter 5 discusses how to utilize intentional time delays as part of controllers to improve the damping characteristics in electromechanical oscillations of power system synchronous machines. First, stability theory on the spectral analysis of small and large time-delay systems is provided. The control parameter settings for which time delays in PSSs improve the small-signal stability of a power system are systematically identified. Analytical results are presented by applying a Proportional Retarded (PR)

control scheme to the One-Machine Infinite-Bus (OMIB) electromechanical power system model. Finally, to demonstrate the opportunities in more realistic models, the obtained results are tested via numerical analysis on the IEEE 14-bus system.

Chapter 6 proposes the inclusion of a delay – equal to the time step of the numerical integration – to reduce the coupling of the equations of the non-linear DAE power system model. At first, the conventional implicit numerical integration of power systems is described. Subsequently, the proposed one-step delay approximation is presented. The selection of the variables that when subjected to one-step delay leave practically unchanged the system trajectories, as well as estimation of the maximum admissible delay, are discussed using small-signal stability analysis. Finally, the proposed approach is evaluated in terms of accuracy, convergence and computational burden, by means of (i) the IEEE 39-bus system; (ii) the 21,177-bus model of the European Network of Transmission System Operators for Electricity (ENTSO-E).

Finally, Chapter 7 summarizes the most relevant conclusions of the thesis and suggests directions for future work.

1.2.3 Publications

This section provides the list of publications that gave rise to the work presented in this thesis.

Journal papers

(Closely related to the content of the thesis)

1. **G. Tzounas**, R. Sipahi, and F. Milano, Damping power system electromechanical oscillations using time delays, *IEEE Transactions on Circuits and Systems I: Regular Papers*, accepted in Feb. 2021, in press.
2. **G. Tzounas**, I. Dassios, M. Liu, and F. Milano, Comparison of numerical methods and open-source libraries for eigenvalue analysis of large-scale power systems, *Applied Sciences*, MDPI, *Special Issue: Methods in Dynamical Systems, Mathematics of Networks, and Optimization for Modelling in Engineering*, vol. 10, no. 21, 7592, Oct. 2020. DOI: 10.3390/app10217592.

3. **G. Tzounas**, F. Milano, Delay-based decoupling of power system models for transient stability analysis, *IEEE Transactions on Power Systems*, vol. 36, no 1, pp. 464-473, Jan. 2021. DOI: 10.1109/TPWRS.2020.3009172.
4. I. Dassios, **G. Tzounas**, F. Milano, Generalized fractional controller for singular systems of differential equations, *Journal of Computational and Applied Mathematics*, Elsevier, vol. 378, Nov. 2020. DOI: 10.1016/j.cam.2020.112919.
5. **G. Tzounas**, I. Dassios, M. A. A. Murad, F. Milano, Theory and implementation of fractional order controllers for power system applications, *IEEE Transactions on Power Systems*, vol. 35, no. 6, pp. 4622-4631, Nov. 2020. DOI: 10.1109/TPWRS.2020.2999415.
6. **G. Tzounas**, I. Dassios, F. Milano, Modal participation factors of algebraic variables, *IEEE Transactions on Power Systems*, vol. 35, no. 1, pp. 742-750, Jan. 2020. DOI: 10.1109/TPWRS.2019.2931965.
7. I. Dassios, **G. Tzounas**, F. Milano, Participation factors for singular systems of differential equations, *Circuits, Systems, and Signal Processing*, Springer, vol. 39, no. 1, pp. 83-110, Jan. 2020. DOI: 10.1007/s00034-019-01183-1.

(Other)

8. I. Dassios, **G. Tzounas**, F. Milano, Robust stability criterion for perturbed singular systems of linearized differential equations, *Journal of Computational and Applied Mathematics*, Elsevier, vol. 381, Jan. 2021. DOI: 10.1016/j.cam.2020.113032.
9. M. Liu, I. Dassios, **G. Tzounas**, F. Milano, Model-independent derivative control delay compensation methods for power systems, *Energies*, MDPI, *Special Issue: Advanced Solutions for Monitoring, Protection and Control of Modern Power Transmission System*, vol. 13, no. 2, Jan. 2020. DOI: 10.3390/en13020342.
10. I. Dassios, **G. Tzounas**, and F. Milano, The Möbius transform effect in singular systems of differential equations, *Applied Mathematics and Computation*, Elsevier, vol. 361, pp. 338-353, Nov. 2019. DOI: 10.1016/j.amc.2019.05.047.

11. M. Liu, I. Dassios, **G. Tzounas**, and F. Milano, Stability analysis of power systems with inclusion of realistic-modeling WAMS delays, *IEEE Transactions on Power Systems*, vol. 34, no. 1, pp. 627-636, Jan. 2019. DOI: 10.1109/tpwrs.2018.2865559.

Books

12. F. Milano, I. Dassios, M. Liu, and **G. Tzounas**, *Eigenvalue Problems in Power Systems*, CRC Press, Taylor & Francis Group, 2020. ISBN: 9780367343675.

Conference Papers

13. M. A. A. Murad, **G. Tzounas** and F. Milano, Modeling and simulation of fractional order PI control limiters for power systems, 21st IFAC World Congress (IFAC 2020), Berlin, Germany, 12-17 Jul. 2020.
14. **G. Tzounas** and F. Milano, Impact of the estimation of synchronous machine rotor speeds on wide area damping controllers, IEEE PES General Meeting, Atlanta, GA, 4-8 Aug. 2019. DOI: 10.1109/pesgm40551.2019.8973611.
15. M. A. A. Murad, **G. Tzounas**, M. Liu, and F. Milano, Frequency control through voltage regulation of power system using SVC devices, IEEE PES General Meeting, Atlanta, GA, 4-8 Aug. 2019. DOI: 10.1109/pesgm40551.2019.8973807.
16. **G. Tzounas**, M. Liu, M. A. A. Murad, and F. Milano, Impact of realistic bus frequency measurements on wide-area power system stabilizers, IEEE PowerTech, Milano, Italy, 23-27 Jun. 2019. DOI: 10.1109/ptc.2019.8810695.
17. M. Liu, **G. Tzounas**, and F. Milano, A model-independent delay compensation method for power systems, IEEE PowerTech, Milano, Italy, 23-27 Jun. 2019. DOI: 10.1109/ptc.2019.8810975.
18. **G. Tzounas**, M. Liu, M. A. A. Murad, and F. Milano, Stability analysis of wide area damping controllers with multiple time delays, 10th Symposium on Control of Power and Energy Systems (IFAC CPES), Tokyo, Japan, 4-6 Sep. 2018. DOI: 10.1016/j.ifacol.2018.11.753.

Chapter 2

Small-Signal Stability Analysis

2.1 Introduction

The objective of this chapter is to provide definitions, formulations, theorems, and software tools related to SSSA and linearized power systems. The chapter is organized as follows. Section 2.2 describes the formulation of power system models for transient stability analysis. Section 2.3 discusses the power system model linearized around an equilibrium. Section 2.4 provides the outlines of linear systems of differential equations. In particular, this section discusses the definition of matrix pencils, the solution, the formulation and properties of the Linear Eigenvalue Problem (LEP) and Generalized Eigenvalue Problem (GEP) and defines asymptotic stability. The most relevant numerical methods and open-source libraries for the solution of the eigenvalue problems that arise in power systems are discussed in Section 2.5. A comprehensive comparison of these libraries is carried out through two real-world power system models in the case studies discussed in Section 2.6. Finally, conclusions are drawn in Section 2.7.

2.2 Power System Model

The power system model for transient stability analysis can be formulated as a set of non-linear, *semi-implicit* DAEs, as follows [95]:

$$\begin{bmatrix} \mathbf{T} & \mathbf{0}_{n,m} \\ \mathbf{R} & \mathbf{0}_{m,m} \end{bmatrix} \begin{bmatrix} \dot{\mathbf{x}} \\ \dot{\mathbf{y}} \end{bmatrix} = \begin{bmatrix} \mathbf{f}(\mathbf{x}, \mathbf{y}, \mathbf{u}) \\ \mathbf{g}(\mathbf{x}, \mathbf{y}, \mathbf{u}) \end{bmatrix}, \quad (2.1)$$

where $\mathbf{f} : \mathbb{R}^{n+m+p} \rightarrow \mathbb{R}^n$, $\mathbf{g} : \mathbb{R}^{n+m+p} \rightarrow \mathbb{R}^m$; $\mathbf{x} = \mathbf{x}(t)$, $\mathbf{x} \in \mathbb{R}^n$, are the state variables, $\mathbf{y} = \mathbf{y}(t)$, $\mathbf{y} \in \mathbb{R}^m$, are the algebraic variables; $\mathbf{u} = \mathbf{u}(t)$, $\mathbf{u} \in \mathbb{R}^p$, are controlled and/or uncontrolled inputs; $\mathbf{T} \in \mathbb{R}^{n \times n}$, $\mathbf{R} \in \mathbb{R}^{m \times n}$, are assumed to be constant matrices; and $t \in [0, \infty)$ is the simulation time. Finally, $\mathbf{0}_{n,m}$ denotes the zero matrix of dimensions $n \times m$.

In the formulation of (2.1), discrete variables are modeled implicitly, i.e. each discontinuous change in the system leads to a new continuous set of equations in the form of (2.1). In addition, dynamic components of (2.1) are modeled following the *phasor* or *quasi sinusoidal* approximation. That is, the three phases of AC electric networks and machines are assumed symmetric; stator transients of electric machines, as well as Electro-Magnetic Transient (EMT) phenomena of transmission lines are ignored.

A special case of (2.1) is when

$$\mathbf{T} = \mathbf{I}_n, \quad \mathbf{R} = \mathbf{0}_{m,n}, \quad (2.2)$$

where \mathbf{I}_n denotes the $n \times n$ identity matrix. This case leads to an *explicit* set of DAEs, that is the formulation most commonly employed for transient stability analysis. In this thesis, the more general form of (2.1) is used, unless otherwise explicitly stated.

2.3 Linearized Power System Model

2.3.1 DAE Formulation

The objective of SSSA is to study the stability properties of a power system model around an equilibrium point. An equilibrium point $(\mathbf{x}_o, \mathbf{y}_o, \mathbf{u}_o)$ of (2.1) satisfies:

$$\mathbf{0}_{n,1} = \mathbf{f}(\mathbf{x}_o, \mathbf{y}_o, \mathbf{u}_o),$$

$$\mathbf{0}_{m,1} = \mathbf{g}(\mathbf{x}_o, \mathbf{y}_o, \mathbf{u}_o).$$

For sufficiently small disturbances, (2.1) can be linearized around $(\mathbf{x}_o, \mathbf{y}_o, \mathbf{u}_o)$ for the purpose of analysis, as follows:

$$\begin{bmatrix} \mathbf{T} & \mathbf{0}_{n,m} \\ \mathbf{R} & \mathbf{0}_{m,m} \end{bmatrix} \begin{bmatrix} \Delta \dot{\mathbf{x}} \\ \Delta \dot{\mathbf{y}} \end{bmatrix} = \begin{bmatrix} \mathbf{f}_x \Delta \mathbf{x} + \mathbf{f}_y \Delta \mathbf{y} + \mathbf{f}_u \Delta \mathbf{u} \\ \mathbf{g}_x \Delta \mathbf{x} + \mathbf{g}_y \Delta \mathbf{y} + \mathbf{g}_u \Delta \mathbf{u} \end{bmatrix}, \quad (2.3)$$

where $\Delta \mathbf{x} = \mathbf{x} - \mathbf{x}_o$, $\Delta \mathbf{y} = \mathbf{y} - \mathbf{y}_o$, $\Delta \mathbf{u} = \mathbf{u} - \mathbf{u}_o$; $\mathbf{f}_x, \mathbf{f}_y, \mathbf{f}_u, \mathbf{g}_x, \mathbf{g}_y, \mathbf{g}_u$, are the Jacobian matrices calculated at $(\mathbf{x}_o, \mathbf{y}_o, \mathbf{u}_o)$. Obtaining the linear DAE system (2.3) from (2.1) is straightforward, by considering Taylor's expansion and ignoring all derivative terms of order higher than one. System (2.3) is an autonomous linear system, i.e. the elements of the Jacobian matrices are not functions of time t . This system can be rewritten in the following form:

$$\mathbf{E}_a \dot{\mathbf{z}} = \mathbf{A}_a \mathbf{z} + \mathbf{B}_a \Delta \mathbf{u}, \quad (2.4)$$

where

$$\mathbf{z} = \begin{bmatrix} \Delta \mathbf{x} \\ \Delta \mathbf{y} \end{bmatrix}, \quad \mathbf{E}_a = \begin{bmatrix} \mathbf{T} & \mathbf{0}_{n,m} \\ \mathbf{R} & \mathbf{0}_{m,m} \end{bmatrix}, \quad \mathbf{A}_a = \begin{bmatrix} \mathbf{f}_x & \mathbf{f}_y \\ \mathbf{g}_x & \mathbf{g}_y \end{bmatrix}, \quad \mathbf{B}_a = \begin{bmatrix} \mathbf{f}_u \\ \mathbf{g}_u \end{bmatrix}.$$

In the special case of (2.2), system (2.3) takes the following explicit DAE form:

$$\begin{bmatrix} \mathbf{I}_n & \mathbf{0}_{n,m} \\ \mathbf{0}_{m,n} & \mathbf{0}_{m,m} \end{bmatrix} \begin{bmatrix} \Delta \dot{\mathbf{x}} \\ \Delta \dot{\mathbf{y}} \end{bmatrix} = \begin{bmatrix} \mathbf{f}_x \Delta \mathbf{x} + \mathbf{f}_y \Delta \mathbf{y} + \mathbf{f}_u \Delta \mathbf{u} \\ \mathbf{g}_x \Delta \mathbf{x} + \mathbf{g}_y \Delta \mathbf{y} + \mathbf{g}_u \Delta \mathbf{u} \end{bmatrix}. \quad (2.5)$$

In this case, matrix \mathbf{E}_a has the diagonal form:

$$\mathbf{E}_a = \begin{bmatrix} \mathbf{I}_n & \mathbf{0}_{n,m} \\ \mathbf{0}_{m,n} & \mathbf{0}_{m,m} \end{bmatrix}.$$

2.3.2 ODE Formulation

Under the assumption that \mathbf{g}_y is not singular, system (2.5) can be reduced to a system of ODEs, by eliminating the deviations of the algebraic variables. Rewrite (2.5) as:

$$\Delta \dot{\mathbf{x}} = \mathbf{f}_x \Delta \mathbf{x} + \mathbf{f}_y \Delta \mathbf{y} + \mathbf{f}_u \Delta \mathbf{u}, \quad (2.6)$$

$$\mathbf{0}_{m,1} = \mathbf{g}_x \Delta \mathbf{x} + \mathbf{g}_y \Delta \mathbf{y} + \mathbf{g}_u \Delta \mathbf{u}. \quad (2.7)$$

Solving (2.7) for $\Delta \mathbf{y}$ yields:

$$\Delta \mathbf{y} = -\mathbf{g}_y^{-1} \mathbf{g}_x \Delta \mathbf{x} - \mathbf{g}_y^{-1} \mathbf{g}_u \Delta \mathbf{u}. \quad (2.8)$$

Substitution of (2.8) in (2.6) leads to the following linear system:

$$\Delta \dot{\mathbf{x}} = \mathbf{A}_s \Delta \mathbf{x} + \mathbf{B}_s \Delta \mathbf{u}, \quad (2.9)$$

where $\mathbf{A}_s = \mathbf{f}_x - \mathbf{f}_y \mathbf{g}_y^{-1} \mathbf{g}_x$, $\mathbf{B}_s = \mathbf{f}_u - \mathbf{f}_y \mathbf{g}_y^{-1} \mathbf{g}_u$, are the state matrix and input matrix, respectively, of the ODE system. System (2.9) is the model conventionally used in power system SSSA.

In general, (2.9) (or (2.3)) can be employed to accurately assess the small-signal stability of the non-linear power system model (2.1). An exception occurs at points where the system undergoes structural changes, e.g. at bifurcation points, where linearization as a technique to assess the stability of equilibria is inconclusive and where, thus, the non-linear dynamics of the system must be taken into account.

2.4 Linear System of Differential Equations

2.4.1 Formulation

The properties of a linearized power system model can be systematically studied using theory of linear differential equations. To this aim, this section considers the following system:

$$\mathbf{E} \dot{\mathbf{x}}(t) = \mathbf{A} \mathbf{x}(t) + \mathbf{B} \mathbf{u}(t), \quad (2.10)$$

where $\mathbf{E}, \mathbf{A} \in \mathbb{R}^{r \times r}$, $\mathbf{x} : [0, +\infty) \rightarrow \mathbb{R}^r$.

Matrix \mathbf{E} in (2.10) can be:

- non-singular, i.e. $\det(\mathbf{E}) \neq 0$. This is the case of the ODE power system model (2.9). In particular, (2.9) can be obtained from (2.10) for $r = n$, $\mathbf{x} \equiv \Delta \mathbf{x}$, $\mathbf{A} \equiv \mathbf{A}_s$, $\mathbf{E} \equiv \mathbf{I}_n$, $\mathbf{B} \equiv \mathbf{B}_s$.

- singular, i.e. $\det(\mathbf{E}) = 0$. This is the case of the DAE power system model (2.3). In particular, (2.3) can be obtained from (2.10) for $r = n + m$, $\mathbf{x} \equiv \mathbf{z}$, $\mathbf{A} \equiv \mathbf{A}_a$, $\mathbf{E} \equiv \mathbf{E}_a$, $\mathbf{B} \equiv \mathbf{B}_a$.

In case that \mathbf{E} in (2.10) is a singular matrix, system (2.10) is called a *singular system* of differential equations. Singular systems are relevant in many fields of engineering, such as automatic control, circuits, and robotic systems [28, 37, 82]. Note that, the theory of singular systems of differential equations involves a class of systems that is more general than (2.10), e.g. it includes systems with non-square matrices. However, for the needs of this thesis, it is adequate to study systems in the form of (2.10). The reader interested in a comprehensive theory on singular systems of differential equations may refer to [45], while some applications of that theory to power systems can be found in [30, 33, 101].

This section studies next some important properties of system (2.10), and in particular, defines its matrix pencil, discusses existence and uniqueness of its solutions, and provides the conditions for its stability.

2.4.2 Matrix Pencil

Applying the Laplace transform to (2.10), one gets:

$$\mathbf{E} \mathcal{L}\{\dot{\mathbf{x}}(t)\} = \mathbf{A} \mathcal{L}\{\mathbf{x}(t)\} + \mathbf{B} \mathcal{L}\{\mathbf{u}(t)\}, \quad (2.11)$$

where $s \in \mathbb{C}$ denotes the complex Laplace variable. Employing Laplace transform properties, one has:

$$\mathbf{E} (s \mathcal{L}\{\mathbf{x}(t)\} - \mathbf{x}(0)) = \mathbf{A} \mathcal{L}\{\mathbf{x}(t)\} + \mathbf{B} \mathcal{L}\{\mathbf{u}(t)\}, \quad (2.12)$$

or, equivalently,

$$(s\mathbf{E} - \mathbf{A}) \mathcal{L}\{\mathbf{x}(t)\} = \mathbf{E} \mathbf{x}(0) + \mathbf{B} \mathcal{L}\{\mathbf{u}(t)\}. \quad (2.13)$$

The structure of the polynomial matrix $s\mathbf{E} - \mathbf{A}$, hereafter referred as the *matrix pencil* of system (2.10), defines the existence of solutions and the stability properties of (2.10).

This thesis considers only matrix pencils that are *regular*, i.e. the associated matrices are square and, in addition, $\det(s\mathbf{E} - \mathbf{A}) = \varphi(s) \neq 0$, where $\varphi(s)$ is a polynomial of s of

degree $\deg(\varphi(s)) \leq r$. This is, in fact, the form of matrix pencils that most commonly appear for the purpose of power system SSSA.

2.4.3 Solutions

Remark 2.1. (*Existence of Solutions*). Consider system (2.10) with $\det(s\mathbf{E} - \mathbf{A}) \neq 0$. Then, $s\mathbf{E} - \mathbf{A}$ is invertible and (2.13) can always be solved for $\mathcal{L}\{\mathbf{x}(t)\}$ as:

$$\mathcal{L}\{\mathbf{x}(t)\} = (s\mathbf{E} - \mathbf{A})^{-1} \mathbf{E} \mathbf{x}(0) + (s\mathbf{E} - \mathbf{A})^{-1} \mathbf{B} \mathcal{L}\{\mathbf{u}(t)\}.$$

Consequently, a solution $\mathbf{x}(t)$ always exists and is given by:

$$\mathbf{x}(t) = \mathcal{L}^{-1}\{(s\mathbf{E} - \mathbf{A})^{-1} \mathbf{E} \mathbf{x}(0) + (s\mathbf{E} - \mathbf{A})^{-1} \mathbf{B} \mathcal{L}\{\mathbf{u}(t)\}\}. \quad (2.14)$$

Remark 2.2. (*Uniqueness of Solutions*). There are two types of initial conditions $\mathbf{x}(0)$: *consistent* and *non-consistent*. If \mathbf{E} is non-singular, then for any given initial conditions the solution is unique. However, it is not guaranteed that for given initial conditions a singular system with a regular pencil has a unique solution. In this case, if the given initial conditions are consistent, then the solution is unique. Otherwise, there are infinitely many solutions, the general solution (2.14) holds for $t > 0$ and the system is called *impulsive*.

2.4.4 Eigenvalue Problem

2.4.4.1 Formulation

The stability of (2.10) can be assessed by calculating its eigenvalues, which are defined as the roots of the *characteristic equation*:

$$\det(s\mathbf{E} - \mathbf{A}) = 0. \quad (2.15)$$

where $\det(s\mathbf{E} - \mathbf{A})$ is called the *characteristic polynomial* of system (2.10). In general, analytical solution of (2.15) is possible only if $r \leq 4$. For higher degrees, general formulas do not exist and only the application of a numerical method is possible. In addition, algorithms that explicitly determine the characteristic polynomial $\det(s\mathbf{E} - \mathbf{A})$ and

then numerically calculate its roots, may be extremely slow even for small problems. Alternatively, the eigenvalues of $s\mathbf{E} - \mathbf{A}$ can be found from the solution of the GEP:

$$\begin{aligned}(s\mathbf{E} - \mathbf{A})\mathbf{v} &= \mathbf{0}_{r,1}, \\ \mathbf{w}(s\mathbf{E} - \mathbf{A}) &= \mathbf{0}_{1,r},\end{aligned}\tag{2.16}$$

where $\mathbf{v} \in \mathbb{C}^{r \times 1}$ and $\mathbf{w} \in \mathbb{C}^{1 \times r}$. Every value of s that satisfies (2.16) is an eigenvalue of the pencil $s\mathbf{E} - \mathbf{A}$, with the vectors \mathbf{v} , \mathbf{w} being the corresponding right and left eigenvectors, respectively. Thus, the solution of the GEP consists in calculating the eigenpairs, i.e. eigenvalues and eigenvectors, that satisfy (2.16). Depending on the analysis that needs to be carried out, it may be required that only right (or left) or both right and left eigenvectors are calculated. In general, the pencil $s\mathbf{E} - \mathbf{A}$ has $\nu = \text{rank}(s\mathbf{E} - \mathbf{A})$ finite eigenvalues and the infinite eigenvalue with multiplicity $\mu = r - \text{rank}(s\mathbf{E} - \mathbf{A})$. Note that, unless otherwise stated, when this thesis refers to infinite eigenvalues, it implies eigenvalues that are at infinity and not infinitely many. Note also that, if \mathbf{E} is singular, the pencil will have the infinite eigenvalue with multiplicity at least one.

In the special case that the left-hand side matrix of (2.10) is the identity matrix (as is the case of system (2.9)), (2.16) is equivalent to the LEP:

$$\begin{aligned}(s\mathbf{I}_r - \mathbf{A})\mathbf{v} &= \mathbf{0}_{r,1}, \\ \mathbf{w}(s\mathbf{I}_r - \mathbf{A}) &= \mathbf{0}_{1,r}.\end{aligned}\tag{2.17}$$

Every value of s that satisfies (2.17) is an eigenvalue of the pencil $s\mathbf{I}_r - \mathbf{A}$, with the vectors \mathbf{v} , \mathbf{w} being the corresponding right and left eigenvectors, respectively. Thus, the solution of the LEP consists in calculating the eigenvalues and eigenvectors of $s\mathbf{I}_r - \mathbf{A}$. In particular, the pencil $s\mathbf{I}_r - \mathbf{A}$, has r finite eigenvalues.

2.4.4.2 Properties

Remark 2.3. (*Jordan Decomposition*). Consider the pencil $s\mathbf{E} - \mathbf{A}$, with $\det(s\mathbf{E} - \mathbf{A}) \neq 0$. There exist non-singular matrices \mathbf{W} , $\mathbf{V} \in \mathbb{C}^{r \times r}$ such that [45]:

$$\begin{aligned}\mathbf{W}\mathbf{E}\mathbf{V} &= \mathbf{I}_\nu \oplus \mathbf{H}_\mu, \\ \mathbf{W}\mathbf{A}\mathbf{V} &= \mathbf{J}_\nu \oplus \mathbf{I}_\mu,\end{aligned}\tag{2.18}$$

where $\nu + \mu = r$; $\mathbf{J}_\nu, \mathbf{J}_\nu \in \mathbb{C}^{\nu \times \nu}$, is constructed by the ν finite eigenvalues $\lambda_1, \lambda_2, \dots, \lambda_\nu$, and their multiplicities, and has the Jordan canonical form [45]; $\mathbf{H}_\mu, \mathbf{H}_\mu \in \mathbb{C}^{\mu \times \mu}$, is a nilpotent matrix with index μ_* , constructed by using the algebraic multiplicity μ of the infinite eigenvalue. Alternatively, the matrix \mathbf{H}_μ can be perceived as the Jordan matrix of the zero eigenvalue of the dual pencil $z\mathbf{A} - \mathbf{E}$, where $z = 1/s$.

The following notation is used:

$$\mathbf{W} = \begin{bmatrix} \mathbf{W}_\nu \\ \mathbf{W}_\mu \end{bmatrix}, \quad \mathbf{V} = \begin{bmatrix} \mathbf{V}_\nu & \mathbf{V}_\mu \end{bmatrix},$$

with $\mathbf{W}_\nu \in \mathbb{C}^{\nu \times r}$, $\mathbf{W}_\mu \in \mathbb{C}^{\mu \times r}$ and $\mathbf{V}_\nu \in \mathbb{C}^{r \times \nu}$, $\mathbf{V}_\mu \in \mathbb{C}^{r \times \mu}$. \mathbf{W}_ν is a matrix with rows ν linear independent left eigenvectors (including the generalized) of the ν finite eigenvalues of $s\mathbf{E} - \mathbf{A}$; \mathbf{W}_μ is a matrix with rows μ linear independent (including the generalized) left eigenvectors of the infinite eigenvalue of $s\mathbf{E} - \mathbf{A}$ with algebraic multiplicity μ ; \mathbf{V}_ν is a matrix with columns ν linear independent (including the generalized) right eigenvectors of the ν finite eigenvalues of $s\mathbf{E} - \mathbf{A}$; and \mathbf{V}_μ is a matrix with columns μ linear independent (including the generalized) right eigenvectors of the infinite eigenvalue of $s\mathbf{E} - \mathbf{A}$ with algebraic multiplicity μ . By applying the above expressions into (2.10), one gets the following eight equalities:

$$\begin{aligned} \mathbf{W}_\nu \mathbf{A} \mathbf{V}_\nu &= \mathbf{J}_\nu, & \mathbf{W}_\nu \mathbf{E} \mathbf{V}_\nu &= \mathbf{I}_\nu, \\ \mathbf{W}_\nu \mathbf{A} \mathbf{V}_\mu &= \mathbf{0}_{\nu, \mu}, & \mathbf{W}_\nu \mathbf{E} \mathbf{V}_\mu &= \mathbf{0}_{\nu, \mu}, \\ \mathbf{W}_\mu \mathbf{A} \mathbf{V}_\nu &= \mathbf{0}_{\mu, \nu}, & \mathbf{W}_\mu \mathbf{E} \mathbf{V}_\nu &= \mathbf{0}_{\mu, \nu}, \\ \mathbf{W}_\mu \mathbf{A} \mathbf{V}_\mu &= \mathbf{I}_\mu, & \mathbf{W}_\mu \mathbf{E} \mathbf{V}_\mu &= \mathbf{H}_\mu. \end{aligned}$$

Theorem 2.1. Consider system (2.10) with a regular pencil. Then the general solution of (2.10) is given by:

$$\mathbf{x}(t) = \mathbf{V}_\nu e^{\mathbf{J}_\nu t} \mathbf{c} + \mathbf{V}_\nu \int_0^\infty e^{\mathbf{J}_\nu(t-\tau)} \mathbf{W}_\nu \mathbf{B} \mathbf{u}(\tau) d\tau - \mathbf{V}_\mu \sum_{i=0}^{\mu_*-1} \mathbf{H}_\mu^i \mathbf{W}_\mu \mathbf{B} \mathbf{u}^{(i)}(t), \quad (2.19)$$

where $\mathbf{c} \in \mathbb{C}^{\nu \times \nu}$ is constant vector and $e^{\mathbf{J}_\nu t}$ is the matrix exponential of $\mathbf{J}_\nu t$.

The proof of Theorem 2.1 is given in Appendix A.

2.4.5 Stability

Definition 2.1. (*Asymptotic stability*) Consider an autonomous non-linear system $\dot{\mathbf{x}}(t) = \mathbf{h}(\mathbf{x}(t))$ with equilibrium \mathbf{x}_o . Then, the equilibrium \mathbf{x}_o is said to be *asymptotically stable* if there exists $\delta > 0$ such that if $\|\mathbf{x}(0) - \mathbf{x}_o\| < \delta$, then $\lim_{t \rightarrow \infty} \|\mathbf{x}(t) - \mathbf{x}_o\| = 0$.

Simply put, asymptotic stability implies that solutions starting close enough to the equilibrium will eventually converge to it. Asymptotic stability of equilibria is a local property for non-linear systems. On the other hand, for linear systems, asymptotic stability is a global property, which means that the solution will eventually converge to the equilibrium for any given initial condition. In this case, applying the above definition to the general solution (2.19) of system (2.10), yields that stability is guaranteed if and only if no element of the matrix exponential $e^{\mathbf{J}\nu t}$ goes to infinity, when $t \rightarrow \infty$, which, in turn, leads to the following well-known stability criterion.

Definition 2.2. System (2.10) is said to be *asymptotically stable* if all finite eigenvalues λ^* of its matrix pencil $s\mathbf{E} - \mathbf{A}$ satisfy:

$$\operatorname{Re}(\lambda^*) < 0. \quad (2.20)$$

The stability condition (2.20) can be also obtained using Lyapunov stability theory [61, 155]. In particular, condition (2.20) is equivalent to considering the Lyapunov function:

$$\mathcal{V}(\mathbf{x}) = \mathbf{x}^T \mathbf{E}^T \mathbf{M} \mathbf{x}, \quad (2.21)$$

with $\mathbf{E}^T \mathbf{M}$ symmetric and positive definite, and

$$\mathbf{A}^T \mathbf{M} + \mathbf{M}^T \mathbf{A} \quad (2.22)$$

negative definite. If such a matrix \mathbf{M} exists, then (2.10) is asymptotically stable and, hence, also Lyapunov stable.

Finally, calculation of eigenvalues allows measuring the characteristics of the most critical or *dominant* for the stability dynamic modes on the system. In particular, the *damping ratio* and *natural frequency* of a dynamic mode are defined as follows.

Definition 2.3. Let $\lambda = a + jb$ be a finite, complex eigenvalue of $s\mathbf{E} - \mathbf{A}$. The damping ratio and the natural frequency of λ are defined as follows:

$$\zeta = -\frac{a}{|\lambda|} = -\frac{a}{\sqrt{a^2 + b^2}}, \quad (\text{Damping ratio}) \quad (2.23)$$

$$f_n = \frac{|\lambda|}{2\pi} = \frac{\sqrt{a^2 + b^2}}{2\pi}, \quad (\text{Natural frequency}) \quad (2.24)$$

The power system is said to be well-damped, if for all eigenvalues λ^* , the damping ratio is higher than a threshold, typically $\zeta^* > 5\%$.

2.5 Numerical Methods

2.5.1 Eigenvalue Algorithms

There is a rich literature on numerical algorithms that compute the full or a partial solution of a given LEP or GEP. Relevant monographs on the topic are, for example, [136] and [70]. However, not all available algorithms are suitable for SSSA of power systems. The vast majority of numerical algorithms, in fact, solve exclusively symmetric eigenvalue problems. Such algorithms are, for example, the ones described in [67, 147]. However, the matrices that describe a linearized power system model are typically non-symmetric. Compared to symmetric problems, non-symmetric eigenvalue problems are more difficult and computationally demanding to solve.

The scalability of the numerical solution of eigenvalue problems is also very important since, real-world power networks are large-scale dynamic systems. Unfortunately, the most reliable methods to find the full spectrum of an eigenvalue problem are dense-matrix methods, and their computational complexity and memory requirements increase more than quadratically (in some cases even cubically) as the size of the matrix increases. This is further discussed in Section 2.5.4. Even using sparse matrices and limiting the search to a subset of the spectrum, the solution of large-scale power system eigenvalue problems is challenging.

A coarse taxonomy of existing algorithms for the solution of non-symmetric eigenvalue problems is as follows: vector iteration methods, Schur decomposition methods, Krylov subspace methods, and contour integration methods.

Vector iteration methods are in turn separated to single and simultaneous vector iteration methods. Single vector iteration methods include the power method and its variants, such as the inverse power and Rayleigh quotient iteration. Simultaneous vector iteration methods include the subspace iteration method [14] and its variants, such as the inverse subspace method.

Schur decomposition methods mainly include the QR algorithm [42], the QZ algorithm [104], and their variants, such as the QR algorithm with shifts. Schur decomposition based methods have been the standard methods employed for the eigenvalue analysis of small to medium size power systems [73, 100].

Krylov subspace methods basically include the Arnoldi iteration [10] and its variants, such as the implicitly restarted Arnoldi [79] and the Krylov-Schur method [150]. In this category belong also preconditioned extensions of the Lanczos algorithm, such as the non-symmetric versions of the Generalized Davidson and Jacobi-Davidson method.

Finally, contour integration methods include a moment-based Hankel method [137] and a Rayleigh-Ritz-based projection method [138] proposed by Sakurai; and the FEAST algorithm [127].

2.5.2 Open-Source Libraries

Available free and open-source software libraries that solve non-symmetric eigenvalue problems are a small subset of all existing eigensolvers. This section provides an overview of the open-source solvers that implement state-of-art numerical algorithms for non-symmetric eigenvalue problems [167]. These are LAPACK, ARPACK, Anasazi, SLEPc, FEAST and z-PARES.

LAPACK [8] is a standard library aimed at solving problems of numerical linear algebra, such as systems of linear equations and eigenvalue problems. A large part of the computations required by the routines of LAPACK are performed by calling the BLAS [77]. As an eigensolver, LAPACK includes the QR and QZ algorithms. Although it cannot handle general sparse matrices, LAPACK is functional with dense matrices and, in fact, is the standard dense matrix data interface used by all other eigenvalue libraries.

A powerful GPU-based implementation of LAPACK routines is provided by MAGMA which, for general non-symmetric matrices, supports only the solution of the LEP.

ARPACK [80] is a library developed for solving large eigenvalue problems with the IR-Arnoldi method. ARPACK depends on a number of subroutines from LAPACK/BLAS. An important feature of ARPACK is the support of a Reverse Communication Interface (RCI), which provides to the user the freedom to customize the matrix data format as desired. An implementation of ARPACK for parallel computers is provided by PARPACK. The message parsing layers supported by PARPACK are Message Passing Interface (MPI) [146] and BLACS.

Anasazi [13] is a library that implements block versions of both symmetric and non-symmetric algorithms for the solution of large-scale eigenvalue problems. Regarding non-symmetric problems, it provides a block extension of the Krylov-Schur method and the Generalized Davidson (GD) method. Anasazi depends on Trilinos [160] and uses LAPACK as an interface for dense matrix and Epetra as an interface for sparse Compressed Sparse Row (CSR) matrix formats.

SLEPc [56] is a library that includes a variety of symmetric and non-symmetric methods, for the solution of large sparse eigenproblems. For non-symmetric problems, it provides the following methods: power/inverse, power/Rayleigh quotient in a single implementation; subspace iteration with Rayleigh-Ritz projection and locking; Explicitly Restarted and Deflated (ERD) Arnoldi; Krylov-Schur; GD; Jacobi-Davidson (JD); Contour Integration with Hankel matrices (CIH) and Contour Integration with Rayleigh-Ritz (CIRR) methods. SLEPc depends on PETSc [9] and employs LAPACK as an interface for dense matrix, MUMPS [5] as an interface for sparse CSR matrix formats and supports custom data formats, enabled by RCI.

FEAST [128] is the eigensolver that implements the FEAST algorithm, first proposed in [127]. It depends on LAPACK as an interface for dense matrix, on SPIKE as an interface for banded matrix and on MKL-PARDISO [140] for sparse CSR matrix formats. In addition, FEAST includes RCI and thus, data formats can be customized by the user. Using the sparse interface requires linking FEAST with Intel MKL. Finally, FEAST includes parallel implementations which support 3-Level MPI message parsing layer.

z-PARES [44] is a complex moment-based contour integration eigensolver for GEPs that implements the CIH, and CIRR methods to find the eigenvalues (and corresponding

eigenvectors) that lie into a contour path defined by the user. The library depends on LAPACK for dense matrices, on MUMPS for sparse CSR matrices, while it supports custom data formats, enabled by RCI. Moreover, z-PARES includes a parallel version, which exploits 2-Level MPI layer and employs MUMPS as its sparse solver.

Tables 2.1 and 2.2 provide a synoptic summary of the methods and relevant features of open-source libraries that solve non-symmetric eigenvalue problems. As it can be seen from Table 2.2, all libraries can handle both real and complex arithmetic types. On the other hand, not all libraries are 2-sided, i.e provide algorithms that allow calculating both left and right eigenvectors at once.

Table 2.1: Methods of open-source libraries for non-symmetric eigenvalue problems.

Library	Method
LAPACK	QR, QZ
ARPACK	IR-Arnoldi
SLEPc	Power/Inverse Power/Rayleigh Quotient Iteration, Subspace, ERD-Arnoldi, Krylov-Schur, GD, JD, CIH, CIRR
Anasazi	Block Krylov-Schur, GD
FEAST	FEAST
z-PARES	CIH, CIRR

Table 2.2: Relevant features of open-source libraries for non-symmetric eigenvalue problems.

Library	Data formats				Computing		2-sided	Real/ complex	Releases	
	dense	CSR	band	RCI	GPU	parallel			first	latest
LAPACK	✓	✗	✗	✗	✓ ^a	✓ ^b	✓	✓	1992	2016
ARPACK	✗	✗	✗	✓	✗	✓	✗	✓	1995	2019 ^c
SLEPc	✓	✓	✗	✓	✓	✓	✓ ^d	✓	2002	2020
Anasazi	✓	✓	✗	✗	✗	✗	✗	✓	2008	2014
FEAST	✓	✓	✓	✓	✗	✓	✓	✓	2009	2020
z-PARES	✓	✓	✗	✓	✗	✓	✗	✓	2014	2014

^aWith MAGMA.

^bParallel implementations of LAPACK routines are provided by ScaLAPACK [18].

^cARPACK has been forked into ARPACK-NG.

^dIn SLEPc, only the power and the Krylov-Schur methods are 2-sided.

2.5.3 Spectral Transforms

In general, solving the eigenvalue problem involves finding the full or partial spectrum of the pencil $s\mathbf{E} - \mathbf{A}$. However, depending on the applied numerical method as well as on the structure of the system matrices, it is common that the eigenvalues are not found by using directly $s\mathbf{E} - \mathbf{A}$, but through the pencil that arises after the application of a proper spectral transform. Spectral transforms are utilized by eigenvalue numerical methods to find the eigenvalues of interest, address a singularity issue, or accelerate convergence.

The Möbius transformation, which is a general variable transformation that includes as special cases all spectral transforms used in practice by eigenvalue algorithms, is discussed here. The formulation of the Möbius transformation is:

$$s := \frac{az + b}{cz + d}, \quad a, b, c, d \in \mathbb{C}, \quad ad - bc \neq 0. \quad (2.25)$$

Applying the transform (2.25) in (2.15) one has

$$\det\left(\frac{az + b}{cz + d}\mathbf{E} - \mathbf{A}\right) = 0,$$

or, equivalently, by using determinant properties

$$\det((az + b)\mathbf{E} - (cz + d)\mathbf{A}) = 0,$$

or, equivalently,

$$\det((a\mathbf{E} - c\mathbf{A})z - (d\mathbf{A} - b\mathbf{E})) = 0,$$

which is the characteristic equation of the linear dynamical system

$$(a\mathbf{E} - c\mathbf{A})\dot{\tilde{\mathbf{x}}}(t) = (d\mathbf{A} - b\mathbf{E})\tilde{\mathbf{x}}(t), \quad (2.26)$$

with pencil $z(a\mathbf{E} - c\mathbf{A}) - (d\mathbf{A} - b\mathbf{E})$. System (2.10) will be referred as the prime system, and the family of systems (2.26) will be defined as the proper “M-systems”. An important property is that the solutions and stability properties of system (2.10) can be studied through (2.26) without resorting to any further computations, see [30]. The utilities of the family of systems of type (2.26) have been further emphasized by the features of some particular special cases. The most commonly employed Möbius transforms and

the corresponding matrix pencils for the GEP are summarized in Table 2.3. The values of the parameters a, b, c, d that lead to each of these transforms are given in Table 2.4. In case that $\sigma > 0$, the Cayley transform is equivalent to the bilinear transform $z := (\frac{T}{2}s + 1)/(\frac{T}{2}s - 1)$, where $T = \frac{2}{\sigma}$. Finally, the selection of the best transform for a specific system and eigenvalue problem is a challenging task to solve, since the selection of shift values is, ultimately, heuristic.

Table 2.3: Common linear spectral transforms.

Name	z	Pencil	s
Prime system	s	$s\mathbf{E} - \mathbf{A}$	z
Invert	$1/s$	$z\mathbf{A} - \mathbf{E}$	$1/z$
Shift & invert	$1/s - \sigma$	$z(\sigma\mathbf{E} - \mathbf{A}) + \mathbf{E}$	$1/z + \sigma$
Cayley	$(s + \sigma)/(s - \sigma)$	$z(\sigma\mathbf{E} - \mathbf{A}) - (\mathbf{A} + \sigma\mathbf{E})$	$\sigma(z - 1)/(z + 1)$
Gen. Cayley	$(s + \nu)/(s - \sigma)$	$z(\sigma\mathbf{E} - \mathbf{A}) - (\mathbf{A} + \nu\mathbf{E})$	$(\sigma z - \nu)/(z + 1)$
Möbius	$(-ds + b)/(cs - a)$	$z(a\mathbf{E} - c\mathbf{A}) - (d\mathbf{A} - b\mathbf{E})$	$(az + b)/(cz + d)$

Table 2.4: Coefficients of special Möbius transformations.

M-system	a	b	c	d
Prime	-1	0	0	-1
Dual	0	1	1	0
Shift & invert	σ	1	1	0
Cayley	σ	$-\sigma$	1	1
Gen. Cayley	σ	$-\nu$	1	1

2.5.4 Computational Complexity

The computational complexity of an eigenvalue algorithm is in general dependent upon the particular implementation provided by a given software library. However, library manuals typically do not detail their memory and computational requirements, and thus to provide a systematic and precise comparison with this regard is not a trivial task. Yet, for an eigenvalue problem with a pencil of size n , one may provide a rough summary of the costs associated to a generic algorithm that searches for $k \leq n$ eigenvalues. That is, the algorithm:

- constructs a subspace of order k associated to the eigenvalue problem*. A basis of the subspace, that is k vectors of size n , needs to be stored.
- carries out computations to guarantee that the basis vectors of the subspace are orthogonal. The associated cost of such computations is $\mathcal{O}(k^2n)$.
- projects the matrix pencil to the subspace which yields a reduced eigenvalue problem with a pencil of size k . The dense matrices of dimensions $k \times k$ that comprise this pencil need to be stored.
- solves the projected dense eigenvalue problem. This problem is typically solved using QR factorization, with an associated cost of $\mathcal{O}(k^3)$.

The total computational cost sums to $\mathcal{O}(k^2n + k^3)$. For a dense matrix method, i.e. the QR algorithm and its variants, a complete basis of vectors is used, which yields a computational complexity of $\mathcal{O}(n^3)$. It follows that the cost of the resources required to solve a very large problem using a dense-matrix algorithm is very high. As a matter of fact, the largest ever eigenvalue analysis with a dense algorithm to date was the solution of a $10^6 \times 10^6$ problem in about 1 h, and it was carried out in 2014 by the Japanese K computer in Riken. To be able to obtain this result, the K computer includes 88,000 processors that draw a peak power of 12.6 MW, while its operation costs annually US\$10 million.

The computational burden associated to the numerical algorithms and open-source libraries described in this thesis is further discussed through numerical simulations in the case study of Section 2.6.

2.6 Case Studies

In this section simulation results are presented based on two real-world size power system models. The first system is a detailed model of the AIITS which includes 1,443 state variables and 7,197 algebraic variables. The second system is a dynamic model of the ENTSO-E system, which includes 49,396 state variables and 96,770 algebraic variables. The versions and dependencies of the open-source libraries considered in this section are

*Note this is a rough estimation. In order to accurately capture k eigenvalues, practical algorithms often work with subspaces of size that is larger than k , thus increasing the overall computational cost.

summarized in Table 2.5. Note that this section considers only the open-source libraries that were successfully compiled and installed on Linux and Mac OS X operating systems and that worked for relatively “large” eigenvalue problems.

Table 2.5: Versions and dependencies of open-source libraries for non-symmetric eigenvalue problems.

Library (Version)	Dependencies (Version)
LAPACK (3.8.0)	ATLAS (3.10.3)
MAGMA (2.2.0)	NVidia CUDA (10.1)
ARPACK-NG (3.5.0)	SuiteSparse KLU (1.3.9)
z-PARES (0.9.6a)	OpenMPI (3.0.0), MUMPS (5.1.2)
SLEPc (3.8.2)	PETSc (3.8.4), MUMPS (5.1.2)

All simulations are obtained using Dome [93]. The Dome version utilized for this chapter is based on Fedora Linux 28, Python 3.6.8, CVXOPT 1.1.9 and KLU 1.3.9. Regarding the computing times reported in both examples, two comments are relevant. First, all simulations were executed on a server mounting two quad-core Intel Xeon 3.50 GHz CPUs, 1 GB NVidia Quadro 2000 GPU, 12 GB of RAM, and running a 64-bit Linux OS. Second, since, not all method implementations include 2-sided versions and in order to provide as a fair comparison as possible, all eigensolvers are called so as to return only the calculated eigenvalues and not eigenvectors.

2.6.1 All-Island Irish Transmission System

This case study considers a real-world model of the AIITS. The topology and the steady-state operation data of the system have been provided by the Irish transmission system operator, EirGrid Group. Dynamic data have been determined based on current knowledge about the technology of the generators and the controllers. The system consists of 1,479 buses, 796 lines, 1,055 transformers, 245 loads, 22 synchronous machines, with Automatic Voltage Regulators (AVRs) and Turbine Governors (TGs), 6 PSSs and 176 wind generators. In total, the dynamic model has $n = 1,443$ state variables and $m = 7,197$ algebraic variables. The map of the AIITS is given in Appendix B.

Results of the eigenvalue analysis of the AIITS are discussed for both LEP and GEP and for a variety of different numerical methods, namely, QR and QZ algorithms

Table 2.6: AIITS: dimensions of the LEP and GEP.

Problem	Pencil	Size
LEP	$s\mathbf{I}_n - \mathbf{A}_s$	$1,443 \times 1,443$
GEP	$s\mathbf{E}_a - \mathbf{A}_a$	$8,640 \times 8,640$

by LAPACK, GPU-based QR algorithm by MAGMA, subspace iteration, ERD-Arnoldi and Krylov-Schur methods by SLEPc, IR-Arnoldi by ARPACK; and CIRRE by z-PARES.

The results obtained with Schur decomposition methods are presented in Table 2.7. Both QR and QZ algorithms find all 1,443 finite eigenvalues of the system. For the GEP, the QZ algorithm also finds the additional infinite eigenvalue with its algebraic multiplicity. The obtained rightmost eigenvalues are the same for both LEP and GEP. Since LAPACK is the most mature software tool among those considered in this section, the accuracy of the eigenvalues found with all other libraries is evaluated by comparing them with the reference solution computed with LAPACK. The system root loci plot is shown in Figure 2.1. Regarding the computational time, it is seen that, for the LEP, both LAPACK and the GPU-based MAGMA are very efficient at this scale, with MAGMA providing only a marginal speedup. On the other hand, when it comes to solving the GEP with LAPACK’s QZ method, scalability becomes a serious issue.

Table 2.7: AIITS: Schur decomposition methods, LEP and GEP.

Library	LAPACK	MAGMA	LAPACK
Problem	LEP	LEP	GEP
Method	QR	QR	QZ
Spectrum	All	All	All
Time [s]	3.94	3.54	3,669.77
Found	1,443 eigs.	1,443 eigs.	8,640 eigs.
LRP eigs.	0.0000 -0.0869 $-0.1276 \pm j0.1706$ $-0.1322 \pm j0.4353$ -0.1376 -0.1382 -0.1386 -0.1390 -0.1391 -0.1393 -0.1394	0.0000 -0.0869 $-0.1276 \pm j0.1706$ $-0.1322 \pm j0.4353$ -0.1376 -0.1382 -0.1386 -0.1390 -0.1391 -0.1393 -0.1394	0.0000 -0.0869 $-0.1276 \pm j0.1706$ $-0.1322 \pm j0.4353$ -0.1376 -0.1382 -0.1386 -0.1390 -0.1391 -0.1393 -0.1394

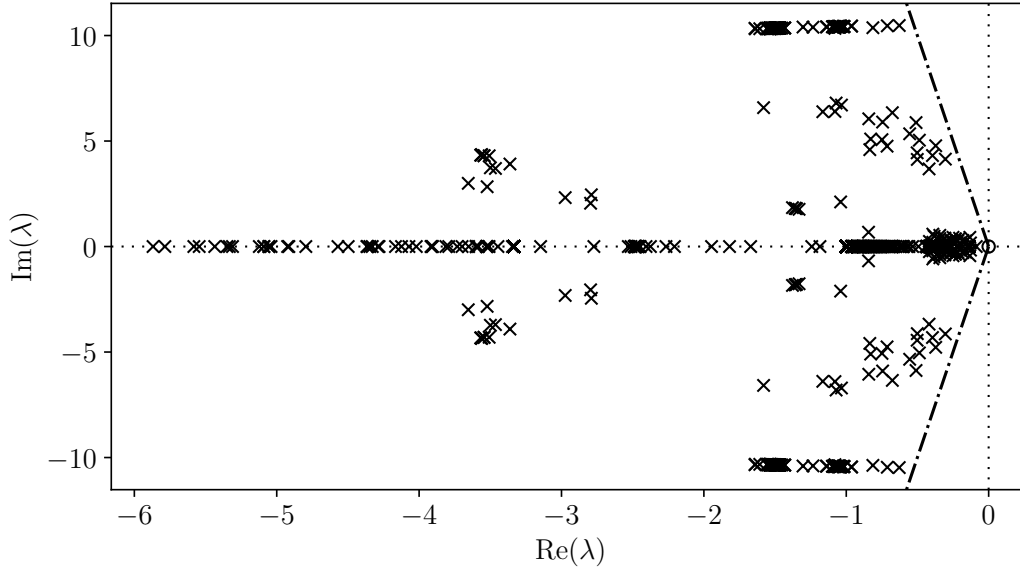


Figure 2.1: AIITS: root loci computed with LAPACK.

Figures 2.2 and 2.3 show the spectrum of the AIITS system for a couple of common special Möbius transforms, in particular for the shift & invert and the Cayley transform. In these figures, $\hat{\lambda}$ denotes an eigenvalue of the transformed pencil. These results refer to the LEP, and are obtained using LAPACK. In each figure, the stable region is shaded, while the stability boundary is indicated with a solid line. The 5 % damping boundary is indicated with a dash-dotted line. For the shift & invert transform, the stability boundary is defined by the circle with center $c = (1/2\sigma, 0)$ and radius $\rho = 1/2\sigma$. If $\sigma < 0$, that is the case of Figure 2.2, stable eigenvalues are mapped outside the circle. On the other hand, if $\sigma > 0$, stable eigenvalues are mapped inside the circle. If $\sigma = 0$, the dual pencil is obtained with the corresponding invert transform, and the stable region is the full negative right half plane. Finally, Figure 2.3 shows the image of the Cayley transform of the AIITS for $\sigma = 1.2$. All stable eigenvalues are located inside the unit circle with center the origin.

The implementation of the subspace iteration by SLEPc only finds the desired number of LM eigenvalues. However, in the s -domain, the relevant eigenvalues from the stability point of view are not the LM ones, but the ones with Largest Real Part (LRP) or Smallest Magnitude (SM). Especially for the GEP, the Largest Magnitude (LM) eigenvalue is infinite and, hence, does not provide any meaningful information on the system dynamics. For this reason and for the needs of power system SSSA, the subspace method and, in general, any method that looks for LM eigenvalues, must always be combined with a

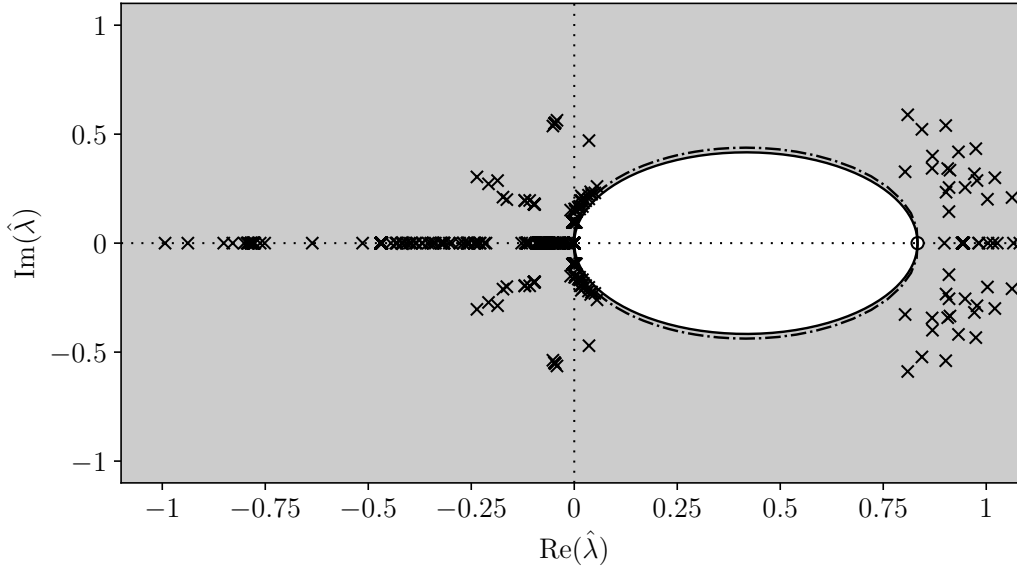


Figure 2.2: AITTS: shift & invert transform image of the spectrum, $\sigma = -1.2$.

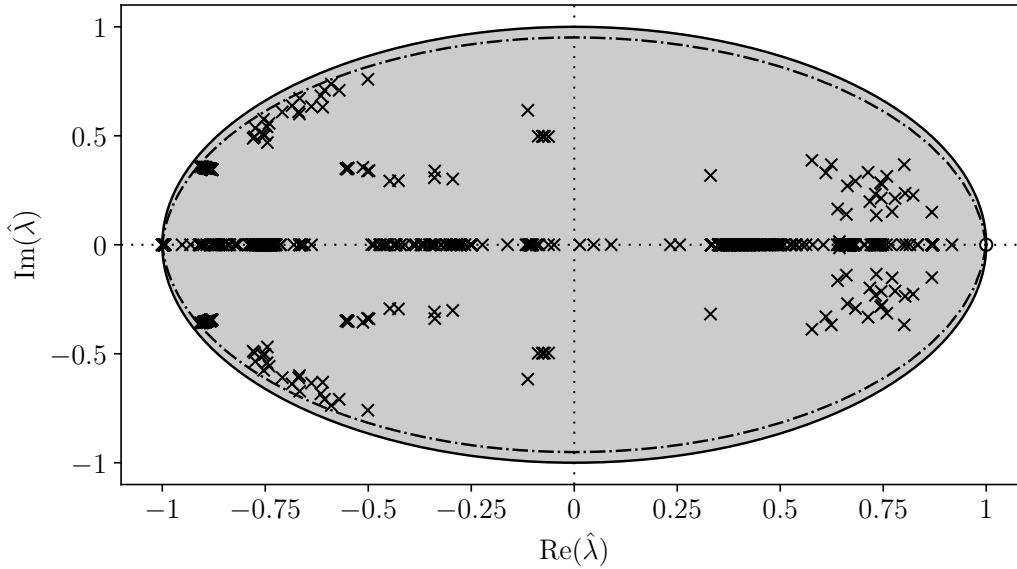


Figure 2.3: AITTS: Cayley transform image of the spectrum, $\sigma = 2$.

spectral transform. For the needs of this example, the invert transform is applied and the pencil of the dual system, i.e. $z\mathbf{A} - \mathbf{E}$, is passed to SLEPc. Then, the method looks for the 50 LM eigenvalues of the dual system, which correspond to the 50 SM eigenvalues of the prime system. With this setup, the eigenvalues found by the subspace iteration for the GEP are shown in Table 2.8. As it can be seen, the pair $-0.1322 \pm j0.4353$ is not captured, since its magnitude is larger than the magnitudes of the 50 SM eigenvalues. To obtain also this pair, one can customize the spectral transform or simply increase the number of the eigenvalues to be returned. However, the best setup is not known a priori

and thus, some heuristic parameter tuning is required. Finally, the method does not scale well, since solution of the GEP is completed in 6,807.24 s.

Table 2.8: AIITS: subspace iteration method, GEP.

Library	SLEPc
Method	Subspace
Spectrum	50 LM
Transform	Invert
Time [s]	6,807.24
Found	50
LRP eigs.	-0.0000 -0.0869 $-0.1276 \pm j0.1706$ -0.1376 -0.1382 -0.1386 -0.1390 -0.1391 -0.1393 -0.1394 -0.1397

The rightmost eigenvalues found with Krylov subspace methods for the LEP and GEP are shown in Table 2.9 and Table 2.10, respectively. For the LEP, ARPACK is set up to find the 50 LRP eigenvalues. Although all eigenvalues shown in Table 2.9 for ARPACK are actual eigenvalues of the system, some of the LRP ones are missed. Furthermore, no correct eigenvalues were found for the GEP, since a non-symmetric \mathbf{E} is not supported. In SLEPc methods, both for LEP and GEP and in order to obtain the eigenvalues with good accuracy, the option “Target Real Part” (TRP) is used, which allows targeting eigenvalues with specified real part. In particular, the TRP parameter is set to -0.01 , and a shift & invert transform with $\sigma = -0.01$ is applied. Both ERD-Arnoldi and Krylov-Schur methods are able to accurately capture all rightmost eigenvalues. Note that, the eigenvalues obtained with SLEPc, when compared to the ones found by LAPACK, appeared to be shifted by a constant offset $-\sigma$, i.e. 0.01 was returned instead of 0, and so on. The results shown in Table 2.9 and Table 2.10 take into account such a shift by adding σ to all output values returned by SLEPc. Finally, the Krylov subspace methods by SLEPc appear to be more efficient than ARPACK’s IR-Arnoldi. Compared to Schur decomposition methods, at this scale, Krylov methods,

although they require some tuning, appear to be by far more efficient for the GEP, but less efficient for the LEP.

Table 2.9: AIITS: Krylov subspace methods, LEP.

Library Method Spectrum	ARPACK IR-Arnoldi 50 LRP	SLEPc ERD-Arnoldi 50 TRP	SLEPc Krylov-Schur 50 TRP
Transform	-	Shift & invert $\sigma = -0.01$	Shift & invert $\sigma = -0.01$
Time [s] Found	76.96 26 eigs.	17.84 54 eigs.	16.58 55 eigs.
LRP eigs.	-0.0000 -0.0869 $-0.1276 \pm j0.1706$ $-0.1322 \pm j0.4353$ $-0.1615 \pm j0.2689$ $-0.1809 \pm j0.2859$ $-0.2042 \pm j0.3935$ $-0.2172 \pm j0.2646$ $-0.2335 \pm j0.3546$ $-0.2344 \pm j0.3644$ $-0.2503 \pm j0.4363$	0.0000 -0.0869 $-0.1276 \pm j0.1706$ $-0.1322 \pm j0.4353$ -0.1376 -0.1382 -0.1386 -0.1390 -0.1391 -0.1393 -0.1394	0.0000 -0.0869 $-0.1276 \pm j0.1706$ $-0.1322 \pm j0.4353$ -0.1376 -0.1382 -0.1386 -0.1390 -0.1391 -0.1393 -0.1394

Table 2.10: AIITS: Krylov subspace methods, GEP.

Library Method Spectrum	SLEPc ERD-Arnoldi 50 TRP	SLEPc Krylov-Schur 50 TRP
Transform	Shift & invert $\sigma = -0.01$	Shift & invert $\sigma = -0.01$
Time [s] Found	8.93 51 eigs.	7.64 53 eigs.
LRP eigs.	0.0000 -0.0869 $-0.1276 \pm j0.1706$ $-0.1322 \pm j0.4353$ -0.1376 -0.1382 -0.1386 -0.1390 -0.1391 -0.1393 -0.1394	0.0000 -0.0869 $-0.1276 \pm j0.1706$ $-0.1322 \pm j0.4353$ -0.1376 -0.1382 -0.1386 -0.1390 -0.1391 -0.1393 -0.1394

The results obtained with z-PARES' CIRR method are presented in Table 2.11 and Figure 2.4. The method is set to look for solutions in the circle with center the point $c = (-0.01, 4)$ and radius $\rho = 8$. In both cases, the eigenvalues found by z-PARES are actual eigenvalues of the system, although the eigenvalues found for the GEP include noticeable errors, when compared to the results obtained with LAPACK.

Table 2.11: AIITS: contour integration method, LEP and GEP.

Library Method Spectrum	z-PARES CIRR $c = (-0.01, 4), \rho = 8$	
Problem	LEP	GEP
Time [s]	10.81	17.10
Found	49 eigs.	52 eigs.
LRP eigs.	$-0.3041 + j4.1425$	$-0.3040 + j4.1429$
	$-0.3720 + j4.7773$	$-0.3715 + j4.7774$
	$-0.3945 + j4.3121$	$-0.3947 + j4.3122$
	$-0.4184 \pm j3.6794$	$-0.4187 \pm j3.6794$
	$-0.4866 + j5.0405$	$-0.4865 + j5.0405$
	$-0.5011 + j4.1276$	$-0.5007 + j4.1274$
	$-0.5022 + j4.4417$	$-0.5018 + j4.4417$
	$-0.5077 + j5.8727$	$-0.5097 + j5.8747$
	$-0.5555 + j5.3444$	$-0.5542 + j5.3436$
	$-0.6765 + j6.3426$	$-0.6761 + j6.3412$

The most relevant issue is that the eigenvalues obtained with z-PARES are not the most important ones for the stability of the system, which means that critical eigenvalues are missed. This issue occurs despite the defined search contour being reasonable. Of course, there may be some region for which the critical eigenvalues are captured but, this can not be known *a priori*. Regarding the simulation time, the method for the AIITS is faster than SLEPc's Krylov subspace methods for the LEP, but slower for the GEP. The search contour and the location of the characteristic roots found by z-PARES for the LEP are depicted in Figure 2.4.

2.6.2 21,177-bus ENTSO-E

This example presents simulation results for a dynamic model of the ENTSO-E. The system includes 21,177 buses (1,212 off-line); 30,968 transmission lines and transformers (2,352 off-line); 1,144 zero-impedance connections (420 off-line); 4,828 power plants

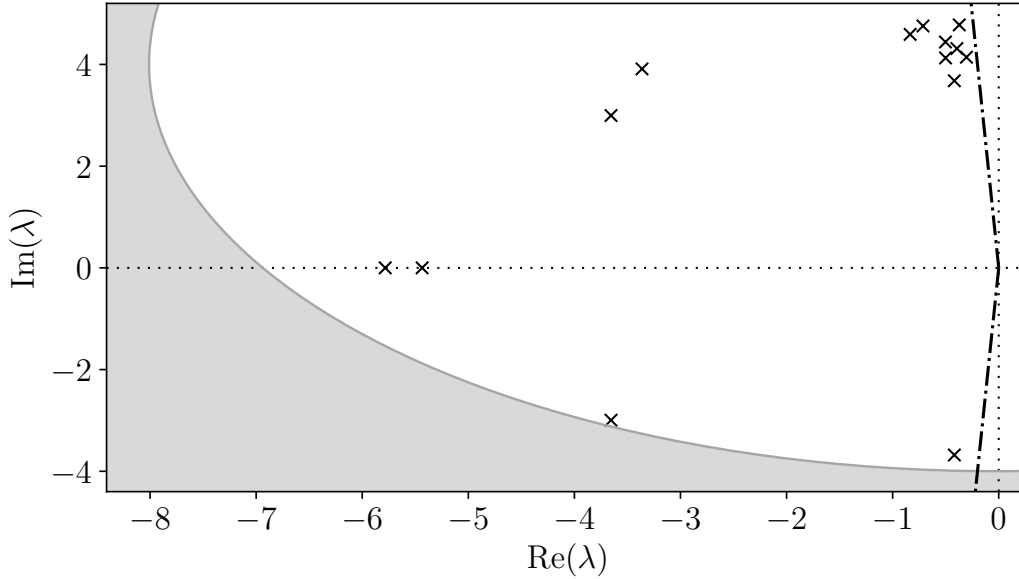


Figure 2.4: AIITS: root loci obtained with z-PARES, LEP.

represented by 6-th order and 2-nd order synchronous machine models; and 15,756 loads (364 off-line), modeled as constant active and reactive power consumption. Synchronous machines represented by 6-th order models are also equipped with dynamic AVR and TG models. The system also includes 364 PSSs.

As summarized in Table 2.12, the system has in total $n = 49,396$ state variables and $m = 96,770$ algebraic variables. The pencil $s\mathbf{E} - \mathbf{A}$ has dimensions $146,166 \times 146,166$ and the matrix \mathbf{A} has 654,950 non-zero elements, which represent the 0.003% of the total number of elements of the matrix.

Table 2.12: ENTSO-E: statistics.

n	49,396
m	96,770
Dimensions of \mathbf{A}	$146,166 \times 146,166$
Sparsity degree of \mathbf{A} [%]	99.997

Neither the LEP or GEP could be solved using Schur decomposition methods. At this scale, the dense matrix representation required by LAPACK and MAGMA leads to massive memory requirements, and a segmentation fault error is returned by the CPU. Among the algorithms that support sparse matrices, only z-PARES is tested. This, in fact, was the library that was able to tackle this large problem on the available hardware.

The effect of changing the search region of z-PARES' CIRP method on the eigenvalue analysis of the ENTSO-E is shown in Table 2.13. Interestingly, simulations showed that

shrinking the defined contour may lead to a marginal increase of the computation time. Although not intuitive, this result indicates that the mass of the computational burden is mainly determined by the large size of the ENTSSO-E, and that, at this scale, smaller subspaces are not necessarily constructed faster by the CIRR algorithm. Regarding the number of eigenvalues obtained, using a region that is too small leads, as expected, to missing an important number of critical eigenvalues.

Table 2.13: ENTSSO-E: impact of the search region of the CIRR method.

Library Problem Method	z-PARES		
	GEP		
	CIRR		
c	$(-0.01, 4)$	$(-0.01, 3)$	$(-0.01, 3)$
ρ	8	4	2
Time [s]	364.85	375.67	378.71
Found	349 eigs.	350 eigs.	110 eigs.

Table 2.14: ENTSSO-E: impact of spectral transforms of the CIRR method.

Library Problem Method Spectrum	z-PARES		
	GEP		
	CIRR		
	$c = (-0.01, 4), \rho = 8$		
Transform	-	Invert	Inverted Cayley
Time [s]	364.85	350.82	337.43
Found	349 eigs.	297 eigs.	349 eigs.

The impact of applying spectral transforms to the matrix pencil $s\mathbf{E} - \mathbf{A}$ is examined. In particular, two transforms are tested. The invert transform, which yields the dual pencil $z\mathbf{A} - \mathbf{E}$; and the inverted Cayley transform, i.e. $s = (z + 1)/(\sigma z - \sigma)$, which yields the pencil $z(\mathbf{E} - \sigma\mathbf{A}) - (-\sigma\mathbf{A} - \mathbf{E})$. The results are shown in Table 2.14. Passing the transformed matrices to z-PARES provides a marginal speedup to the eigenvalue computation. In addition, considering either the prime system or the inverted Cayley transform with $\sigma = -1$, results in finding the same number of eigenvalues, whereas when the dual system is considered a number of eigenvalues is missed.

2.7 Concluding Remarks

This chapter provides fundamental concepts of power system SSSA and linear systems of differential equations that are employed throughout the thesis.

The chapter also provides a comprehensive comparison of state-of-art software implementations for the numerical solution of the eigenvalue problems that arise in power systems. With this regard, the following discussion is relevant.

The main disadvantage of dense matrix methods is that they are computationally expensive. In addition, they generate complete fill-in in general sparse matrices and therefore, cannot be applied to large sparse matrices simply because of massive memory requirements. Even so, LAPACK is the most mature among all computer-based eigensolvers and, as opposed to basically all sparse solvers, requires practically no parameter tuning. For small to medium size problems, the QR algorithm with LAPACK remains the standard and most reliable algorithm for finding the full spectrum for the conventional LEP.

As for sparse matrix methods, convergence of vector iteration methods can be very slow, and thus in practice, if not completely avoided, these algorithms should be used only for the solution of simple eigenvalue problems. With regard to Krylov subspace methods, the main shortcoming of ARPACK's implementation is the lack of support for general, non-symmetric left-hand side coefficient matrices, which is the form that commonly appears when dealing with the GEP of large power system models. On the other hand, the implementations of ERD-Arnoldi and Krylov-Schur by SLEPc do not have this limitation and exploit parallelism while providing good accuracy, although some parameter tuning effort is required. In addition, for the scale of the AIITS system and for the GEP, these methods appear to be by far more efficient than LAPACK. Moreover, the implementation of contour integration by z-PARES is very efficient and can handle systems at the scale of the ENTSO-E. The most relevant issue for z-PARES is that, depending on the problem, it may miss some critical eigenvalues, despite the defined search contour being reasonable. Although there may be some parameter settings for which this problem does not occur, those cannot be known *a priori*.

Chapter 3

Participation Factors

3.1 Introduction

Modal participation analysis was first introduced by Pérez-Arriaga *et al.* in [123] and [174]. These studies employed the analytical solution that determines the time response of a linear time-invariant dynamic system and applied initial conditions appropriate to define the relative contribution of a system state in a dynamic mode and *vice versa*. Participation Factors (PFs) were introduced as an approach to selective modal analysis. They have been also utilized in model reduction [26], as well as in control signal and input placement selection [58]. The properties of PFs were summarized and extended in [46]. In [3, 54], the authors studied the effect of the uncertainty in the initial conditions in the definition of the PFs. Nowadays, PFs are considered a fundamental tool for power system SSSA. Recent efforts have focused on the modal participation analysis of non-linear systems [110, 159].

Dominant states in lightly damped modes of power systems are typically the synchronous machine rotor angles and speeds. The state variables of poorly tuned controllers, e.g. the AVRs and PSSs, can also show high PFs in critical modes. Nevertheless, measurement units installed on the transmission system buses provide information on the local voltage, frequency and active and reactive power flows, which in angle and voltage stability studies are modeled as algebraic variables [92]. Moreover, these quantities are typically utilized by Flexible AC Transmission System (FACTS) devices as signals for the implementation of various controllers including Power Oscillation Damper (POD) [1].

This chapter provides a tool to study how algebraic variables are coupled with power system dynamic modes. It is precisely recognized that the algebraic variables of a set of DAEs can be interpreted as functions of the state variables and, in turn, as *outputs* of the state-space representation of the power system model. Until now, algebraic variables were mostly interpreted either as *constraints* and thus eliminated when calculating the state matrix of the system; or as *states with infinitely fast dynamics* and, as such, their PFs to system modes were considered to be null. The focus is on the PFs of bus voltages, frequencies, and power injections; Rate of Change of Frequency (ROCOF) of synchronous machines; Center of Inertia (COI) speed of different areas; and any system parameters. However, the formulation provided in this chapter is general and can be extended to any non-linear function of the system states and algebraic variables.

The remainder of the chapter is organized as follows. Section 3.2 describes the classical modal participation analysis of a power system model. Section 3.3 provides a new interpretation of the PFs as eigen-sensitivities – which is derived from the partial differentiation of the analytical solution of the linearized power system around a valid equilibrium point – and provides their formulation for a singular dynamical system with eigenvalue multiplicities. Based on this interpretation, the proposed approach to measure the participation of algebraic variables and, in general, of any function of the variables in power system modes is presented in Section 3.4. The case studies are discussed in Section 3.5. Finally, conclusions are drawn in Section 3.6.

3.2 Classical Participation Factors

3.2.1 Definition

Consider the following system of ODEs:

$$\dot{\mathbf{x}} = \mathbf{A} \mathbf{x}, \quad (3.1)$$

where $\mathbf{x} \in \mathbb{R}^r$ is the vector of state variables and $\mathbf{A} \in \mathbb{R}^{r \times r}$ is the state matrix. System (3.1) can be obtained from (2.10) for $\mathbf{E} \equiv \mathbf{I}_r$ and by assuming that no inputs are included.

Let λ_i be an eigenvalue of $s\mathbf{I}_r - \mathbf{A}$ and all eigenvalues be distinct, i.e. $\lambda_i \neq \lambda_j$, $i \neq j$, and $i, j = 1, 2, \dots, r$. Let also \mathbf{v}_i , \mathbf{w}_i be the right and left eigenvectors associated to λ_i ,

respectively. The PF is defined as the following dimensionless number:

$$\pi_{k,i} = w_{i,k} v_{k,i}, \quad (3.2)$$

where $v_{k,i}$ is the k -th row element of \mathbf{v}_i and $w_{i,k}$ is the k -th column element of \mathbf{w}_i .

The right and left eigenvectors are usually normalized so that the sum of all PFs that correspond to the same eigenvalue equals to 1 [123]. However, this is not always the case [75]. In addition, the PFs of a system are typically collected to form the participation matrix $\mathbf{\Pi}_{\text{PF}}$, which is defined as follows:

$$\mathbf{\Pi}_{\text{PF}} = \mathbf{W}^T \circ \mathbf{V}, \quad (3.3)$$

where \circ denotes the Hadamard product, i.e. the element-wise multiplication; and \mathbf{V} , \mathbf{W} , are the right and left *modal matrices*, respectively. That is, the columns of \mathbf{V} are the right eigenvectors \mathbf{v}_i and the rows of \mathbf{W} are the left eigenvectors \mathbf{w}_i .

3.2.2 Residues

The PF $\pi_{k,i}$ in (3.2) basically expresses the relative contribution of x_k in the structure of the eigenvalue λ_i , and *vice versa*, but has also various other interpretations. It is also known to represent the sensitivity of an eigenvalue to variations of an element of the state matrix [119] and it has been also viewed as modal energy in the MacFarlane sense [52].

In the state space representation, PFs can be studied as an important case of residue analysis of the system transfer function and thus, as joint observabilities/controllabilities of the geometric approach, which play an important role during the design of control systems [46, 53]. Consider the following single-input single-output system:

$$\begin{aligned} \dot{\mathbf{x}} &= \mathbf{A} \mathbf{x} + \mathbf{b} u, \\ w &= \mathbf{c} \mathbf{x}, \end{aligned} \quad (3.4)$$

where \mathbf{b} is the column vector of the input u ; \mathbf{c} is the row vector of the output w . Then, the residue of the transfer function of system (3.4) associated with the eigenvalue λ_i of

the pencil $s\mathbf{I}_r - \mathbf{A}$ is given by:

$$\mathbf{R}_i = \mathbf{c} \mathbf{v}_i \mathbf{w}_i \mathbf{b}. \quad (3.5)$$

The PF of the k -th state x_k in λ_i can be viewed as the residue of the transfer function of system (3.4) associated with λ_i , when the input is a perturbation in the differential equation that defines \dot{x}_k and the output is x_k . Indeed, if

$$\begin{aligned} \mathbf{c} &= [c_1 \quad \dots \quad c_k \quad \dots \quad c_r] = [0 \quad \dots \quad 1 \quad \dots \quad 0], \\ \mathbf{b}^\top &= [b_1 \quad \dots \quad b_k \quad \dots \quad b_r]^\top = [0 \quad \dots \quad 1 \quad \dots \quad 0]^\top, \end{aligned}$$

equation (3.5) becomes:

$$\mathbf{R}_i = w_{i,k} v_{k,i} = \pi_{k,i}. \quad (3.6)$$

In the case of a multiple-input multiple-output system, the PFs appear as the diagonal elements of the emerging residue matrix. The ability to calculate only a subset of all residue elements and acquire an approximate but yet accurate measure of the contribution of system states in system modes (and *vice versa*), features the physical importance and the computational efficiency of the PFs.

3.3 Generalized Participation Factors

3.3.1 Formulation

From the definition of PFs given in (3.2), it follows that the main assumptions of classical modal participation analysis are:

- All eigenvalues are distinct.
- The system is modeled as a set of ODEs, i.e. all eigenvalues are finite.

On the other hand, it is common in the simulation of dynamic models that some eigenvalues are repeated. For small size systems, it may be possible to avoid multiplicities, e.g. by perturbation of some parameters. But this is impractical for real-world size

systems. Moreover, for large-scale systems, available algorithms are typically able to find a partial solution only of the GEP and provided that the matrices are sparse, which implies that the system is modeled as a set of singular differential equations. Section 2.5 further elaborates on this point.

This section presents an alternative interpretation of the PFs as eigen-sensitivities. In the view of addressing the issues mentioned above, the focus is on the modal participation analysis of a singular system of differential equations with eigenvalue multiplicities. The proposed approach requires the solution of the GEP, as opposed to the conventional LEP, and thus fully exploits the sparsity of Jacobian matrices [100]. This allows utilizing solvers for eigenvalue analysis that scale well and are suitable for large real-world systems. Finally, classical PFs are extracted from the provided formulation as a special case.

Consider system (2.10) without any inputs, i.e.:

$$\mathbf{E} \dot{\mathbf{x}}(t) = \mathbf{A} \mathbf{x}(t), \quad (3.7)$$

where $\mathbf{E}, \mathbf{A} \in \mathbb{R}^{r \times r}$, $\mathbf{x}(t) : \mathbb{R}^+ \rightarrow \mathbb{R}^r$. From Theorem 2.1, and by applying $\mathbf{B} = \mathbf{0}_{r,p}$ in (2.19), the analytical solution of system (3.7) is:

$$\mathbf{x}(t) = \mathbf{V}_\nu e^{\mathbf{J}_\nu t} \mathbf{c}. \quad (3.8)$$

In order to study the effects of eigenvalue multiplicities in (3.7), (2.19) has to be rewritten so that the generalized eigenvectors appear in the solution of the system explicitly [32].

Firstly, let:

- α be the number of Jordan blocks and $\hat{\lambda}_i \in \mathbb{C}$, $i = 1, 2, \dots, \alpha$, be finite eigenvalue that corresponds to the i -th Jordan block and β_i be the rank of the block, where $\sum_{i=1}^{\alpha} \beta_i = \nu$.
- the infinite eigenvalue have algebraic multiplicity μ .

The following theorem is relevant.

Theorem 3.1. Consider system (3.7) with pencil $s\mathbf{E} - \mathbf{A}$ and $\det(s\mathbf{E} - \mathbf{A}) \neq 0$. Let $\hat{\lambda}_i$, $i = 1, 2, \dots, \alpha$, be a finite eigenvalue of the pencil, where α is the number of Jordan blocks. Let also β_i be rank of the corresponding Jordan block, $\sum_{i=1}^{\alpha} \beta_i = \nu$, $\alpha \leq \nu$, and $\mathbf{v}_i^{[j]}$, $\mathbf{w}_i^{[j]}$, $j = 1, 2, \dots, \beta_i$, denote the j -th right, left, linear independent (generalized) eigenvectors corresponding to the eigenvalue $\hat{\lambda}_i$, respectively. Then [161]:

(a) The solution of (3.7) with initial condition $\mathbf{x}(0)$ can be written as follows:

$$\mathbf{x}(t) = \sum_{i=1}^{\alpha} e^{\hat{\lambda}_i t} \sum_{j=1}^{\beta_i} \left(\sum_{k=1}^j t^{k-1} \mathbf{w}_i^{[j-k+1]} \mathbf{E} \mathbf{x}(0) \right) \mathbf{v}_i^{[j]}. \quad (3.9)$$

(b) Let $x_k(t)$ be the k -th element of $\mathbf{x}(t)$. Then the participation of $\hat{\lambda}_i$ in $x_k(t)$, $k = 1, 2, \dots, r$, is given by:

$$\frac{\partial x_k(t)}{\partial e^{\hat{\lambda}_i t}} = \sum_{j=1}^{\beta_i} \left(\sum_{\sigma=1}^j t^{\sigma-1} \mathbf{w}_i^{[j-\sigma+1]} \mathbf{E} \mathbf{x}(0) \right) v_{k,i}^{[j]}, \quad (\text{Participation Factor}) \quad (3.10)$$

where $v_{k,i}^{[j]}$ is the k -th row element of the eigenvector $\mathbf{v}_i^{[j]}$.

The proof of Theorem 3.1 is given in Appendix A.

The following corollary is relevant.

Corollary 3.1. Consider system (3.7) with a regular pencil. Let the finite eigenvalues be either distinct, or with algebraic multiplicity equal to geometric, i.e. $\beta_i = 1$ is the rank of corresponding Jordan block. Then in Theorem 3.1, one has $\alpha = \nu$, $\mathbf{v}_i^{[j]} = \mathbf{v}_i$, and:

(a) The solution of (3.7) with initial condition $\mathbf{x}(0)$ is given by:

$$\mathbf{x}(t) = \sum_{i=1}^{\nu} \mathbf{w}_i \mathbf{E} \mathbf{x}(0) \mathbf{v}_i e^{\lambda_i t}.$$

(b) Let $x_k(t)$ be the k -th element of $\mathbf{x}(t)$. Then the participation of the i -th eigenvalue, $i = 1, 2, \dots, \nu$, in $x_k(t)$, $k = 1, 2, \dots, r$, is given by:

$$\frac{\partial x_k(t)}{\partial e^{\lambda_i t}} = \mathbf{w}_i \mathbf{E} \mathbf{x}(0) v_{k,i}, \quad (\text{Participation Factor}) \quad (3.11)$$

where $v_{k,i}$ is the k -th row element of the eigenvector \mathbf{v}_i .

The following remarks are relevant.

Remark 3.1. Since only the finite eigenvalues appear in (3.9), the participation matrix of system (3.7) has dimensions $r \times \alpha$. Determining the PFs associated with the infinite eigenvalue to obtain the full matrix is possible by applying a spectral transform to system (3.7). In particular, by applying $z = 1/s$ into (3.7), one arrives at the dual system $\mathbf{A} \dot{\hat{\mathbf{x}}} = \mathbf{E} \hat{\mathbf{x}}$. Let $x_k(t)$ be the k -th element of $\mathbf{x}(t)$, and $\hat{x}_k(t)$ be the k -th element of $\hat{\mathbf{x}}(t)$. Then the participation of the infinite eigenvalue of $s\mathbf{E} - \mathbf{A}$ in $x_k(t)$, $k = 1, 2, \dots, r$, is equal to the participation of the zero eigenvalue of $z\mathbf{A} - \mathbf{E}$ in $\hat{x}_k(t)$, $k = 1, 2, \dots, r$. This is a direct result from the duality between (3.7) and its dual system, or, additionally, between their pencils $s\mathbf{E} - \mathbf{A}$, and $z\mathbf{A} - \mathbf{E}$ respectively, see [100]. Note that this discussion, although interesting from a mathematical viewpoint, is not of practical interest in power system SSSA, since an infinite eigenvalue does not represent any particularly meaningful dynamics.

Remark 3.2. Applying appropriate initial conditions in (3.10), i.e. $x_k(0) = 1$, and $x_h(0) = 0$, $h \neq k$, and imposing $t \rightarrow 0$, allows obtaining the PFs in the classical sense [123]. Furthermore, as already discussed, algorithms that are suitable for large sparse matrices allow finding only a partial solution of the GEP, typically including the most critical dynamic modes of the system. This solution allows determining only the part of the participation matrix that is associated with the most critical modes. Therefore, by applying the above initial conditions, the (critical) participation matrix, i.e. the part of the participation matrix that is associated with the most critical eigenvalues of the system, can be expressed as:

$$\mathbf{\Pi}_{\text{PF},\kappa} = \mathbf{W}_{\kappa}^{\text{T}} \circ (\mathbf{E} \mathbf{V}_{\kappa}) , \quad (3.12)$$

where κ , $\kappa \leq \alpha$, be the number of the calculated finite eigenvalues and \mathbf{V}_{κ} , \mathbf{W}_{κ} are the corresponding right and left modal matrices.

3.3.2 Illustrative Example

As an illustrative example, consider system (3.7) with

$$\mathbf{E} = \begin{bmatrix} 12 & -3 & 0 & 0 & 0 \\ 4 & 1 & -1 & 3 & 0 \\ 0 & -4 & -5 & 1 & 0 \\ 8 & 2 & -5 & 9 & 0 \\ 0 & 0 & 0 & 0 & 0 \end{bmatrix}, \quad \mathbf{A} = \begin{bmatrix} -17 & 8 & -2 & 5 & 3 \\ -7 & -3 & 3 & -8 & 1 \\ 13 & 9 & 9 & 3 & 1 \\ -12 & -7 & 13 & -22 & 0 \\ 1 & 0 & 0 & 0 & 1 \end{bmatrix}.$$

The pencil $s\mathbf{E} - \mathbf{A}$ has $\alpha = 2$ finite eigenvalues $\hat{\lambda}_1 = -2$, $\hat{\lambda}_2 = -3$, of algebraic multiplicity $\nu_1 = 2$, $\nu_2 = 1$ and the infinite eigenvalue with multiplicity $\mu = 2$. The geometric multiplicity γ_i of the finite eigenvalue $\hat{\lambda}_i$ is found as the dimension of the null space of $\hat{\lambda}_i\mathbf{E} - \mathbf{A}$. In this example, $\gamma_1 = 1$, $\gamma_2 = 1$. The right and left eigenvectors of $s\mathbf{E} - \mathbf{A}$ associated with the finite eigenvalue $\hat{\lambda}_1 = -2$ are:

$$\mathbf{v}_1^{[1]} = \begin{bmatrix} 0 \\ -1 \\ -1 \\ 0 \\ 0 \end{bmatrix}, \quad \mathbf{v}_1^{[2]} = \begin{bmatrix} 0.0049 \\ -3.282 \cdot 10^7 \\ -3.282 \cdot 10^7 \\ 0 \\ 0.0049 \end{bmatrix}, \quad \mathbf{w}_1^{[1]} = \begin{bmatrix} -0.2308 \\ -0.3846 \\ 0.0769 \\ 0 \\ 1 \end{bmatrix}^T, \quad \mathbf{w}_1^{[2]} = \begin{bmatrix} -0.1426 \\ -0.2376 \\ 0.0475 \\ 0 \\ 0.6178 \end{bmatrix}^T,$$

where $\mathbf{v}_1^{[2]}$, $\mathbf{w}_1^{[2]}$ are generalized eigenvectors determined from $(\mathbf{A} - \hat{\lambda}_1\mathbf{E})\mathbf{v}_1^{[2]} = \mathbf{E}\mathbf{v}_1^{[1]}$ and $\mathbf{w}_1^{[2]}(\mathbf{A} - \hat{\lambda}_1\mathbf{E}) = \mathbf{w}_1^{[1]}\mathbf{E}$ respectively. The right and left eigenvectors of $s\mathbf{E} - \mathbf{A}$ associated with the finite eigenvalue $\hat{\lambda}_2 = -3$ are:

$$\mathbf{v}_2^{[1]} = \begin{bmatrix} 0 \\ 1 \\ -0.5 \\ 0 \\ 0 \end{bmatrix}, \quad \mathbf{w}_2^{[1]} = \begin{bmatrix} -0.3333 \\ 1 \\ 0.1111 \\ 0 \\ -0.1111 \end{bmatrix}^T.$$

The sensitivities $\frac{\partial \mathbf{x}_k(t)}{\partial e^{\hat{\lambda}_i t}}$ are obtained from Theorem 3.1 as follows:

$$\frac{\partial \mathbf{x}_k(t)}{\partial e^{\hat{\lambda}_i t}} = \sum_{j=1}^{\beta_i} \left(\sum_{k=1}^j t^{k-1} \mathbf{w}_i^{[j-(k-1)]} \mathbf{E} \mathbf{x}(0) \right) \mathbf{v}_{k,i}^{[j]}.$$

For $\hat{\lambda}_1$ and $\hat{\lambda}_2$ one has respectively:

$$\begin{aligned}\frac{\partial x_k(t)}{\partial e^{\hat{\lambda}_1 t}} &= \sum_{j=1}^2 \left(\sum_{k=1}^j t^{k-1} \mathbf{w}_1^{[j-(k-1)]} \mathbf{E} \mathbf{x}(0) \right) v_{k,1}^{[j]} \\ &= \mathbf{w}_1^{[1]} \mathbf{E} \mathbf{x}(0) v_{k,1}^{[1]} + \left(\sum_{k=1}^2 t^{k-1} \mathbf{w}_1^{[2-(k-1)]} \mathbf{E} \mathbf{x}(0) \right) v_{k,1}^{[2]} \\ &= \mathbf{w}_1^{[1]} \mathbf{E} \mathbf{x}(0) v_{k,1}^{[1]} + \mathbf{w}_1^{[2]} \mathbf{E} \mathbf{x}(0) v_{k,1}^{[2]} + t \mathbf{w}_1^{[1]} \mathbf{E} \mathbf{x}(0) v_{k,1}^{[2]},\end{aligned}$$

$$\frac{\partial x_k(t)}{\partial e^{\hat{\lambda}_2 t}} = \mathbf{w}_2^{[1]} \mathbf{E} \mathbf{x}(0) v_{k,2}^{[1]}.$$

Consider $x_k(0) = 1$, and $x_i(0) = 0$, $i \neq k$, which lead to the PFs related to the system finite modes. One has:

- For $\frac{\partial x_1(t)}{\partial e^{\hat{\lambda}_1 t}}$, one has $\mathbf{x}(0) = \begin{bmatrix} 1 & 0 & 0 & 0 & 0 \end{bmatrix}^T$. Hence,

$$\pi_{1,1} = 0.0130 + 0.0209t, \quad \pi_{1,2} = 0.$$

- For $\frac{\partial x_2(t)}{\partial e^{\hat{\lambda}_1 t}}$, one has $\mathbf{x}(0) = \begin{bmatrix} 0 & 1 & 0 & 0 & 0 \end{bmatrix}^T$. Hence,

$$\pi_{2,1} = 0.3290 + 1.0839t, \quad \pi_{2,2} = 0.6667.$$

- For $\frac{\partial x_3(t)}{\partial e^{\hat{\lambda}_1 t}}$, one has $\mathbf{x}(0) = \begin{bmatrix} 0 & 0 & 1 & 0 & 0 \end{bmatrix}^T$. Hence,

$$\pi_{3,1} = 0.6580 + 2.1678t, \quad \pi_{3,2} = 0.3333.$$

- For $\frac{\partial x_4(t)}{\partial e^{\hat{\lambda}_1 t}}$, one has $\mathbf{x}(0) = \begin{bmatrix} 0 & 0 & 0 & 1 & 0 \end{bmatrix}^T$. Hence,

$$\pi_{4,1} = 0, \quad \pi_{4,2} = 0.$$

- For $\frac{\partial x_5(t)}{\partial e^{\hat{\lambda}_1 t}}$, one has $\mathbf{x}(0) = \begin{bmatrix} 0 & 0 & 0 & 0 & 1 \end{bmatrix}^T$. Hence,

$$\pi_{5,1} = 0, \quad \pi_{5,2} = 0.$$

Results are summarized in Table 3.1, where $t \rightarrow 0$. Since \mathbf{E} , \mathbf{A} are 5×5 matrices and $\text{rank}(s\mathbf{E} - \mathbf{A}) = 3$, there exist $5 - 3 = 2$ variables the participation of which to the system finite eigenvalues is zero. These variables are x_4 and x_5 . Moreover, Table 3.1 shows that x_3 is dominant in $\hat{\lambda}_1$, while x_2 is dominant in $\hat{\lambda}_2$.

Table 3.1: Illustrative example: PFs associated to finite modes.

	$\hat{\lambda}_1$	$\hat{\lambda}_2$
x_1	0.0130	0
x_2	0.3290	0.6667
x_3	0.6580	0.3333
x_4	0	0
x_5	0	0

3.4 Participation Factors of Algebraic Variables

Consider the explicit DAE power system model (2.5) without inputs, i.e. $\mathbf{B}_a = \mathbf{0}_{(n+m),p}$. Let $z_k(t)$ be the k -th element of $\mathbf{z}(t)$. Then, the following cases are relevant:

- $k \leq n$, that is z_k is a state variable. Then, substitution of appropriate initial conditions (see Remark 3.2) gives $\mathbf{w}_i^{[1]} \mathbf{E}_a \mathbf{z}(0) = \mathbf{w}_{i,k}^{[1]}$. In the special case that the eigenvectors form a complete basis for the rational vector space of the matrix pencil, which means that all eigenvalues are either distinct or their algebraic multiplicity is equal with the geometric, one has $\nu_i = 1$, $\nu = n$, and thus $\mathbf{v}_{k,i}^{[1]} = \mathbf{v}_{k,i}$, $\mathbf{w}_{i,k}^{[1]} = \mathbf{w}_{i,k}$ in (3.13). Substitution in (3.10) gives:

$$\frac{\partial z_k(t)}{\partial e^{\lambda_i t}} = \mathbf{w}_i^{[1]} \mathbf{E}_a \mathbf{z}(0) \mathbf{v}_{k,i}^{[1]} = \mathbf{w}_{i,k}^{[1]} \mathbf{v}_{k,i}^{[1]} = \pi_{k,i}. \quad (3.13)$$

- $n < k \leq n + m$, i.e. z_k is an algebraic variable. Then $\mathbf{w}_i^{[1]} \mathbf{E}_a \mathbf{z}(0) = 0$. The m rightmost columns of \mathbf{E}_a which contain only zero elements, impose that the PFs of the algebraic variables in the system finite modes are found to be null. This is a consequence of the fact that the coefficients of the first derivatives of the algebraic variables are zero, which implies that the algebraic variables introduce only infinite eigenvalues to the system. Nevertheless, the algebraic variables constrain the system and, in this sense, do participate in the system finite modes.

It follows that, for this system, the critical participation matrix (3.12) takes the following form:

$$\mathbf{\Pi}_{\text{PF},\kappa} = \mathbf{W}_{\kappa}^{\text{T}} \circ (\mathbf{E} \mathbf{V}_{\kappa}) = \begin{bmatrix} \mathbf{\Pi}_{\text{PF},\mathbf{x}} \\ \mathbf{0}_{m,\kappa} \end{bmatrix}, \quad (3.14)$$

where $\mathbf{\Pi}_{\text{PF},\mathbf{X}} \subset \mathbf{\Pi}_{\text{PF}}$, $\mathbf{\Pi}_{\text{PF},\mathbf{X}} \in \mathbb{C}^{(n+m) \times \kappa}$. The matrix $\mathbf{\Pi}_{\text{PF},\mathbf{X}}$ contains all the information on the dynamics of interest and is the matrix that is utilized in the remainder of the chapter.

This section introduces an approach to measure the participation of algebraic variables in power system dynamic modes, based on the PFs of the system states [161]. These can be algebraic variables included in the DAE system model, or, in general, any algebraic output that is defined as a function of the states and algebraic variables of the DAE system.

Let the output vector \mathbf{w} , $\mathbf{w} \in \mathbb{R}^q$, be defined as:

$$\mathbf{w} = \mathbf{h}(\mathbf{x}, \mathbf{y}),$$

where \mathbf{h} ($\mathbf{h} : \mathbb{R}^{n+m} \rightarrow \mathbb{R}^q$) is a non-linear function of \mathbf{x} , \mathbf{y} . Then differentiation around $(\mathbf{x}_o, \mathbf{y}_o)$ yields:

$$\Delta \mathbf{w} = \mathbf{h}_x \Delta \mathbf{x} + \mathbf{h}_y \Delta \mathbf{y}. \quad (3.15)$$

Substitution of (2.8) to the last equation gives:

$$\Delta \mathbf{w} = \mathbf{C} \Delta \mathbf{x}, \quad (3.16)$$

where $\mathbf{C} = \mathbf{h}_x - \mathbf{h}_y \mathbf{g}_y^{-1} \mathbf{g}_x$, $\mathbf{C} \in \mathbb{R}^{q \times n}$, is the output matrix.

Let Δw_{ρ} be the ρ -th system output. Then, the following expression is a candidate as the PF of Δw_{ρ} in the mode λ_i :

$$\hat{\pi}_{\rho,i} = \frac{\partial \Delta w_{\rho}}{\partial e^{\lambda_i t}}. \quad (3.17)$$

From the state-space viewpoint, $\hat{\pi}_{\rho,i}$ expresses the residue (or the joint observability/controllability) of the i -th mode, when the input is, exactly as it holds for $\pi_{k,i}$, a perturbation in the differential equation that defines $\Delta \dot{\mathbf{x}}_k$. The output however is Δw_{ρ} , which can be, in principle, any function of the system state variables. The fact that the

perturbation that leads from (3.10) and (3.17) to the classical PFs is the same, is also the reason that $\hat{\pi}_{\varrho,i}$ is called PF.

Proposition 3.1. Let the PF $\hat{\pi}_{\varrho,i}$ be the ϱ -th row, i -th column element of the participation matrix $\hat{\mathbf{\Pi}}_{\text{PF},(\mathbf{w})}$. Then:

$$\hat{\mathbf{\Pi}}_{\text{PF},(\mathbf{w})} = \mathbf{C} \mathbf{\Pi}_{\text{PF},\mathbf{x}} . \quad (3.18)$$

Proof. Let $\mathbf{c}_{\varrho} = [c_{\varrho,1} \ \dots \ c_{\varrho,n}]$ be the ϱ -th row of \mathbf{C} . Then:

$$\Delta w_{\varrho} = \mathbf{c}_{\varrho} \Delta \mathbf{x} = c_{\varrho,1} \Delta x_1 + c_{\varrho,2} \Delta x_2 + \dots + c_{\varrho,n} \Delta x_n .$$

Partial differentiation over $e^{\lambda_i t}$ leads to:

$$\begin{aligned} \frac{\partial \Delta w_{\varrho}}{\partial e^{\lambda_i t}} &= c_{\varrho,1} \frac{\partial \Delta x_1}{\partial e^{\lambda_i t}} + c_{\varrho,2} \frac{\partial \Delta x_2}{\partial e^{\lambda_i t}} + \dots + c_{\varrho,n} \frac{\partial \Delta x_n}{\partial e^{\lambda_i t}} + \\ &\quad + \frac{\partial c_{\varrho,1}}{\partial e^{\lambda_i t}} \Delta x_1 + \frac{\partial c_{\varrho,2}}{\partial e^{\lambda_i t}} \Delta x_2 + \dots + \frac{\partial c_{\varrho,n}}{\partial e^{\lambda_i t}} \Delta x_n \\ &\Rightarrow \hat{\pi}_{\varrho,i} = c_{\varrho,1} \pi_{1,i} + c_{\varrho,2} \pi_{2,i} + \dots + c_{\varrho,n} \pi_{n,i} , \end{aligned}$$

where $\frac{\partial c_{\varrho,1}}{\partial e^{\lambda_i t}} = \frac{\partial c_{\varrho,2}}{\partial e^{\lambda_i t}} = \dots = \frac{\partial c_{\varrho,n}}{\partial e^{\lambda_i t}} = 0$, since the elements of \mathbf{C} do not depend on functions of t . By applying the same steps for all outputs and representing in matrix form, one arrives at (3.18). ■

The main feature of (3.18) is that it allows defining the participation matrix not only of the algebraic variables of the DAEs, but also of any defined output vector that is a function of the system state and algebraic variables. One has only to specify the gradients $\mathbf{h}_{\mathbf{x}}$ and $\mathbf{h}_{\mathbf{y}}$ at the operating point, and then calculate the output matrix \mathbf{C} . The proposed participation matrix $\hat{\mathbf{\Pi}}_{\text{PF},(\mathbf{w})}$ provides meaningful information for the system coupling that, to the best of the authors' knowledge, has not been exploited in the literature.

Remark 3.3. The following special cases for the participation matrix of (3.18) are relevant:

- (a) *State variables:* If $\mathbf{w} = \mathbf{x}$, the gradients in (3.15) become $\mathbf{h}_{\mathbf{x}} = \mathbf{I}_n$, $\mathbf{h}_{\mathbf{y}} = \mathbf{0}_{q,m}$. The output matrix is $\mathbf{C} = \mathbf{I}_n$ and hence the participation matrix of the system states

is, as expected:

$$\hat{\mathbf{\Pi}}_{\text{PF},(\mathbf{x})} = \mathbf{\Pi}_{\text{PF},\mathbf{x}} . \quad (3.19)$$

- (b) *Algebraic variables:* If $\mathbf{w} = \mathbf{y}$, the gradients in (3.15) become $\mathbf{h}_x = \mathbf{0}_{q,n}$, $\mathbf{h}_y = \mathbf{I}_m$. The output matrix is $\mathbf{C} = -\mathbf{g}_y^{-1} \mathbf{g}_x$. Thus:

$$\hat{\mathbf{\Pi}}_{\text{PF},(\mathbf{y})} = -\mathbf{g}_y^{-1} \mathbf{g}_x \mathbf{\Pi}_{\text{PF},\mathbf{x}} , \quad (3.20)$$

which is the participation matrix of the algebraic variables in system modes included in the DAE model.

- (c) *Rates of change of state variables:* If the output is defined as $\mathbf{w} = \dot{\mathbf{x}} = \mathbf{f}(\mathbf{x}, \mathbf{y})$, the gradients in (3.15) become $\mathbf{h}_x = \mathbf{f}_x$, $\mathbf{h}_y = \mathbf{f}_y$. The output matrix is $\mathbf{C} = \mathbf{A}$. Thus:

$$\hat{\mathbf{\Pi}}_{\text{PF},(\dot{\mathbf{x}})} = \mathbf{A} \mathbf{\Pi}_{\text{PF},\mathbf{x}} . \quad (3.21)$$

The ROCoF of the synchronous machines ($\dot{\omega}_r$) is a relevant case.

- (d) *Parameters:* Finally, consider the scalar output $w = \eta$, where η is a parameter. If η appears only in the j -th algebraic equation $0 = g^j(\mathbf{x}, \mathbf{y}, \eta)$, then the linearization of the j -th algebraic equation around the operating point yields:

$$0 = \mathbf{g}_x^j \Delta \mathbf{x} + \mathbf{g}_y^j \Delta \mathbf{y} + g_\eta^j \Delta \eta , \quad (3.22)$$

where $\mathbf{g}_x^j \in \mathbb{R}^{1 \times n}$, $\mathbf{g}_y^j \in \mathbb{R}^{1 \times m}$ and $g_\eta^j \in \mathbb{R}_{\neq 0}$. Solving (3.22) for $\Delta \eta$ and comparing with (3.15), $\mathbf{h}_x = -\mathbf{g}_x^j / g_\eta^j$ and $\mathbf{h}_y = -\mathbf{g}_y^j / g_\eta^j$. The participation vector is obtained from (3.18) for $\mathbf{C} = (-\mathbf{g}_x^j + \mathbf{g}_y^j \mathbf{g}_y^{-1} \mathbf{g}_x) / g_\eta^j$.

Note, finally, that once the eigenvalue analysis is completed and the modal matrices are known, calculating the proposed participation matrices involves few matrix multiplications. From the computational burden viewpoint, the cost of calculating the PFs is marginal compared to the eigenvalue analysis.

3.5 Case Studies

This case study presents two practical applications of the proposed approach and shows how defining PFs of algebraic variables in system modes can help design more effective and robust controllers. In particular, Section 3.5.1 is based on the well-known two-area system [74] and shows how the calculation of PFs can help select the most effective algebraic variable to be measured to damp inter-area oscillations. Section 3.5.2 utilizes a realistic detailed model of the AIITS and shows how PFs can help define the impact of a given system mode on the network. This second case study also serves to discuss the robustness and the scalability of the proposed approach. Simulations of this section are carried using Dome [93].

3.5.1 Two-Area System

The two-area system is depicted in Figure 3.1. It comprises two areas connected through a relatively weak tie; eleven buses and four synchronous machines. Each generator is equipped with an AVR of type IEEE DC-1 and a TG. The system feeds two loads connected to buses 7 and 9 and which are modeled as constant active and reactive power consumption.

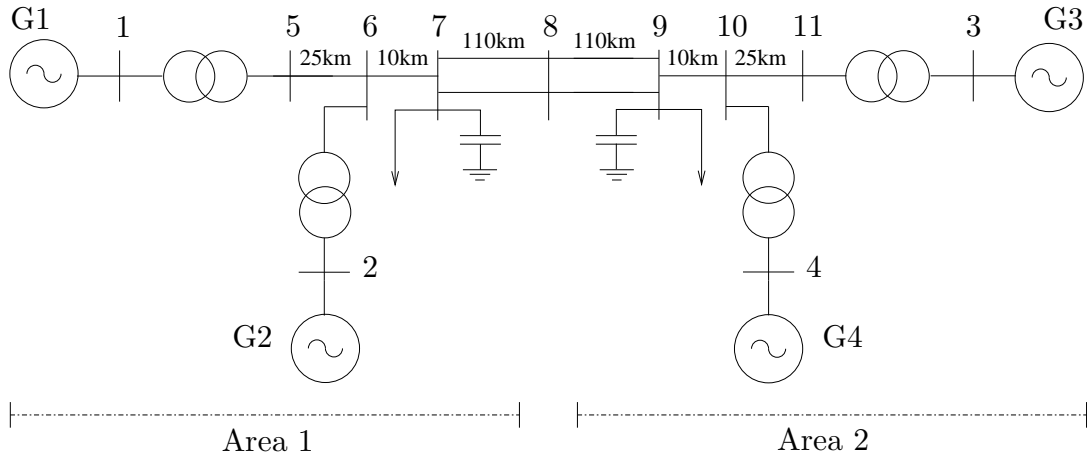


Figure 3.1: Two-area four-machine system: single-line diagram.

The system model has 52 state variables. For a system with this dynamic order, the dense state matrix \mathbf{A}_s can be efficiently calculated and handled. The most critical modes and the mostly participating states to these modes are presented in Table 3.2. Area 1 presents a critical local mode $-0.599 \pm j6.604$ with natural frequency 1.06 Hz and

dominant state the rotor speed $\omega_{r,2}$. Area 2 presents a critical local mode as well, which is $-0.514 \pm j6.843$ with natural frequency 1.09 Hz and dominant state the rotor speed $\omega_{r,4}$. For these modes, the damping ratio is $> 5\%$. Finally, the most lightly damped mode is $-0.096 \pm j3.581$, which is an inter-area mode with natural frequency 0.57 Hz. The mostly participating state in the inter-area mode is the rotor speed $\omega_{r,3}$.

Table 3.2: Two-area system: critical modes.

Mode	f_n (Hz)	ζ (%)	x -dom.	$ \pi _{\max}$
$-0.096 \pm j3.581$	0.57	2.67	$\omega_{r,3}$	0.1696
$-0.514 \pm j6.843$	1.09	7.50	$\omega_{r,4}$	0.2945
$-0.599 \pm j6.604$	1.06	9.04	$\omega_{r,2}$	0.2530

The participation matrix of the algebraic variables for these modes is calculated from (3.20). Note that in this section, each $\hat{\pi}_{g,i}$ is divided over the Euclidean norm of the respective output \mathbf{c}_g , so that the results are normalized and comparable according to the geometric approach. Of course, since the PFs are a relative measure, one may apply any further normalization, e.g. the maximum or the sum of the values to be equal to 1.

The following simple test shows how the proposed PFs of the algebraic variables are linked to their sensitivities in eigenvalue changes. Imposing a perturbation in the active power and voltage of the PV buses 1, 4, changes the most critical mode $-0.096 \pm j3.581$ by $|d\lambda| = 3 \cdot 10^{-5}$. The calculated eigen-sensitivities $|d\Delta y_k|/|d\lambda|$ are then compared with the PFs of the algebraic variables P_1 , P_4 , v_1 , v_4 , in Table 3.3. As expected, a highly participating variable in a mode indicates that this mode is sensitive to small variations of this variable.

Table 3.3: Sensitivity test for the inter-area mode, $|d\lambda| = 3 \cdot 10^{-5}$.

y_k (pu)	$ \hat{\pi}_{k,i} $	$ d\Delta y_k $ (pu)	$ d\Delta y_k / d\lambda $
$P_1 = 5.88$	0.3642	$0.43 \cdot 10^{-3}$	14.42
$P_4 = 7.00$	0.9766	$0.54 \cdot 10^{-3}$	18.00
$v_1 = 1.03$	0.0036	$0.27 \cdot 10^{-4}$	0.90
$v_4 = 1.01$	0.0028	$0.11 \cdot 10^{-4}$	0.35

For illustration, consider now the simple example of finding the participation vector of one system parameter. Let P_7 be the active power consumption of the load connected to bus 7. Since P_7 is also the active power injection at bus 7, the following algebraic

equation (see Figure 3.1) holds:

$$\begin{aligned}
0 &= v_7 v_6 (G_{76} \cos(\theta_7 - \theta_6) + B_{76} \sin(\theta_7 - \theta_6)) \\
&+ v_7 v_8 (G_{78} \cos(\theta_7 - \theta_8) + B_{78} \sin(\theta_7 - \theta_8)) - P_7 \\
&= g(v_6, v_7, v_8, \theta_6, \theta_7, \theta_8, P_7) .
\end{aligned}$$

Linearization and solving for ΔP_7 yields:

$$\Delta P_7 = \left(\frac{\partial g}{\partial v_6} \Delta v_6 + \frac{\partial g}{\partial v_7} \Delta v_7 + \frac{\partial g}{\partial v_8} \Delta v_8 + \frac{\partial g}{\partial \theta_6} \Delta \theta_6 + \frac{\partial g}{\partial \theta_7} \Delta \theta_7 + \frac{\partial g}{\partial \theta_8} \Delta \theta_8 \right) ,$$

where, the gradients are calculated at $(v_{6,o}, v_{7,o}, v_{8,o}, \theta_{6,o}, \theta_{7,o}, \theta_{8,o})$; and $\partial g / \partial P_7 = -1$. Therefore, $\mathbf{h}_x = \mathbf{0}_{q,n}$, and \mathbf{h}_y is the $1 \times m$ row vector which contains the gradients calculated above in the indices of $v_6, v_7, v_8, \theta_6, \theta_7, \theta_8$; all other elements of \mathbf{h}_y are zero. The output matrix \mathbf{C} is $\mathbf{C} = -\mathbf{h}_y \mathbf{g}_y^{-1} \mathbf{g}_x$, $\mathbf{C} \in \mathbb{R}^{1 \times n}$. The resulting participation matrix is given by (3.18).

Table 3.4: Two-area system: PFs.

Mode	$-0.096 \pm j3.581$		$-0.514 \pm j6.843$		$-0.599 \pm j6.604$	
Output	Dom.	$ \hat{\pi} $	Dom.	$ \hat{\pi} $	Dom.	$ \hat{\pi} $
\mathbf{v}_B	v_{11}	0.0192	v_8	0.0375	v_7	0.0345
$\boldsymbol{\theta}_B$	θ_8	0.1429	θ_4	0.2385	θ_6	0.2250
$\boldsymbol{\omega}_B$	ω_8	0.2065	ω_{10}	0.3247	ω_6	0.3113
\mathbf{P}_B	P_6	0.1447	P_{10}	0.2518	P_6	0.2719
\mathbf{Q}_B	Q_{11}	0.0258	Q_8	0.0544	Q_{10}	0.0631
$\dot{\boldsymbol{\omega}}_r$	$\dot{\omega}_{r,4}$	0.0401	$\dot{\omega}'_{r,4}$	0.0917	$\dot{\omega}_{r,2}$	0.0539
$\boldsymbol{\omega}_{CoI}$	$\omega_{CoI,2}$	0.1700	$\omega_{CoI,2}$	0.3151	$\omega_{CoI,1}$	0.3137

The active (\mathbf{P}_B) and reactive (\mathbf{Q}_B) power injections on all system buses, as well as the COI speeds ($\boldsymbol{\omega}_{CoI}$) of the two areas are defined as outputs and their PFs are obtained from (3.18). Correspondingly, the system bus voltages (\mathbf{v}_B), angles ($\boldsymbol{\theta}_B$) and frequencies ($\boldsymbol{\omega}_B$) are included in the algebraic variables of the DAEs. Thus, their PFs are determined from (3.20). With this aim, ideal frequency estimations of the system buses are obtained by employing the frequency divider formula, proposed in [99]. The formulation of the frequency divider in per units is as follows:

$$\mathbf{B}_{BB} \Delta \boldsymbol{\omega}_B = -\mathbf{B}_{BG} \Delta \boldsymbol{\omega}_r ,$$

where $\Delta\omega_B$ are the estimated bus frequency deviations with respect to the reference synchronous speed; $\Delta\omega_r$ are the synchronous machines rotor speed deviations; and \mathbf{B}_{BB} , \mathbf{B}_{BG} are system susceptance matrices that include the internal reactances of the synchronous machines. The accuracy, the numerical robustness and the computational efficiency of the frequency divider have been discussed in [99, 115, 164].

The PFs of the RoCoF of the synchronous machines ($\dot{\omega}_r$) are determined from (3.21). The mostly participating of the above variables in the system critical modes are summarized in Table 3.4. It is worth observing that the bus voltages, the reactive power injections and the RoCoF have a low participation in the system critical modes. Mostly participating in the inter-area mode is the bus frequency ω_8 . Similarly, the bus frequency ω_{10} is the one mostly participating in the local mode of Area 2. Finally, the CoI speed of Area 1 ($\omega_{CoI,1}$) is the one mostly participating in $-0.599 \pm j6.604$, which is a local mode of this area.

Finally, the calculated PFs can be utilized to improve the dynamic behavior of the system. As already discussed, the critical mode of the system is the inter-area mode and the mostly participating variable (Table 3.4) is the bus frequency ω_8 . A Static Var Compensator (SVC) is installed at bus 8 with a POD loop [1]. The POD input signal is ω_8 . The POD output is considered as an additional input to the SVC voltage reference algebraic equation. The results are summarized in Table 3.5. The eigenvalue analysis shows that, after the inclusion of the controller, the system is stable and all modes are properly damped.

Table 3.5: Impact of SVC-POD installation in the critical mode.

SVC-POD	Mode	ζ (%)
No	$-0.096 \pm j3.581$	2.67
Yes	$-0.256 \pm j3.562$	7.16

3.5.2 All-Island Irish Transmission System

This section considers the real-world model of the AIITS which has been also discussed in Section 2.6.1. The dynamic order of the system is 1,480. Eigenvalue analysis shows that the system is stable when subject to small disturbances. The system presents both local machine modes and inter-machine modes. Recall that, a local machine mode refers to a single machine oscillating against the rest of the system. On the other hand, an

Table 3.6: AIITS: examined modes.

Mode Name	Mode 1		Mode 2	
Eigenvalue	$-0.586 \pm j7.248$		$-0.722 \pm j4.618$	
f_n (Hz)	1.16		0.74	
ζ (%)	8.06		15.44	
Type	Local		Inter-machine	
Dominant States	State	$ \pi _{\max}$	State	$ \pi _{\max}$
1-st	$\delta_{r,16}$	0.4456	$\omega_{r,2}$	0.2883
2-nd	$\omega_{r,16}$	0.4456	$\delta_{r,2}$	0.2872

inter-machine mode refers to a group of machines of the same area oscillating against each other [74]. The remainder of this section shows two modes with different damping ratios and natural frequencies. The examined modes are summarized in Table 3.6.

Mode 1 has eigenvalue $-0.586 \pm j7.248$, with natural frequency 1.16 Hz and damping ratio 8.06%. The dominant states in this mode are the rotor angle and speed of synchronous generator 16. The PFs of these states sum to 0.8912. The mode is local with generator 16 oscillating against the rest of the system. Mode 2 has eigenvalue $-0.722 \pm j4.618$, with frequency 0.74 Hz and damping ratio 15.44 %. The mostly participating states are the rotor speed and angle of synchronous generator 2. The corresponding PFs sum to 0.5755. The natural frequency and the distribution of the PFs indicate that this is an inter-machine mode [74].

The Python module *graph-tool* [122] is utilized to generate a graph of the studied network. The resulting graph has 1,479 vertices, which correspond to the system buses and 1,851 edges, which correspond to lines and transformers. Note that the coordinates of the graph vertices and edges do not represent the actual geography of the system. The participation matrices of the bus active power injections are calculated for the examined modes. Then, the sizes and the colors of the graph vertices are adjusted with respect to the magnitude of the calculated PFs.

The generated graph with the PFs of all bus active power injections in the local Mode 1 is illustrated in Figure 3.2. The mostly participating active power injection is the one of the bus 552, that is adjacent to generator 16, with $|\hat{\pi}|_{\max} = 0.3218$. The PFs of all bus active power injections in the inter-machine Mode 2 is illustrated in Figure 3.3. The mostly participating active power injection is the one of the bus 1,405, that is close to synchronous generator 2, with $|\hat{\pi}|_{\max} = 0.2508$. Figure 3.3 shows that the lower frequency

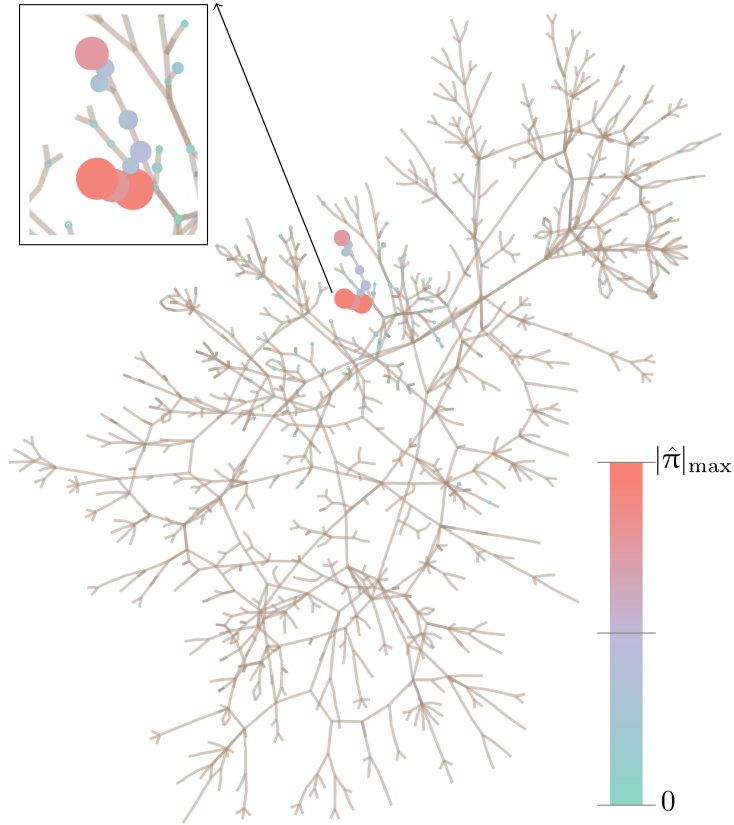


Figure 3.2: AIITS: participation of bus active power injections to Mode 1.

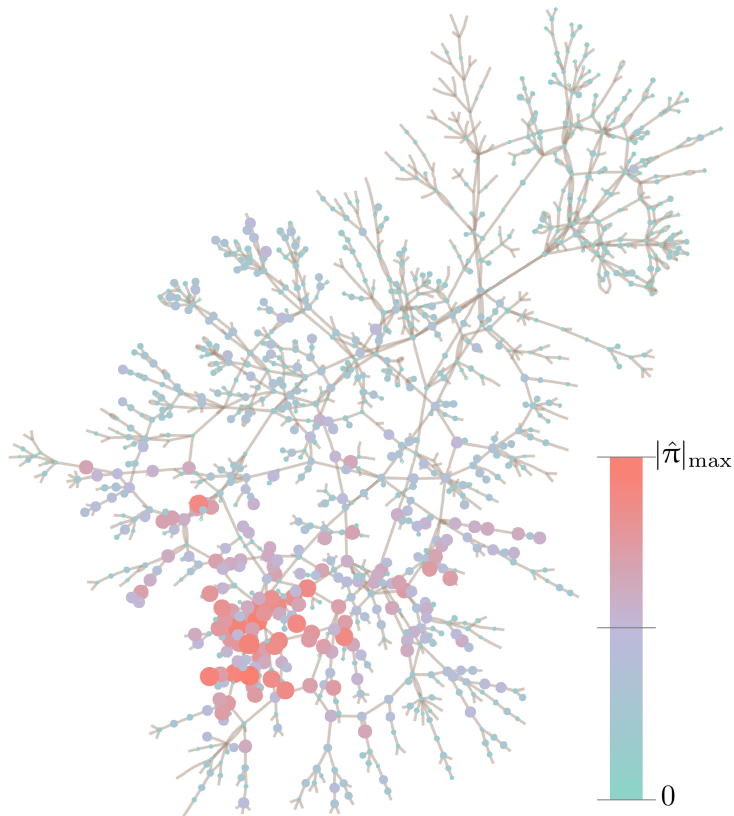


Figure 3.3: AIITS: participation of bus active power injections to Mode 2.

oscillations spread over the power system. In fact, there are several buses in a large area that have a high participation to the inter-machine mode.

3.6 Conclusions

The chapter proposes a systematic analytical approach to quantify the participation of the algebraic variables of a power system model, and to general of any function of the system variables in the system modes, through the definition of output vectors of the system's state-space formulation. The proposed approach, which describes an alternative interpretation of the PFs as eigen-sensitivities, provides a high flexibility, since it allows determining PFs of states, algebraic variables, rates of change of system variables, as well as of system parameters.

Regarding the computational burden of the participation analysis, once the eigenvalue analysis is completed, the cost of calculating the proposed PFs is negligible. Moreover, the proposed approach allows exploiting the sparsity of the GEP matrix pencil and can lead to a significant speedup, provided that a proper eigenvalue solver is employed.

Chapter 4

Fractional Order Control

4.1 Introduction

Fractional calculus is the analysis of non-integer order differentials and integrals. Although the first discussion on derivatives with non-integer order dates back to Leibniz [81], major studies on fractional calculus started with Liouville [85]. The application of fractional calculus in control was introduced with the definition of the ideal cut-off characteristic by Bode [19] and the first systematic study of the frequency response of FOCs was done by Oustaloup [116]. In [125, 126], Podlubny provided a comprehensive analysis of fractional systems with applications to automatic control, and proposed the use of the Fractional-Order Proportional Integral Derivative (FOPID) controller. The FOPID controller is an extension of the classical PID, and is characterized by five parameters: three gains, namely proportional, integral, and derivative; and two fractional orders, namely integral (α) and derivative (β). Employing a FOPID extends the four control points of the PID strategy to the plane defined by the fractional orders α and β [105]. This is illustrated in Figure 4.1. FOCs have been applied to various engineering fields, e.g. heat diffusion [62] and robotic time-delay systems [78]. Recent efforts on FOCs have tackled several issues, such as modeling and studying the impact of control limiters, see [121], and variable-order fractional orders, see [27]. Finally, it is relevant to mention here that fractional calculus is a promising tool for applications not only in control systems, but in many other applications, for example physics [57] and biology [60].

The potential of FOCs for power system applications has not been discussed until very recently. Applications include automatic voltage regulation of synchronous machines

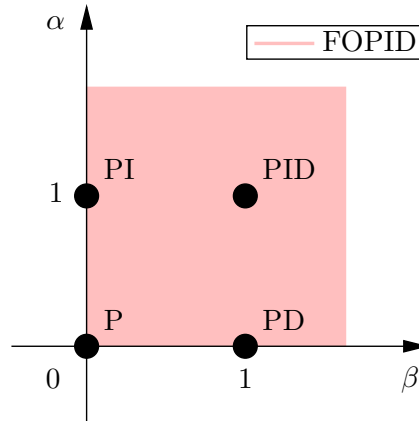


Figure 4.1: PID vs FOPID: from point to plane.

[120,156,183]; load frequency control [139,154]; damping control [24]; and voltage control of distributed energy resource systems [36]. These works mainly focus on the tuning of FOPID controllers through heuristic algorithms, such as particle swarm [183], chaotic multi-objective [120], and imperialist competitive algorithm [154]. Analytical methods employ frequency response criteria such as the desired gain crossover frequency [139].

From a practical and simulation point of view, fractional dynamics are typically approximated using appropriate rational order transfer functions. Although various techniques have been proposed to define such transfer functions [175], the most commonly utilized continuous method is the ORA [117]. Therefore, the ORA is the method considered in this chapter. The works cited above focus on applications and rely, for the implementation of FOCs, on proprietary software tools which are utilized as a *black-box*. This approach is indeed fostered by the availability of several software tools for the design and simulation of FOCs, see, for example, the Matlab toolboxes CRONE [118], Ninteger [172], and FOMCON [158].

The main goal of this chapter is to provide a systematic study of FOCs for power system applications. The remainder of the chapter is organized as follows. Section 4.2 outlines the theory of fractional calculus. Section 4.3 discusses the stability of power systems with inclusion of FOCs. Section 4.4 focuses on the modeling, computer implementation and tuning of ORA-based FOCs. Two case studies are presented in Sections 4.5.1 and 4.5.2. Finally, conclusions are drawn in Section 4.6.

4.2 Essentials of Fractional Calculus

Fractional calculus is the analysis of non-integer order differentials and integrals. That is, it deals with the problem of extending the differentiation and integration operators $\frac{d^n}{dt^n}$, $\int_0^t d^n(\tau)$, $n \in \mathbb{N}$, for real (or complex) number powers. There exist several approaches that address this problem. A precise formulation is given by the Riemann-Liouville (RL) definition. Consider a function $\phi : [0, \infty) \rightarrow \mathbb{R}$. The idea behind the RL definition is to first consider the n -fold integration of $\phi(t)$ and then extend $n \in \mathbb{N}$ to any $\gamma \in \mathbb{R}^+$. In its derivative form, the RL definition reads [105]:

$$\phi^{(\gamma)}(t) = \frac{1}{\Gamma(\mu - \gamma)} \frac{d^\mu}{dt^\mu} \left(\int_0^t \frac{\phi(\tau)}{(t - \tau)^{\gamma - \mu + 1}} d\tau \right), \quad (4.1)$$

where γ , $\mu - 1 < \gamma < \mu$, $\mu \in \mathbb{N}$, is the fractional order; and $\phi^{(\gamma)}(t) = d^\gamma \phi / dt^\gamma$. The Laplace transform of (4.1) is:

$$\mathcal{L}\{\phi^{(\gamma)}(t)\} = s^\gamma \Phi(s) - \sum_{j=0}^{\mu-1} s^j \phi^{(\gamma-j-1)}(0), \quad (4.2)$$

where $s \in \mathbb{C}$ and $\mathcal{L}\{\phi(t)\} = \Phi(s)$. Equation (4.2) requires the knowledge of the fractional order initial conditions $\phi^{(\gamma-j-1)}(0)$, $j = 0, 1, \dots, \mu - 1$. This raises an issue for engineering systems since, currently, only integer order initial conditions are well understood and known for physical variables. Other properties of the RL definition are also counter-intuitive in the sense of classical differentiation. For example, the RL derivative of a constant function is typically unbounded at $t = 0$ [126].

With the aim of meeting the requirements of known physical variables and systems, (4.1) was revisited by Caputo [23]. Caputo's definition of $\phi^{(\gamma)}(t)$ reads:

$$\phi^{(\gamma)}(t) = \frac{1}{\Gamma(\mu - \gamma)} \int_0^t \frac{\phi^{(\mu)}(\tau)}{(t - \tau)^{\gamma - \mu + 1}} d\tau. \quad (4.3)$$

The Laplace transform of (4.3) is:

$$\mathcal{L}\{\phi^{(\gamma)}(t)\} = s^\gamma \Phi(s) - \sum_{j=0}^{\mu-1} s^{\gamma-j-1} \phi^{(j)}(0). \quad (4.4)$$

Equation (4.4) requires the knowledge of the initial conditions $\phi^{(j)}(0)$, $j = 0, 1, \dots, \mu - 1$, which in this case are of integer order. This property is crucial for the solution of initial value problems. In fact, for the purpose of fractional control, that is of concern here, one needs to use a definition with integer order initial conditions. This work utilizes the Caputo definition of fractional derivative given in (4.3), which is more consistent for control applications and follows the properties of differentiation in the classical sense. For example, the Caputo fractional derivative of a constant function is zero.

In the special case that $0 < \gamma < 1$, the Caputo definition (4.3) reduces to [20]:

$$\phi^{(\gamma)}(t) = \frac{1}{\Gamma(1 - \gamma)} \int_0^t \frac{\dot{\phi}(\tau)}{(t - \tau)^\gamma} d\tau. \quad (4.5)$$

There are several other definitions of fractional derivatives/integrals and choosing the appropriate one depends on the application. For example, the Grünwald-Letnikov's derivative is relevant for the numerical solution of fractional differential equations. It is important to emphasize that the theory of fractional calculus applicable to the stability analysis and control of physical dynamical systems is an active research topic and yet to be fully understood. Recent efforts have addressed issues related to Caputo's formulation, for example its singular kernel for $t = \tau$ [12, 23]. Finally, note that fractional-order operators are not a straightforward generalization of the classical integer-order operators and, despite the several advances and interesting recent studies, see e.g. [20, 29, 35, 63, 84, 89, 142, 152, 178], the existing theory of fractional differential equations is far from complete.

4.3 Power System with Fractional Order Control

This chapter focuses on the modeling and stability of power systems with inclusion of FOCs. Since a general theory of the stability of non-linear fractional differential equations is not available, we proceed as follows [162]. This section considers the conditions for the stability of a linear (or linearized) singular power system model with inclusion of a FOC. These conditions help design the FOCs discussed in Section 4.4. However, power system models are non-linear. For this reason, the design of FOCs is checked by solving numerical time domain simulations of the fully-fledged non-linear model of the system and its controllers in the case studies presented in Section 4.5.

4.3.1 Modeling

Consider the DAE linearized power system model (2.4), which is repeated here for clarity:

$$\mathbf{E}_a \dot{\mathbf{z}} = \mathbf{A}_a \mathbf{z} + \mathbf{B}_a \Delta \mathbf{u}, \quad (4.6)$$

where $l = n + m$ and $\mathbf{E}_a, \mathbf{A}_a \in \mathbb{R}^{l \times l}$, $\mathbf{B}_a \in \mathbb{R}^{l \times p}$.

Let the vector of the system output measurements \mathbf{w} , $\mathbf{w} \in \mathbb{R}^q$, be:

$$\mathbf{w} = \mathbf{C}_a \mathbf{z} + \mathbf{D}_a \Delta \mathbf{u}, \quad (4.7)$$

where $\mathbf{C}_a \in \mathbb{R}^{q \times l}$, $\mathbf{D}_a \in \mathbb{R}^{q \times p}$. Then, a multiple-input, multiple-output FOC for the system (4.6)-(4.7), can be described by a set of fractional DAEs as follows:

$$\begin{aligned} \mathbf{E}_{c,1} \dot{\mathbf{x}}_c + \mathbf{E}_{c,\gamma} \mathbf{x}_c^{(\gamma)} &= \mathbf{A}_c \mathbf{x}_c + \mathbf{B}_c \mathbf{w}, \\ \mathbf{0}_{p,1} &= \mathbf{C}_c \mathbf{x}_c + \mathbf{D}_c \mathbf{w} - \Delta \mathbf{u}, \end{aligned} \quad (4.8)$$

where γ is the controller's fractional order; $\mathbf{x}_c, \mathbf{x}_c \in \mathbb{R}^s$, is the vector of the controller states; $\mathbf{E}_{c,1}, \mathbf{E}_{c,\gamma}, \mathbf{A}_c \in \mathbb{R}^{s \times s}$, $\mathbf{B}_c \in \mathbb{R}^{s \times q}$, $\mathbf{C}_c \in \mathbb{R}^{p \times s}$, $\mathbf{D}_c \in \mathbb{R}^{p \times q}$. It is relevant to mention that there are FOCs that introduce multiple, distinct fractional orders. Combining (4.6), (4.7) and (4.8) yields the closed-loop system representation. In matrix form:

$$\begin{aligned} \begin{bmatrix} \mathbf{E} & \mathbf{0}_{l,s} & \mathbf{0}_{l,p} \\ \mathbf{0}_{s,l} & \mathbf{E}_{c,1} & \mathbf{0}_{s,p} \\ \mathbf{0}_{p,l} & \mathbf{0}_{p,s} & \mathbf{0}_{p,p} \end{bmatrix} \begin{bmatrix} \dot{\mathbf{z}} \\ \dot{\mathbf{x}}_c \\ \Delta \dot{\mathbf{u}} \end{bmatrix} + \begin{bmatrix} \mathbf{0}_{l,l} & \mathbf{0}_{l,s} & \mathbf{0}_{l,p} \\ \mathbf{0}_{s,l} & \mathbf{E}_{c,\gamma} & \mathbf{0}_{s,p} \\ \mathbf{0}_{p,l} & \mathbf{0}_{p,s} & \mathbf{0}_{p,p} \end{bmatrix} \begin{bmatrix} \mathbf{z}^{(\gamma)} \\ \mathbf{x}_c^{(\gamma)} \\ \Delta \mathbf{u}^{(\gamma)} \end{bmatrix} \\ = \begin{bmatrix} \mathbf{A} & \mathbf{0}_{l,s} & \mathbf{B} \\ \mathbf{B}_c \mathbf{C} & \mathbf{A}_c & \mathbf{B}_c \mathbf{D} \\ \mathbf{D}_c \mathbf{C} & \mathbf{C}_c & \mathbf{D}_c \mathbf{D} - \mathbf{I}_p \end{bmatrix} \begin{bmatrix} \mathbf{z} \\ \mathbf{x}_c \\ \Delta \mathbf{u} \end{bmatrix}, \end{aligned}$$

or equivalently,

$$\mathbf{M} \dot{\boldsymbol{\psi}} + \mathbf{M}_\gamma \boldsymbol{\psi}^{(\gamma)} = \mathbf{A}_{cl} \boldsymbol{\psi}, \quad (4.9)$$

where

$$M = \begin{bmatrix} \mathbf{E} & \mathbf{0}_{l,\varsigma} & \mathbf{0}_{l,p} \\ \mathbf{0}_{\varsigma,l} & \mathbf{E}_{c,1} & \mathbf{0}_{\varsigma,p} \\ \mathbf{0}_{p,l} & \mathbf{0}_{p,\varsigma} & \mathbf{0}_{p,p} \end{bmatrix}, \quad M_\gamma = \begin{bmatrix} \mathbf{0}_{l,l} & \mathbf{0}_{l,\varsigma} & \mathbf{0}_{l,p} \\ \mathbf{0}_{\varsigma,l} & \mathbf{E}_{c,\gamma} & \mathbf{0}_{\varsigma,p} \\ \mathbf{0}_{p,l} & \mathbf{0}_{p,\varsigma} & \mathbf{0}_{p,p} \end{bmatrix},$$

$$\mathbf{A}_{\text{cl}} = \begin{bmatrix} \mathbf{A} & \mathbf{0}_{l,\varsigma} & \mathbf{B} \\ \mathbf{B}_c \mathbf{C} & \mathbf{A}_c & \mathbf{B}_c \mathbf{D} \\ \mathbf{D}_c \mathbf{C} & \mathbf{C}_c & \mathbf{D}_c \mathbf{D} - \mathbf{I}_p \end{bmatrix}, \quad \boldsymbol{\psi} = \begin{bmatrix} \mathbf{z} \\ \mathbf{x}_c \\ \Delta \mathbf{u} \end{bmatrix},$$

with $M, M_\gamma, \mathbf{A}_{\text{cl}} \in \mathbb{R}^{\rho \times \rho}$, and $\rho = l + \varsigma + p$.

4.3.2 Stability

This section studies the stability of the closed-loop system (4.9), which is a singular system of differential equations having both first, and fractional order derivatives. With this aim, the following property of the Caputo fractional derivative is relevant [84]:

Proposition 4.1. Let $\boldsymbol{\phi}(t), \boldsymbol{\phi}(t) \in \mathcal{C}^1[0, T]^n$ for some $T > 0$, where \mathcal{C}^1 denotes the set of continuously differentiable functions. Then:

$$[\boldsymbol{\phi}^{(a)}(t)]^{(b)} = [\boldsymbol{\phi}^{(b)}(t)]^{(a)} = \boldsymbol{\phi}^{(a+b)}(t), \quad (4.10)$$

where $a, b \in \mathbb{R}^+$, and $a + b \leq 1$. Note that (4.10) does not hold for the RL derivative.

Equation (4.9) can be rewritten as:

$$\mathbf{M} \boldsymbol{\psi}^{(\gamma+\beta)} + \mathbf{M}_\gamma \boldsymbol{\psi}^{(\gamma)} = \mathbf{A}_{\text{cl}} \boldsymbol{\psi}, \quad (4.11)$$

where $\gamma + \beta = 1$.

Adopting the notation

$$\mathbf{x}_1 = \boldsymbol{\psi}, \quad \mathbf{x}_2 = \boldsymbol{\psi}^{(\gamma)},$$

one obtains $\mathbf{x}_1^{(\gamma)} = \boldsymbol{\psi}^{(\gamma)} = \mathbf{x}_2$. Making use of (4.10) yields $\mathbf{x}_2^{(\beta)} = \boldsymbol{\psi}^{(\gamma+\beta)}$. Substitution to (4.11) gives:

$$\begin{aligned} \mathbf{M} \mathbf{x}_2^{(\beta)} + \mathbf{M}_\gamma \mathbf{x}_2 &= \mathbf{A}_{\text{cl}} \mathbf{x}_1 \Rightarrow \\ \mathbf{M} \mathbf{x}_2^{(\beta)} &= \mathbf{A}_{\text{cl}} \mathbf{x}_1 - \mathbf{M}_\gamma \mathbf{x}_2 . \end{aligned} \quad (4.12)$$

Equivalently:

$$\begin{bmatrix} \mathbf{I}_\rho & \mathbf{0}_{\rho,\rho} \\ \mathbf{0}_{\rho,\rho} & \mathbf{M} \end{bmatrix} \begin{bmatrix} \mathbf{x}_1^{(\gamma)} \\ \mathbf{x}_2^{(\beta)} \end{bmatrix} = \begin{bmatrix} \mathbf{0}_{\rho,\rho} & \mathbf{I}_\rho \\ \mathbf{A}_{\text{cl}} & -\mathbf{M}_\gamma \end{bmatrix} \begin{bmatrix} \mathbf{x}_1 \\ \mathbf{x}_2 \end{bmatrix} . \quad (4.13)$$

System (4.13) can be rewritten as:

$$\tilde{\mathbf{E}} \mathbf{x}^\Delta = \tilde{\mathbf{A}} \mathbf{x} , \quad (4.14)$$

or, by recovering the time dependency, as:

$$\tilde{\mathbf{E}} \mathbf{x}^\Delta(t) = \tilde{\mathbf{A}} \mathbf{x}(t) , \quad (4.15)$$

where

$$\tilde{\mathbf{E}} = \begin{bmatrix} \mathbf{I}_\rho & \mathbf{0}_{\rho,\rho} \\ \mathbf{0}_{\rho,\rho} & \mathbf{M} \end{bmatrix} , \quad \tilde{\mathbf{A}} = \begin{bmatrix} \mathbf{0}_{\rho,\rho} & \mathbf{I}_\rho \\ \mathbf{A}_{\text{cl}} & -\mathbf{M}_\gamma \end{bmatrix} , \quad \mathbf{x} = \begin{bmatrix} \mathbf{x}_1 \\ \mathbf{x}_2 \end{bmatrix} , \quad \mathbf{x}^\Delta = \begin{bmatrix} \mathbf{x}_1^{(\gamma)} \\ \mathbf{x}_2^{(\beta)} \end{bmatrix} .$$

We have $\tilde{\mathbf{E}}, \tilde{\mathbf{A}} \in \mathbb{R}^{r \times r}$, $\mathbf{x} : [0, +\infty) \rightarrow \mathbb{R}^r$, and $\beta, \gamma \in (0, 1)$, where for simplicity the notation $r = 2\rho$ is used.

Theorem 4.1. Consider system (4.15). Then its matrix pencil is given by [31]:

$$z(s) \tilde{\mathbf{E}} - \tilde{\mathbf{A}} , \quad (4.16)$$

where

$$z(s) = \begin{bmatrix} s^\gamma \mathbf{I}_\rho & \mathbf{0}_{\rho,\rho} \\ \mathbf{0}_{\rho,\rho} & s^\beta \mathbf{I}_\rho \end{bmatrix} .$$

The proof of Theorem 4.1 is given in Appendix A.

Assuming that the pencil (4.16) is regular, or equivalently, $\det(z\tilde{\mathbf{E}} - \tilde{\mathbf{A}}) \not\equiv 0$, it can be proven that there always exist solutions of (4.15). Then, similarly to the discussions of

Chapter 2, uniqueness of solutions depends on the given initial condition. The interested reader may find a comprehensive theory for the existence and uniqueness of solutions of systems in the form of (4.15) – with either regular or singular pencil – in [31].

The eigenvalues of the matrix pencil (4.16) provide insight on the stability of system (4.15), or equivalently, of system (4.9). Since the pencil of system (4.15) is a regular pencil, $s\tilde{\mathbf{E}} - \tilde{\mathbf{A}}$ is also a regular pencil. Hence and because of the structure of $\tilde{\mathbf{E}}$ there exist invariants of the following type:

- κ finite eigenvalues of algebraic multiplicity ν_i , $i = 1, 2, \dots, \kappa$;
- an infinite eigenvalue of algebraic multiplicity μ ,

where $\sum_{i=1}^{\kappa} \nu_i = \nu$, $\nu + \mu = r$.

Let

$$\mathbf{W} = \begin{bmatrix} \mathbf{W}_{\nu,\gamma} \\ \mathbf{W}_{p,\beta} \\ \mathbf{W}_{q,\gamma} \\ \mathbf{W}_{q,\beta} \end{bmatrix}, \quad \mathbf{V} = \begin{bmatrix} \mathbf{V}_{\nu,\gamma} & \mathbf{V}_{\nu,\beta} & \mathbf{V}_{q,\gamma} & \mathbf{V}_{q,\beta} \end{bmatrix},$$

where $\mathbf{W}_{\nu,\gamma} \in \mathbb{C}^{\hat{\nu} \times r}$, $\mathbf{W}_{\nu,\beta} \in \mathbb{C}^{\bar{\nu} \times r}$, $\mathbf{W}_{\mu,\gamma} \in \mathbb{C}^{\hat{\mu} \times r}$, $\mathbf{W}_{\mu,\beta} \in \mathbb{C}^{\bar{\mu} \times r}$, and $\mathbf{V}_{\nu,\gamma} \in \mathbb{C}^{r \times \hat{\nu}}$, $\mathbf{V}_{\nu,\beta} \in \mathbb{C}^{r \times \bar{\nu}}$, $\mathbf{V}_{\mu,\gamma} \in \mathbb{C}^{r \times \hat{\mu}}$, $\mathbf{V}_{\mu,\beta} \in \mathbb{C}^{r \times \bar{\mu}}$. Equivalently, setting:

$$\mathbf{W}_{\nu} = \begin{bmatrix} \mathbf{W}_{\nu,\gamma} \\ \mathbf{W}_{\nu,\beta} \end{bmatrix}, \quad \mathbf{V}_{\nu} = \begin{bmatrix} \mathbf{V}_{\nu,\gamma} & \mathbf{V}_{\nu,\beta} \end{bmatrix},$$

$$\mathbf{W}_{\mu} = \begin{bmatrix} \mathbf{W}_{\mu,\gamma} \\ \mathbf{W}_{\mu,\beta} \end{bmatrix}, \quad \mathbf{V}_{\mu} = \begin{bmatrix} \mathbf{V}_{\mu,\gamma} & \mathbf{V}_{\mu,\beta} \end{bmatrix},$$

one has

$$\mathbf{W} = \begin{bmatrix} \mathbf{W}_{\nu} \\ \mathbf{W}_{\mu} \end{bmatrix}, \quad \mathbf{V} = \begin{bmatrix} \mathbf{V}_{\nu} & \mathbf{V}_{\mu} \end{bmatrix}. \quad (4.17)$$

with $\mathbf{W}_{\nu} \in \mathbb{C}^{\nu \times r}$, $\mathbf{W}_{\mu} \in \mathbb{C}^{\mu \times r}$, and $\mathbf{V}_{\nu} \in \mathbb{C}^{r \times \nu}$, $\mathbf{V}_{\mu} \in \mathbb{C}^{r \times \mu}$.

Employing (2.18) for $\tilde{\mathbf{A}}, \tilde{\mathbf{E}}$, and using the notation $\mathbf{I}_{\nu} = \mathbf{I}_{\hat{\nu}} \oplus \mathbf{I}_{\bar{\nu}}$, $\mathbf{J}_p = \mathbf{J}_{\hat{\nu}} \oplus \mathbf{J}_{\bar{\nu}}$, one has:

$$\mathbf{W}\tilde{\mathbf{E}}\mathbf{V} = \mathbf{I}_{\hat{\nu}} \oplus \mathbf{I}_{\bar{\nu}} \oplus \mathbf{H}_{\hat{\mu}} \oplus \mathbf{H}_{\bar{\mu}},$$

$$\mathbf{W}\tilde{\mathbf{A}}\mathbf{V} = \mathbf{J}_{\hat{\nu}} \oplus \mathbf{J}_{\bar{\nu}} \oplus \mathbf{I}_{\hat{\mu}} \oplus \mathbf{I}_{\bar{\mu}}.$$

Finally, the following proposition is relevant:

Proposition 4.2. Consider system (4.15) with a regular pencil. Then:

a) using the spectrum of the pencil $s\tilde{\mathbf{E}} - \tilde{\mathbf{A}}$, the general solution is given by:

$$\mathbf{x}(t) = \mathbf{V}_\nu \sum_{k=0}^{\infty} \begin{bmatrix} \frac{t^{\gamma k}}{\Gamma(k\gamma+1)} \mathbf{I}_{\hat{\nu}} & \mathbf{0}_{\hat{\nu}, \hat{\nu}} \\ \mathbf{0}_{\bar{\nu}, \bar{\nu}} & \frac{t^{\beta k}}{\Gamma(k\beta+1)} \mathbf{I}_{\bar{\nu}} \end{bmatrix} \mathbf{J}_\nu^k \mathbf{c}, \quad (4.18)$$

where $\mathbf{J}_\nu \in \mathbb{C}^{\nu \times \nu}$ is a Jordan matrix constructed by the finite eigenvalues of the pencil $s\tilde{\mathbf{E}} - \tilde{\mathbf{A}}$, and their algebraic multiplicity, while $\mathbf{V}_\nu \in \mathbb{C}^{r \times \nu}$ is a matrix constructed by the linear independent eigenvectors related to the finite eigenvalues of the pencil $s\tilde{\mathbf{E}} - \tilde{\mathbf{A}}$, and $\mathbf{c} \in \mathbb{C}^\nu$ is a constant vector.

b) the system (4.15) is asymptotically stable if all eigenvalues $\hat{\lambda}^*$ of the pencil $s\tilde{\mathbf{E}} - \tilde{\mathbf{A}}$ satisfy:

$$|\text{Arg}(\hat{\lambda}^*)| > \tilde{\gamma} \frac{\pi}{2} \text{ (rad)}, \quad (4.19)$$

where $\tilde{\gamma} = \min\{\gamma, 1 - \gamma\}$.

The proof of Proposition 4.2 can be found in [31]. For a more general survey on the stability conditions for systems of fractional differential equations, the interested reader may refer to [124]. Finally, for linearized systems, as it is the case of power systems, the condition (4.19) guarantees stability in a neighborhood of the operating point utilized to calculate the pencil (4.16). For this reason, in the case studies discussed in Sections 4.5.1 and 4.5.2, numerical integration rather than (4.19) is utilized to check the stability and the dynamic response of power systems with inclusion of FOCs.

4.3.3 Properties of Fractional Order Controllers

Consider the simple FOC with transfer function $H_c(s) = Ks^\gamma$. Consider the frequency response of $H_c(s)$, i.e. its steady-state response to sinusoidal, periodic input signals. In this case, it is $s \in \mathbb{I}$, or $s = j\omega$.

Frequency Response: The magnitude and phase of $H_c(s)$ can be written as follows:

$$\begin{aligned} \text{Mag}(H_c(s)) \text{ (dB)} &= 20 \log|Ks^\gamma| = 20 \gamma \log(K\omega), \\ \text{Arg}(H_c(s)) \text{ (}^\circ\text{)} &= \text{Arg}(K(j\omega)^\gamma) = 90 \gamma. \end{aligned} \quad (4.20)$$

Hence, $H_c(s)$ has a magnitude Bode plot with constant slope of 20γ dB/dec, while the phase plot is a horizontal line at 90γ degrees. The Integer Order (IO) versions of $H_c(s)$ are obtained for $\gamma = n$, $n \in \mathbb{Z}$. Then, from (4.20), it is clear that $H_c(s)$ is an extension of its IO versions in frequency domain. This result is general, so that all FOCs can be viewed as extensions of the respective IO ones.

Robustness: FOCs have an inherent property of iso-damping, which implies that the closed-loop system is robust against gain uncertainties and variations. Let $H_o(s)$ be the transfer function of the open-loop, linearized power system. Then, the iso-damping property is defined as:

$$\left| \frac{d \operatorname{Arg}(H_c(j\omega) H_o(j\omega))}{d\omega} \right|_{\omega=\omega_{gc}} = 0, \quad (4.21)$$

where ω_{gc} is the system gain crossover frequency. (4.21) indicates that the system maintains its phase margin around ω_{gc} .

4.3.4 Examples

This section provides two illustrative examples on the SSSA of power systems with inclusion of FOCs. The first example considers a small linear singular system of differential equations with regular pencil. The second example discusses the damping of the electro-mechanical oscillations of the WSCC 9-bus system through a Fractional-Order Power System Stabilizer (FOPSS).

4.3.4.1 Illustrative Example

Consider system (2.10) with:

$$\mathbf{E} = \begin{bmatrix} 4 & 9 & 9 & -2 & 10 & 7 & 3 \\ 1 & 5 & 2 & 2 & 3 & 1 & 1 \\ 1 & 0 & -2 & -2 & 6 & 4 & 1 \\ 5 & -2 & -3 & 18 & 3 & 16 & 2 \\ 6 & 8 & 6 & 8 & 6 & 14 & 2 \\ 2 & 11 & 3 & 6 & 6 & 2 & 2 \\ 4 & 5 & 5 & 6 & 2 & 9 & 1 \end{bmatrix},$$

$$\mathbf{A} = \begin{bmatrix} -15 & -43 & -39 & 4 & -35 & -22 & -5 \\ -3 & -19 & -2 & -5 & -12 & -2 & 1 \\ -4 & -16 & -30 & 6 & -9 & -1 & -7 \\ -25 & -2 & 3 & -72 & -3 & -74 & -4 \\ -27 & -32 & -23 & -39 & -24 & -66 & -5 \\ -8 & -41 & -15 & -18 & -24 & -8 & -8 \\ -18 & -15 & -9 & -29 & -13 & -48 & -1 \end{bmatrix}, \quad \mathbf{B} = \begin{bmatrix} 0 \\ 0 \\ 0 \\ 0 \\ 0 \\ 1 \\ 0 \end{bmatrix}.$$

The matrix pencil $s\mathbf{E} - \mathbf{A}$ has $\nu = 5$ finite, distinct eigenvalues $\lambda_1 = -5$, $\lambda_2 = -4$, $\lambda_3 = 1$, $\lambda_4 = -2$ and $\lambda_5 = -3$. The pencil also has the eigenvalue $\lambda_6 \rightarrow \infty$ with algebraic multiplicity $\mu = 2$. The rightmost eigenvalue of the pencil is $\lambda_3 > 0$, and thus the system is unstable.

Consider that the output of the system is given by (4.7), where:

$$\mathbf{C} = \begin{bmatrix} 0 & 0 & 0 & 0 & 0 & 1 & 0 \end{bmatrix}, \quad \mathbf{D} = 0.$$

In order to stabilize the system, the following simple form of controller (4.8) is considered:

$$\begin{aligned} x_c^{(\gamma)} &= K_i u, \\ w &= x_c + K_p u. \end{aligned} \tag{4.22}$$

Equation (4.22) describes a Fractional-Order Proportional Integral (FOPI) controller, where $K_p = 7$, $K_i = 10$, are the proportional and integral gains, respectively; $\gamma = 0.6$ is

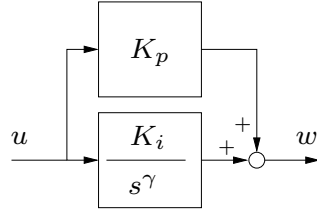


Figure 4.2: FOPI block diagram.

the controller's fractional order. The block diagram of the FOPI is shown in Figure 4.2.

Then, the closed-loop system is described by (4.9), where

$$\mathbf{M} = \begin{bmatrix} 4 & 9 & 9 & -2 & 10 & 7 & 3 & 0 & 0 \\ 1 & 5 & 2 & 2 & 3 & 1 & 1 & 0 & 0 \\ 1 & 0 & -2 & -2 & 6 & 4 & 1 & 0 & 0 \\ 5 & -2 & -3 & 18 & 3 & 16 & 2 & 0 & 0 \\ 6 & 8 & 6 & 8 & 6 & 14 & 2 & 0 & 0 \\ 2 & 11 & 3 & 6 & 6 & 2 & 2 & 0 & 0 \\ 4 & 5 & 5 & 6 & 2 & 9 & 1 & 0 & 0 \\ 0 & 0 & 0 & 0 & 0 & 0 & 0 & 0 & 0 \\ 0 & 0 & 0 & 0 & 0 & 0 & 0 & 0 & 0 \end{bmatrix}, \quad \mathbf{M}_\gamma = \begin{bmatrix} 0 & 0 & 0 & 0 & 0 & 0 & 0 & 0 & 0 \\ 0 & 0 & 0 & 0 & 0 & 0 & 0 & 0 & 0 \\ 0 & 0 & 0 & 0 & 0 & 0 & 0 & 0 & 0 \\ 0 & 0 & 0 & 0 & 0 & 0 & 0 & 0 & 0 \\ 0 & 0 & 0 & 0 & 0 & 0 & 0 & 0 & 0 \\ 0 & 0 & 0 & 0 & 0 & 0 & 0 & 0 & 0 \\ 0 & 0 & 0 & 0 & 0 & 0 & 0 & 0 & 0 \\ 0 & 0 & 0 & 0 & 0 & 0 & 0 & 1 & 0 \\ 0 & 0 & 0 & 0 & 0 & 0 & 0 & 0 & 0 \end{bmatrix},$$

$$\mathbf{A}_{\text{cl}} = \begin{bmatrix} -15 & -43 & -39 & 4 & -35 & -22 & -5 & 0 & 0 \\ -3 & -19 & -2 & -5 & -12 & -2 & 1 & 0 & 0 \\ -4 & -16 & -30 & 6 & -9 & -1 & -7 & 0 & 0 \\ -25 & -2 & 3 & -72 & -3 & -74 & -4 & 0 & 0 \\ -27 & -32 & -23 & -39 & -24 & -66 & -5 & 0 & 0 \\ -8 & -41 & -15 & -18 & -24 & -8 & -8 & 0 & 1.0 \\ -18 & -15 & -9 & -29 & -13 & -48 & -1 & 0 & 0 \\ 0 & 0 & 0 & 0 & 0 & 10 & 0 & 0 & 0 \\ 0 & 0 & 0 & 0 & 0 & 7 & 0 & 1 & -1 \end{bmatrix}.$$

The stability of the closed-loop system can be checked by calculating the eigenvalues of the matrix pencil $s\tilde{\mathbf{E}} - \tilde{\mathbf{A}}$, where $\tilde{\mathbf{E}}, \tilde{\mathbf{A}}$, are defined in (4.15). In this case:

The pencil $s\tilde{\mathbf{E}} - \tilde{\mathbf{A}}$ has $\hat{p} = 11$ distinct finite eigenvalues $\hat{\lambda}_{1,2} = 1.816 \pm j2.679$, $\hat{\lambda}_3 = -1.130$, $\hat{\lambda}_{4,5} = 1.840 \pm j0.996$, $\hat{\lambda}_{6,7} = -0.0109 \pm j1.751$, $\hat{\lambda}_{8,9} = -0.044 \pm j1.940$, $\hat{\lambda}_{10,11} = 0.0211 \pm j2.2004$, and the infinite eigenvalue $\hat{\lambda}_{12} \rightarrow \infty$ with algebraic multiplicity $\hat{q} = 7$. For fractional order $\gamma = 0.6$, $\tilde{\gamma} = \min\{0.6, 0.4\} = 0.4$ in equation (4.19), and thus, the closed-loop system is stable if the arguments $\text{Arg}(\hat{\lambda}^*)$ of all finite eigenvalues $\hat{\lambda}^*$ satisfy:

$$|\text{Arg}(\hat{\lambda}^*)| > \frac{\pi}{5} = 0.628 \text{ rad.}$$

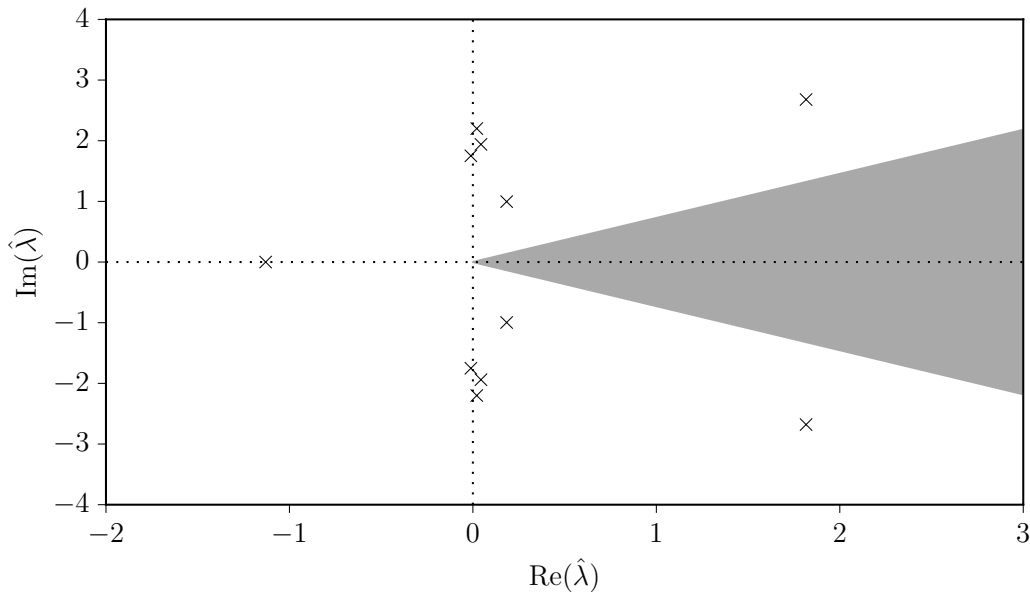


Figure 4.3: Numerical example 1: root loci of $s\tilde{\mathbf{E}} - \tilde{\mathbf{A}}$. Shaded is the region of instability $|\text{Arg}(\hat{\lambda}^*)| < 0.628$ rad.

The finite eigenvalues of $s\tilde{\mathbf{E}} - \tilde{\mathbf{A}}$ are illustrated in Figure 4.3. The system is stable, since all eigenvalues lie in the region given in (4.23).

4.3.4.2 WSCC 9-bus System

This example is based on the well-known WSCC 9-bus system, the data of which are provided in [7]. The system consists of 3 synchronous machines, 6 transmission lines, 3 transformers and 3 loads, modeled as constant power consumption. Each machine provides primary voltage and frequency control through an AVR and a TG, respectively. The original system model does not include any fractional dynamics.

Suppose that a FOPSS is installed at the synchronous machine connected at bus 2. The FOPSS employed has the following transfer function:

$$H_{\text{FOPSS}} = K_w \left(\frac{T_1 s^\gamma + 1}{T_2 s^\gamma + 1} \right)^2.$$

The controller input is the local rotor speed, while the output is an additional input to the algebraic equation of the local AVR reference. The FOPSS can be written in the form of (4.8), where:

$$\mathbf{E}_{c,\gamma} = \begin{bmatrix} T_2 & 0 & 0 & 0 \\ T_1 & 0 & 0 & 0 \\ 0 & 0 & T_2 & 0 \\ 0 & 0 & T_1 & 0 \end{bmatrix}, \quad \mathbf{A}_c = \begin{bmatrix} -1 & 0 & 0 & 0 \\ -1 & 1 & 0 & 0 \\ 0 & 1 & -1 & 0 \\ 0 & 0 & -1 & 1 \end{bmatrix},$$

$$\mathbf{B}_c = [K_w \ 0 \ 0 \ 0]^T, \quad \mathbf{C}_c = [0 \ 0 \ 0 \ 1], \quad \mathbf{D}_c = 0.$$

Suppose that $T_1 = 0.01$ s, $T_2 = 0.22$ s, $\gamma = 0.75$. Then, small-signal stability is assessed by calculating the eigenvalues of (4.16). From (4.19), the system is stable if all finite eigenvalues λ^* satisfy:

$$|\text{Arg}(\lambda^*)| > \tilde{\gamma} \frac{\pi}{2} = 0.393 \text{ rad},$$

where $\tilde{\gamma} = \min\{0.75, 0.25\} = 0.25$. The most critical eigenvalues of the closed-loop system are shown in Figure 4.4, where the shaded region is unstable. As it can be seen, the system with the FOPSS is in this case stable.

4.4 Oustaloup's Recursive Approximation

4.4.1 Formulation

The theoretical analysis based on fractional calculus is essential for a better understanding of “ideal” FOCs and hence, for a robust FOC design. In practice, however, the implementation of FOCs is typically done by approximating the fractional derivatives and integrals with rational transfer functions. Although this is an important aspect of FOCs implementation, some studies omit mentioning what approximation technique

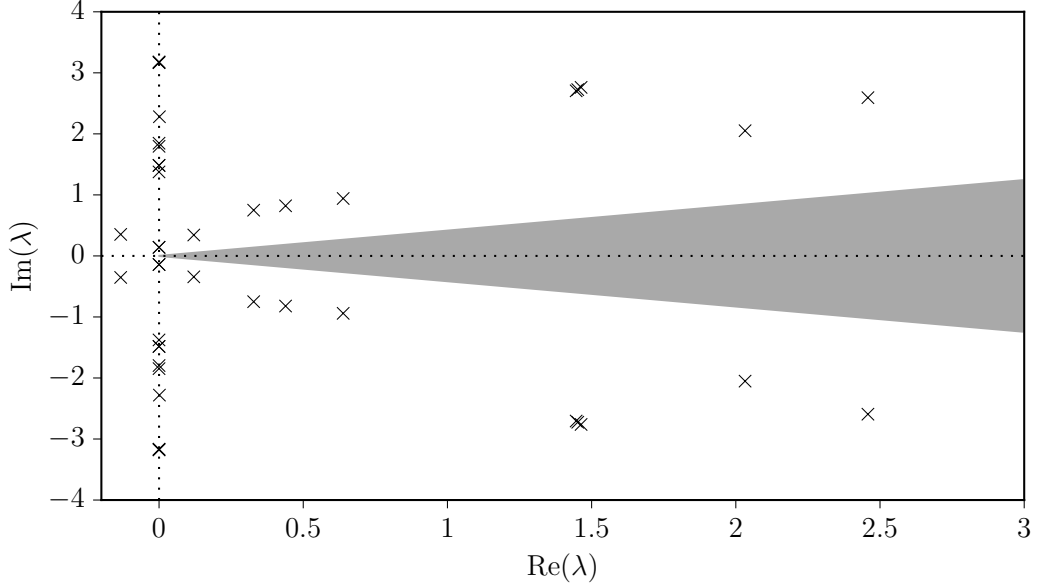


Figure 4.4: WSCC system with FOPSS: most critical eigenvalues. Shaded is the region of instability.

and/or parameters they use, effectively forcing the adoption of a black-box approach. In the following the ORA method, which is arguably the most common continuous approximation technique, is employed. The generalized ORA of a fractional derivative of order γ is defined as [105]:

$$s^\gamma \approx \omega_h^\gamma \prod_{k=1}^N \frac{s + \omega'_k}{s + \omega_k}, \quad (4.23)$$

where

$$\begin{aligned} \omega'_k &= \omega_b \omega_v^{(2k-1-\gamma)/N}, \\ \omega_k &= \omega_b \omega_v^{(2k-1+\gamma)/N}, \\ \omega_v &= \sqrt{\frac{\omega_h}{\omega_b}}. \end{aligned}$$

In the above expressions, $[\omega_b, \omega_h]$ is the frequency range for which the approximation is designed to be valid; N is the order of the polynomial approximation; The term “generalized” implies that, in (4.23), N can be either even or odd [105], while the term “recursive” implies that the values of ω'_k, ω_k result from a set of recursive equations [117]. The block diagram of ORA is shown in Figure 4.5.

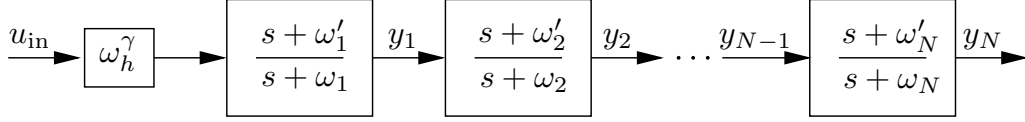


Figure 4.5: Oustaloup's recursive approximation block diagram.

Figure 4.6 compares the theoretical frequency response of $s^{-0.7}$, which is given by (4.20) for $K = 1$, with the respective plots provided by ORAs of different dynamic orders. This simple example shows the typical behavior of the ORA: the approximation is more accurate for higher dynamic orders and for frequencies closer to the middle of the interval $[\omega_b, \omega_h]$.

A final remark on equation (4.23) is that the ORA of s^γ is typically accurate enough for fractional orders that satisfy $0 \leq |\gamma| \leq 1$. For higher fractional orders, accuracy can be maintained by implementing s^γ as a multiplication of a suitable integer order block and a fractional order block, as follows:

$$s^\gamma = s^n s^{\gamma-n}, \quad n \in \mathbb{Z}, \quad (\gamma - n) \in [0, 1]. \quad (4.24)$$

4.4.2 DAE Model

In time-domain, the ORA can be described by the following set of explicit DAEs:

$$\begin{aligned} \dot{\chi}_E &= \mathbf{A}_{E,ORA} \chi_E + \mathbf{B}_{E,ORA} u_{in} \\ 0 &= y_N - \mathbf{C}_{E,ORA} \chi_E + \omega_h^\gamma u_{in}, \end{aligned} \quad (4.25)$$

where $\chi_E = [\chi_{E,1} \ \chi_{E,2} \ \cdots \ \chi_{E,N}]^T$ is the ORA state vector; and

$$\begin{aligned} \mathbf{A}_{E,ORA} &= \begin{bmatrix} -\omega_1 & & & & & \\ \omega'_2 - \omega_2 & -\omega_2 & & & & \\ \omega'_3 - \omega_3 & \omega'_3 - \omega_3 & -\omega_3 & & & \\ \vdots & \vdots & \vdots & \ddots & & \\ \omega'_N - \omega_N & \omega'_N - \omega_N & \cdots & \omega'_N - \omega_N & -\omega_N & \end{bmatrix}, \\ \mathbf{B}_{E,ORA} &= \begin{bmatrix} \omega_h^\gamma (\omega'_1 - \omega_1) & \omega_h^\gamma (\omega'_2 - \omega_2) & \cdots & \omega_h^\gamma (\omega'_N - \omega_N) \end{bmatrix}^T, \\ \mathbf{C}_{E,ORA} &= \begin{bmatrix} 1 & 1 & \cdots & 1 \end{bmatrix}^T. \end{aligned}$$

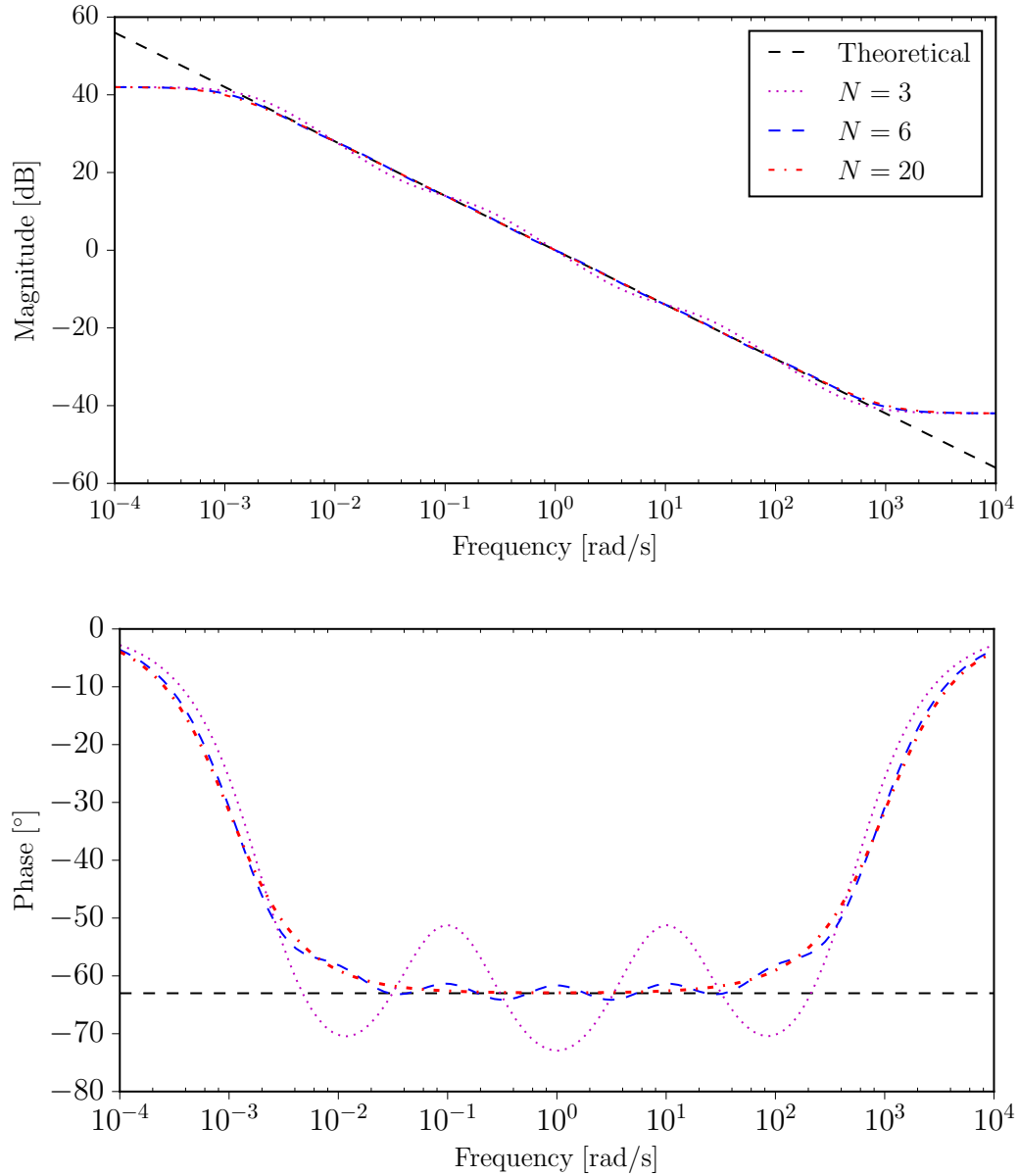


Figure 4.6: Bode plot of the ORA for different approximation orders N ($\gamma = -0.7$, $[\omega_b, \omega_h] = [10^{-3}, 10^3]$ rad/s).

The dimensions of $\mathbf{A}_{E,ORA}$, $\mathbf{B}_{E,ORA}$, $\mathbf{C}_{E,ORA}$, are $N \times N$, $N \times 1$ and $1 \times N$, respectively. As discussed in Chapter 2, an alternative way to describe a dynamic model is by using a

4.4.3 Steady State Error

Consider the simple FOC with transfer function $H_c(s) = Ks^\gamma$. By approximating s^γ from (4.23), $H_c(s)$ can be written as:

$$H_c(s) \approx K \omega_h^\gamma \prod_{k=1}^N \frac{s + \omega'_k}{s + \omega_k} = \frac{c_1 s^N + c_2 s^{N-1} + \dots + c_N}{d_1 s^N + d_2 s^{N-1} + \dots + d_N}, \quad (4.27)$$

with

$$\begin{aligned} c_N &= K \omega_h^\gamma \prod_{k=1}^N \omega'_k = K \omega_h^\gamma \omega_b^N \omega_v^{(N-\gamma)}, \\ d_N &= \prod_{k=1}^N \omega_k = \omega_b^N \omega_v^{(N+\gamma)}, \end{aligned} \quad (4.28)$$

where the expressions for ω_k and ω'_k have been substituted as in (4.23) and $\sum_{k=1}^N = \frac{N(N+1)}{2}$. From (4.27), one can deduce that the controller's unity feedback closed-loop steady state error $e(t \rightarrow \infty)$ for an arbitrary input $U(s)$ is:

$$\begin{aligned} e(t \rightarrow \infty) &= \lim_{s \rightarrow 0} \frac{s U(s)}{1 + H_c(s)} \\ &= \frac{d_N}{c_N + d_N} \lim_{s \rightarrow 0} s U(s) \\ &= \frac{1}{K + \omega_b^\gamma} \lim_{s \rightarrow 0} s U(s), \end{aligned} \quad (4.29)$$

where $\omega_v = \sqrt{\omega_h/\omega_b}$. The steady-state error in (4.29) depends on K , ω_b^γ , and the applied input $U(s)$. Evaluating the controller's unit step input response yields $U(s) = 1/s$ and $e_{\text{step}}(t \rightarrow \infty) = 1/(K + \omega_b^\gamma)$. Considering $\gamma < 0$ yields that an ORA-based Fractional Order (FO) integral controller is not perfect tracking. This result is not consistent with the theoretical behavior of Ks^γ , $\gamma < 0$, which has $e_{\text{step}}(t \rightarrow \infty) = 0$. However, the design of an almost perfect-tracking FOC is possible with appropriate selection of ORA parameters.

4.4.4 Parameters Selection

While the value of N is usually constrained due to computational concerns, most studies that consider ORA-based FOCs in power systems provide a rather arbitrary selection of

the range of frequencies $[\omega_b, \omega_h]$. This section discusses the tuning of ORA parameters and provides an empirical rule that simplifies the design of FOCs.

- *Low frequency ω_b* : A very small ω_b reduces the steady state error in (4.29). However, a poor choice can significantly degrade the phase fitting of ORA. An example is shown in Figure 4.7, where ω_b is varied from 10^{-3} to 10^{-8} rad/s.
- *High frequency ω_h* : A very high ω_h may increase the system gain margin. Large gains lead to fast response and stability enhancement, as well as to elimination of steady state errors. However, increasing excessively the speed of the system response may trigger closed-loop resonant points. Note that such resonant points can remain undetected if they stem from unmodeled high frequency dynamics.
- *Approximation order N* : The phase fitting degradation caused by the decrease of ω_b can be compensated by increasing the dynamic order N , e.g. from 7 to 11 (see Figure 4.7). Increasing N has an impact on the computational complexity, which can be a serious constraint, especially if multiple filters are required and if a large system (like real-world power systems) is studied. Another possible problem of a very high N is that multiple poles are placed very close to each other and close to the imaginary axis. For digital filters, such a pole-placement may affect the discretization process, with multiple poles being mapped on the unity circle, due e.g. to rounding errors.

Control parameters need to provide an adequate compromise among accuracy, computational burden and performance. A good practice is to limit the range of $[\omega_b, \omega_h]$ to the frequencies of the dynamics of interest. This also avoids unexpected resonances, as discussed above. Then, given a range let's say $\omega_b = 10^{-\nu_b}$ and $\omega_h = 10^{\nu_h}$, $\nu_b, \nu_h \in \mathbb{N}$, a choice that provides a very good compromise is $N = \nu_b + \nu_h$, with $N \geq 4$.

4.5 Case Studies

4.5.1 WSCC 9-bus System

This section presents three power system applications of FOCs. (i) a FO integral controller for secondary frequency regulation; (ii) a FO lead-lag controller for primary frequency regulation of an ESS; and (iii) the voltage regulation provided by a STATCOM

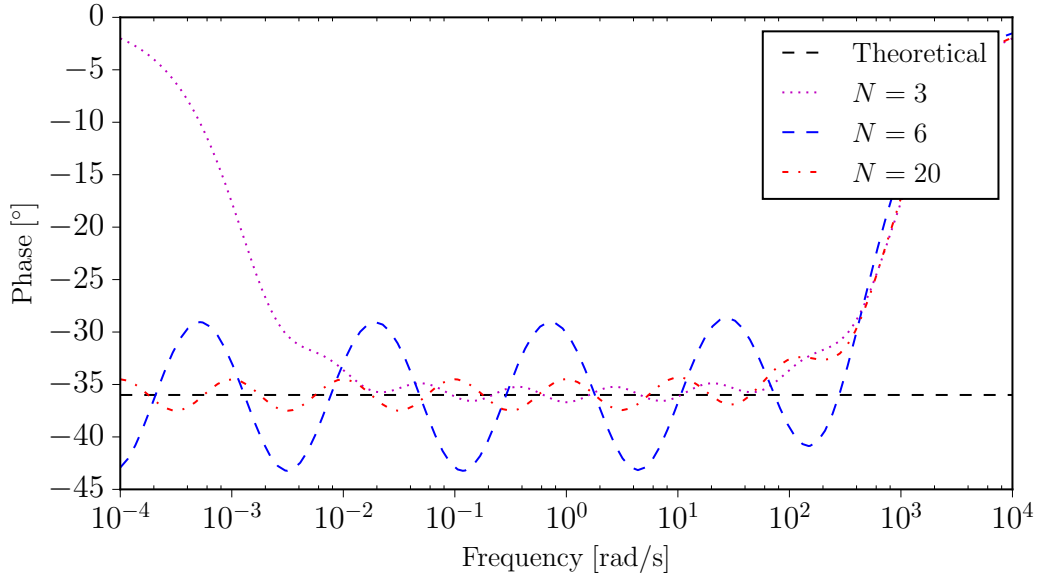


Figure 4.7: Effect of ω_b on ORA frequency response ($\gamma = -0.4$, $\omega_h = 10^3$ rad/s).

with inclusion of multiple FOPI controllers. In these three examples, the pre-disturbance equilibrium of the fractional DAE model is stable, i.e. condition (4.19) holds. The focus is on time-domain simulations carried to discuss the dynamic performance of ORA-based FOCs and check the system stability under large disturbances. In all cases, the system is numerically integrated using the implicit trapezoidal method. A brief description of implicit integration of power systems is provided in Section 6.2. Examples of this section are based on the WSCC 9-bus system. All simulation results are obtained with Dome.

Automatic Generation Control

In this example, an AGC, that coordinates the three generators and provides secondary frequency regulation, is included in the WSCC system. The AGC measures the COI frequency (ω_{CoI}) and produces a dynamic active power signal (P_s), which is sent to the synchronous generator turbine governors, and is proportional to their droops. The power order ($P_{\text{ord},i}$) received by the i -th governor is:

$$P_{\text{ord},i} = \frac{\mathcal{R}_i}{\mathcal{R}_T} P_s, \quad i = \{1, 2, 3\}, \quad (4.30)$$

where \mathcal{R}_i is the i -th TG droop constant; and $\mathcal{R}_T = \mathcal{R}_1 + \mathcal{R}_2 + \mathcal{R}_3$. The simplest model of an AGC assumes an integral controller. The differential equation that describes the

dynamic behavior of a Fractional-Order Integral (FOI) AGC is:

$$P_s^{(\gamma)} = K_i (\omega^{\text{ref}} - \omega_{\text{CoI}}) , \quad (4.31)$$

where K_i is the FOI-AGC gain; ω^{ref} is the reference angular frequency; and γ is the order of integration. The IO version of this controller (I-AGC) is obtained for $\gamma = 1$.

It is of interest to compare the performance of the I-AGC and the ORA-based FOI-AGC. With this aim, a three-phase fault is considered at bus 4 occurring at $t = 3$ s. After 80 ms, the line that connects buses 4 and 5 trips and the fault is cleared.

The parameters of both controllers are tuned by optimizing the CoI frequency profile through trial-and-error. The I-AGC gain is $K_i = 15$, while the parameters of the FOI-AGC are $K_i = 50$ and $\gamma = 0.7$.

Taking into account the discussion in Section 4.4.4, the ORA parameters are set to $[\omega_b, \omega_h] = [10^{-3}, 10^1]$ rad/s, $N = 4$. Figure 4.8 shows the CoI frequency response of the system without AGC; with I-AGC; with FOI-AGC. The FOI-AGC improves significantly the dynamic response of the frequency of the system. Note that, with the selected parameters, the FOI-AGC achieves practically a perfect-tracking behavior.

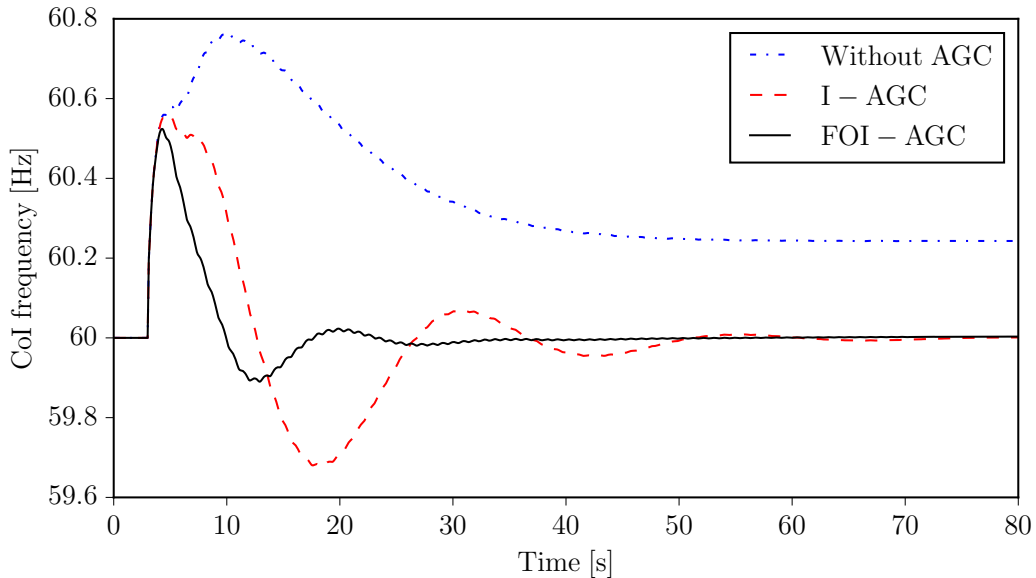


Figure 4.8: WSCC system with AGC: CoI frequency.

Energy Storage System

In this example, a converter-interfaced ESS is installed at bus 6 of the 9-bus system. A simplified model is employed to describe the ESS dynamics. Figure 4.9 shows the block diagram of the ESS active power control. The ESS measures the local frequency at bus 6 and regulates its active power P_{ESS} to provide frequency support. The frequency error $\omega_6^{\text{ref}} - \omega_6$ is filtered. $T_{f,P}$ is the time constant of the applied filter and $x_{f,P}$ is the filtered signal as well as the input of the frequency control transfer function $H(s)$. Finally, $T_{\text{ESS},P}$ is the time constant of the ESS active power dynamics. The interested reader can find more details on the employed ESS model in [102].

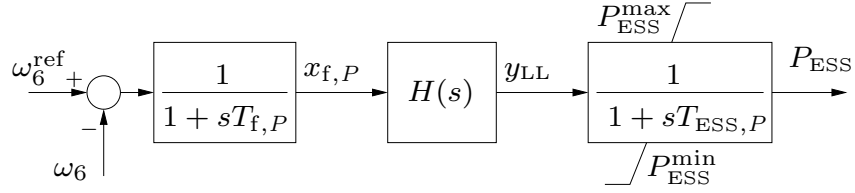


Figure 4.9: Active power flow of simplified ESS model.

In this example, $H(s)$ is assumed to be a FO lead-lag controller defined as:

$$H(s) = K \frac{T_1 s^\gamma + 1}{T_2 s^\gamma + 1}. \quad (4.32)$$

The equations that describe the FO lead-lag are:

$$\begin{aligned} T_2 x_{\text{LL}}^{(\gamma)} &= K x_{f,P} - x_{\text{LL}}, \\ y_{\text{LL}} &= x_{\text{LL}} + T_1 x_{\text{LL}}^{(\gamma)}, \end{aligned} \quad (4.33)$$

where x_{LL} is the controller's state. The IO version of this controller (IO lead-lag) is obtained for $\gamma = 1$.

We consider the same disturbance examined at the previous example (fault at bus 4 cleared after 80 ms). Two implementations of the IO lead-lag are compared, namely, the IO lead-lag and the ORA-based IO lead-lag controller for $\gamma = 1$, $[\omega_b, \omega_h] = [10^{-4}, 10^4]$ rad/s. The results are shown in Figure 4.10. The value $\omega_h = 10^4$ rad/s is high enough to trigger a closed-loop high frequency resonant point, which significantly impacts the control output. Figure 4.10 also shows that, while it is independent from the approximation order, the overshoot can be avoided by properly reducing the value of ω_h .

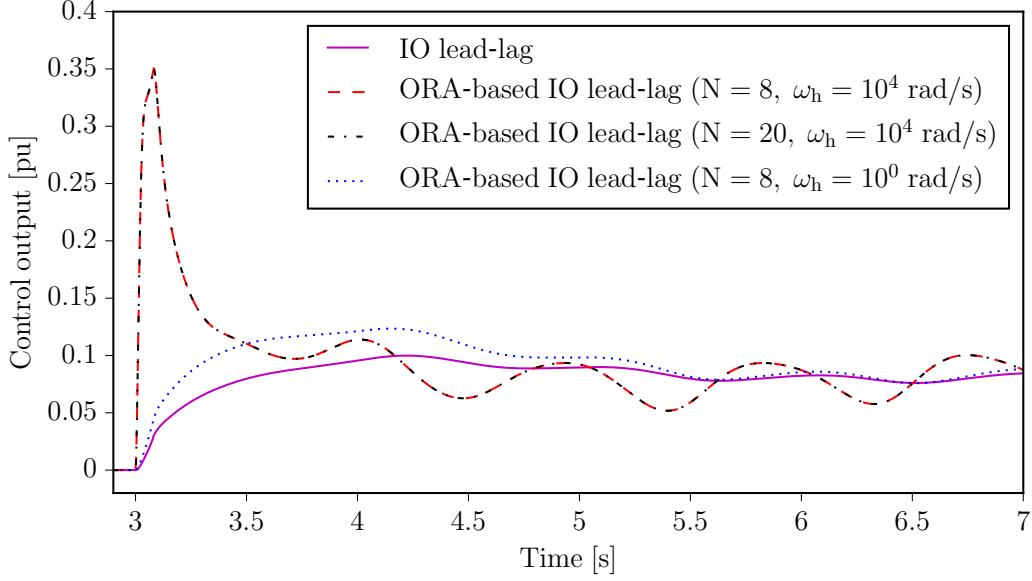


Figure 4.10: WSCC system with ESS frequency control: lead-lag parameters: $T_1 = 2$ s, $T_2 = 0.01$ s, $K = 10$. ORA parameters: $\omega_b = 10^{-4}$ rad/s, $\gamma = 1$.

Next, the dynamic performance of the IO lead-lag is compared with two ORA-based FO lead-lags, namely FOLL1 and FOLL2, which have different tuning. The parameters of the three controllers are shown in Table 4.1. For comparison, the gain and time constants of FOLL1 have been set equal to the ones of the IO lead-lag. In this case, only the order γ needs to be tuned. In general, however, the control parameters of a FOC are not directly mapped onto those of its IO version and should be retuned. FOLL2 represents the retuned controller.

To tune FOLL2, $T_1 = 2$ s is fixed and the rest of the parameters are selected by optimizing the local bus frequency profile through trial-and-error.

The response of the frequency at bus 6 is shown in Figure 4.11. Shifting the fractional order γ (FOLL1) allows reducing both the frequency overshoot and the steady state error of the local bus frequency. Retuning all control parameters leads to a further performance improvement (FOLL2).

Table 4.1: Parameters of the ESS lead-lag frequency controllers.

IO lead-lag	$T_1 = 2$ s, $T_2 = 0.01$ s, $K = 20$,
FOLL1	$T_1 = 2$ s, $T_2 = 0.01$ s, $K = 20$, $\gamma = 0.3$
FOLL2	$T_1 = 2$ s, $T_2 = 0.005$ s, $K = 60$, $\gamma = 0.2$

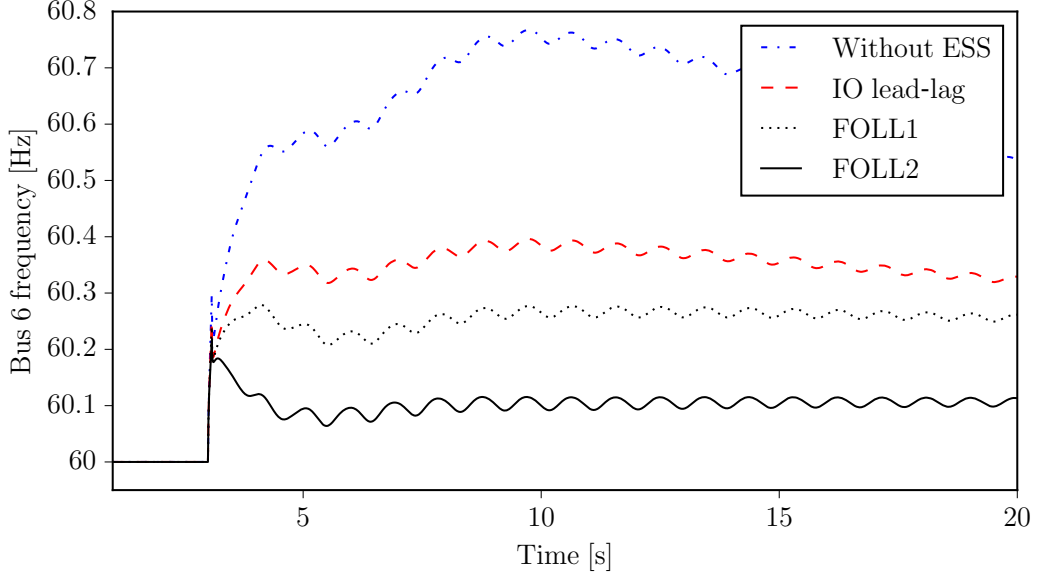


Figure 4.11: WSCC system with ESS frequency control: ORA parameters: $[\omega_b, \omega_h] = [10^{-3}, 10^1]$ rad/s, $N = 4$.

STATCOM

In this example, a STATCOM connected to bus 8 provides reactive power support. The reactive power variations provided by the STATCOM rely on the control of a Voltage Source Converter (VSC). The VSC is represented by an average value model. It consists of an AC/DC converter, an AC-side high voltage/medium voltage transformer, and a DC-side condenser. The VSC parameters are given in [109].

The VSC is controlled by employing a vector-current control strategy. The control is based on a dq-axis reference frame and a phase-locked loop refers all phases to the AC side voltage phasor angle [6]. The block diagram of the considered vector-current control is depicted in Figure 4.12. The d- and q- axis current components are decoupled by the inner control loop, through the controllers $H_{i,d}(s)$ and $H_{i,q}(s)$, respectively. In the STATCOM configuration, the outer control loop utilizes the d-axis and q-axis current components to provide regulation of the DC and AC voltages, through the controllers $H_{o,d}(s)$ and $H_{o,q}(s)$, respectively.

$H_{i,d}(s)$, $H_{i,q}(s)$, $H_{o,d}(s)$ and $H_{o,q}(s)$, are assumed to be FOPI controllers. The equations that describe the behavior of the FOPI are:

$$\begin{aligned} x_G^{(\gamma)} &= K_i u_G , \\ y_G &= K_p u_G + x_G , \end{aligned} \tag{4.34}$$

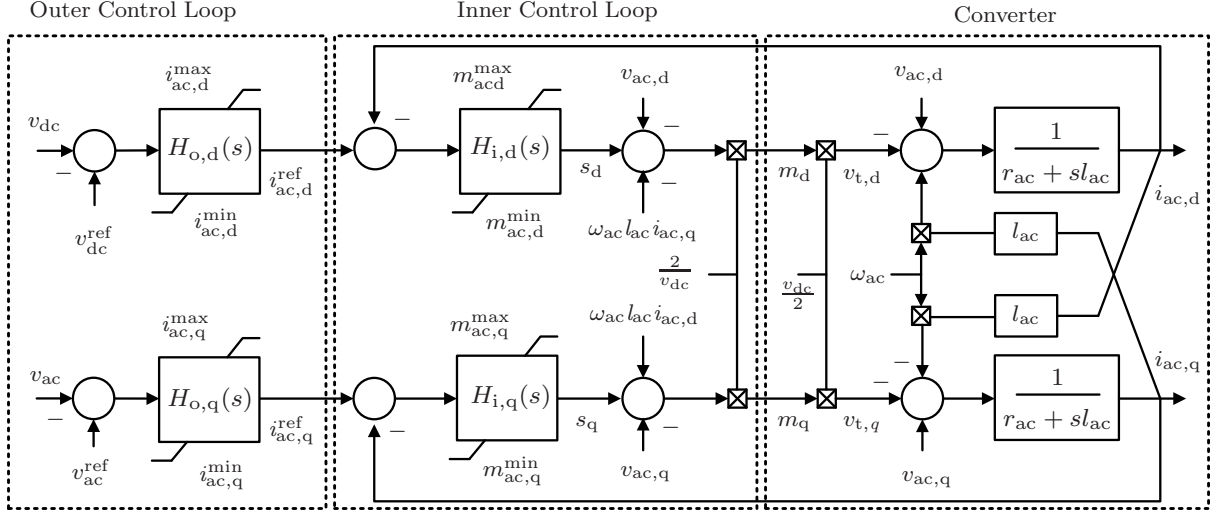


Figure 4.12: VSC outer and inner control in dq-frame.

where K_p and K_i , are the proportional and integral gains, respectively; x_G , y_G , are the state and output variable of the controller, respectively; and u_G is the controller input. The IO version of this controller, i.e. the classical PI controller, is obtained for $\gamma = 1$.

To study the impact of the STATCOM voltage regulation, a stressed operating condition of the WSCC system is considered. With this aim, the consumed power is increased by 60% compared to the base case. Then, for the purpose of transient analysis, an additional 15% consumption increase of the load connected at bus 8 is considered, occurring at $t = 3$ s. The system response is compared for the three following scenarios: without the STATCOM; with the STATCOM connected and all four controllers modeled as classical PIs; with the STATCOM connected and the four controllers modeled as ORA-based FOPIs.

The values of the STATCOM control parameters are shown in Table 4.2. The inner control loop parameters are tuned based on the pole cancellation technique as in [106], while the outer control loop parameters are tuned by optimizing the local bus voltage profile though trial-and-error.

Regarding the ORA parameters of the FOPIs, we have set the frequency range at $[10^{-3}, 10^2]$ rad/s for the inner control loop; at $[10^{-4}, 10^1]$ rad/s for the outer control loop. The dynamic order is $N = 5$ for all FOPI controllers.

Simulation results are presented in Figure 4.13. The use of multiple FOPIs for STATCOM voltage regulation is able to provide a significant improvement to the local voltage response.

Table 4.2: Parameters of the STATCOM controllers.

	PI		FOPI		
	K_p	K_i	K_p	K_i	γ
$H_{i,d}(s)$	0.2	20	0.2	20	0.20
$H_{i,q}(s)$	0.2	20	0.2	20	0.25
$H_{o,d}(s)$	50	25	50	25	0.40
$H_{o,q}(s)$	2.3	6	2.3	80	0.50

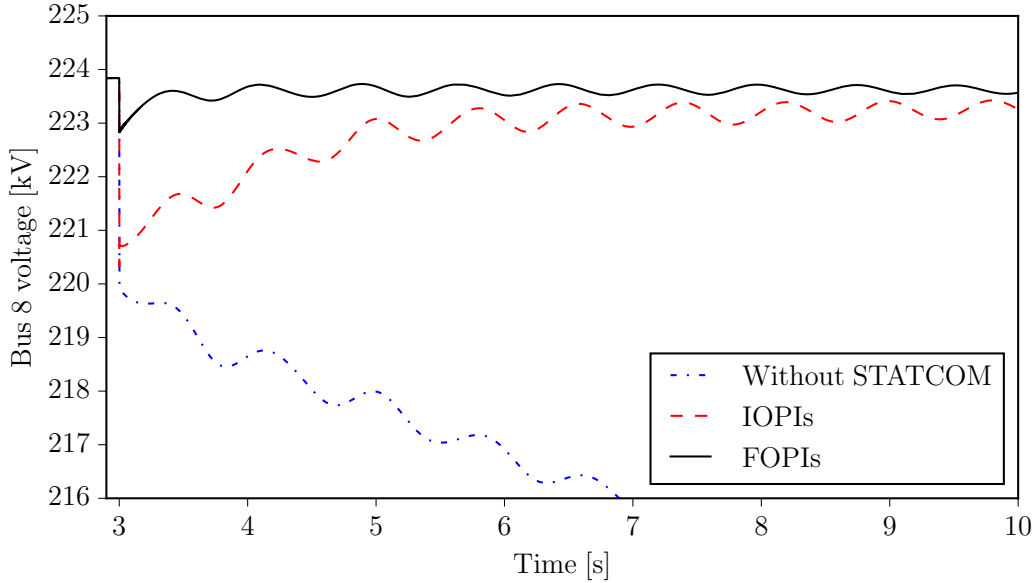


Figure 4.13: WSCC system with STATCOM: voltage at bus 8.

4.5.2 All-Island Irish Transmission System

This section presents simulation results based on a detailed model of the AIITS, which has been described in the case study of Section 2.6.1. In addition to the components described in Section 2.6.1, in the system is connected also an I-AGC.

For the needs of this case study, the AIITS model has been validated by utilizing the frequency data from a severe event that occurred in the real system [107]. The examined event refers to the tripping – on the 28-th of February 2018 – of the VSC-based HVDC link East-West Inter-Connector (EWIC) that connects the AIITS with the Great Britain transmission system. At that moment, Ireland was exporting 470 MW to Great Britain. Following the loss of the EWIC, the frequency in the Irish grid showed a peak of 50.42 Hz, which led to the triggering of over-frequency protections and wind farm active power generation curtailment.

A comparison of the actual system response and the one simulated with Dome is shown in Figure 4.14. As it can be seen, the simulated transient closely follows the real system behavior.

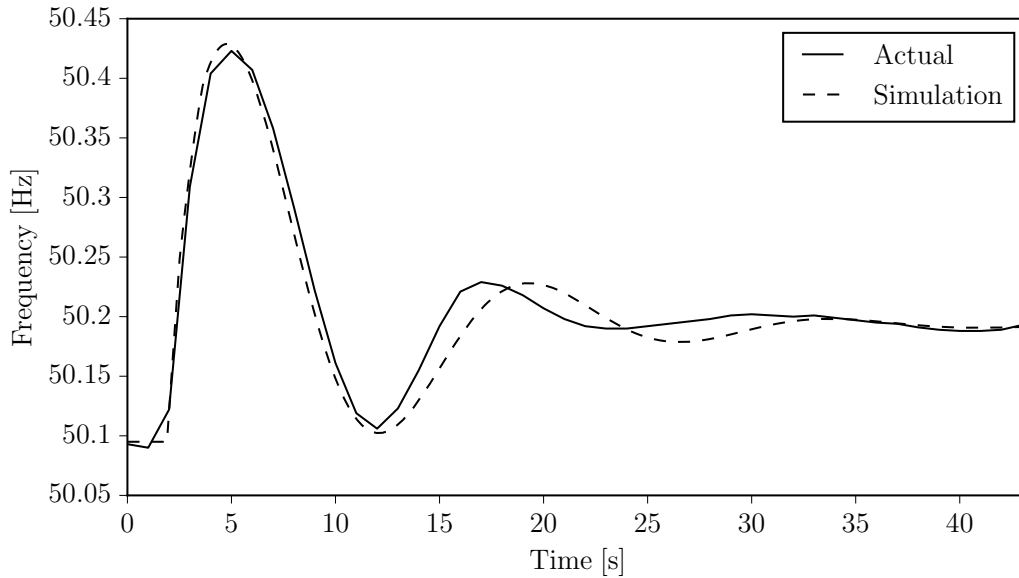


Figure 4.14: AIITS: frequency response following the loss of EWIC.

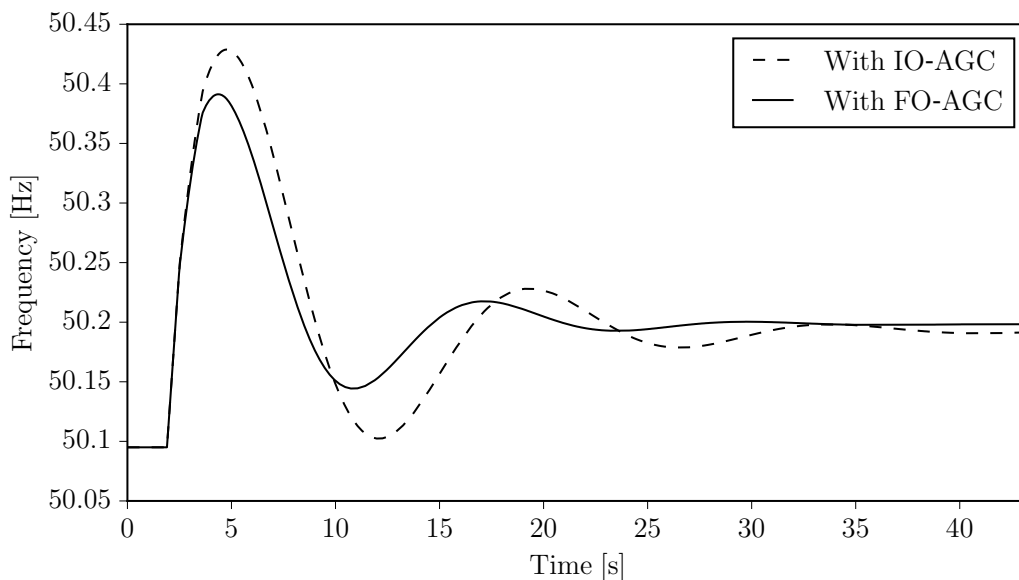


Figure 4.15: AIITS: impact of FO-AGC on frequency response.

We examine the impact of FOC on the secondary frequency regulation of the system. To this aim, the I-AGC is substituted with the FOI-AGC model described by (4.31). The parameters of the FOI-AGC are tuned to $K_i = 500$, $\gamma = 0.15$. The ORA parameters are $[\omega_b, \omega_h] = [10^{-3}, 10^1]$ rad/s, $N = 4$. Figure 4.15 shows the frequency response of the

system with I-AGC and FOI-AGC. The FOI-AGC is able to improve the frequency regulation of the AIITS.

4.6 Conclusions

The chapter studies the theory, stability analysis, computer implementation and practical design aspects of FOCs for power system applications. It provides a comprehensive theory on fractional calculus for control, as well as a detailed description of ORA-based FOCs. In all considered examples, the proposed FOCs are shown to perform better than the conventional IO versions while requiring only a little additional tuning effort. This is a general result that shows the potential of FOCs for power system applications.

Chapter 5

Time-Delay-based Control

5.1 Introduction

Time delays appear in many control systems mainly because it takes time to measure/acquire information, formulate a decision based on this information, and implement the decision to achieve a particular control mission. Delays arise in many applications, such as in network control systems when sending/receiving information between physical locations [4, 143]; in connected vehicle models due to delays in communication/sensing lines and human reaction times [55, 114]; and in the dynamics of multi-agent systems [112, 130].

Since delays are in general a source of poor performance and instability, many studies have focused on the fundamentals of explaining these characteristics within a control theoretic approach [17, 47, 51]. Along these lines, stability theory has been developed to address the peculiarities of systems with delays and these results were more recently combined with powerful convex optimization tools to study the stability of and design controllers for time-delay systems, see, e.g. [43].

While most results in the literature treat delays as undesirable, there is also a large amount of work that has focused on the advantages of having delays in a closed-loop setting. In these studies, the goal is to incorporate delays intentionally into the closed-loop and systematically analyze the dynamics to show that for certain delays and controllers, the closed-loop dynamics can behave more desirably based on certain metrics, such as response time [69, 131, 169]. A simple “delay-based” controller is the one in which a

derivative of a signal $\dot{x}(t)$ is approximated using a first order Euler's approximation:

$$\dot{x}(t) \approx \frac{x(t) - x(t - \tau)}{\tau}, \quad (5.1)$$

where $\tau > 0$ is the delay [69].

Delay-based controllers have a rich history with many promising directions [64, 129, 145]. Recent studies have focused on analytical tractability. This is a challenging effort since delays cause infinite dimensional system dynamics, study of which cannot be performed using standard tools available for finite-dimensional systems. A remedy to this was proposed by utilizing some salient features of algebraic geometry on a class of delay systems, and deriving analytical formulae that prescribe how to tune the delays and control gains to achieve a desired performance from these systems [131, 132, 134]. These results have been recently extended to distributed control of multi-agent systems with the goal to achieve fast consensus of agents [133].

Despite the aforementioned advances, benefits of utilizing time delays as part of controllers are yet to be fully explored in engineering applications. In electric power engineering, the vast majority of studies have emphasized only the destabilizing effects of time delays, e.g. in WADCs, see, [97, 148, 179]. Some studies have focused on modeling of delays that arise in a Wide-Area Measurement System (WAMS) [86, 176], while others have explored numerical methods for the stability analysis of power systems with inclusion of delays [83, 96]. Only very recently were delays in power systems viewed as tunable control design parameters [11, 135].

In light of the above discussion, there exists an opportunity to connect the recent results in time-delay systems literature toward improving the stability of power systems [166]. The main goal of this chapter is to systematically assess the impact of the structure and control parameter settings of delay-based PSSs on the small-signal stability and in particular on the damping characteristics of power system electromechanical oscillations.

The remainder of the chapter is organized as follows. Section 5.2 describes a comprehensive treatment for the stability analysis of small and large scale time-delay systems. Section 5.3 provides analytical results on the OMIB power system. Section 5.4 discusses a case study based on the IEEE standard 14-bus system model. Finally, conclusions are drawn in Section 5.6.

5.2 Spectral Analysis of Time-Delay Systems

This section provides first some preliminaries on the spectral properties of Linear Time-Invariant (LTI) systems with time delay. This is followed by further discussions on a benchmark second-order time-delay system. Then, for this system, the conditions that have to be satisfied to guarantee stability independently from the magnitude of the delay are rigorously deduced. Finally, this section shows how delay-independent stability enables “connected” stability regions.

5.2.1 Preliminaries

Since the study is concerned with the dynamics following small perturbations, it is relevant to provide here a concise discussion on the stability properties of linear systems affected by time delays. Given that the focus is on time-invariant systems, consider the following LTI system:

$$\dot{\mathbf{x}}(t) = \mathbf{A}_0 \mathbf{x}(t) + \mathbf{A}_1 \mathbf{x}(t - \tau), \quad (5.2)$$

where \mathbf{A}_0 and \mathbf{A}_1 are matrices with constant entries, delay is denoted by $\tau \geq 0$, and \mathbf{x} , $\mathbf{x} \in \mathbb{R}^n$, is the state vector. System (5.2) is a set of linear functional differential equations of retarded type, also known as linear Delay Differential Equations (DDEs). Moreover, this system is of retarded type, i.e. the highest derivative of the state is not influenced by the delay term.

To assess exponential stability of system (5.2), one must study its characteristic roots, which are the zeros of the system characteristic function given by:

$$\varphi(s, \tau) = \det(s\mathbf{I}_n - \mathbf{A}_0 - \mathbf{A}_1 e^{-\tau s}), \quad (5.3)$$

where the delay appears in the exponents as per Laplace transform. Due to the presence of the exponential function, this equation is not in polynomial form in s , and is often called a *quasi-polynomial* [111].

For a given delay τ , system (5.2) is exponentially stable if and only if all its characteristic roots have negative real parts. That is, for all λ satisfying $\varphi(\lambda, \tau) = 0$, $\text{Re}(\lambda^*) < 0$ holds [149]. While in principle stability definition is not different from that

for ODEs*, computing λ to assess stability is challenging due to the transcendental exponential terms in $\varphi(s, \tau)$ that arise due to the delay τ . This is because these terms bring about infinitely many characteristic roots, computation of which is prohibitive [143].

A remedy to the above issue is to recognize that the characteristic roots of the system vary on the complex plane in a continuum as the delay parameter changes in a continuum [34]. Hence, the only way the system may become unstable is that a characteristic root (or a pair of roots) touches the imaginary axis of the complex plane at $s = j\omega$, $\omega \in \mathbb{R}^+$. That is, whenever $\varphi(j\omega, \tau) = 0$ for some $\omega \geq 0$ and τ , the system “may be” in transition from stability to instability, or vice versa[†].

Definition 5.1. Consider that $\lambda_{i,i+1} = \alpha_i \pm j\beta_i$ define a pair of roots of (5.3). Then, the system is called:

- σ -stable, if $\forall i \in \mathbb{N}^*$, $\alpha_i < -\sigma$, where $\sigma > 0$ is a prescribed exponential decay rate [131].
- ζ -stable, if $\forall i \in \mathbb{N}^*$, $\frac{-\alpha}{\sqrt{\alpha^2 + \beta^2}} < \zeta$, where ζ is a prescribed dominant oscillation damping ratio.

In contrast to the concept of σ -stability, which has been employed in several studies, the term ζ -stability is, to the best of the author’s knowledge, first introduced for the needs of this thesis and, in particular, to the aim of studying the structure of the delay-gain parameter space and the damping characteristics of the system discussed in the case study of Section 5.4.

5.2.2 Analytical Study of Second-Order LTI Systems

This section presents some salient stability characteristics of second-order LTI systems, namely, a subset of the systems described by equation (5.2). These results are critical to establish the stability features of the OMIB power system.

*This is mainly because the spectrum of ‘retarded’ type LTI systems exhibit similar characteristics as those of ordinary differential equations [149].

[†]Note that it is necessary, but not sufficient, that the system has at least one root on the imaginary axis for its transition from stable to unstable behavior. For sufficiency, the system must be stable for $\tau - |\varepsilon|$, $|\varepsilon| \ll 1$.

5.2.2.1 System Description

Consider the LTI system:

$$\ddot{x}(t) + c_1 \dot{x}(t) + c_2 x(t) = -u(t), \quad (5.4)$$

where $c_1, c_2, \in \mathbb{R}$ and $u(t)$ is a scalar input. Next, let $u(t)$ be defined as a delay-based controller. Specifically, u is designed as PR controller:

$$u(t) = K_p \dot{x}(t) - K_r \dot{x}(t - \tau_r), \quad (5.5)$$

where K_p, K_r , are the proportional, retarded gains, respectively; and $\tau_r \geq 0$ is a constant delay. Combining (5.4) and (5.5), and taking the Laplace transform of the arising dynamics leads to the closed-loop system characteristic equation $q(s, \tau_r, K_r) = 0$, where

$$q(s, \tau_r, K_r) = s^2 + (c_1 + K_p) s + c_2 - K_r s e^{-s\tau_r}, \quad (5.6)$$

is the system characteristic equation.

5.2.2.2 Stability Analysis

In order to study the σ -stability of system (5.4), the change of variable $s \rightarrow (s - \sigma)$ is applied to (5.6). This yields the following quasi-polynomial:

$$\tilde{q}(\sigma, s, \tau_r, K_r) = \tilde{q}_0(\sigma, s) + \tilde{q}_1(\sigma, s) K_r e^{\sigma\tau_r} e^{-s\tau_r}, \quad (5.7)$$

where

$$\begin{aligned} \tilde{q}_0(\sigma, s) &= (s - \sigma)^2 + (c_1 + K_p)(s - \sigma) + c_2, \\ \tilde{q}_1(\sigma, s) &= -(s - \sigma). \end{aligned}$$

Recall that the roots of the characteristic equation change continuously with respect to variations of system parameters and time delays. The system can thus change from stable to unstable, and vice versa, only if a root (or a pair of roots) crosses the imaginary axis of the complex plane. Hence, the σ -stability of (5.4) can be assessed by finding the set

of crossing points $(\tau_r^{\text{cr}}, K_r^{\text{cr}})$, that satisfy:

$$\tilde{q}(\sigma, j, \tau_r^{\text{cr}}, K_r^{\text{cr}}) = 0, \quad (5.8)$$

where $s = j\omega$. The set $(\tau_r^{\text{cr}}, K_r^{\text{cr}})$ can be determined by considering the magnitude and the argument of (5.8), as follows [132]:

$$\tau_r^{\text{cr}} = \frac{1}{j\omega} \left(\text{Arg}(\tilde{q}_1(\sigma, j\omega)) - \text{Arg}(\tilde{q}_0(\sigma, j\omega)) + \frac{\pi}{2}(4\mu + \nu + 1) \right), \quad (5.9)$$

$$K_r^{\text{cr}} = \nu e^{-\sigma\tau_r^{\text{cr}}} \left| \frac{\tilde{q}_0(\sigma, j\omega)}{\tilde{q}_1(\sigma, j\omega)} \right|, \quad (5.10)$$

where $\nu = \pm 1$, $\mu = 0, \pm 1, \pm 2, \dots$. Equations (5.9) and (5.10), allow tracing the domains of stability that correspond to specified exponential decay rates, i.e. the σ -stability map in the (τ_r, K_r) space.

Finally, note that if the time-delayed state in (5.4) is not utilized, i.e. $K_r = 0$, then the closed-loop system behavior is determined by the polynomial $\tilde{q}_0(\sigma, s)$. In this case, dissipative terms included in the system are defined by the coefficient of s corresponding to the first derivative of the state:

$$c = c_1 + K_p. \quad (5.11)$$

Here, the coefficient c_1 defines the damping of the open-loop system oscillatory mode, while K_p defines the amount of non-delayed artificial damping introduced by the PR controller.

5.2.2.3 Delay-Independent Stability

Under certain conditions, LTI systems with delays can remain stable no matter how large/small the delays are. This phenomenon, known as delay-independent stability, offers the advantage of rendering the dynamics robustly stable against the delays.

The system (5.4) is stable regardless the magnitude of the time delay τ_r provided that certain conditions on the gain $K_r \in \mathcal{K}$, $\mathcal{K} \subset \mathbb{R}$, are satisfied. For a given set \mathcal{K} , a necessary condition for delay independent stability is that the roots of the system

characteristic equation never cross the imaginary axis, or equivalently:

$$q(j\omega, \tau_r, K_r) \neq 0, \quad \forall \tau_r \geq 0, \quad \forall K_r \in \mathcal{K}. \quad (5.12)$$

Using (5.11) in (5.12) yields:

$$\begin{aligned} & -\omega^2 + c j\omega + c_2 - K_r j\omega e^{-j\omega\tau_r} \neq 0 \\ \Rightarrow & \frac{-\omega^2 + c j\omega + c_2}{K_r j\omega} \neq e^{-j\omega\tau_r} \\ \Rightarrow & \frac{c}{K_r} + j \frac{1}{K_r} \left(\omega - \frac{c_2}{\omega} \right) \neq e^{-j\omega\tau_r}. \end{aligned} \quad (5.13)$$

Note that the real part of (5.13) does not depend on w , and thus, in the complex plane, the left hand side defines the vertical line with abscissa c/K_r . In addition, $e^{-j\omega\tau_r}$ defines in the complex plane a unit circle centred at $(0,0)$, regardless of the value of the delay τ_r . Then, the critical condition for delay independent stability is that the line c/K_r is tangent to the unit circle. Equivalently:

$$\frac{c}{K_r} = \pm 1 \quad \Rightarrow \quad c = \pm K_r. \quad (5.14)$$

From equation (5.14), the following cases are of interest [166]:

- If $c = -K_r^0 < 0$, $K_r = K_r^0 > 0$, the system is delay independent unstable in $\mathcal{K} = (-K_r^0, K_r^0)$. Moreover, since $c < 0$, the system is unstable around the origin of the τ_r - K_r plane. Hence, even if stable regions exist, these regions are guaranteed to be disconnected.
- If $c = 0$, there are no delay independent stable or unstable regions.
- If $c = K_r^0 > 0$, $K_r = K_r^0 > 0$, the system is delay independent stable in $\mathcal{K} = (-K_r^0, K_r^0)$. The existence of a delay independent stable region around the zero gain guarantees that there is a large connected stable domain in the τ_r - K_r plane. This feature is very important for two reasons: (i) there is the possibility that the dynamics can be characterized by high exponential decay rates for large delay values, (ii) the presence of a delay-independent stable region indicates that there exists at least one large, “connected” stable region from zero to infinite delay.

Notice that delay independent stable/unstable region is symmetric with respect to the gain K_r .

5.2.3 Linear Large-Scale Time-Delay Systems

For a second-order LTI system with PR control, such as the one discussed above, one can analytically identify the parameter regions with specified exponential decay rates, as well as the conditions for delay independent stability. However, real-world dynamical systems are larger in size and much more complex. Capturing the impact of delays on the behavior of large system models can be achieved only by carrying out a numerical analysis. Nevertheless, such studies must be carefully guided by the analytical understanding of small scale dynamical systems. This is the approach utilized below.

This section describes next how to assess the stability of large scale linear time-delay systems. To this aim, system (5.2) is extended to include multiple delays τ_i . The resulting LTI dynamical system is described through the following set of DDEs:

$$\dot{\mathbf{x}}(t) = \mathbf{A}_0 \mathbf{x}(t) + \sum_{i=1}^{\rho} \mathbf{A}_i \mathbf{x}(t - \tau_i), \quad (5.15)$$

where $\tau_i \geq 0$, $i = 1, 2, \dots, \rho$, The characteristic matrix of (5.15) has the following form [96]:

$$s\mathbf{I}_n - \mathbf{A}_0 - \sum_{i=1}^{\rho} \mathbf{A}_i e^{-s\tau_i}. \quad (5.16)$$

Since (5.16) is transcendental, it has infinitely many eigenvalues, and only an approximation of the solution is possible. Different approaches have been proposed to overcome this problem [96]. In this chapter, the DDE system (5.15) is transformed to a formally equivalent set of Partial Differential Equations (PDEs), which has infinite dimensions. The PDE system is then reduced to a finite dimensional problem through Chebyshev discretization [16, 21]. If N_C is the number of points of the Chebyshev differentiation matrix [96], then discretization leads to an approximate linear matrix pencil in the form:

$$s\mathbf{I}_{nN_C} - \mathbf{M}, \quad (5.17)$$

where the matrix \mathbf{M} has dimensions $nN_C \times nN_C$. The spectrum of (5.17) – which can be found using any common numerical method, e.g. the QR algorithm [42] – represents an approximate spectrum of (5.16). The Chebyshev discretization technique has been successfully applied to single and multiple time-delay systems, e.g. to power systems with constant and stochastic delays affecting damping controllers [86, 168].

After the above analysis is complete, one can reveal the most critical eigenvalue(s), by comparing the damping ratios ζ_i of all computed eigenvalues. This work is concerned with the parametric analysis in a delay versus control gain space. The above analysis therefore allows building a map of specified dominant oscillation damping ratio ζ . In the remainder of the chapter, this map is referred to as the ζ -*stability map*.

5.2.4 Non-Linear Large-Scale Time-Delay Systems

Consider the non-linear DAE power system model (2.1), where for simplicity, but without loss of generality, no inputs are included and $\mathbf{T} = \mathbf{I}_n$, $\mathbf{R} = \mathbf{0}_{m,n}$, see (2.2). This system can be written as:

$$\begin{aligned}\dot{\mathbf{x}} &= \mathbf{f}(\mathbf{x}, \mathbf{y}), \\ \mathbf{0}_{m,1} &= \mathbf{g}(\mathbf{x}, \mathbf{y}).\end{aligned}\tag{5.18}$$

The presence of time delays, for example, in control loops, changes the set of DAEs (5.18) into a set of Delay Differential-Algebraic Equations (DDAEs). Inclusion of time delays in (5.18) yields the following system:

$$\begin{aligned}\dot{\mathbf{x}} &= \mathbf{f}(\mathbf{x}, \mathbf{y}, \mathbf{x}_d, \mathbf{y}_d), \\ \mathbf{0}_{m,1} &= \mathbf{g}(\mathbf{x}, \mathbf{y}, \mathbf{x}_d, \mathbf{y}_d),\end{aligned}\tag{5.19}$$

where $\mathbf{x}_d, \mathbf{x}_d \in \mathbb{R}^{n_d}$, and $\mathbf{y}_d, \mathbf{y}_d \in \mathbb{R}^{m_d}$ are the delayed state and algebraic variables, respectively. Suppose that the system includes a single constant delay τ . Then, one has:

$$\begin{aligned}\mathbf{x}_d &= \mathbf{x}(t - \tau), \\ \mathbf{y}_d &= \mathbf{y}(t - \tau),\end{aligned}\tag{5.20}$$

where t is the current time.

The equilibrium of (5.20) is defined in the time interval $[-\tau, 0]$. This implies the assumption that a time equal to τ has to elapse before a valid equilibrium of the system

is reached. Although there is no theoretical upper bound to τ , the aforementioned assumption may render the consideration of a very large value impractical. A limit case example is a PSS whose control signal is affected by an infinite delay. In principle, infinite time has to pass before the equilibrium of a system with inclusion of such PSS is obtained. The issue is resolved by modeling only delays that lie in the time-scale of the dynamics of interest. Variables affected by delays that are much larger than the time-constants of the system dynamics are, in fact, irrelevant to the model under study which, in turn, can be conveniently modified to disregard such variables. In the above limit case example, the delayed PSS does not have any effect on the system and thus, it can be simply disregarded from the system model. In this thesis, only delays that lie in the same time scale with the rest of the system dynamics are considered.

When \mathbf{y}_d does not appear in the algebraic equations of (5.19), this leads to the index-1 Hessenberg form of DDAEs:

$$\begin{aligned}\dot{\mathbf{x}} &= \mathbf{f}(\mathbf{x}, \mathbf{y}, \mathbf{x}_d, \mathbf{y}_d), \\ \mathbf{0}_{m,1} &= \mathbf{g}(\mathbf{x}, \mathbf{y}, \mathbf{x}_d).\end{aligned}\tag{5.21}$$

Model (5.21) is adopted instead of (5.19), since it allows simplifying the form of the characteristic equation of the corresponding linearized system, while being adequate for the applications considered in this chapter. The interested reader can find a detailed study on the SSSA for non-index 1 Hessenberg form systems of DDAEs in [98].

For sufficiently small disturbances, and for the purpose of SSSA, see Chapter 2, (5.21) can be linearized around a valid stationary point, as follows:

$$\Delta\dot{\mathbf{x}} = \mathbf{f}_x\Delta\mathbf{x} + \mathbf{f}_y\Delta\mathbf{y} + \mathbf{f}_{x_d}\Delta\mathbf{x}_d + \mathbf{f}_{y_d}\Delta\mathbf{y}_d,\tag{5.22}$$

$$\mathbf{0}_{m,1} = \mathbf{g}_x\Delta\mathbf{x} + \mathbf{g}_y\Delta\mathbf{y} + \mathbf{g}_{x_d}\Delta\mathbf{x}_d,\tag{5.23}$$

where \mathbf{f}_x , \mathbf{f}_y , \mathbf{g}_x , \mathbf{g}_y , are the Jacobian matrices of the delay-free variables; and \mathbf{f}_{x_d} , \mathbf{f}_{y_d} , \mathbf{g}_{x_d} , are the Jacobian matrices of the delayed variables of (5.22) and (5.23).

In the linearized system (5.22), (5.23), the algebraic variables $\Delta\mathbf{y}$, $\Delta\mathbf{y}_d$ can be eliminated, under the assumption that \mathbf{g}_y is not singular. Substitution of (5.23) into

(5.22) yields:

$$\Delta \dot{\mathbf{x}}(t) = \mathbf{A}_0 \Delta \mathbf{x}(t) + \mathbf{A}_1 \Delta \mathbf{x}(t - \tau) + \mathbf{A}_2 \Delta \mathbf{x}(t - 2\tau), \quad (5.24)$$

where

$$\begin{aligned} \mathbf{A}_0 &= \mathbf{f}_x - \mathbf{f}_y \mathbf{g}_y^{-1} \mathbf{g}_x, \\ \mathbf{A}_1 &= \mathbf{f}_{x_d} - \mathbf{f}_y \mathbf{g}_y^{-1} \mathbf{g}_{x_d} - \mathbf{f}_{y_d} \mathbf{g}_y^{-1} \mathbf{g}_x, \\ \mathbf{A}_2 &= -\mathbf{f}_{y_d} \mathbf{g}_y^{-1} \mathbf{g}_{x_d}. \end{aligned}$$

Applying the Laplace transform in (5.24) yields the following, quasi-polynomial characteristic matrix:

$$s\mathbf{I}_n - \mathbf{A}_0 - \mathbf{A}_1 e^{-s\tau} - \mathbf{A}_2 e^{-2s\tau}. \quad (5.25)$$

Note that the form of the characteristic matrix (5.25) can be retrieved from (5.16) for $\rho = 2$ and $\tau_2 = 2\tau_1$.

5.3 One-Machine Infinite-Bus System

Consider the simple example of the OMIB system shown in Figure 5.1. This section first describes the classical machine model and then includes in such a model a simplified PSS with a PR control, i.e. with two input signals, one instantaneous and one delayed.

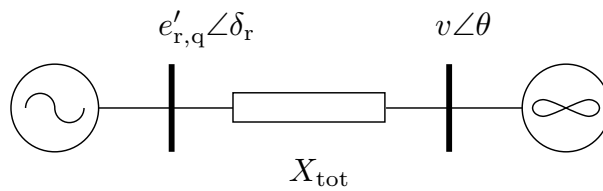


Figure 5.1: OMIB system: single-line diagram.

5.3.1 Classical Model

The classical per-unit model of this system is as follows [74]:

$$\begin{aligned} \dot{\delta}_r &= \Omega_b(\omega_r - 1), \\ M\dot{\omega}_r &= P_m - P_e(\delta) - D(\omega_r - 1), \end{aligned} \quad (5.26)$$

where δ_r , ω_r , are the rotor angle and the rotor speed of the synchronous machine, respectively; P_m and P_e are the mechanical, electrical power output of the machine, respectively. In addition, M is the machine mechanical starting time; D is the machine rotor damping coefficient; and Ω_b is the nominal synchronous angular frequency in rad/s.

The electrical power P_e is described by the following non-linear expression:

$$P_e(\delta_r) = \frac{e'_{r,q}v}{X_{\text{tot}}}\sin(\delta_r - \theta), \quad (5.27)$$

where v , θ , are the (constant) voltage magnitude and angle at the infinite bus; $e'_{r,q}$ is the internal electromotive force of the synchronous machine, which is taken as constant, by assuming an integral AVR. X_{tot} is the total reactance, comprising the machine transient reactance (X'_d) and the line reactance (X), where the latter is referred to the machine power base.

Defining the system state vector as $[\delta_r \ \omega_r]^T$, making use of (5.27) and linearizing (5.26) around a valid equilibrium $[\delta_{r,o} \ \omega_{r,o}]^T$ yield:

$$\Delta\dot{\delta}_r = \Omega_b\Delta\omega_r, \quad (5.28)$$

$$M\Delta\dot{\omega}_r = -\frac{e'_{r,q}v\cos(\delta_{r,o} - \theta)}{X_{\text{tot}}}\Delta\delta_r - D\Delta\omega_r, \quad (5.29)$$

where $\Delta\delta_r = \delta_r - \delta_{r,o}$ and $\Delta\omega_r = \omega_r - \omega_{r,o}$. Equations (5.28) and (5.29) can be rewritten as a second-order LTI system:

$$\Delta\ddot{\delta}_r + d\Delta\dot{\delta}_r + b\Delta\delta_r = 0, \quad (5.30)$$

where $\Delta\delta_r \equiv x$ and

$$b = \frac{\Omega_b e'_{r,q} v \cos(\delta_{r,o})}{M X_{\text{tot}}}, \quad d = \frac{D}{M}. \quad (5.31)$$

5.3.2 Power System Stabilizer with PR Control

In its simplest form, the PSS measures the machine rotor speed, i.e. $\dot{\delta}_r = \omega_r$, and introduces a fictitious damping into the swing equation (5.28). The linearized closed-loop system can therefore be written as:

$$\Delta\ddot{\delta}_r + d\Delta\dot{\delta}_r + b\Delta\delta_r = -u(\Delta\dot{\delta}_r). \quad (5.32)$$

The damping controller is modeled here as a proportional PSS with two control channels, one with and one without delay. The PSS diagram is shown in Figure 5.2.

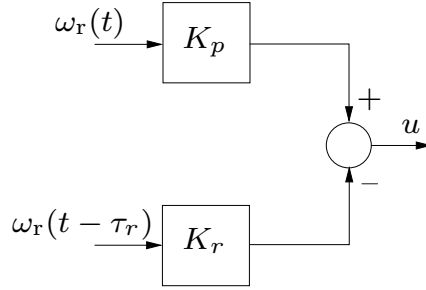


Figure 5.2: PR control based PSS diagram.

Dual-channel PSSs have been employed in the past, e.g. as decentralized-hierarchical schemes for wide-area stabilizing control [65]. The dual-channel PSS output is described as:

$$u = K_p \Delta\dot{\delta}_r - K_r \Delta\dot{\delta}_r(t - \tau_r). \quad (5.33)$$

Merging (5.28), (5.32) and (5.33) leads to the following closed-loop system representation:

$$\Delta\ddot{\delta}_r + \left(d + \frac{K_p}{\Omega_b}\right) \Delta\dot{\delta}_r + b\Delta\delta_r - \frac{K_r}{\Omega_b} \Delta\dot{\delta}_r(t - \tau_r) = 0, \quad (5.34)$$

which is exactly in the form of (5.4)-(5.5). Applying the Laplace transform and substituting the initial conditions $\Delta\delta_r(0) = \Delta\dot{\delta}_r(0) = 0$, yields the following characteristic quasi-polynomial:

$$q(s, \tau_r, K_r) = s^2 + \left(d + \frac{K_p}{\Omega_b}\right) s + b - \frac{K_r}{\Omega_b} s e^{-s\tau_r}. \quad (5.35)$$

Comparing the quasi-polynomial (5.35) with the one in (5.6), one has $c_1 = d$, $c_2 = b$, $= \Omega_b^{-1}$. Therefore, the analysis of σ -stability and the conditions for delay independent

stability can be studied through the derivations of Section 5.2.2. The amount of friction included in the delay-free OMIB system is according to (5.11):

$$c = d + \frac{K_p}{\Omega_b}. \quad (5.36)$$

The critical condition for which the OMIB system is delay independent stable is that $\Omega_b c / K_r$ is tangent to the unit circle. Equivalently, one has:

$$\frac{\Omega_b c}{K_r} = \pm 1 \quad \Rightarrow \quad c = \pm \frac{K_r}{\Omega_b}. \quad (5.37)$$

5.3.3 Illustrative Example

We provide a numerical example on the closed-loop OMIB system. Let $e'_{r,q} = 1.22$ pu, $v = 1$ pu, $\theta = 0$ rad, $P_m = 1$ pu, $X_{\text{tot}} = 0.7$ pu. Then, the initial value $\delta_{r,o}$ of the rotor angle is given by:

$$\delta_{r,o} = \arcsin \left(\frac{P_m X_{\text{tot}}}{v e'_{r,q}} \right). \quad (5.38)$$

The examined equilibrium is hence $[0.61, 1]^T$. Let also $M = 5$ MW s/MVA, and $\Omega_b = 100\pi$ rad/s (50 Hz system). Then, $b = 89.756$ pu in (5.30). The following sections discuss the σ -stability map of the system for the three cases of negative, zero and positive values of c .

Case 1

For $c = -0.4 < 0$, the stability map is shown in Figure 5.3. The map has a symmetric delay independent unstable region obtained for $K_r \in (-125.6, 125.6)$. In addition, PR control can stabilize the system, provided that the delay is $\tau_r < 0.131$ s and a proper $K_r > 0$ is selected (see e.g. point $\Sigma_1(0.05, 729)$).

There also exist stable regions of the map in Figure 5.3 for delays higher than 0.131 s. For example, the system is stable around the point $\Sigma_3(0.30, -763.4)$. Note, however, that obtaining the equilibrium of a delayed system implies that a time equal to the maximum delay included in the system has elapsed but, meanwhile, the system may have been already rendered unstable. Indeed, Figure 5.3 indicates that there is no path

to Σ_3 without crossing the system stability boundary, which implies that the system necessarily becomes unstable before actually reaching Σ_3 .

The effect of crossing the stability boundary of the closed-loop OMIB system is illustrated with a time domain simulation. Suppose that the non-linear system (5.26) with the inclusion of the PR controller (5.33), operates around the stable equilibrium defined by the point Σ_1 of Figure 5.3.

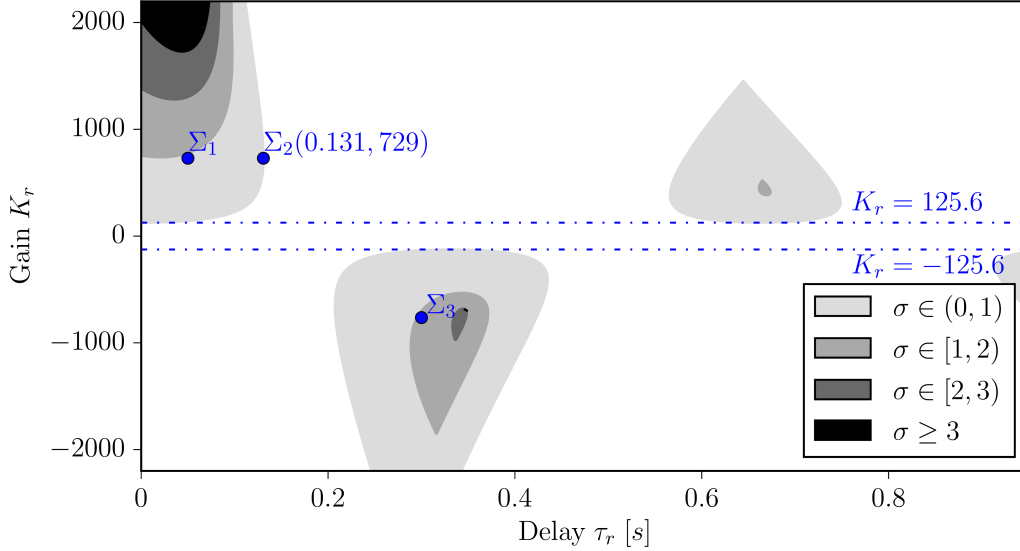


Figure 5.3: Closed-loop linearized OMIB system: σ -stability map in the τ_r - K_r plane, $c = -0.4$.

The system is numerically integrated considering a small noise on the measurement of the OMIB rotor speed. The noise is a normal process with zero mean and standard deviation of 0.0002. The noise amplitude is set to a small value with the purpose of showing the dynamics of the system in a neighbourhood of the equilibrium point. At $t = 2$ s, the gain and delay are switched to $K_r = -765$ and $\tau_r = 0.3$, respectively, so that the system is set at the new equilibrium point Σ_3 .

Figure 5.4 shows the simulation result, and indicates that, as expected, attempting to jump to a different, not connected stable region by crossing the stability boundary during a transient, renders the system unstable. Thus, Σ_3 is an example of infeasible stationary point, and thus, the delay margin of the system is 0.131 s.

Case 2

The σ -stability map for $c = 0$ is presented in Figure 5.5. In this case, the stability of the system depends on the magnitude of the delay, regardless of the value of the gain K_r . In

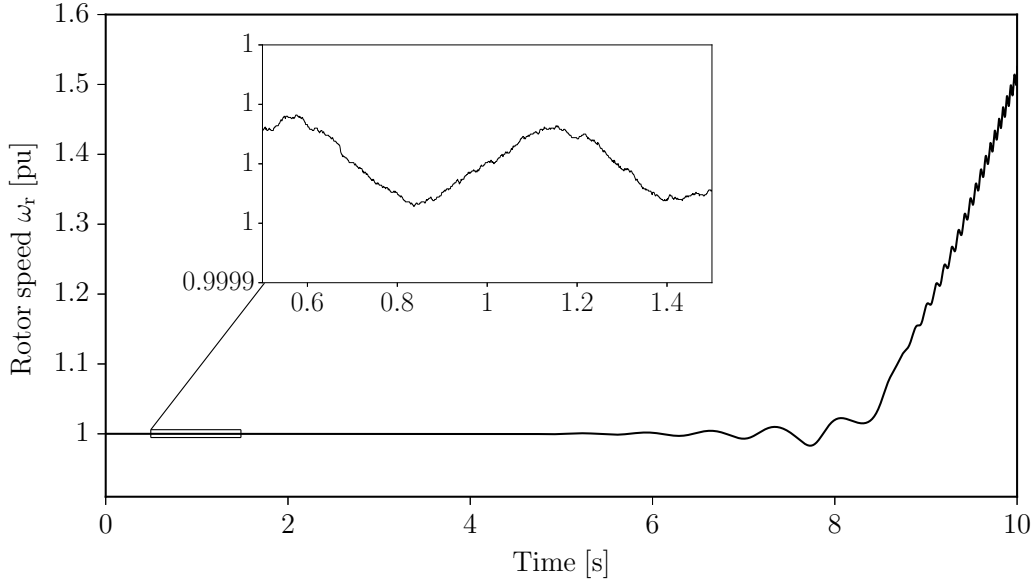


Figure 5.4: Closed-loop non-linear OMIB system (5.26) with noisy rotor speed measurement: the equilibrium is switched from Σ_1 to Σ_3 at $t = 2$ s.

fact, the horizontal line $K_r = 0$ comprises bifurcation points. The delay-free closed-loop system is stable for $K_r > 0$ and unstable for $K_r < 0$. Provided that a proper positive K_r value is selected and that $\tau_r < 0.166$ s (see point Σ_4), the delayed system is stable.

There also exist stable regions for $\tau_r > 0.166$ s. For example, the system is small-signal stable around Σ_5 . However, similarly to the discussion of Case 1, the system will likely lose stability before actually reaching e.g. Σ_5 . An exception occurs if the system crosses Σ_4 , which is a bifurcation point that connects two stable regions. In this scenario, the first order information provided by the linearized system in Figure 5.5 is inconclusive on the feasibility of operating at Σ_5 .

Case 3

The stability map for $c = 0.4 > 0$ is shown in Figure 5.6. In this case, the stable region is compact. For $K_r \in (-125.6, 125.6)$ the system is stable regardless of the magnitude of the delay τ_r . Moreover, all points of Figure 5.6 with $\sigma > 0$ represent stable and feasible stationary points of the linearized OMIB system. For example, such points are $\Sigma_6(0.13, 400)$ and $\Sigma_7(0.35, -410)$.

The results of a time domain simulation, including the same noise model on the rotor speed measurement as in Case 1, are shown in Figure 5.7. At $t = 2$ s, the system

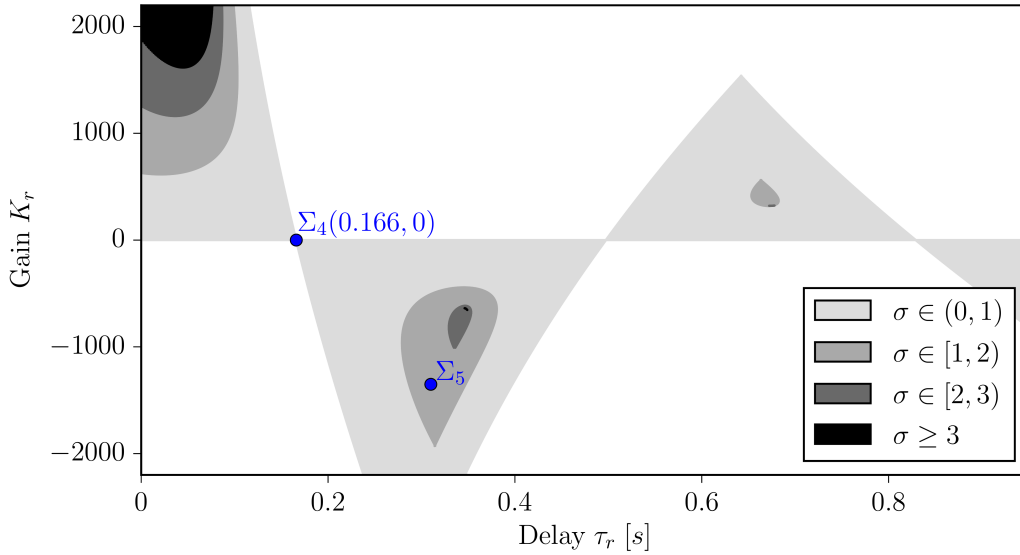


Figure 5.5: Closed-loop linearized OMIB system: σ -stability map in the τ_r - K_r plane, $c = 0$.

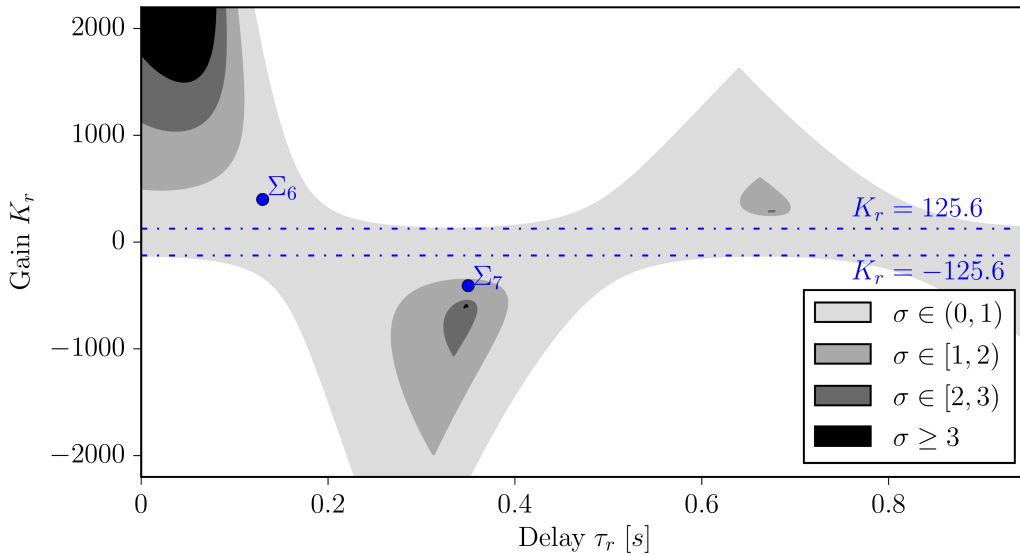


Figure 5.6: Closed-loop linearized OMIB system: σ -stability map in the τ_r - K_r plane, $c = 0.4$.

equilibrium is switched from Σ_6 to Σ_7 . The trajectory shows that the machine maintains synchronism.

Overall, proper design of the PSS given by the PR law (5.33) allows unifying the σ -stable regions, and thus allows one to operate the OMIB system under the presence of large delays. In particular, this is achieved by properly adjusting the control parameter K_p which introduces delay-free artificial damping to the system.

Finally, the delay τ_r in this example is assumed to be a fully controlled parameter. However, the above discussion is relevant also for systems with inherent delays. For the sake of example, consider again point Σ_6 of Figure 5.6. Suppose that the corresponding

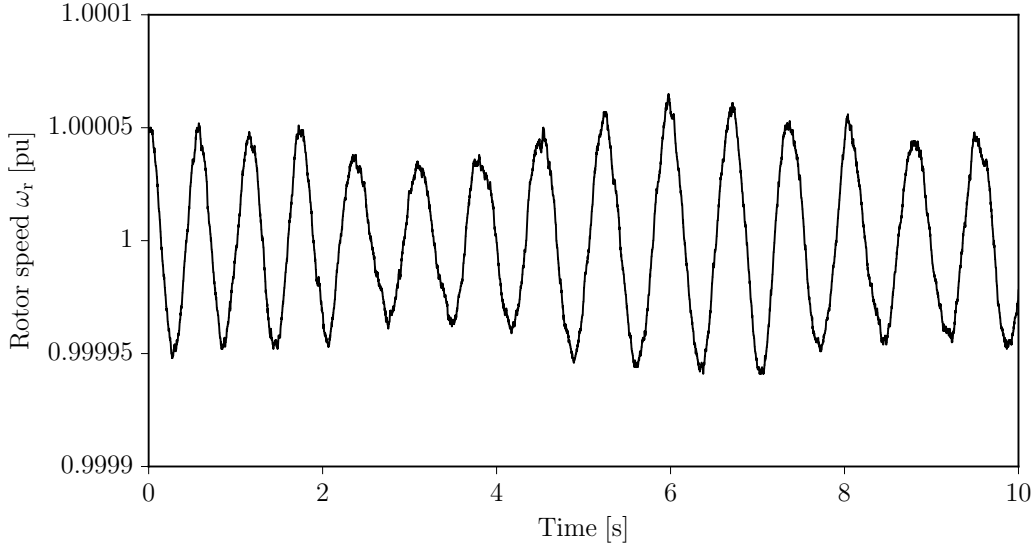


Figure 5.7: Closed-loop non-linear OMIB system with noisy rotor speed measurement: the equilibrium is switched from Σ_6 to Σ_7 at $t = 2$ s.

delay, i.e. 0.13 s, represents an uncontrolled physical phenomenon, e.g. the latency of a measurement transmitted through a communication system. In power systems, this situation describes, for example, the behavior of a wide area measurement system [86]. In such a scenario, the parameter τ_r can be adaptively adjusted to add an artificial delay, which ensures that the system under the total delay $0.13 + \tau_r$ always operates at a region of high exponential decay rate. Along these lines, see, for example, the idea of delay scheduling in [113].

5.4 Case Study: IEEE 14-bus System

We next study the stability characteristics of the IEEE 14-bus system. The single-line diagram of this system is depicted in Figure 5.8. The system consists of fourteen buses, five synchronous machines, twelve loads, twelve transmission lines and four transformers. All machines are equipped with AVRs. The static and dynamic data of the system can be found in [92]. Simulations in this section are carried out using Dome.

Without any PSS installed to the system, SSSA shows that the rightmost pair of eigenvalues is $0.3522 \pm j9.12$, and thus, the system is unstable around the examined equilibrium. A PSS is utilized to stabilize the system. The PSS model employed in this

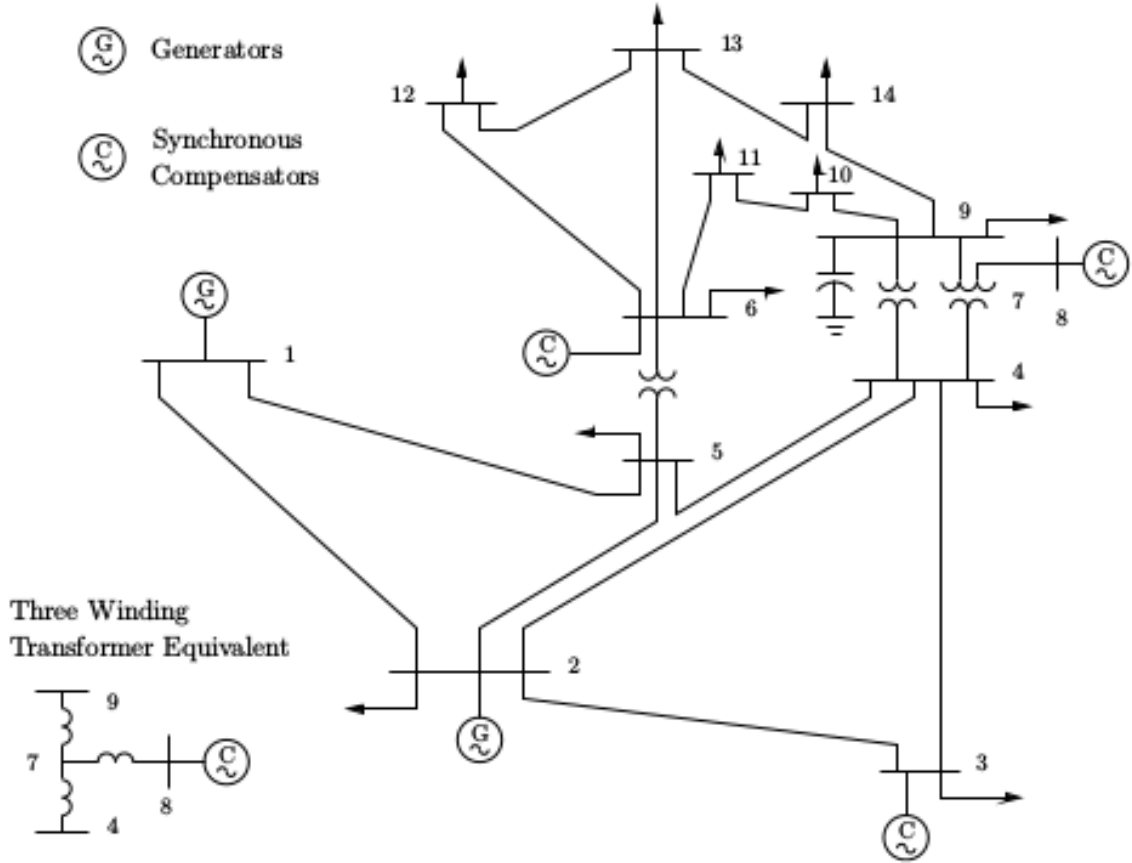


Figure 5.8: IEEE 14-bus system: single-line diagram.

section is described by the following DAEs:

$$\begin{aligned}
 T_w \dot{v}_1 &= -K_w v_{si} - v_1, \\
 T_2 \dot{v}_2 &= \left(1 - \frac{T_1}{T_2}\right) (K_w v_{si} + v_1) - v_2, \\
 T_4 \dot{v}_3 &= \left(1 - \frac{T_3}{T_4}\right) \left(v_2 + \frac{T_1}{T_2} (K_w v_{si} + v_1)\right) - v_3, \\
 0 &= v_3 + \frac{T_3}{T_4} \left(v_2 + \frac{T_1}{T_2} (K_w v_{si} + v_1)\right) - v_{so},
 \end{aligned}$$

where v_1, v_2, v_3 are the PSS state variables; T_w, T_1, T_2, T_3, T_4 are time constants; K_w is the PSS gain. In addition, the input v_{si} is the local rotor speed, which, depending on the examined scenario, may be delayed or not. Finally, the output signal v_{so} is an additional input to the local AVR reference, so that the PSS provides damping of electromechanical oscillations through excitation control. The PSS block diagram is depicted in Figure 5.9.

To study the effect of time-delayed damping control on the small signal stability of the IEEE 14-bus system, two damping control configurations are compared, namely, a

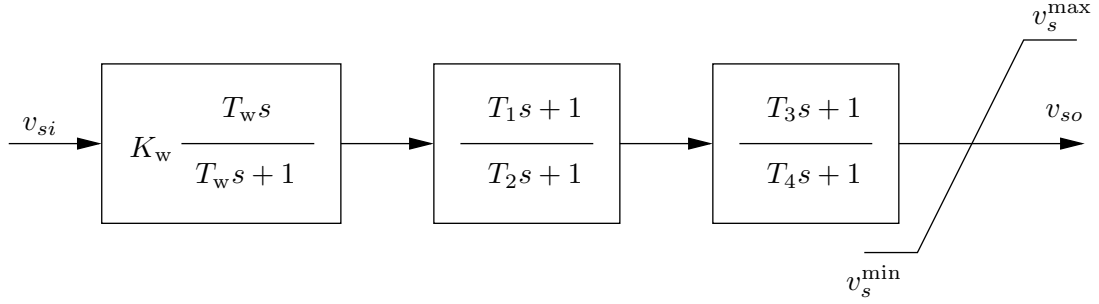


Figure 5.9: Power system stabilizer block diagram.

conventional PSS with delayed input signal; and a PSS that consists of two channels, one delayed and one non-delayed. In both cases, the damping controller is installed at the AVR of the synchronous machine connected at bus 1.

The impact of time delay in each case is evaluated by means of constructing the ζ -stability map in the delay-control gain space. For each point of the plane, an eigenvalue analysis is carried out by applying the Chebyshev discretization technique (see Section 5.2.3). The spectrum of the approximate matrix pencil is calculated using the QR algorithm with LAPACK [8]. Then, comparison among the eigenvalues allows obtaining the most poorly damped one determining the ζ -stability.

Standard PSS with Delayed Input Signal

The employed PSS model is as shown in Figure 5.9. The control input signal is considered to be the delayed local rotor speed measurement:

$$v_{si} = \omega_{r,1}(t - \tau), \quad (5.39)$$

where τ is an intentional constant delay. The PSS time constant values are summarized in Table 5.1.

Table 5.1: IEEE 14-bus system: PSS parameters.

$$T_1 = T_3 = 0.28 \text{ s}, T_2 = T_4 = 0.02 \text{ s}, T_w = 10 \text{ s}$$

The dynamic order of the system is 54. Setting the number of points of the Chebyshev differentiation matrix to $N_C = 10$, 540 eigenvalues are found in total. The system ζ -stability map in the τ - K_w plane is shown in Figure 5.10. The map consists of distinct and not compact stable regions, which stems from the fact that, without the PSS, the

system is unstable. For $K_w \in (-0.55, 0.65)$, the system is unstable regardless of the magnitude of the delay. The delay margin of the system is 0.104 s and is obtained for $K_w = 1.5$. Thus, operation under the presence of a large delay, e.g. 0.35 s, is infeasible.

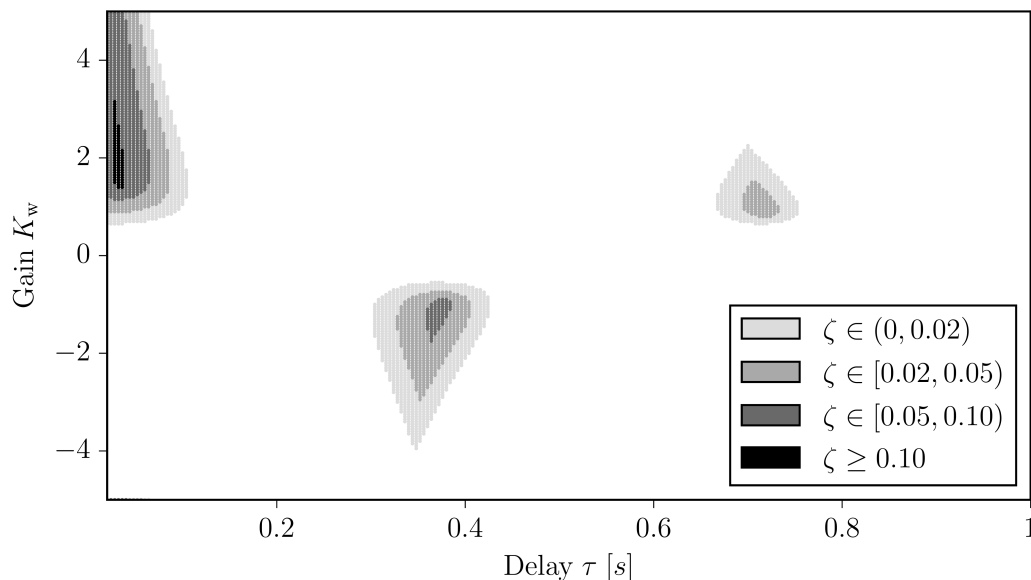


Figure 5.10: IEEE 14-bus system: ζ -stability map in the τ - K_w plane.

Dual-channel PSS

In the OMIB system example of Section 5.3, a compact stable region in the delay-control gain plane can be achieved by employing a PR-based PSS scheme, tuned to operate the system at a point with good damping characteristics.

We apply the same principle in the IEEE 14-bus system. To this aim, we test a PSS with two control channels: first channel is not delayed; second channel is delayed. The examined dual-channel PSS configuration is shown in Figure 5.11.

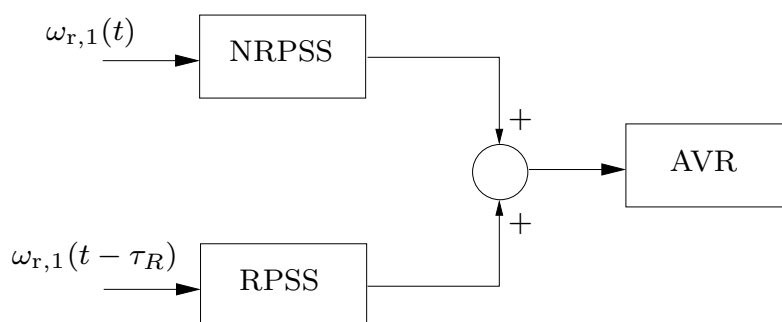


Figure 5.11: Dual-channel PSS configuration.

The first channel, namely Not Retarded PSS (NRPSS), is tuned to render the non-delayed system small-signal stable. The control input of NRPSS is the local rotor speed $\omega_{r,1}(t)$. The second channel, namely Retarded PSS (RPSS), tunes the delay dynamics so that the system operates at a point with good damping characteristics. The input signal of the RPSS is the delayed rotor speed $\omega_{r,1}(t - \tau_R)$, where $\tau_R \geq 0$ is the magnitude of the delay. The time constants of both NRPSS and RPSS are as summarized in Table 5.1. In addition, $K_{w,P}$ and $K_{w,R}$ denote the gains of NRPSS and RPSS, respectively. An analogy between the dual-channel PSS configuration and the PR-based PSS of the OMIB system example of Section 5.3 is given in Table 5.2.

Table 5.2: Analogy between the examined dual-channel PSS configuration and the PR controller of Section 5.3.

System	OMIB	IEEE 14-bus
Non-retarded control	Proportional K_p	NRPSS
Retarded control	K_r, τ_r	RPSS

The NRPSS gain is tuned so that the system without delayed control is small-signal stable. For $K_{w,P} = 5$, $K_{w,R} = 0$, SSSA shows that the rightmost pair of eigenvalues is $-0.1376 \pm j0.0203$. The most poorly damped pair is $-0.5171 \pm j7.2516$, which yields a damping ratio 0.071.

Considering $K_{w,P} = 5$, the ζ -stability map of the system is constructed in the $K_{w,R}-\tau_R$ plane. In this case, the dynamic order of the system is 57 and, using $N_C = 10$, 570 eigenvalues are in total calculated to obtain each point of the map. The resulting map, presented in Figure 5.12, shows that the stable region is compact, while the area with $K_{w,R} \in (-2.4, 2.5)$ is delay independent stable. In Figure 5.12, maximum damping is 0.178 and is achieved for $\tau_R = 0.34$ s, i.e. a relatively large delay value.

5.5 Remarks

Delays arising in power system damping controllers are typically not tunable but inherent, i.e. they represent measurement and/or communication latencies. Although studying the impact of inherent delays is not the main focus of this chapter, this section briefly discusses their relevance to the results presented above.

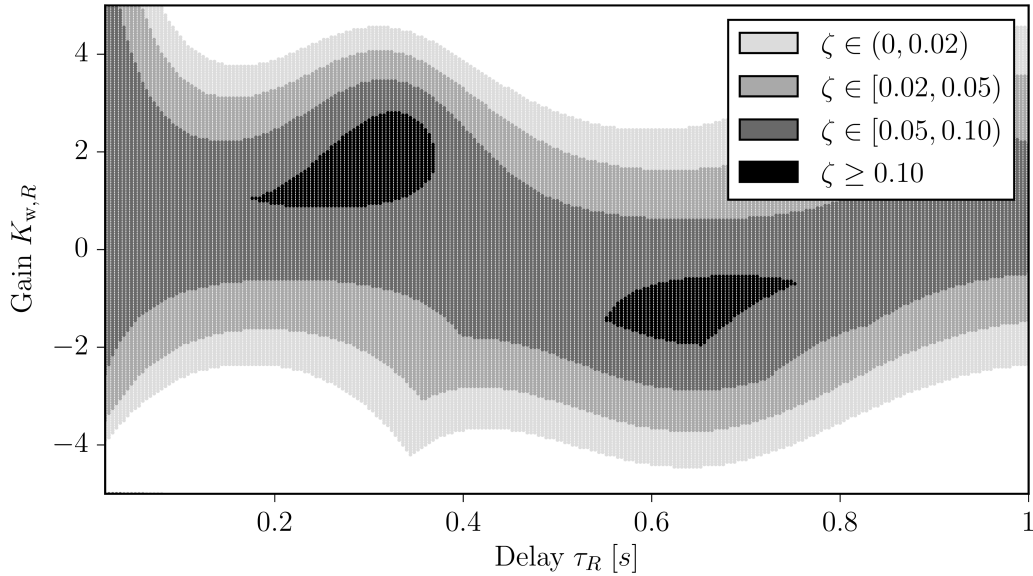


Figure 5.12: IEEE 14-bus system: ζ -stability map in the τ_R - $K_{w,R}$ plane.

Regarding the standard PSS with delayed input signal of Section 5.4, assuming that τ is inherent does not change the structure of the stability map in Figure 5.10 but only changes the interpretation of the role of delay. Since in this case τ is not tunable, the small delay margin of 0.104 s may be a severe stability issue. For inherent delays that have a small magnitude, a delay-dependent design of a standard PSS allows increasing the delay margin and avoid instability.

In fact, in Figure 5.10, the region of the highest damping $\zeta \geq 0.10$ is obtained for a non-zero delay value. The closed-loop loci related to the critical system mode have an angle of departure closer to 180° when $\tau = 0.03$ s. In other words, the phase shift introduced by the PSS is optimal when a small delay is present.

In the case of the dual-channel PSS of Section 5.4, if the delay is inherent, the structure of Figure 5.12 implies that if one introduces a proper artificial delay on top of the inherent delay, the system can be led to a region of better damping characteristics. This extra delay can be introduced, for example, by a properly designed controller that adjusts both the delay and gain values following a stable path, through consecutive quasi-steady state shifts of the system equilibrium.

5.6 Conclusions

This chapter presents new results on time-delayed damping control of power system synchronous machine electromechanical oscillations. The chapter focuses on the delay-control gain space, and studies the stability boundaries, as well as the relationship between the existence of delay-independent stability and connected stability domains. Connected stable regions are obtained by employing a PSS with two control channels and indicate that best damping characteristics may be achieved for large delay values.

The OMIB system with inclusion of a PSS is a relevant example of power system model that allows an analytical assessment of its stability when delays are considered. This chapter shows the conditions for which the stability of the linearized OMIB equations is guaranteed independently from the magnitude of the delay, and present how system response time as measured by the concept of σ -stability can be understood in view of recent results [131].

On the plane of controller gain vs. intentional delay, the linearized equations of the OMIB system typically exhibit stable regions that are separated by unstable regions. This however does not allow tuning the “non-linear” dynamics to operate in separate stable regions as this would require the non-linear dynamics to first cross through an unstable region. This practically-relevant aspect of delayed dynamical systems is addressed by presenting the conditions under which the stable region of the OMIB system can be all “connected” so that the non-linear dynamics can be tuned for any settings inside this region. Finally, the analytical results based on the benchmark OMIB system are extended through numerical methods and the concept of ζ -stability. Specifically, the IEEE 14-bus system model serves to illustrate how to achieve improved damping characteristics for a set of controller gains and intentional delays, and how to achieve a fully connected stability region to be able to fully explore the parameter space, without introducing instability.

Chapter 6

One-Step Delay Approximation

6.1 Introduction

As discussed in Chapter 5, introducing time delays in a set of DAEs turns it into a set of functional DAEs of retarded type, also known as DDAEs. DDAEs are typically employed to model physical time delays. In power systems, apart from their application to automatic control, mostly due to the inevitable latencies that are present in measurement and communication systems, see Chapter 5, delays have been also considered to study the effect of long transmission lines [173]. In addition, time delays are inherent to phenomena occurring in many other engineering applications, such as circuit and microwave theory [15, 103].

A property of constant delays is that the Jacobian elements with respect to retarded variables are null. This feature has been utilized for the simulation of EMTs that include long transmission lines [177] or control systems [76, 90]. The sending- and receiving-end variables of long overhead lines, in fact, are decoupled by the transmission delay and, hence, sections of circuits connected through long lines are naturally decoupled. In [90], on the other hand, the control system is solved at the previous step of the EMT circuit equations which, *de facto*, introduces a delay in the control equations. This allows ordering the Jacobian matrix of the DAEs with a block diagonal structure (see Figure 6.1.a). Each block can be handled separately at each time step – which is of the same order of the delay, i.e. μs – and allows exploiting parallelization techniques.

The effort of developing parallel algorithms in EMTs simulations stems from the fact that simulations of this type are slow for large systems [171]. For systems with the same

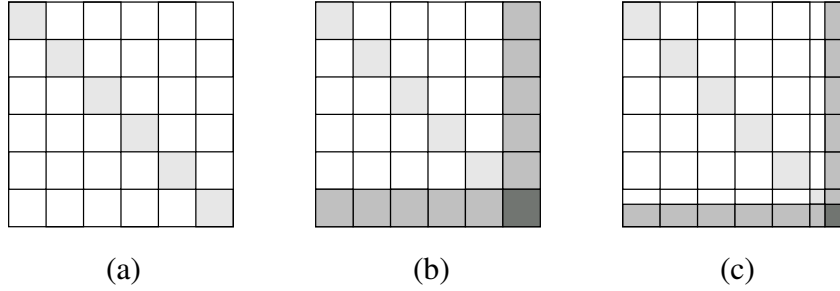


Figure 6.1: Types of Jacobian matrices: (a) block-diagonal matrix of a fully decoupled system; (b) coupled system ordered to exploit the BBD structure; and (c) coupled system with ordered BBD structure and extra decoupling obtained through fictitious delays.

number of buses, simulations based on quasi-steady state phasors and electromechanical models are much faster. However, the Time Domain Integration (TDI) of large power systems requires iteratively solving stiff non-linear hybrid DAEs, which is still a time-consuming task to complete. The time required to complete a $N - 1$ contingency analysis, in fact, can be a critical constraint, e.g. for on-line dynamic security assessment (see, for example, Chapter 15 of [48]).

The DAEs for transient stability analysis are naturally coupled through the admittance matrix of the grid, which is modeled with a set of algebraic equations, as well as by secondary frequency controllers, and generally do not include delays. This leads to a Bordered-Block Diagonal (BBD) structure of the Jacobian matrix (see Figure 6.1.b) [141]. The BBD structure can be enforced in any set of DAEs through *diakoptics*, i.e. by introducing additional algebraic equations [71, 170]. These equations increase the order of the system but tend to increase sparsity and, in some cases, may also speed up the factorization of the Jacobian matrix of the system. A technique conceptually similar to diakoptics, called MANA, namely Modified Augmented Nodal Analysis, has been utilized in unbalanced power flow analysis [68] and EMTs [66] but has no clear application for single-phase equivalent phasor-based transient stability models.

The main idea of this chapter is that, if one includes fictitious delays in the power system transient stability model, the Jacobian matrix can be further decoupled (see Figure 6.1.c) without increasing the system's order, thus increasing sparsity and reducing the computational burden of numerical methods. In this vein, in [39], the authors proposed the use of the COI at the previous time step to decouple the equations of the rotor angles of the synchronous machines. In [39], the “slightly” delayed COI was

tested on a 4-bus system using the Implicit Trapezoidal Method (ITM) with time step 0.01 s and showed not to affect the system transient response.

This chapter proposes a systematic way to implement and evaluate the idea of including *one-step-delays* to a DAE model for transient stability analysis. In order to ensure that the inclusion of fictitious one-step delays in the non-linear DAE power system model does not have a noticeable impact on the system trajectories, the following crucial aspects of the technique are addressed: (i) only variables that do not contribute to critical dynamic modes of the system are delayed. Such variables are systematically identified based on the values of their residues at the frequency range of the dynamics of interest; and (ii) given a set of selected variables, a proper upper bound of the integration time-step is established. This is done by recognizing that the one-step-delay approximation in a coupled system can be formally studied as a set of DDAEs [165].

The remainder of the chapter is organized as follows. Section 6.2 recalls a conventional implicit TDI scheme for power systems. Section 6.3 discusses the proposed approach to one-step-delay approximation. Section 6.4 discusses how to select the variables of a DAE model to be delayed. Section 6.5 provides a method to calculate the maximum admissible delay for a given DDAE model. The case study is discussed in Section 6.6. Conclusions are drawn in Section 6.7.

6.2 Implicit Integration of Power Systems

Consider the non-linear DAE power system model (2.1), where for simplicity, but without loss of generality, no inputs are included and $\mathbf{T} = \mathbf{I}_n$, $\mathbf{R} = \mathbf{0}_{m,n}$, see (2.2). This system can be written as:

$$\begin{aligned}\dot{\mathbf{x}} &= \mathbf{f}(\mathbf{x}, \mathbf{y}), \\ \mathbf{0}_{m,1} &= \mathbf{g}(\mathbf{x}, \mathbf{y}).\end{aligned}\tag{6.1}$$

Equations of system (6.1) are *stiff*, i.e. some numerical methods, when employed for the solution of (6.1), are unstable. This happens for two reasons:

- (a) the time constants of the differential equations typically span multiple time scales;
- (b) and the algebraic equations can be viewed as *infinitely fast* differential equations associated with zero time constants.

There exist both explicit and implicit methods for the numerical integration of (6.1). Explicit numerical methods are known to be impractical for the integration of this system, since for stiff problems they require very small time steps which in turn leads to poor performance. Thus, a more common approach to numerically integrate (6.1) is to use an implicit method with a direct solver. Employing an implicit method allows a simultaneous solution of both state and algebraic variables [151], and requires the solution of the following set of non-linear equations:

$$\begin{aligned}\mathbf{0}_{n,1} &= \boldsymbol{\phi}(\mathbf{x}, \mathbf{y}, h), \\ \mathbf{0}_{m,1} &= \boldsymbol{\psi}(\mathbf{x}, \mathbf{y}, h),\end{aligned}\tag{6.2}$$

where $\boldsymbol{\phi}$, ($\boldsymbol{\phi} : \mathbb{R}^{(n+m)} \rightarrow \mathbb{R}^n$) and $\boldsymbol{\psi}$, ($\boldsymbol{\psi} : \mathbb{R}^{(n+m)} \rightarrow \mathbb{R}^m$) are non-linear functions that depend on the differential and algebraic equations, respectively, as well as on the applied implicit method. The update of the state and algebraic variables at each time step can be expressed as follows:

$$\begin{bmatrix} \mathbf{x}^{[i+1]}(t+h) \\ \mathbf{y}^{[i+1]}(t+h) \end{bmatrix} = \begin{bmatrix} \mathbf{x}^{[i]}(t+h) \\ \mathbf{y}^{[i]}(t+h) \end{bmatrix} + \begin{bmatrix} \Delta \mathbf{x}^{[i]} \\ \Delta \mathbf{y}^{[i]} \end{bmatrix},\tag{6.3}$$

where h is the time step length; $\mathbf{x}^{[i]}(t+h)$ denotes the vector \mathbf{x} at the i -th iteration of time $t+h$. The increments $\Delta \mathbf{x}^{[i]}$, $\Delta \mathbf{y}^{[i]}$ are obtained by employing the Newton method, as follows:

$$\begin{bmatrix} \Delta \mathbf{x}^{[i]} \\ \Delta \mathbf{y}^{[i]} \end{bmatrix} = - \left[\mathbf{A}^{[i]} \right]^{-1} \begin{bmatrix} \boldsymbol{\phi}^{[i]} \\ \boldsymbol{\psi}^{[i]} \end{bmatrix},\tag{6.4}$$

where $\mathbf{A}^{[i]}$, $\mathbf{A}^{[i]} \in \mathbb{R}^{(n+m) \times (n+m)}$, is defined as:

$$\mathbf{A}^{[i]} = \begin{bmatrix} \boldsymbol{\phi}_x^{[i]} & \boldsymbol{\phi}_y^{[i]} \\ \boldsymbol{\psi}_x^{[i]} & \boldsymbol{\psi}_y^{[i]} \end{bmatrix},\tag{6.5}$$

where $\boldsymbol{\phi}_x^{[i]}$, $\boldsymbol{\phi}_y^{[i]}$, $\boldsymbol{\psi}_x^{[i]}$, $\boldsymbol{\psi}_y^{[i]}$ are the Jacobian matrices of $\boldsymbol{\phi}$ and $\boldsymbol{\psi}$ at the i -th iteration of time t .

Among the various implicit numerical methods utilized by power system software tools to define equations (6.2), for simplicity but without lack of generality, this chapter considers only one, namely the ITM, which is a well-known and widely utilized A -stable

integration scheme particularly adequate to handle DAE stiffness. The ITM leads to the following form of (6.2):

$$\begin{aligned}\mathbf{0}_{n,1} &= \boldsymbol{\phi}^{[i]} = \mathbf{x}^{[i]} - \mathbf{x}(t-h) - 0.5h(\mathbf{f}^{[i]} + \mathbf{f}(t-h)), \\ \mathbf{0}_{m,1} &= \boldsymbol{\psi}^{[i]} = \mathbf{g}^{[i]},\end{aligned}\tag{6.6}$$

where h is the time step length; $\mathbf{f}^{[i]} = \mathbf{f}(\mathbf{x}^{[i]}, \mathbf{y}^{[i]})$, $\mathbf{g}^{[i]} = \mathbf{g}(\mathbf{x}^{[i]}, \mathbf{y}^{[i]})$ and $\mathbf{f}(t-h) = \mathbf{f}(\mathbf{x}(t-h), \mathbf{y}(t-h))$. The Jacobian matrix (6.5) at the i -th iteration of time t is defined as:

$$\begin{aligned}\boldsymbol{\phi}_{\mathbf{x}}^{[i]} &= \mathbf{I}_n - 0.5h\mathbf{f}_{\mathbf{x}}^{[i]}, \\ \boldsymbol{\phi}_{\mathbf{y}}^{[i]} &= -0.5h\mathbf{f}_{\mathbf{y}}^{[i]}, \\ \boldsymbol{\psi}_{\mathbf{x}}^{[i]} &= \mathbf{g}_{\mathbf{x}}^{[i]}, \\ \boldsymbol{\psi}_{\mathbf{y}}^{[i]} &= \mathbf{g}_{\mathbf{y}}^{[i]},\end{aligned}\tag{6.7}$$

where $\mathbf{f}_{\mathbf{x}}^{[i]}$, $\mathbf{f}_{\mathbf{y}}^{[i]}$, $\mathbf{g}_{\mathbf{x}}^{[i]}$, $\mathbf{g}_{\mathbf{y}}^{[i]}$ are the Jacobian matrices of the DAEs.

6.3 One-Step-Delay Approximation

Assume that some variables – how to select such variables is discussed later in this chapter – of the DAE system (6.1) are substituted with their values at the previous time step. This system can be formally studied as a system of non-linear DDAEs with a constant delay, as follows:

$$\begin{aligned}\dot{\mathbf{x}} &= \tilde{\mathbf{f}}(\mathbf{x}, \mathbf{y}, \mathbf{x}_d, \mathbf{y}_d), \\ \mathbf{0}_{m,1} &= \tilde{\mathbf{g}}(\mathbf{x}, \mathbf{y}, \mathbf{x}_d, \mathbf{y}_d),\end{aligned}\tag{6.8}$$

where $\mathbf{x}_d, \mathbf{x}_d \in \mathbb{R}^{n_d}$, $\mathbf{y}_d, \mathbf{y}_d \in \mathbb{R}^{m_d}$, are the delayed state and algebraic variables, respectively, as follows:

$$\begin{aligned}\mathbf{x}_d &= \mathbf{x}(t-h), \\ \mathbf{y}_d &= \mathbf{y}(t-h).\end{aligned}\tag{6.9}$$

Note that (6.8) is an approximation of (6.1). The delay h , in fact, is fictitious as it does not model any physical phenomenon.

The numerical integration of (6.8) requires the solution of the following set of non-linear equations [97]:

$$\begin{aligned}\mathbf{0}_{n,1} &= \tilde{\boldsymbol{\phi}}(\mathbf{x}, \mathbf{y}, \mathbf{x}_d, \mathbf{y}_d, h), \\ \mathbf{0}_{m,1} &= \tilde{\boldsymbol{\psi}}(\mathbf{x}, \mathbf{y}, \mathbf{x}_d, \mathbf{y}_d, h).\end{aligned}\tag{6.10}$$

If at the i -th iteration of time t , $\tilde{\mathbf{f}}_{\mathbf{x}}^{[i]}$, $\tilde{\mathbf{f}}_{\mathbf{y}}^{[i]}$, $\tilde{\mathbf{g}}_{\mathbf{x}}^{[i]}$, $\tilde{\mathbf{g}}_{\mathbf{y}}^{[i]}$, are the delay-free and $\tilde{\mathbf{f}}_{\mathbf{x}_d}^{[i]}$, $\tilde{\mathbf{f}}_{\mathbf{y}_d}^{[i]}$, $\tilde{\mathbf{g}}_{\mathbf{x}_d}^{[i]}$, $\tilde{\mathbf{g}}_{\mathbf{y}_d}^{[i]}$, are the Jacobian matrices of the delayed variables of system (6.8), then the following identities apply:

$$\begin{aligned}\mathbf{f}_{\mathbf{x}}^{[i]} &= \tilde{\mathbf{f}}_{\mathbf{x}}^{[i]} + \tilde{\mathbf{f}}_{\mathbf{x}_d}^{[i]}, \\ \mathbf{f}_{\mathbf{y}}^{[i]} &= \tilde{\mathbf{f}}_{\mathbf{y}}^{[i]} + \tilde{\mathbf{f}}_{\mathbf{y}_d}^{[i]}, \\ \mathbf{g}_{\mathbf{x}}^{[i]} &= \tilde{\mathbf{g}}_{\mathbf{x}}^{[i]} + \tilde{\mathbf{g}}_{\mathbf{x}_d}^{[i]}, \\ \mathbf{g}_{\mathbf{y}}^{[i]} &= \tilde{\mathbf{g}}_{\mathbf{y}}^{[i]} + \tilde{\mathbf{g}}_{\mathbf{y}_d}^{[i]}.\end{aligned}\tag{6.11}$$

The main difference between (6.10) and (6.2) is that the Jacobian matrices of (6.10) do not include the terms that depend on \mathbf{x}_d and \mathbf{y}_d , as these variables are ‘‘constants’’ at time t . One has:

$$\begin{bmatrix} \Delta \mathbf{x}^{[i]} \\ \Delta \mathbf{y}^{[i]} \end{bmatrix} = - \left[\tilde{\mathbf{A}}^{[i]} \right]^{-1} \begin{bmatrix} \tilde{\boldsymbol{\phi}}^{[i]} \\ \tilde{\boldsymbol{\psi}}^{[i]} \end{bmatrix},\tag{6.12}$$

where

$$\tilde{\mathbf{A}}^{[i]} = \begin{bmatrix} \tilde{\boldsymbol{\phi}}_{\mathbf{x}}^{[i]} & \tilde{\boldsymbol{\phi}}_{\mathbf{y}}^{[i]} \\ \tilde{\boldsymbol{\psi}}_{\mathbf{x}}^{[i]} & \tilde{\boldsymbol{\psi}}_{\mathbf{y}}^{[i]} \end{bmatrix}.\tag{6.13}$$

The terms $\tilde{\boldsymbol{\phi}}_{\mathbf{x}}^{[i]}$, $\tilde{\boldsymbol{\phi}}_{\mathbf{y}}^{[i]}$, $\tilde{\boldsymbol{\psi}}_{\mathbf{x}}^{[i]}$, $\tilde{\boldsymbol{\psi}}_{\mathbf{y}}^{[i]}$ are the delay-free Jacobian matrices of $\tilde{\boldsymbol{\phi}}^{[i]}$ and $\tilde{\boldsymbol{\psi}}^{[i]}$. For a detailed description on the modifications required by the ITM in order to integrate a set of DDAEs with inclusion of more general (time-varying and state-dependent) delays, the interested reader may refer to [97]. Since matrix $\tilde{\mathbf{A}}$ is composed only of the delay-free Jacobian matrix elements of $\tilde{\boldsymbol{\phi}}$ and $\tilde{\boldsymbol{\psi}}$, $\tilde{\mathbf{A}}$ is sparser than \mathbf{A} . The scope of this chapter is to take advantage of the fact that approximating (6.1) with (6.8) leads to a sparser Jacobian matrix.

6.4 Selection of Variables to be Delayed

Inclusion of fictitious time delays in a set of DAEs introduces an inevitable approximation in its transient response. It is thus crucial to identify the variables and the equations

that, if subject to a small variation, do not lead to a significant change in the system trajectories. With this regard, delaying variables that are slower than the dynamics of main interest, causes a smaller variation in the system trajectories.

Another aspect is the position of the selected elements in the Jacobian matrix. Removing elements that introduce dense rows/columns in the Jacobian leads not only to a sparsity increase, but also to decoupling of the system equations, which in turn allows exploiting state-of-the-art algorithms that parallelize the factorization. Such algorithms usually exploit the specific formulation of current-injection power system models and the admittance matrix to take advantage of the BBD structure of the Jacobian matrix [38,41]. Exploiting parallelization, however, is out of the scope of this chapter. Thus the general DAE model (6.1) is considered.

6.4.1 Systematic Selection of Variables

This section provides a systematic small-signal based method to select the delayed variables \mathbf{x}_d and \mathbf{y}_d of a model, based on the geometric approach [53, 163]. The geometric approach has been widely employed in control design to provide a measure for (i) the observability of a dynamic mode from a signal; (ii) the controllability of a mode from a control input placement. The product of these two measures provides the joint observability/controllability index. The smaller this index is, the less the examined mode is affected by the specific signal-control input set. In the following, the geometric approach is utilized to determine the sensitivity of system modes to variations of all non-zero elements of the DAE Jacobian matrices.

Differentiating (6.1) around an equilibrium point yields:

$$\begin{aligned}\Delta\dot{\mathbf{x}} &= \mathbf{f}_x \Delta\mathbf{x} + \mathbf{f}_y \Delta\mathbf{y}, \\ \mathbf{0}_{m,1} &= \mathbf{g}_x \Delta\mathbf{x} + \mathbf{g}_y \Delta\mathbf{y}.\end{aligned}\tag{6.14}$$

Elimination of $\Delta\mathbf{y}$ leads to $\Delta\dot{\mathbf{x}} = \mathbf{A}_s \Delta\mathbf{x}$, where the matrix $\mathbf{A}_s = \mathbf{f}_x - \mathbf{f}_y \mathbf{g}_y^{-1} \mathbf{g}_x$ has n finite eigenvalues $\lambda_1, \lambda_2, \dots, \lambda_n$. For rotor angle stability studies, eigenvalues of interest are those that define oscillatory modes with natural frequency $f_{n,i} \in [0.1, 2]$ Hz [174]. In the remainder of the chapter, these modes (and the respective eigenvalues) are referred to as *relevant*.

A perturbation is introduced into (6.14) as follows:

$$\begin{aligned}\Delta \dot{\mathbf{x}} &= \mathbf{f}_x \Delta \mathbf{x} + \mathbf{f}_y \Delta \mathbf{y} + \mathbf{B}_f \Delta \mathbf{u}_f, \\ \mathbf{0}_{m,1} &= \mathbf{g}_x \Delta \mathbf{x} + \mathbf{g}_y \Delta \mathbf{y} + \mathbf{B}_g \Delta \mathbf{u}_g,\end{aligned}\tag{6.15}$$

where $\Delta \mathbf{u}_f \in \mathbb{R}^n$, $\Delta \mathbf{u}_g \in \mathbb{R}^m$ are the perturbation vectors of the differential, algebraic equations, respectively; and \mathbf{B}_f , \mathbf{B}_g are the perturbation matrices associated with $\Delta \mathbf{u}_f$ and $\Delta \mathbf{u}_g$, respectively. Eliminating $\Delta \mathbf{y}$ from (6.15) yields:

$$\Delta \dot{\mathbf{x}} = \mathbf{A}_s \Delta \mathbf{x} + \mathbf{B}_f \Delta \mathbf{u}_f - \mathbf{f}_y \mathbf{g}_y^{-1} \mathbf{B}_g \Delta \mathbf{u}_g.\tag{6.16}$$

Considering zero perturbation matrices in (6.16), as discussed in [53], the output matrices of the state and algebraic variable variations can be defined as $\mathbf{C}_x = \mathbf{I}_n$, $\mathbf{C}_y = -\mathbf{g}_y^{-1} \mathbf{g}_x$, respectively.

Let $\mathbf{f}_x(\mu_f, \nu_x)$, be the μ_f -th row, ν_x -th column element of \mathbf{f}_x ; $\mathbf{f}_y(\mu_f, \nu_y)$ the element of \mathbf{f}_y ; $\mathbf{g}_x(\mu_g, \nu_x)$ the μ_g -th row, ν_x -th column element of \mathbf{g}_x ; and $\mathbf{g}_y(\mu_g, \nu_y)$ the μ_g -th row, ν_y -th column element of \mathbf{g}_y . Then, the geometric controllability/observability (gco) measures of λ_i from the Jacobian matrix elements of the system are determined as follows:

$$\text{gco}(\mathbf{f}_x(\mu_f, \nu_x)) = \frac{|\mathbf{c}_{x,\mu_f} \mathbf{v}_i \mathbf{w}_i \mathbf{b}_{f,\nu_x}|}{\|\mathbf{v}_i\| \|\mathbf{c}_{x,\mu_f}\| \|\mathbf{w}_i\| \|\mathbf{b}_{f,\nu_x}\|},\tag{6.17}$$

where \mathbf{c}_{x,μ_f} is the μ_f -th row of \mathbf{C}_x ; \mathbf{b}_{f,ν_x} is the ν_x -th column of \mathbf{B}_f ; $|\cdot|$ and $\|\cdot\|$ denote the modulus and Euclidean norm, respectively;

$$\text{gco}(\mathbf{f}_y(\mu_f, \nu_y)) = \frac{|\mathbf{c}_{y,\mu_f} \mathbf{v}_i \mathbf{w}_i \mathbf{b}_{f,\nu_y}|}{\|\mathbf{v}_i\| \|\mathbf{c}_{y,\mu_f}\| \|\mathbf{w}_i\| \|\mathbf{b}_{f,\nu_y}\|},\tag{6.18}$$

where \mathbf{c}_{y,μ_f} is the μ_f -th row of \mathbf{C}_y ; \mathbf{b}_{f,ν_y} is the ν_y -th column of \mathbf{B}_f ;

$$\text{gco}(\mathbf{g}_x(\mu_g, \nu_x)) = \frac{|\mathbf{c}_{x,\mu_g} \mathbf{v}_i \mathbf{w}_i \mathbf{b}_{g,\nu_x}|}{\|\mathbf{v}_i\| \|\mathbf{c}_{x,\mu_g}\| \|\mathbf{w}_i\| \|\mathbf{b}_{g,\nu_x}\|},\tag{6.19}$$

where \mathbf{c}_{x,μ_g} is the μ_g -th row of \mathbf{C}_x ; \mathbf{b}_{g,ν_x} is the ν_x -th column of \mathbf{B}_g ; and

$$\text{gco}(\mathbf{g}_y(\mu_g, \nu_y)) = \frac{|\mathbf{c}_{y,\mu_g} \mathbf{v}_i \mathbf{w}_i \mathbf{b}_{g,\nu_y}|}{\|\mathbf{v}_i\| \|\mathbf{c}_{y,\mu_g}\| \|\mathbf{w}_i\| \|\mathbf{b}_{g,\nu_y}\|},\tag{6.20}$$

where \mathbf{c}_{y,μ_g} is the μ_g -th row of the output matrix \mathbf{C}_y ; \mathbf{b}_{g,ν_y} is the ν_y -th column of the perturbation matrix \mathbf{B}_g .

Expressions (6.17)-(6.20) allow selecting the elements of the Jacobians of (6.14) that can be delayed and thus can be eliminated from the matrices \mathbf{f}_x , \mathbf{f}_y , \mathbf{g}_x and \mathbf{g}_y . Specifically, elements of such matrices that have low gco values for all relevant modes of the system, do not noticeably impact the dynamic behavior of the system. Therefore, a candidate to be delayed is any element whose gco value is below a given threshold gco_{\max} . Note that \mathbf{f}_x , \mathbf{f}_y , \mathbf{g}_x and \mathbf{g}_y are stored as sparse matrices, hence only non-zero elements are considered for the analysis above, which leads to an efficient implementation.

6.4.2 Illustrative Examples

The criteria described above are further discussed through some illustrative examples, which are based on well-known devices and models utilized in transient stability analysis. In particular, this chapter considers devices and controllers that are slow and/or couple several variables of the system.

6.4.2.1 Center of Inertia

The algebraic variable of the COI speed (ω_{CoI}) is defined by the following algebraic equation:

$$g_{(\omega_{\text{CoI}})} := 0 = \omega_{\text{CoI}} - \sum_{i=1}^{\kappa} \frac{M_i}{M_T} \omega_{r,i}, \quad (6.21)$$

where $\omega_{r,i}$, $i = 1, 2, \dots, \kappa$, is the state of the speed of the i -th machine; M_i is the mechanical starting time of the i -th machine; and $M_T = M_1 + M_2 + \dots + M_\kappa$. The COI speed is used as a reference in the differential equations of the generator rotor angles:

$$f_{(\dot{\delta}_{r,i})} := \dot{\delta}_{r,i} = \Omega_b (\omega_{r,i} - \omega_{\text{CoI}}), \quad (6.22)$$

where Ω_b is the angular frequency base. The COI provides the “average” frequency trend of the system and thus represents a relatively slow dynamic. Delaying $\omega_{r,i}$ and ω_{CoI} in (6.21), (6.22), respectively, allows removing the elements $\partial g_{(\omega_{\text{CoI}})} / \partial \omega_{r,i}$ and $\partial f_{(\dot{\delta}_{r,i})} / \partial \omega_{\text{CoI}}$, which constitute a dense row in \mathbf{g}_x and a dense column in \mathbf{f}_y , respectively.

6.4.2.2 Turbine Governor

The action of some TGs can be significantly slow, as compared to primary damping and voltage controllers and hence, adding one-step delays in some TG DAE models, e.g. the ones described in [92], leads to increased sparsity without jeopardizing the TDI accuracy. On the other hand, since TG variables typically do not constitute dense segments in the Jacobian matrix, the increased sparsity does not come with significant decoupling.

6.4.2.3 Automatic Generation Control

The AGC is used to provide secondary frequency regulation to the power system. Consider a simplified continuous AGC model that measures the COI frequency and produces a dynamic active power command (P_s) which is distributed to the machine TGs proportionally to their droops [157]. The algebraic variable of the power order received by the i -th TG is defined by the following algebraic equation:

$$g_{(P_{\text{ord},i})} := 0 = P_{\text{ord},i} - \frac{\mathcal{R}_i}{\mathcal{R}_T} P_s, \quad (6.23)$$

where $P_{\text{ord},i}$ is the TG power order; \mathcal{R}_i is the droop constant; and $\mathcal{R}_T = \mathcal{R}_1 + \mathcal{R}_2 + \dots + \mathcal{R}_\kappa$. Delaying $P_{\text{ord},i}$ in (6.23) removes $\partial g_{(P_{\text{ord},i})} / \partial P_s$, which forms a dense column in \mathbf{g}_x , while accuracy is not impacted, because of the AGC slow action.

6.4.2.4 Secondary Voltage Regulation

The Secondary Voltage Regulation (SVR) model employed in this chapter is based on the scheme proposed in the grid code of the Italian system. For a detailed description of this scheme, the interested reader may refer to [153]. The SVR mainly consists of two control levels. The external loop receives the voltage measurement of a selected pilot bus and computes the vector \mathbf{Q}_{ref} that represents reactive power limits for the participating to the SVR generators. \mathbf{Q}_{ref} is compared with the actual reactive power generation vector \mathbf{Q} and the error $\mathbf{Q}_{\text{err}} = \mathbf{Q}_{\text{ref}} - \mathbf{Q}$ is further processed by a dynamic decoupling matrix \mathbf{D} . The produced vector is finally sent to the Generator Reactive Power Regulators (GRPRs). Each GRPR is basically a PI control, the output of which is considered as input to the voltage reference of the generator's AVR. The dynamic

behavior of the the i -th GRPR state variable $x_{r,i}$ is given by the PI differential equation:

$$f_{(x_{r,i})} := \dot{x}_{r,i} = K_I \mathbf{D}_i \mathbf{Q}_{\text{err}}, \quad (6.24)$$

where K_I is the integral gain of the GRPR; \mathbf{D}_i is the i -th row of \mathbf{D} . Delaying \mathbf{Q}_{err} in (6.24) allows eliminating $\partial f_{(x_{r,i})}/\partial \mathbf{Q}_{\text{err}}$, which constitutes a dense block of columns and rows in \mathbf{f}_y . The accuracy of the integration is maintained, due to the relatively slow time scale of the SVR action.

6.5 Maximum Delay / Time Step

This section presents a technique based on SSSA, which for a selected set of \mathbf{x}_d and \mathbf{y}_d , estimates the maximum admissible delay h_{max} that allows keeping the errors between the original DAEs and the modified DDAEs below a threshold. To this aim, first one has to solve the eigenvalue problem of the linearized delayed system. Linearizing (6.8) around a valid operating point yields:

$$\begin{aligned} \Delta \dot{\mathbf{x}} &= \tilde{\mathbf{f}}_x \Delta \mathbf{x} + \tilde{\mathbf{f}}_y \Delta \mathbf{y} + \tilde{\mathbf{f}}_{x_d} \Delta \mathbf{x}_d + \tilde{\mathbf{f}}_{y_d} \Delta \mathbf{y}_d, \\ \mathbf{0}_{m,1} &= \tilde{\mathbf{g}}_x \Delta \mathbf{x} + \tilde{\mathbf{g}}_y \Delta \mathbf{y} + \tilde{\mathbf{g}}_{x_d} \Delta \mathbf{x}_d + \tilde{\mathbf{g}}_{y_d} \Delta \mathbf{y}_d. \end{aligned} \quad (6.25)$$

Eliminating the algebraic variables from (6.25) is possible under the assumption that $\tilde{\mathbf{g}}_y$ is not singular, as follows:

$$\Delta \dot{\mathbf{x}} = \mathbf{A}_0 \Delta \mathbf{x} + \mathbf{A}_1 \Delta \mathbf{x}_d + \sum_{k=2}^{\infty} (\mathbf{A}_k \mathbf{x}(t - kh)), \quad (6.26)$$

where \mathbf{A}_0 is the delay-free system matrix; \mathbf{A}_k , $k \geq 2$, are the delayed system matrices. A rigorous proof of (6.26), as well as the condition under which the series in (6.26) converges, are provided in [98]. The series typically converges rapidly as k increases and, thus, it is acceptable to assume a finite maximum value for k , say ρ , in the summation of (6.26), and hence, the characteristic matrix of (6.26) can be approximated with the following pencil:

$$s \mathbf{I}_n - \mathbf{A}_0 - \sum_{k=1}^{\rho} (e^{-skh} \mathbf{A}_k). \quad (6.27)$$

Based on the above, the following proposition on the continuity of the eigenvalues of (6.27) is relevant.

Proposition 6.1. Let $\hat{\lambda}$ be an eigenvalue of (6.27) with multiplicity α . There exists a constant $\hat{\epsilon}$ such that for all $\epsilon > 0$ satisfying $\epsilon < \hat{\epsilon}$, there is a number $\xi > 0$ such that the pencil:

$$s \mathbf{I}_\nu - (1 + \xi) \left(\mathbf{A}_0 - \sum_{k=1}^{\rho} e^{-sk(1+\xi)h} \mathbf{A}_k \right), \quad (6.28)$$

where

$$\begin{aligned} \xi h \in \mathbb{R}, \quad \|\xi h\| < \xi, \quad h + \xi h \geq 0, \\ \xi \mathbf{A}_k \in \mathbb{R}^{n \times n}, \quad \|\xi \mathbf{A}_k\|_2 < \xi, \quad k = 0, 1, \dots, \rho, \end{aligned}$$

has exactly α eigenvalues in the disk: $\{s \in \mathbb{C} : |s - \hat{\lambda}| < \epsilon\}$. The notation $\|\cdot\|_2$ implies the induced matrix 2-norm.

The proposition above states that the characteristic roots of a delayed system behave continuously with respect to variations of system matrices and delays [91].

In the proposed scheme, the modes of the time-delay system are viewed as approximations of the modes of the delay-free system. Let λ_i and $\hat{\lambda}_i$ be the i -th rightmost, non-null eigenvalues of the delay-free and the delayed system, respectively. The associated relative error is:

$$\eta_i = \frac{|\hat{\lambda}_i - \lambda_i|}{|\lambda_i|}. \quad (6.29)$$

The limit case $h = 0$ leads to $\eta_i = 0$, $0 \leq i \leq n$; and, for $h > 0$, $\eta_i \geq 0$. Assigning a maximum admissible error, say η_{\max} , allows finding the delay upper bound h_{\max} , as follows:

$$\eta_{\max} \geq \frac{|\hat{\lambda}_i(h_{\max}) - \lambda_i|}{|\lambda_i|}, \quad \forall i = 1, 2, \dots, \nu, \quad \nu \leq n. \quad (6.30)$$

The calculation of h_{\max} requires to find the eigenvalues of (6.27), which implies solving a non-linear, transcendental characteristic equation. Transforming (6.27) into a linear pencil is possible by using a partial differential equations representation of the system,

which however, has infinite dimensions. A reduced set of eigenvalues can be found by employing Chebyshev discretization, a brief description of which was given in Section 5.2.3.

The following remarks are relevant.

Remark 6.1. (*Delay vs time step*): In general, the time step of the numerical integration is determined based on the fastest dynamics of the system, whereas the variables that are delayed in this work are typically associated with slow dynamics. This means that the time step is always smaller than the time scale of delayed variables. Regarding the magnitude of the time delay, if the delay is greater than the integration time step, an extra, undesirable approximation is introduced into the system, as Proposition 6.1 indicates that the difference between the DAEs and DDAEs are the smaller, the smaller is the delay. On the other hand, for delays smaller than the time step, the numerical integration has to interpolate the delayed values, which introduces an additional source of error in the trajectories of the DDAEs. In general, handling delays smaller than the step size is an open research topic, as it creates difficulties even for special integration methods for stiff DDEs [49]. For the reasons above, in the proposed formulation, the delay is always equal to the time step.

Remark 6.2. (*Stiffness*): Apart from the approximation introduced with the delay, the maximum step h_{\max} is also constrained by the stiffness of the DDAEs and the numerical integration method. In the following, the system is integrated using the ITM.

Remark 6.3. (*Computational burden*): The approach presented in Section 6.4.1 and Section 6.5 is based on SSSA, which is valid around an equilibrium. SSSA based techniques in this chapter are used to capture a feature of the power system model that is “robust”, i.e. does not substantially change by varying the operating point. Hence, the analysis can be carried out only once per network. Some references have addressed a similar problem. For example, see the discussion on the participation matrix and identification of relevant state variables in [174]; and the use of SSSA techniques for non-linear dynamic model reduction in [26].

6.6 Case Studies

Two power system models are considered in this section. In particular, Section 6.6.1 is based on the IEEE 39-bus system and employs the discussions of Sections 6.4 and 6.5 for selection of variables and estimation of the maximum admissible time step. Then, Section 6.6.2 considers a 21,177-bus model of the ENTSO-E. This system is large enough to allow properly discussing the impact of the proposed approach on the convergence and the computational burden of the TDI.

6.6.1 IEEE 39-bus System

This section presents simulation results based on the IEEE 39-bus system, also known as the New England 10-machine system. Detailed static and dynamic data of the IEEE 39-bus system can be found in [102]. It consists of 10 synchronous generators, all represented by 4-th order (two-axis) models [92]; 34 transmission lines; 12 transformers; and 19 loads. Each generator is equipped with AVR, TG and PSS, and thus provides primary voltage, primary frequency and damping control, respectively, to the system. In this chapter, all generators are assumed to participate to secondary frequency and voltage control through AGC and SVR schemes, respectively. Note that the CoI speed is used as angular frequency reference of the generators. In total, the system has 141 state variables and 253 algebraic variables.

The state matrix \mathbf{A} has 141 finite eigenvalues, 48 of which have natural frequencies that fall in the range $[0.1, 2]$ Hz and are thus considered *relevant* eigenvalues for the analysis carried out below. Table 6.1 shows the Number of Non-Zero (NNZ) elements of the Jacobian matrix of the original system. The full 394×394 Jacobian matrix \mathbf{A} has 1,704 non-zero elements, which corresponds to density 1.098%.

Table 6.1: IEEE 39-bus system: NNZ Jacobian elements of the original DAE system.

\mathbf{f}_x	\mathbf{f}_y	\mathbf{g}_x	\mathbf{g}_y	Total	Density (%)
281	271	140	1,012	1,704	1.098

The method discussed in Section 6.4.1 is applied to the IEEE 39-bus system. The effect of the selected threshold gco_{\max} on the density of the system Jacobian matrices is shown in Figure 6.2. As expected, the higher gco_{\max} , the more elements are selected and the sparser the delayed Jacobian matrices become.

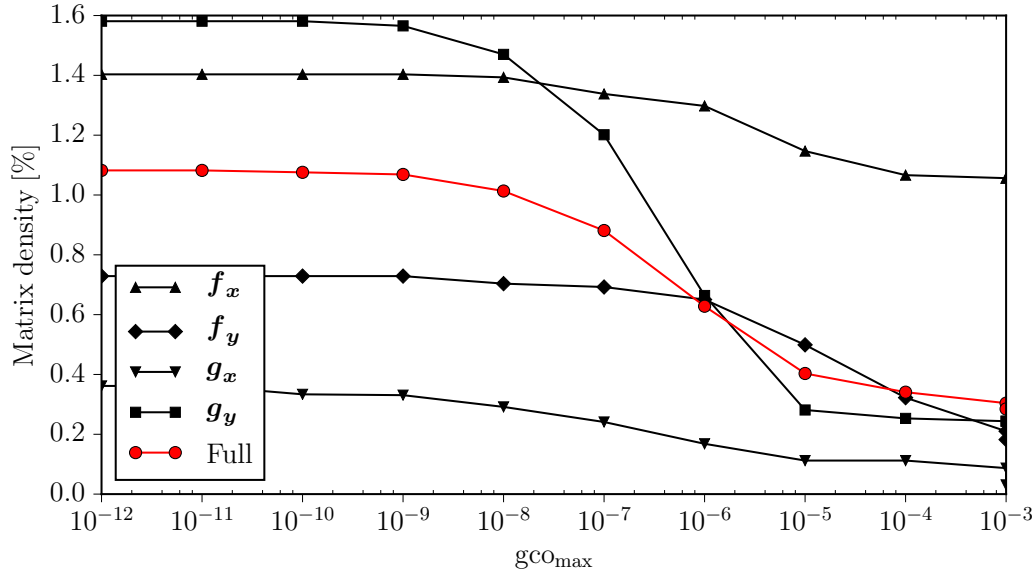


Figure 6.2: IEEE 39-bus system: density of Jacobians as gco_{max} varies.

Table 6.2: IEEE 39-bus system without delays: rightmost eigenvalues.

-0.00782
$-0.01400 \pm j0.03721$
-0.02000
-0.02890
-0.02998
-0.04009
-0.04368
-0.05554
-0.05776
-0.06160
-0.06179
-0.06312
$-0.08362 \pm j0.02745$
-0.10001
-0.10002

For example, consider $gco_{max} = 10^{-10}$. In this case, selected variables include variables of TGs; rotor speeds that appear in the equation of the COI; variables of the SVR. The method suggests first variables of slow acting devices, which is also consistent to the discussion of Section 6.4. The 35 rightmost eigenvalues of the system without and with inclusion of different delays are shown in Tables 6.2 and 6.3. The relative errors of the system for these eigenvalues are calculated according to (6.29) and results are presented in Table 6.4. If $h = 0.01$ s, all relative eigenvalue errors are below 0.05%. The relative eigenvalue errors increase for larger delays. According to the discussion of Section 6.5, if

Table 6.3: IEEE 39-bus system with one-step delay: rightmost eigenvalues, $\text{gco}_{\max} = 10^{-10}$.

$h = 0.01$ s	$h = 0.2$ s	$h = 0.24$ s
$\hat{\lambda}_i$	$\hat{\lambda}_i$	$\hat{\lambda}_i$
-0.00782	-0.00783	-0.00784
$-0.01400 \pm j0.03720$	$-0.01399 \pm j0.03719$	$-0.01397 \pm j0.03717$
-0.02000	-0.02000	-0.02000
-0.02890	-0.02890	-0.02890
-0.02998	-0.02998	-0.02998
-0.04009	-0.04009	-0.04009
-0.04368	-0.04368	-0.04368
-0.05554	-0.05553	-0.05553
-0.05776	-0.05776	-0.05776
-0.06160	-0.06160	-0.06160
-0.06179	-0.06179	-0.06179
-0.06312	-0.06312	-0.06312
$-0.08364 \pm j0.02748$	$-0.08388 \pm j0.02770$	$-0.08426 \pm j0.02804$
-0.10001	-0.10001	-0.10001
-0.10002	-0.10002	-0.10002

Table 6.4: IEEE 39-bus system with one-step-delay: relative errors of rightmost eigenvalues, $\text{gco}_{\max} = 10^{-10}$.

$h = 0.01$ s	$h = 0.2$ s	$h = 0.24$ s
η_i (%)	η_i (%)	η_i (%)
0.00	0.13	0.26
0.03	0.06	0.13
0.00	0.00	0.00
0.00	0.00	0.00
0.00	0.00	0.00
0.00	0.00	0.00
0.00	0.00	0.00
0.00	0.02	0.02
0.00	0.00	0.00
0.00	0.00	0.00
0.00	0.00	0.00
0.00	0.00	0.00
0.04	0.41	0.99
0.00	0.00	0.00
0.00	0.00	0.00

the maximum relative error is $\eta_{\max} = 1$ %, then $h_{\max} = 0.24$ s. Finally, as illustrated in Figure 6.2, constantly increasing gco_{\max} leads to more and more variables being selected, which gradually limits the value of h_{\max} . However, following from (6.17)-(6.20), variables that inherently define relevant modes are consistently not selected.

The geometric approach can provide an insight of the system structure in a systematic and model-agnostic way, unlike for example, the methods proposed in [41] and [38]. This feature is particularly important for modern power systems where converter-interfaced devices can change, in a future not too far away, the overall dynamic response of the system. Still, it is common that variables of a conventional power system DAE model are well-known. Then, \mathbf{x}_d , \mathbf{y}_d can be selected based on the user's experience, and thus without applying a systematic method. The variables that if delayed, do not change or change in a negligible way the overall dynamic behavior of the system, are typically the ones with significantly slower dynamic response as compared to the critical modes of the system. Selected variables are thus naturally decoupled by the critical dynamics of the system due to their different time scale. With this regard, two comments are relevant. First, for any set of selected elements, h_{\max} is not known a priori, so it can be still estimated according to the method described in Section 6.5. Second, while selecting \mathbf{x}_d , \mathbf{y}_d , the user should take into account that, how slow a variable actually is depends on the state matrix \mathbf{A} and, in turn, on the parameters of the examined system. For example, consider again the example of the CoI. Differentiation of (6.21) yields:

$$\dot{\omega}_{\text{CoI}} = \sum_{i=1}^{\kappa} \frac{M_i}{M_T} \dot{\omega}_{r,i}, \quad (6.31)$$

where $\dot{\omega}_{r,i}$ is given by the well-known swing equation:

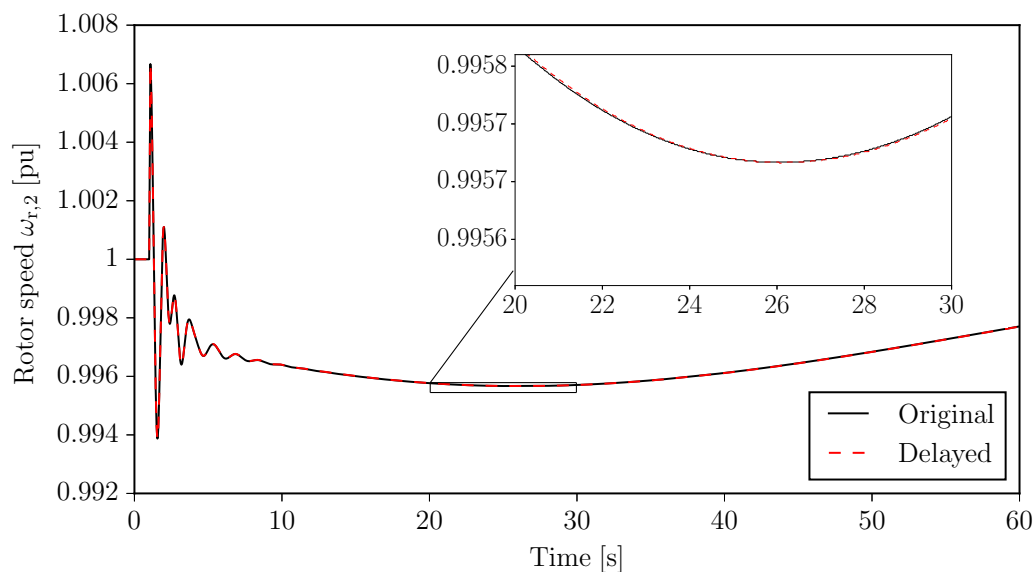
$$\dot{\omega}_{r,i} = \frac{1}{M_i} (\tau_{m,i} - \tau_{e,i} - D_i (\omega_{r,i} - \omega_{\text{CoI}})), \quad (6.32)$$

where $\tau_{m,i}$, $\tau_{e,i}$ are the mechanical and electrical torque, respectively; D_i is the damping coefficient of the i -th machine. Substitution of (6.32) to (6.31) gives:

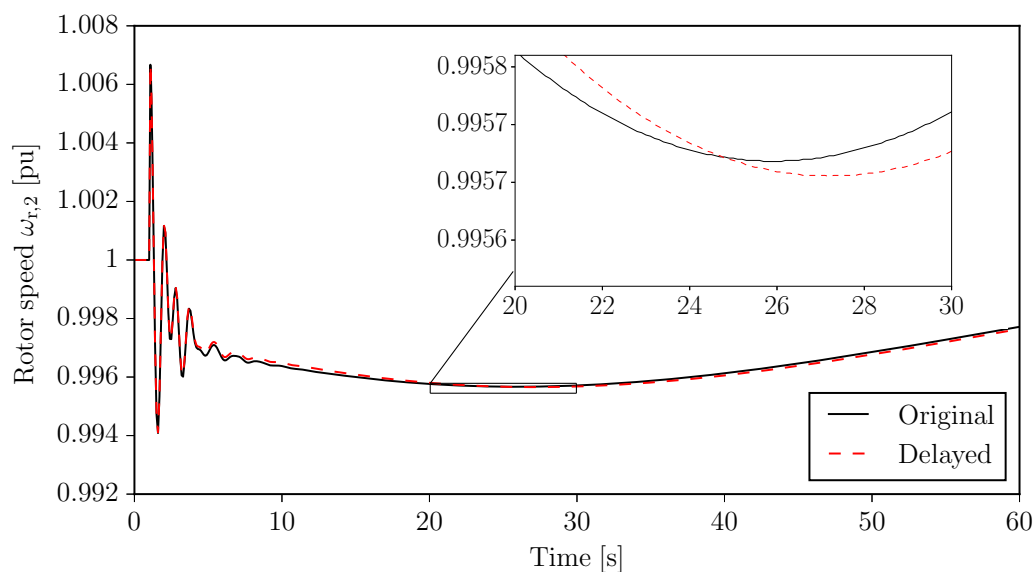
$$\dot{\omega}_{\text{CoI}} = \frac{1}{M_T} (\tau_{m,T} - \tau_{e,T} - \sum_{i=1}^{\kappa} D_i (\omega_i - \omega_{\text{CoI}})), \quad (6.33)$$

where $\tau_{m,T} = \tau_{m,1} + \tau_{m,2} + \dots + \tau_{m,\kappa}$; and $\tau_{e,T} = \tau_{e,1} + \tau_{e,2} + \dots + \tau_{e,\kappa}$. A characteristic of the 39-bus system is that $M_1 \gg M_i$, $i \neq 1$ ($M_1 = 1000$ MWs/MVA, while the second larger mechanical starting time is $M_{10} = 84$ MWs/MVA). In this case, the rate of change of ω_{CoI} is still slow (see Section 6.4.2), but, as seen from (6.33), its rate of change is comparable with that of $\omega_{r,1}$.

Delayed variables are associated with secondary controllers or “slow” variables such as the center of inertia. The dynamic response of these variables cannot change even for relatively big changes of the operating point and topology of the system. As a matter of fact, one could select *a priori* most of these variables. However, the eigenvalue analysis provides a systematic approach that can cope with any system setup and any device and controller. This feature is particularly important for modern power systems where converter-interfaced devices can change, in a future not too far away, the overall dynamic response of the system.



(a) $h = 0.02$ s.



(b) $h = 0.10$ s.

Figure 6.3: IEEE 39-bus system: transient following a three-phase fault.

The next example discusses the effect of the one-step delay approximation in the transient response of the 39-bus system by carrying out non-linear time domain simulations. With this aim and according to the discussion of Section 6.4.2, we eliminate the dense segments $\partial g_{(\omega_{CoI})}/\partial \omega_{r,i}$, $\partial f_{(\delta_{r,i})}/\partial \omega_{CoI}$, $\partial g_{(P_{ord,i})}/\partial P_s$, $\partial f_{(x_{r,i})}/\partial \mathbf{Q}_r$, that arise from (6.21)-(6.24). We simulate the transient following a three-phase fault applied at bus 6 at $t = 1$ s. The fault is cleared after 80 ms by tripping the transmission line that connects buses 5 and 6. The system is numerically integrated using the ITM. Figure 6.3 shows the transient behavior of the rotor speed of generator 2 for integration step sizes $h = 0.02$ s and $h = 0.1$ s. The larger h is, the larger is the mismatch between the two trajectories. In both plots though, the trajectory of the DDAE system closely follows the original trajectory, as expected.

It is relevant to check the accuracy of the proposed one-step delay technique under different operating conditions and contingencies. In addition to the operating condition considered above (from here and on referred as the base case), two other operating conditions are considered, namely, 10% and 20% increase in the total power consumption of the system. For each operating point, the transient response of the system is examined. Two different disturbances are considered: first, the three phase fault applied at bus 6 described above; and second, the loss of the load connected to bus 39 at $t = 1$ s, which leads to a 1.109 GW decrease in the power consumption of the system. In all scenarios, the delayed variables do not change and are the ones used to plot the base case in Figure 6.3.

The response of the rotor speeds of the DAE system are compared with the respective speed trajectories obtained by integrating the DDAE system. Each system is simulated for 100 s and for two time step sizes, $h = 0.02$ s and $h = 0.10$ s. The maximum absolute rotor speed trajectory errors are summarized in Table 6.5. As expected, the proposed technique shows high accuracy for all considered operating conditions and disturbances.

6.6.2 21,177-bus ENTSO-E

This subsection presents simulation results on a dynamic model of the ENTSO-E transmission system, which has been also discussed in Section 2.6.2. In addition to the model components considered in Section 2.6.2, the system examined in this section also includes AGC and SVR mechanisms, which provide secondary frequency and voltage control, respectively, to different areas of the system. In total, the system has 49,930

Table 6.5: IEEE 39-bus system: Maximum absolute rotor speed trajectory mismatches induced by the proposed method.

Operating condition	Applied disturbance	$h = 0.02$ s	$h = 0.10$ s
		– max. error	– max. error
Base case	Fault at bus 6	$6.0 \cdot 10^{-6}$	$8.3 \cdot 10^{-5}$
	Bus 39 load trip	$9.0 \cdot 10^{-6}$	$4.2 \cdot 10^{-5}$
+10% load	Fault at bus 6	$6.0 \cdot 10^{-6}$	$4.8 \cdot 10^{-4}$
	Bus 39 load trip	$1.2 \cdot 10^{-5}$	$5.7 \cdot 10^{-5}$
+20% load	Fault at bus 6	$7.0 \cdot 10^{-6}$	$5.8 \cdot 10^{-4}$
	Bus 39 load trip	$1.7 \cdot 10^{-5}$	$8.4 \cdot 10^{-5}$

state variables and 97,304 algebraic variables. The full Jacobian matrix has dimensions $147,234 \times 147,234$ and 1,226,492 non-zero elements, which yields a density degree of 0.0057 %.

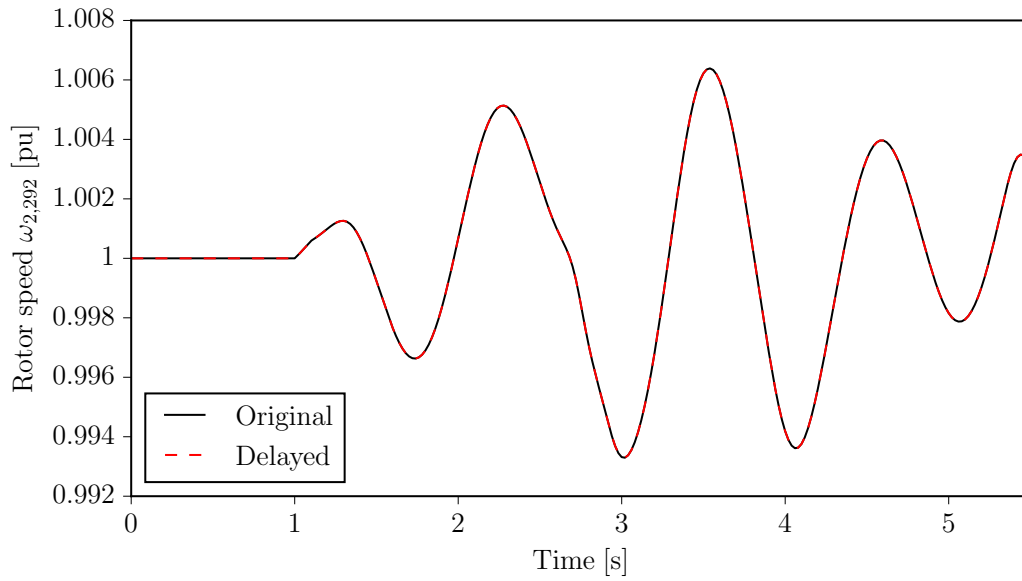
In order to show the impact of the one-step delay approximation on the accuracy, number of factorizations and computational burden of the TDI, the dense segments that arise from (6.21)-(6.24) are eliminated, leading to a sparser and less coupled model. The NNZ Jacobian elements of the original and delayed system are summarized in Table 6.6.

Table 6.6: ENTSO-E system: NNZ Jacobian elements.

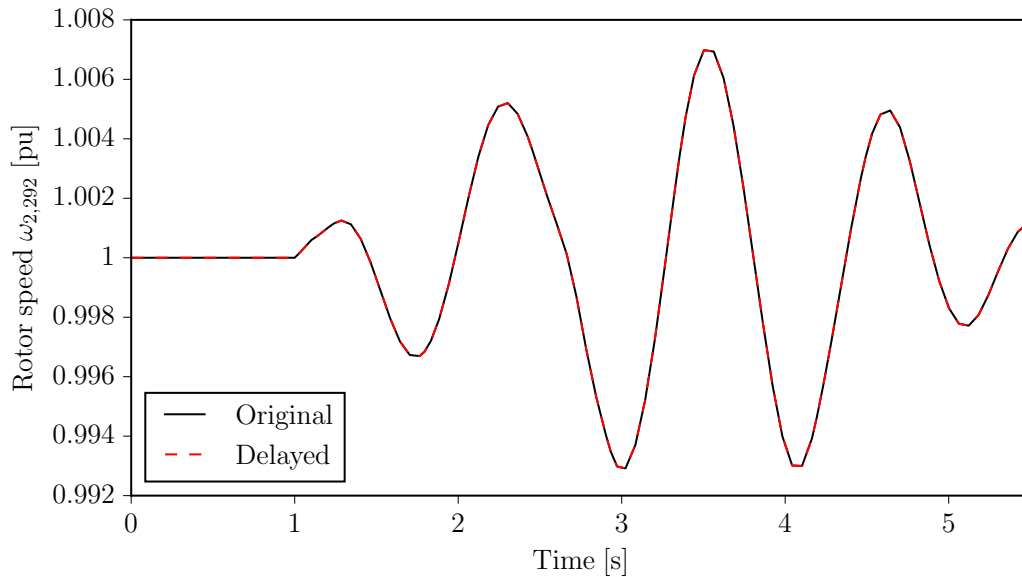
System	NNZ Jacobian elements	Density (%)	Relative difference
Original	1,226,492	0.0057	
Delayed	936,871	0.0043	–23.61 %

We consider a three-phase fault at bus 12,921, occurring at $t = 1$ s. The fault is cleared after 100 ms. The response of the rotor speed of the synchronous generator connected at bus 2,292 during the first seconds following the fault, is shown in Figure 6.4 for two different time step sizes. The difference between the two trajectories is very small, which indicates that accuracy is maintained. In particular, the maximum absolute mismatch between the two trajectories for the cases shown in Figure 6.4 are: (a) $1.0 \cdot 10^{-6}$, (b) $7.0 \cdot 10^{-6}$.

The impact of the one-step delay approximation on the number of factorizations of the TDI is examined next. Following a disturbance, the system shows a transient and, provided that the trajectory is stable, finally reaches a stationary point. While in steady



(a) $h = 0.02$ s.



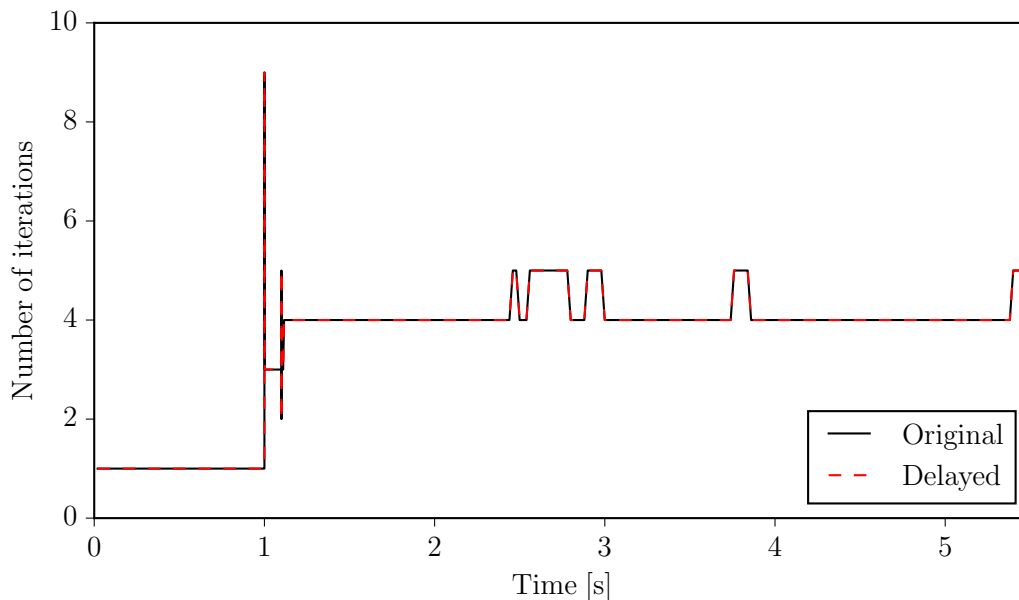
(b) $h = 0.06$ s.

Figure 6.4: ENTSO-E system: transient following a three-phase fault.

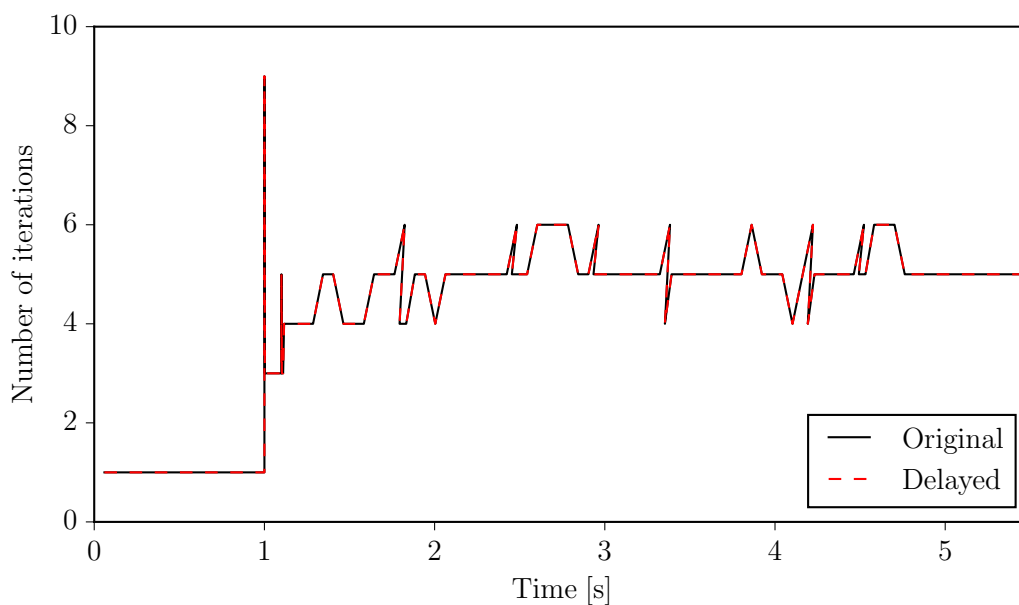
state, the ITM requires exactly one factorization for each time step, both for the original and the delayed system. Hence, any noticeable differences in the number of factorizations required by the original and the delayed system occur during the first seconds following the disturbance.

The number of factorizations required by the original and the delayed system during the first seconds following the three-phase fault, are shown in Figure 6.5. Since the increments of the variables at each time step are updated according to the standard

Newton method (see Section 6.2), the number of factorizations at each time step is equal to the number of Newton iterations. The original and the delayed system require in this case the same number of factorizations at each time step to converge. This indicates that the approximation does not jeopardize the convergence.



(a) $h = 0.02$ s.



(b) $h = 0.06$ s.

Figure 6.5: ENTSO-E system: number of Newton iterations.

Finally, it is relevant to evaluate the effect of the one-step delay approximation on the computational burden of the TDI. The method reduces the coupling of the ENTSO-E system and facilitates the potential application of techniques that factorize decoupled

blocks of the Jacobian matrix in parallel. In turn, enabling parallelization leads to a significant speedup of the simulation. However, as already stated, the goal of this chapter is to provide a technique for decoupling and sparsity increase rather than applying parallel techniques. Hence, the original and delayed ENTSO-E systems are compared in terms of computational effort required for a non-parallel numerical integration.

The full Jacobian matrix without introducing delays requires 0.245 s per each factorization, in average, on a 8×3.5 GHz Intel Xeon CPU desktop computer, while the Jacobian matrix of the delayed system requires 0.223 s, which corresponds to a speedup of 9.04 %.

Apart from the factorization speed-up, one has also to evaluate whether the delayed system requires more or less iterations than the original system to solve the Newton method for each point of the time domain integration. With this regard, Figure 6.5 has already shown an example where the two systems require at each point the same number of iterations. In addition, several cases have been carried out considering a variety of contingencies and time steps and it has been found out that the proposed technique is able to reduce the simulation time in range from 5 to 20%.

For the sake of example, consider the three-phase fault at bus 2,292 discussed above. The system is integrated for 7 s. With a time step $h = 0.02$ s, the original system completes the numerical factorization in 298.63 s, while the delayed system in 262.14 s, which corresponds to a speedup of 12.22 %.

The proposed one-step-delay technique is agnostic with respect to the integration scheme utilized for the TDI. For this reason, the proposed approach can be coupled with any other numerical technique to speed up time domain simulation software. Hence, even if the speed-up provided by the proposed formulation *per se* is not huge, it can be combined with other techniques. Moreover, reducing the computational burden is not the only benefit of the proposed one-step delay technique. A relevant feature is that it increases the decoupling of system variables. This leads to a sparser and more decoupled system Jacobian matrix. The latter is a feature that is expected to be beneficial to further speed up the time domain analysis if combined with parallelization techniques.

6.7 Conclusions

The chapter presents a systematic approach to exploit delays to reduce the coupling of the equations of conventional DAE models of power systems for transient stability analysis. With this aim, the chapter discusses how to select the variables of a power system DAE model that can be delayed and provides an estimation of the maximum admissible time delay so that simulation accuracy is maintained. This analysis has to be carried out only once per network. Numerical simulations support the theoretical appraisal of the proposed approach and show its accuracy, convergence and computational burden.

Chapter 7

Conclusions and Future Work

This thesis proposes novel SSSA-based techniques with application to modal analysis, robust control, and numerical integration of power systems. The objective of this chapter is to summarize the main conclusions of the thesis and support directions for future work.

- *Modal analysis:* The study on modal analysis shows that the classical assumptions made when computing PFs, namely that the system is modeled as a set of ODEs and that all eigenvalues are distinct, are not binding. In fact, considering a singular system of differential equations with eigenvalue multiplicities, allows extracting a generalized expression of PFs in the form of eigen-sensitivities, from which PFs in the classical sense arise as a special case. Moreover, prior to this work, algebraic variables of a power system model were either eliminated or treated as states with infinitely fast dynamics and, as such, their PFs to finite modes were considered to be null. The proposed formulation shows that it is possible to quantify the PFs of algebraic variables of a power system, and in general of any function of the system variables, through the definition of appropriate input/output vectors of the system's state-space model.

Future work will focus on studying the effect of network constraints on the design of control schemes based on the proposed modal analysis. A control signal/actuator selection that is based on the PFs of line power flows and takes into account information on the current/power capacity limits of transmission lines is a relevant example. Such information is readily available to system operators and thus it can be effectively included to the analysis.

Moreover, the proposed formulation of PFs can be extended to include the analysis of systems of fractional differential equations. Such analysis will allow measuring the coupling between the variables of a power system models and its fractional order dynamics, such as the ones introduced by FOCs discussed in Chapter 4. Moreover, extension of the proposed modal participation analysis is also relevant for systems of DDAEs. This will allow an efficient assessment of control signals impacted by time delays, including wide-area controllers and controllers with intentional delays, such as the ones described in Chapter 5. In this case, the calculation of PFs will be a challenging task, since the existence of an infinite dimensional spectrum makes it difficult to determine the coupling between eigenvectors and system variables in an accurate and efficient way.

- *Fractional Control:* The contributions of the thesis are a systematic study of controllers based on fractional calculus and a technique to carry out eigenvalue analysis and assess the small-signal stability of power systems with inclusion of exact fractional dynamics of Caputo type. Furthermore, the properties of ORA are investigated and, through time domain simulations, it is shown that FOCs perform better than their conventional IO versions for synchronous machine AGC, ESS frequency control, and STATCOM voltage control, while they require only a small additional tuning effort.

A relevant extension of the work on FOCs is the study of practical aspects, such as potential modeling and stability issues introduced with the inclusion of control saturation limits. With this regard, a preliminary study on FOC control limits for power system applications can be found in [108]. Furthermore, time domain simulations in Chapter 4 are based on the widely employed ORA, but there exist also other methods that approximate fractional order dynamics, see e.g. [181]. To the best of our knowledge, a systematic study that provides an eigenvalue-based comparison of approximation methods for fractional order dynamics with application to power systems is still missing and it is worth consideration.

- *Delay-based Control:* The study on time-delayed control focuses on the stability boundary of power systems with delay-based PSSs, as well as on the relationship between the existence of delay-independent stability and connected stability

domains in the delay-control gain space. Analytical results based on the OMIB system, as well as a numerical analysis of the IEEE 14-bus system, illustrate that in contrast to their bad reputation, large delays may achieve best damping characteristics, provided that the PSS is properly configured. It is shown that one such possible configuration is to employ a two-channel PSS, which permits a fully connected stability region in the delay-gain space. Then, non-linear dynamics can be tuned to achieve high damping, by fully exploring the parameter space and without introducing instabilities.

A possible future work direction is the design of an adaptive control scheme so that the delay and gain are automatically tuned, following a stable path and through consecutive quasi-steady state shifts of the system equilibrium. This is particularly interesting in case that part of the delay is inherent, i.e. represents measurement and/or communication latency. In this case, high damping can be achieved by adding an artificial controlled delay on top of the inherent delay. This is a novel approach, whose effectiveness can be assessed in comparison with other techniques used for mitigating the destabilizing effect of communication delays, such as delay compensation methods [87, 88].

- *Numerical Integration:* Finally, this work proposes an “one-step delay” approximation technique for the numerical integration of the DAEs utilized to study power system transient stability, and provides a first evaluation of its accuracy, convergence and computational burden. Chapter 6 shows that the proposed approach allows exploiting delays equal to the time step of the numerical integration, in order to reduce the coupling of the equations of conventional power system DAE models for transient stability analysis. SSSA-based techniques are discussed for the selection of the variables of a power system DAE model that can be delayed, as well as for the estimation of the maximum admissible time delay, so that the accuracy of trajectories is not compromised.

The next step is to embed the proposed one-step delay approximation technique in algorithms that apply state-of-the art parallelization techniques. This will typically require to exploit a current injection-based power system model formulation, in

order to take advantage of the BBD structure of the corresponding Jacobian matrix, see e.g. [38, 41].

Appendices

Appendix A

Proofs

A.1 Proof of Theorem 2.1

By substituting the transformation

$$\mathbf{x}(t) = \mathbf{V} \boldsymbol{\xi}(t) \tag{A.1}$$

into (2.10), and by multiplying by \mathbf{W} , one obtains:

$$\mathbf{W} \mathbf{E} \mathbf{V} \dot{\boldsymbol{\xi}}(t) = \mathbf{W} \mathbf{A} \mathbf{V} \boldsymbol{\xi}(t) + \mathbf{W} \mathbf{B} \mathbf{u}(t). \tag{A.2}$$

Let $\mathbf{V}_\nu, \mathbf{V}_\mu$ be the matrices that contain all right eigenvectors of the finite, and infinite eigenvalues respectively. Then by setting $\boldsymbol{\xi} = [\boldsymbol{\xi}_\nu \ \boldsymbol{\xi}_\mu]^\top$, $\mathbf{V} = [\mathbf{V}_\nu \ \mathbf{V}_\mu]$, with $\boldsymbol{\xi}_\nu \in \mathbb{C}^\nu$, $\boldsymbol{\xi}_\mu \in \mathbb{C}^\mu$, and using (2.18), we arrive at two subsystems of (A.2):

$$\begin{aligned} \dot{\boldsymbol{\xi}}_\nu(t) &= \mathbf{J}_\nu \boldsymbol{\xi}_\nu(t) + \mathbf{W}_\nu \mathbf{B} \mathbf{u}(t), \\ \mathbf{H}_\mu \dot{\boldsymbol{\xi}}_\mu(t) &= \boldsymbol{\xi}_\mu(t) + \mathbf{W}_\mu \mathbf{B} \mathbf{u}(t). \end{aligned}$$

The first subsystem has solution:

$$\boldsymbol{\xi}_\nu(t) = e^{\mathbf{J}_\nu t} \mathbf{c} + \int_0^\infty e^{\mathbf{J}_\nu(t-\kappa)} \mathbf{W}_\nu \mathbf{B} \mathbf{u}(\kappa) d\kappa, \tag{A.3}$$

where $\mathbf{c} = \boldsymbol{\xi}_\nu(0)$ is a constant vector. For the second subsystem, let μ_* be the index of the nilpotent matrix \mathbf{H}_μ , i.e. $\mathbf{H}_\mu^{\mu_*} = \mathbf{0}_{\mu,\mu}$. Then following matrix equations are obtained:

$$\begin{aligned} \mathbf{H}_\mu \dot{\boldsymbol{\xi}}_\mu(t) &= \boldsymbol{\xi}_\mu(t) + \mathbf{W}_\mu \mathbf{B} \mathbf{u}(t) \\ \mathbf{H}_\mu^2 \ddot{\boldsymbol{\xi}}_\mu(t) &= \mathbf{H}_\mu \dot{\boldsymbol{\xi}}_\mu(t) + \mathbf{H}_\mu \mathbf{W}_\mu \mathbf{B} \dot{\mathbf{u}}(t) \\ &\vdots \\ \mathbf{H}_\mu^{\mu_*-1} \boldsymbol{\xi}_\mu^{(\mu_*-1)}(t) &= \mathbf{H}_\mu^{\mu_*-2} \boldsymbol{\xi}_\mu^{(\mu_*-2)}(t) + \mathbf{H}_\mu^{\mu_*-2} \mathbf{W}_\mu \mathbf{B} \mathbf{u}^{(\mu_*-2)}(t) \\ \mathbf{H}_\mu^{\mu_*} \boldsymbol{\xi}_\mu^{(\mu_*)}(t) &= \mathbf{H}_\mu^{\mu_*-1} \boldsymbol{\xi}_\mu^{(\mu_*-1)}(t) + \mathbf{H}_\mu^{\mu_*-1} \mathbf{W}_\mu \mathbf{B} \mathbf{u}^{(\mu_*-1)}(t). \end{aligned}$$

By taking the sum of the above equations, the solution for the second subsystem is:

$$\boldsymbol{\xi}_\mu(t) = - \sum_{i=0}^{\mu_*-1} \mathbf{H}_\mu^i \mathbf{W}_\mu \mathbf{B} \mathbf{u}^{(i)}(t). \quad (\text{A.4})$$

Using the solutions (A.3) and (A.4) in (A.1), ones gets:

$$\mathbf{x}(t) = \begin{bmatrix} \mathbf{V}_\nu & \mathbf{V}_\mu \end{bmatrix} \begin{bmatrix} \boldsymbol{\xi}_\nu(t) \\ \boldsymbol{\xi}_\mu(t) \end{bmatrix}, \quad (\text{A.5})$$

or equivalently,

$$\mathbf{x}(t) = \mathbf{V}_\nu e^{\mathbf{J}_\nu t} \mathbf{c} + \mathbf{V}_\nu \int_0^\infty e^{\mathbf{J}_\nu(t-\kappa)} \mathbf{W}_\nu \mathbf{B} \mathbf{u}(\kappa) d\kappa - \mathbf{V}_\mu \sum_{i=0}^{\mu_*-1} \mathbf{H}_\mu^i \mathbf{W}_\mu \mathbf{B} \mathbf{u}^{(i)}(t),$$

which is the general solution (2.19). ■

A.2 Proof of Theorem 3.1

(a) By using the transformation $\mathbf{x}(t) = \mathbf{V} \boldsymbol{\xi}(t)$, from the proof of Theorem 2.1, and in particular from (A.5), one has for $\mathbf{B} = \mathbf{0}_{r,p}$:

$$\mathbf{x}(t) = \mathbf{V}_\nu \boldsymbol{\xi}_\nu(t). \quad (\text{A.6})$$

Let $\mathbf{W}_\nu, \mathbf{W}_\mu$ be the matrices that contain all left eigenvectors of the finite, and infinite eigenvalues of the pencil $s\mathbf{E} - \mathbf{A}$, respectively. Then by using the notation

$\mathbf{W} = [\mathbf{W}_\nu \ \mathbf{W}_\mu]^\top$, and making use of (2.18), there exist $\mathbf{W}_\nu, \mathbf{V}_\nu$, such that $\mathbf{W}_\nu \mathbf{E} \mathbf{V}_\nu = \mathbf{I}_\nu$. Multiplying (A.6) by $\mathbf{W}_\nu \mathbf{E}$ yields:

$$\mathbf{W}_\nu \mathbf{E} \mathbf{x}(t) = \mathbf{W}_\nu \mathbf{E} \mathbf{V}_\nu \boldsymbol{\xi}_\nu(t),$$

or, equivalently,

$$\boldsymbol{\xi}_\nu(t) = \mathbf{W}_\nu \mathbf{E} \mathbf{x}(t).$$

Hence:

$$\boldsymbol{\xi}_\nu(0) = \mathbf{W}_\nu \mathbf{E} \mathbf{x}(0). \quad (\text{A.7})$$

Substitution of (A.7) into the general solution (3.8) gives:

$$\mathbf{x}(t) = \mathbf{V}_\nu e^{\mathbf{J}_\nu t} \mathbf{W}_\nu \mathbf{E} \mathbf{x}(0). \quad (\text{A.8})$$

The matrices $\mathbf{V}_\nu, \mathbf{W}_\nu$ can be written as:

$$\mathbf{V}_\nu = [\mathbf{v}_1^{[\beta_1]} \dots \mathbf{v}_1^{[2]} \mathbf{v}_1^{[1]} \dots \mathbf{v}_\alpha^{[\beta_\alpha]} \dots \mathbf{v}_\alpha^{[2]} \mathbf{v}_\alpha^{[1]}], \quad (\text{A.9})$$

$$\mathbf{W}_\nu = [\mathbf{w}_1^{[\beta_1]} \dots \mathbf{w}_1^{[2]} \mathbf{w}_1^{[1]} \dots \mathbf{w}_\alpha^{[\beta_\alpha]} \dots \mathbf{w}_\alpha^{[2]} \mathbf{w}_\alpha^{[1]}]^\top, \quad (\text{A.10})$$

where $\mathbf{v}_i^{[j]}, \mathbf{w}_i^{[j]}, j = 1, 2, \dots, \beta_i$, linear (generalized) independent right, left eigenvectors of $\hat{\lambda}_i, i = 1, 2, \dots, \alpha$, respectively.

The Jordan matrix \mathbf{J}_ν has the following form:

$$\mathbf{J}_\nu := \mathbf{J}_{\beta_1}(\hat{\lambda}_1) \oplus \dots \oplus \mathbf{J}_{\beta_\alpha}(\hat{\lambda}_\alpha),$$

where

$$\mathbf{J}_{\beta_i}(\hat{\lambda}_i) = \begin{bmatrix} \hat{\lambda}_i & 1 & \dots & 0 & 0 \\ 0 & \hat{\lambda}_i & \dots & 0 & 0 \\ \vdots & \vdots & \ddots & \vdots & \vdots \\ 0 & 0 & \dots & \hat{\lambda}_i & 1 \\ 0 & 0 & \dots & 0 & \hat{\lambda}_i \end{bmatrix} \in \mathbb{C}^{\beta_i \times \beta_i}, \quad i = 1, 2, \dots, \alpha,$$

is the Jordan block that corresponds to the eigenvalue $\hat{\lambda}_i$. The matrix exponential of $\mathbf{J}_\nu t$, denoted as $e^{\mathbf{J}_\nu t}$, is defined as:

$$e^{\mathbf{J}\nu t} := e^{\mathbf{J}_{\beta_1}(\hat{\lambda}_1)t} \oplus \dots \oplus e^{\mathbf{J}_{\beta_\alpha}(\hat{\lambda}_\alpha)t}, \quad (\text{A.11})$$

where

$$e^{\mathbf{J}_{\beta_i}(\hat{\lambda}_i)t} = \begin{bmatrix} e^{\hat{\lambda}_i t} & e^{\hat{\lambda}_i t} t & \dots & e^{\hat{\lambda}_i t} \frac{t^{\beta_i-1}}{(\beta_i-1)!} & e^{\hat{\lambda}_i t} \frac{t^{\beta_i}}{\beta_i!} \\ 0 & e^{\hat{\lambda}_i t} & \dots & e^{\hat{\lambda}_i t} \frac{t^{\beta_i-2}}{(\beta_i-2)!} & e^{\hat{\lambda}_i t} \frac{t^{\beta_i-1}}{(\beta_i-1)!} \\ \vdots & \vdots & \ddots & \vdots & \vdots \\ 0 & 0 & \dots & e^{\hat{\lambda}_i t} & e^{\hat{\lambda}_i t} t \\ 0 & 0 & \dots & 0 & e^{\hat{\lambda}_i t} \end{bmatrix} \in \mathbb{C}^{\beta_i \times \beta_i}, \quad i = 1, 2, \dots, \alpha.$$

By substituting (A.9), (A.10), (A.11) in (A.8), one arrives at (3.9).

(b) From (3.9), the evolution of $\mathbf{x}_k(t)$, i.e. the k -th element of $\mathbf{x}(t)$, is:

$$\mathbf{x}_k(t) = \sum_{i=1}^{\alpha} e^{\hat{\lambda}_i t} \sum_{j=1}^{\beta_i} \left(\sum_{\sigma=1}^j t^{\sigma-1} \mathbf{w}_i^{[j-\sigma+1]} \mathbf{E} \mathbf{x}(0) \right) \mathbf{v}_{k,i}^{[j]}, \quad (\text{A.12})$$

where $\mathbf{v}_{k,i}^{[j]} \in \mathbf{v}_i^{[j]}$.

Partial differentiation of this equation with respect to $e^{\hat{\lambda}_i t}$ leads to:

$$\frac{\partial \mathbf{x}_k(t)}{\partial e^{\hat{\lambda}_i t}} = \sum_{j=1}^{\beta_i} \left(\sum_{\sigma=1}^j t^{\sigma-1} \mathbf{w}_i^{[j-\sigma+1]} \mathbf{E} \mathbf{x}(0) \right) \mathbf{v}_{k,i}^{[j]}, \quad (\text{A.13})$$

which is the PF of $\hat{\lambda}_i$, $i = 1, 2, \dots, \alpha$, in $\mathbf{x}_k(t)$, $k = 1, 2, \dots, r$. ■

A.3 Proof of Theorem 4.1

Let $\mathcal{L}\{\mathbf{x}(t)\}$ be the Laplace transform of $\mathbf{x}(t)$. Using the Caputo fractional derivative, by applying the Laplace transform \mathcal{L} as defined in (4.4) for $\mu = 1$ into (4.15), one gets [63]:

$$\mathcal{L}\{\tilde{\mathbf{E}} \mathbf{x}^\Delta(t)\} = \mathcal{L}\{\tilde{\mathbf{A}} \mathbf{x}(t)\}. \quad (\text{A.14})$$

Note that

$$\mathbf{x}^\Delta(t) = \begin{bmatrix} \frac{d^\gamma}{dt^\gamma} \mathbf{I}_\rho & \mathbf{0}_{\rho,\rho} \\ \mathbf{0}_{\rho,\rho} & \frac{d^\beta}{dt^\beta} \mathbf{I}_\rho \end{bmatrix} \mathbf{x}(t),$$

and hence

$$\tilde{\mathbf{E}}\mathbf{x}^\Delta(t) = \begin{bmatrix} \mathbf{I}_\rho & \mathbf{0}_{\rho,\rho} \\ \mathbf{0}_{\rho,\rho} & \mathbf{M} \end{bmatrix} \begin{bmatrix} \frac{d^\gamma}{dt^\gamma} \mathbf{I}_\rho & \mathbf{0}_{\rho,\rho} \\ \mathbf{0}_{\rho,\rho} & \frac{d^\beta}{dt^\beta} \mathbf{I}_\rho \end{bmatrix} \mathbf{x}(t),$$

or, equivalently,

$$\tilde{\mathbf{E}}\mathbf{x}^\Delta(t) = \begin{bmatrix} \frac{d^\gamma}{dt^\gamma} \mathbf{I}_\rho & \mathbf{0}_{\rho,\rho} \\ \mathbf{0}_{\rho,\rho} & \frac{d^\beta}{dt^\beta} \mathbf{M} \end{bmatrix} \begin{bmatrix} \mathbf{x}_1 \\ \mathbf{x}_2 \end{bmatrix} = \begin{bmatrix} \frac{d^\gamma \mathbf{x}_1}{dt^\gamma} & \mathbf{0}_{\rho,\rho} \\ \mathbf{0}_{\rho,\rho} & \mathbf{M} \frac{d^\beta \mathbf{x}_2}{dt^\beta} \end{bmatrix}.$$

Thus, $\mathcal{L}\{\tilde{\mathbf{E}}\mathbf{x}^\Delta(t)\} = \tilde{\mathbf{E}}\mathcal{L}\{\mathbf{x}^\Delta(t)\}$ and (A.14) becomes:

$$\tilde{\mathbf{E}}\mathcal{L}\{\mathbf{x}^\Delta(t)\} = \tilde{\mathbf{A}}\mathcal{L}\{\mathbf{x}(t)\},$$

or, equivalently,

$$\tilde{\mathbf{E}}\mathcal{L}\left\{ \begin{bmatrix} \mathbf{x}_1^{(\gamma)}(t) \\ \mathbf{x}_2^{(\beta)}(t) \end{bmatrix} \right\} = \tilde{\mathbf{A}}\mathcal{L}\{\mathbf{x}(t)\},$$

or, equivalently,

$$\tilde{\mathbf{E}} \begin{bmatrix} s^\gamma \mathcal{L}\{\mathbf{x}_1(t)\} - s^{\gamma-1} \mathbf{x}_1(0) \\ s^\beta \mathcal{L}\{\mathbf{x}_2(t)\} - s^{\beta-1} \mathbf{x}_2(0) \end{bmatrix} = \tilde{\mathbf{A}}\mathcal{L}\{\mathbf{x}(t)\},$$

or, equivalently,

$$\tilde{\mathbf{E}} \begin{bmatrix} s^\gamma \mathcal{L}\{\mathbf{x}_1(t)\} \\ s^\beta \mathcal{L}\{\mathbf{x}_2(t)\} \end{bmatrix} - \tilde{\mathbf{E}} \begin{bmatrix} s^{\gamma-1} \mathbf{x}_1(0) \\ s^{\beta-1} \mathbf{x}_2(0) \end{bmatrix} = \tilde{\mathbf{A}}\mathcal{L}\{\mathbf{x}(t)\},$$

or, equivalently,

$$\tilde{\mathbf{E}} \begin{bmatrix} s^\gamma \mathbf{I}_\rho & \mathbf{0}_{\rho,\rho} \\ \mathbf{0}_{\rho,\rho} & s^\beta \mathbf{I}_\rho \end{bmatrix} \begin{bmatrix} \mathcal{L}\{\mathbf{x}_1(t)\} \\ \mathcal{L}\{\mathbf{x}_2(t)\} \end{bmatrix} - \tilde{\mathbf{E}} \begin{bmatrix} s^{\gamma-1} \mathbf{I}_\rho & \mathbf{0}_{\rho,\rho} \\ \mathbf{0}_{\rho,\rho} & s^{\beta-1} \mathbf{I}_\rho \end{bmatrix} \begin{bmatrix} \mathbf{x}_1(0) \\ \mathbf{x}_2(0) \end{bmatrix} = \tilde{\mathbf{A}}\mathcal{L}\{\mathbf{x}(t)\},$$

or, equivalently,

$$\left(\tilde{\mathbf{E}} \begin{bmatrix} s^\gamma \mathbf{I}_\rho & \mathbf{0}_{\rho,\rho} \\ \mathbf{0}_{\rho,\rho} & s^\beta \mathbf{I}_\rho \end{bmatrix} - \tilde{\mathbf{A}} \right) \mathcal{L}\{\mathbf{x}(t)\} = \begin{bmatrix} s^{\gamma-1} \mathbf{I}_\rho & \mathbf{0}_{\rho,\rho} \\ \mathbf{0}_{\rho,\rho} & s^{\beta-1} \mathbf{I}_\rho \end{bmatrix} \mathbf{x}(0). \quad (\text{A.15})$$

■

Appendix B

Map of the All-Island Irish Transmission System

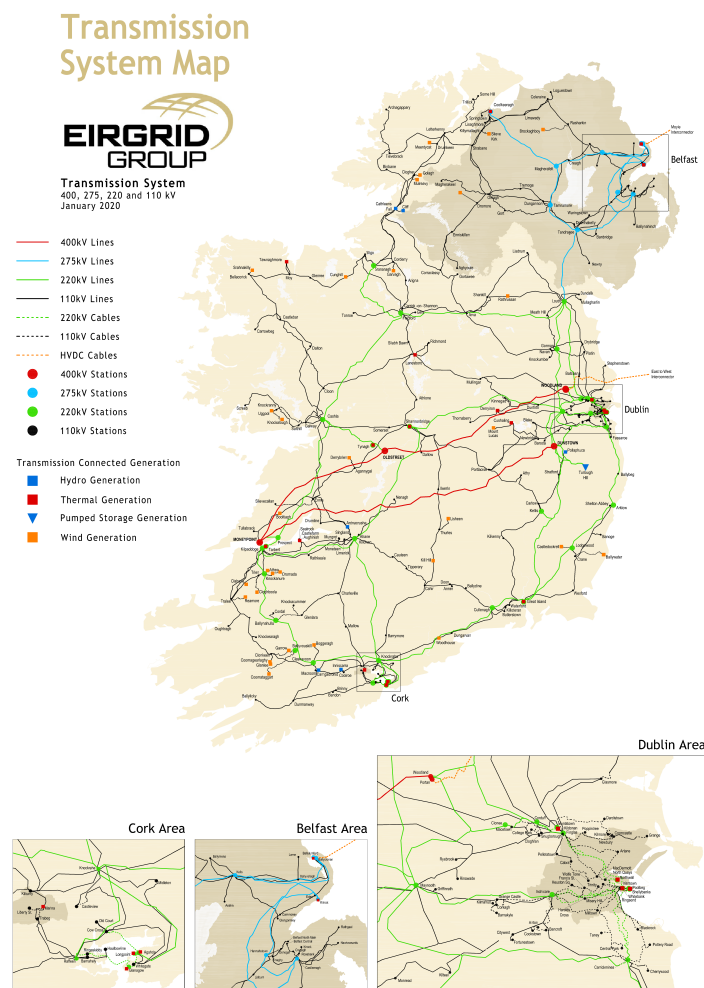


Figure B.1: AIITS: transmission system map, January 2020.

Bibliography

- [1] ABB FACTS Division, “A matter of FACTS deliver more high quality power,” 2015, product guide, available at library.e.abb.com. 37, 53
- [2] C. Abdallah, P. Dorato, J. Benites-Read, and R. Byrne, “Delayed positive feedback can stabilize oscillatory systems,” in *Proceedings of the American Control Conference*, 1993, pp. 3106–3107. 5
- [3] E. H. Abed, D. Lindsay, and W. A. Hashlamoun, “On participation factors for linear systems,” *Automatica*, vol. 36, no. 10, pp. 1489 – 1496, 2000. 37
- [4] K. Abidi, Y. Yildiz, and B. E. Korpe, “Explicit time-delay compensation in teleoperation: An adaptive control approach,” *International Journal of Robust and Nonlinear Control*, vol. 26, no. 15, pp. 3388–3403, 2016. 87
- [5] P. Amestoy, I. S. Duff, J. Koster, and J.-Y. L’Excellent, “A fully asynchronous multifrontal solver using distributed dynamic scheduling,” *SIAM Journal on Matrix Analysis and Applications*, vol. 23, no. 1, pp. 15–41, 2001. 22
- [6] Y. Amirnaser and I. Reza, *Voltage-Sourced Converters in Power Systems: Modeling, Control, and Applications*. Wiley-IEEE Press, 2012. 82
- [7] P. M. Anderson and A. A. Fouad, *Power System Control and Stability*, 2nd ed. IEEE Press: Wiley-Interscience, 2003. 70
- [8] E. Angerson, Z. Bai, J. Dongarra, A. Greenbaum, A. McKenney, J. D. Croz, S. Hammarling, J. Demmel, C. Bischof, and D. Sorensen, “LAPACK: A portable linear algebra library for high-performance computers,” in *Proceedings of the 1990 ACM/IEEE Conference on Supercomputing*, Nov. 1990, pp. 2–11. 21, 106

- [9] Argonne National Laboratory, “PETSc users manual,” 2020. [Online]. Available: <https://www.mcs.anl.gov/petsc> 22
- [10] W. E. Arnoldi, “The principle of minimized iterations in the solution of the matrix eigenvalue problem,” *Quarterly of Applied Mathematics*, vol. 9, no. 1, pp. 17–29, 1951. 21
- [11] R. Asghari, B. Mozafari, M. Salay Naderi, T. Amraee, V. Nurmanova, and M. Bagheri, “A novel method to design delay-scheduled controllers for damping inter-area oscillations,” *IEEE Access*, vol. 6, pp. 71 932–71 946, 2018. 88
- [12] A. Atangana and D. Baleanu, “New fractional derivatives with nonlocal and non-singular kernel: Theory and application to heat transfer model,” *Thermal Science*, vol. 20, no. 2, pp. 763–769, Jan. 2016. 60
- [13] C. Baker, U. Hetmaniuk, R. Lehoucq, and H. Thornquist, “Anasazi software for the numerical solution of large-scale eigenvalue problems,” *ACM Transactions on Mathematical Software*, vol. 36, no. 13, pp. 351–362, Jul. 2009. 22
- [14] K. J. Bathe and E. L. Wilson, “Solution methods for large generalized eigenvalue problems in structural engineering,” *International Journal for Numerical Methods in Engineering*, vol. 6, pp. 213–226, 1973. 21
- [15] A. Bellen, N. Guglielmi, and A. E. Ruehli, “Methods for linear systems of circuit delay differential equations of neutral type,” *IEEE Transactions on Circuits and Systems - I: Fundamental Theory and Applications*, vol. 46, no. 1, pp. 212–215, Jan. 1999. 111
- [16] A. Bellen and S. Maset, “Numerical solution of constant coefficient linear delay differential equations as abstract Cauchy problems,” *Numerische Mathematik*, vol. 84, no. 3, pp. 351–374, Jan. 2000. 94
- [17] R. Bellman and K. L. Cooke, *Differential-Difference Equations*. New York, USA: Academic Press, 1963. 87
- [18] L. S. Blackford, J. Choi, A. Cleary, E. D’Azevedo, J. Demmel, I. Dhillon, J. Dongarra, S. Hammarling, G. Henry, A. Petitet, K. Stanley, D. Walker, and R. C. Whaley, *ScaLAPACK Users’ Guide*. SIAM, 1997. 23

- [19] H. Bode, *Network Analysis and Feedback Amplifier Design*. Princeton, NJ: Van Nostrand, 1945. 57
- [20] B. Bonilla, M. Rivero, and J. Trujillo, “On systems of linear fractional differential equations with constant coefficients,” *Applied Mathematics and Computation*, vol. 187, no. 1, pp. 68–78, 2007. 60
- [21] D. Breda, S. Maset, and R. Vermiglio, *Stability of Linear Delay Differential Equations: A Numerical Approach with MATLAB*. New York, USA: Springer, 2015. 94
- [22] E. F. Camacho and C. Bordons, *Model Predictive Control*. Springer, 2007. 4
- [23] M. Caputo and M. Fabrizio, “A new definition of fractional derivative without singular kernel,” *Progress in Fractional Differentiation and Applications*, vol. 1, no. 2, pp. 73–85, Apr. 2015. 59, 60
- [24] L. Chaib, A. Choucha, and S. Arif, “Optimal design and tuning of novel fractional order PID power system stabilizer using a new metaheuristic Bat algorithm,” *Ain Shams Engineering Journal*, vol. 8, no. 2, pp. 113 – 125, Jun. 2017. 58
- [25] J. H. Chow, J. J. Sanchez-Gasca, H. Ren, and S. Wang, “Power system damping controller design-using multiple input signals,” *IEEE Control Systems Magazine*, vol. 20, no. 4, pp. 82–90, Aug. 2000. 3
- [26] J. H. Chow, *Power System Coherency and Model Reduction*, ser. Power Electronics and Power Systems 94. New York: Springer-Verlag, 2013. 37, 123
- [27] A. Dabiri, B. P. Moghaddam, and J. A. T. Machado, “Optimal variable-order fractional PID controllers for dynamical systems,” *Journal of Computational and Applied Mathematics*, vol. 339, pp. 40–48, 2018. 57
- [28] L. Dai, *Singular Control Systems*. M. Thoma, A. Wyner (Eds.), Lecture Notes in Control and information Sciences, 1988. 15
- [29] I. Dassios and D. Baleanu, “Caputo and related fractional derivatives in singular systems,” *Applied Mathematics and Computation*, vol. 337, pp. 591–606, 2018. 60

- [30] I. Dassios, G. Tzounas, and F. Milano, “The Möbius transform effect in singular systems of differential equations,” *Applied Mathematics and Computation*, vol. 361, pp. 338–353, 2019. 15, 24
- [31] I. Dassios, G. Tzounas, and F. Milano, “Generalized fractional controller for singular systems of differential equations,” *Journal of Computational and Applied Mathematics*, vol. 378, p. 112919, 2020. 63, 64, 65
- [32] I. Dassios, G. Tzounas, and F. Milano, “Participation factors for singular systems of differential equations,” *Circuits, Systems, and Signal Processing*, vol. 39, pp. 83–110, 2020. 41
- [33] I. Dassios, G. Tzounas, and F. Milano, “Robust stability criterion for perturbed singular systems of linearized differential equations,” *Journal of Computational and Applied Mathematics*, vol. 381, p. 113032, 2021. 15
- [34] R. Datko, “A procedure for determination of the exponential stability of certain differential-difference equations,” *Quarterly of Applied Mathematics*, vol. 36, no. 3, pp. 279–292, 1978. 90
- [35] A. Debbouche, “Fractional evolution integro-differential systems with nonlocal conditions,” *Advances in Dynamical Systems and Applications*, vol. 5, no. 1, 2010. 60
- [36] M. B. Delghavi, S. Shoja-Majidabad, and A. Yazdani, “Fractional-order sliding-mode control of islanded distributed energy resource systems,” *IEEE Transactions on Sustainable Energy*, vol. 7, no. 4, pp. 1482–1491, Oct. 2016. 58
- [37] G. R. Duan, *The Analysis and Design of Descriptor Linear Systems*. Springer, 2011. 15
- [38] D. Fabozzi, A. S. Chieh, B. Haut, and T. Van Cutsem, “Accelerated and localized Newton schemes for faster dynamic simulation of large power systems,” *IEEE Transactions on Power Systems*, vol. 28, no. 4, pp. 4936–4947, Nov. 2013. 117, 127, 138

- [39] D. Fabozzi and T. Van Cutsem, “On angle references in long-term time-domain simulations,” *IEEE Transactions on Power Systems*, vol. 26, no. 1, pp. 483–484, Feb. 2011. 112
- [40] M. Fan, V. Ajjarapu, C. Wang, D. Wang, and C. Luo, “RPM-based approach to extract power system steady state and small signal stability information from the time-domain simulation,” *IEEE Transactions on Power Systems*, vol. 26, no. 1, pp. 261–269, 2011. 2
- [41] J. Fong and C. Pottle, “Parallel processing of power system analysis problems via simple parallel microcomputer structures,” *IEEE Transactions on Power Apparatus and Systems*, vol. PAS-97, no. 5, pp. 1834–1841, Sep. 1978. 117, 127, 138
- [42] J. G. F. Francis, “The QR transformation a unitary analogue to the LR transformation – Part 1,” *The Computer Journal*, vol. 4, no. 3, pp. 265–271, 1961. 21, 95
- [43] E. Fridman and L. Shaikhet, “Simple LMIs for stabilization by using delays,” in *Proceedings of the IEEE Conference on Decision and Control*, 2016, pp. 3240–3245. 87
- [44] Y. Futamura and T. Sakurai, *z-Pares Users’ Guide Release 0.9.5*. University of Tsukuba, 2014. 22
- [45] R. F. Gantmacher, *The Theory of Matrices I, II*. New York: Chelsea, 1959. 15, 17, 18
- [46] F. Garofalo, L. Iannelli, and F. Vasca, “Participation factors and their connections to residues and relative gain array,” *IFAC Proceedings Volumes*, vol. 35, no. 1, pp. 125 – 130, 2002, 15th IFAC World Congress. 37, 39
- [47] K. Gopalsamy, *Stability and Oscillations in Delay Differential Equations of Population Dynamics*. Norwell, MA: Kluwer, 1992. 87
- [48] L. L. Grigsby, *Power System Stability and Control*. Boca Raton, CA: CRC Press, 2007. 112

- [49] N. Guglielmi and E. Hairer, “Implementing Radau IIA methods for stiff delay differential equations,” *Computing*, vol. 67, no. 1, pp. 1–12, Jul. 2001. 123
- [50] G. Gurrala and I. Sen, “Power system stabilizers design for interconnected power systems,” *IEEE Transactions on Power Systems*, vol. 25, no. 2, pp. 1042–1051, 2010. 3
- [51] J. K. Hale and S. M. V. Lunel, *Introduction to Functional Differential Equations*. New York, USA: Springer-Verlag, 1993. 87
- [52] A. M. A. Hamdan, “Coupling measures between modes and state variables in power-system dynamics,” *International Journal of Control*, vol. 43, no. 3, pp. 1029–1041, 1986. 3, 39
- [53] H. Hamdan and A. Hamdan, “On the coupling measures between modes and state variables and subsynchronous resonance,” *Electric Power System Research*, vol. 13, no. 3, pp. 165 – 171, 1987. 39, 117, 118
- [54] W. A. Hashlamoun, M. A. Hassouneh, and E. H. Abed, “New results on modal participation factors: Revealing a previously unknown dichotomy,” *IEEE Transactions on Automatic Control*, vol. 54, no. 7, pp. 1439–1449, Jul. 2009. 37
- [55] D. Helbing, S. Lämmer, T. Seidel, P. Šeba, and T. Płatkowski, “Physics, stability, and dynamics of supply networks,” *Physical Review E*, vol. 70, no. 6, 2004, art. no. 066116. 87
- [56] V. Hernandez, J. E. Roman, and V. Vidal, “SLEPc: A scalable and flexible toolkit for the solution of eigenvalue problems,” *ACM Transactions on Mathematical Software*, vol. 31, no. 3, pp. 351–362, 2005. 22
- [57] R. Hilfe, *Applications of Fractional Calculus in Physics*, p. 463. World Scientific, River Edge, NJ, USA, 2000. 57
- [58] Y. Hsu and C. Chen, “Identification of optimum location for stabiliser applications using participation factors,” *IEE Proceedings C - Generation, Transmission and Distribution*, vol. 134, no. 3, pp. 238–244, May 1987. 37

- [59] IEEE, “IEEE Task Force on Stability definitions and characterization of dynamic behavior in systems with high penetration of power electronic interfaced technologies,” *Technical Report PES-TR77*, Apr. 2020. 2
- [60] C. Ionescu, A. Lopes, D. Copot, J. A. T. Machado, and J. H. T. Bates, “The role of fractional calculus in modeling biological phenomena: A review,” *Communications in Nonlinear Science and Numerical Simulation*, vol. 51, pp. 141–159, 2017. 57
- [61] J. Y. Ishihara and M. H. Terra, “On the Lyapunov theorem for singular systems,” *IEEE Transactions on Automatic Control*, vol. 47, no. 11, pp. 1926–1930, 2002. 19
- [62] I. S. Jesus and J. A. T. Machado, “Fractional control of heat diffusion systems,” *Nonlinear Dynamics*, vol. 54, no. 3, pp. 263–282, Nov. 2008. 57
- [63] T. Kaczorek, *Selected Problems of Fractional Systems Theory: Fractional Continuous-Time Linear Systems, 27–52*. Springer Berlin Heidelberg, 2011. 60, 143
- [64] H. E. Kallmann, “Transversal filters,” *Proceedings of the Institute of Radio Engineers*, vol. 28, pp. 302–10, 1940. 88
- [65] I. Kamwa, R. Grondin, and Y. Hebert, “Wide-area measurement based stabilizing control of large power systems—a decentralized/hierarchical approach,” *IEEE Transactions on Power Systems*, vol. 16, no. 1, pp. 136–153, Feb. 2001. 99
- [66] U. Karaagac, J. Mahseredjian, I. Kocar, G. Soykan, and O. Saad, “Partial refactorization based machine modeling techniques for electromagnetic transients,” in *Proceedings of the IEEE PES General Meeting*, Jul. 2017. 112
- [67] A. V. Knyazev, “Toward the optimal preconditioned eigensolver: Locally optimal block preconditioned conjugate gradient method,” *SIAM Journal on Scientific Computing*, vol. 23, no. 2, p. 517–541, 2001. 20
- [68] I. Kocar, J. Mahseredjian, U. Karaagac, G. Soykan, and O. Saad, “Multiphase load-flow solution for large-scale distribution systems using MANA,” *IEEE Transactions on Power Delivery*, vol. 29, no. 2, pp. 908–915, Apr. 2014. 112

- [69] H. Kokame, K. Hirata, K. Konishi, and T. Mori, “Difference feedback fan stabilize uncertain steady states,” *IEEE Transactions on Automatic Control*, vol. 46, no. 12, pp. 1908–1913, 2001. 87, 88
- [70] D. Kressner, *Numerical Methods for General and Structured Eigenvalue Problems*, 4th ed. Springer, 2015. 20
- [71] G. Kron, *The Piecewise Solution of Large-Scale Systems*. London, UK: Macdonald, 1963. 112
- [72] P. Kundur, J. Paserba, V. Ajjarapu, G. Andersson, A. Bose, C. Cañizares, N. Hatziargyriou, D. Hill, A. Stankovic, C. Taylor, T. Van Cutsem, and V. Vittal, “Definition and classification of power system stability IEEE/CIGRE joint task force on stability terms and definitions,” *IEEE Transactions on Power Systems*, vol. 19, no. 3, pp. 1387–1401, 2004. 2
- [73] P. Kundur, G. J. Rogers, D. Y. Wong, L. Wang, and M. G. Lauby, “A comprehensive computer program package for small signal stability analysis of power systems,” *IEEE Transactions on Power Systems*, vol. 5, no. 4, pp. 1076–1083, 1990. 21
- [74] P. Kundur, *Power System Stability and Control*. New York: Mc-Grall Hill, 1994. 50, 54, 97
- [75] L. P. Kunjumammed, B. C. Pal, C. Oates, and K. J. Dyke, “Electrical oscillations in wind farm systems: Analysis and insight based on detailed modeling,” *IEEE Transactions on Sustainable Energy*, vol. 7, no. 1, pp. 51–62, Jan. 2016. 39
- [76] R. H. Lasseter and J. Zhou, “TACS enhancements for the electromagnetic transient program,” *IEEE Transactions on Power Systems*, vol. 9, no. 2, pp. 736–742, 1994. 111
- [77] C. L. Lawson, R. J. Hanson, D. R. Kincaid, and F. T. Krogh, “Basic linear algebra subprograms for FORTRAN usage,” University of Texas at Austin, USA, Tech. Rep., 1977. 21

- [78] M. Lazarević, “Finite time stability analysis of PD^α fractional control of robotic time-delay systems,” *Mechanics Research Communications*, vol. 33, no. 2, pp. 269 – 279, Mar. 2006. 57
- [79] R. B. Lehoucq and D. C. Sorensen, “Deflation techniques for an implicitly restarted Arnoldi iteration,” *SIAM Journal on Matrix Analysis and Applications*, vol. 17, no. 4, 1996. 21
- [80] R. B. Lehoucq, D. C. Sorensen, and C. Yang, “ARPACK users’ guide: Solution of large-scale eigenvalue problems with implicitly restarted Arnoldi methods,” in *SIAM*, 1998. 22
- [81] G. W. Leibniz, “Letter from Hanover, Germany, September 30, 1695 to G. A. L’Hospital,” *Leibnizen Mathemutische Schriften*, vol. 2, no. 1, pp. 301–302, 1962, Olms Verlag., Hildesheim, Germany, Published in 1849. 57
- [82] F. L. Lewis, “A survey of linear singular systems,” *Circuits, Systems, and Signal Processing*, vol. 5, pp. 3–36, 1986. 15
- [83] C. Li, Y. Chen, T. Ding, Z. Du, and F. Li, “A sparse and low-order implementation for discretization-based eigen-analysis of power systems with time-delays,” *IEEE Transactions on Power Systems*, vol. 34, no. 6, pp. 5091–5094, Nov. 2019. 88
- [84] C. Li and W. Deng, “Remarks on fractional derivatives,” *Applied Mathematics and Computation*, vol. 187, no. 2, pp. 777 – 784, Apr. 2007. 60, 62
- [85] J. Liouville, “Mémoire sur quelques quéstions de géometrie et de mécanique, et sur un nouveau genre de calcul pour résoudre ces quéstions,” *Journal Ecole Polytechnique*, vol. 13, pp. 1–69, 1832, Sect. 21. 57
- [86] M. Liu, I. Dassios, G. Tzounas, and F. Milano, “Stability analysis of power systems with inclusion of realistic-modeling WAMS delays,” *IEEE Transactions on Power Systems*, vol. 34, no. 1, pp. 627–636, Jan. 2019. 5, 88, 95, 104
- [87] M. Liu, I. Dassios, G. Tzounas, and F. Milano, “Model-independent derivative control delay compensation methods for power systems,” *Energies*, vol. 13, no. 2, p. 342, 2020. 137

- [88] M. Liu, G. Tzounas, and F. Milano, “A model-independent delay compensation method for power systems,” in *Proceedings of the IEEE PowerTech Conference*, 2019. 137
- [89] C. Lizama, M. Murillo-Arcila, and C. Leal, “Lebesgue regularity for differential difference equations with fractional damping,” *Mathematical Methods in the Applied Sciences*, vol. 41, no. 7, pp. 2535–2545, 2018. 60
- [90] J. Mahseredjian, L. Dube, Ming Zou, S. Denetiere, and G. Joos, “Simultaneous solution of control system equations in EMTP,” *IEEE Transactions on Power Systems*, vol. 21, no. 1, pp. 117–124, Feb 2006. 111
- [91] W. Michiels and S.-I. Niculescu, *Stability and Stabilization of Time-Delay Systems: An Eigenvalue-Based Approach*. Philadelphia, PA: SIAM, 2009. 122
- [92] F. Milano, *Power System Modelling and Scripting*. London: Springer, 2010. 37, 104, 120, 124
- [93] F. Milano, “A Python-based software tool for power system analysis,” in *Proceedings of the IEEE PES General Meeting*, Jul. 2013. 6, 27, 50
- [94] F. Milano, “Delay-based numerical stability of the partitioned-solution approach,” in *Proceedings of the IEEE PES General Meeting*, 2016, pp. 1–5. 3
- [95] F. Milano, “Semi-implicit formulation of differential-algebraic equations for transient stability analysis,” *IEEE Transactions on Power Systems*, vol. 31, no. 6, pp. 4534–4543, Nov. 2016. 11
- [96] F. Milano, “Small-signal stability analysis of large power systems with inclusion of multiple delays,” *IEEE Transactions on Power Systems*, vol. 31, no. 4, pp. 3257–3266, Jul. 2016. 88, 94
- [97] F. Milano and M. Anghel, “Impact of time delays on power system stability,” *IEEE Transactions on Circuits and Systems - I: Fundamental Theory and Applications*, vol. 59, no. 4, pp. 889–900, Apr. 2012. 5, 88, 116
- [98] F. Milano and I. Dassios, “Small-signal stability analysis for non-index 1 Hessenberg form systems of delay differential-algebraic equations,” *IEEE Transactions on*

- Circuits and Systems - I: Regular Papers*, vol. 63, no. 9, pp. 1521–1530, Sep. 2016. 96, 121
- [99] F. Milano and Á. Ortega, “Frequency divider,” *IEEE Transactions on Power Systems*, vol. 32, no. 2, pp. 1493–1501, Mar. 2017. 52, 53
- [100] F. Milano and I. Dassios, “Primal and dual generalized eigenvalue problems for power systems small-signal stability analysis,” *IEEE Transactions on Power Systems*, vol. 32, no. 6, pp. 4626 – 4635, 2017. 21, 41, 43
- [101] F. Milano, I. Dassios, M. Liu, and G. Tzounas, *Eigenvalue Problems in Power Systems*. CRC Press, Taylor & Francis Group, 2020. 15
- [102] F. Milano and Á. Ortega Manjavacas, *Converter-Interfaced Energy Storage Systems: Context, Modelling and Dynamic Analysis*. Cambridge University Press, 2019. 80, 124
- [103] R. A. Minasian, “Photonic signal processing of microwave signals,” *IEEE Transactions on Microwave Theory and Techniques*, vol. 54, no. 2, pp. 832–846, Feb. 2006. 111
- [104] C. B. Moler and G. W. Stewart, “An algorithm for generalized matrix eigenvalue problems,” *SIAM Journal on Numerical Analysis*, vol. 10, no. 2, pp. 241–256, 1973. 21
- [105] C. A. Monje, Y. Chen, B. M. Vinagre, D. Xue, and V. Feliu, *Fractional-order Systems and Controls, Fundamentals and Applications*. Springer, 2010. 57, 59, 72
- [106] M. A. A. Murad and F. Milano, “Modeling and simulation of PI-controllers limiters for the dynamic analysis of VSC-Based devices,” *IEEE Transactions on Power Systems*, vol. 34, no. 5, pp. 3921–3930, Sep. 2019. 83
- [107] M. A. A. Murad, G. Tzounas, M. Liu, and F. Milano, “Frequency control through voltage regulation of power system using SVC devices,” in *Proceedings of the IEEE PES General Meeting*, Aug. 2019. 84

- [108] M. A. A. Murad, G. Tzounas, and F. Milano, “Modeling and simulation of fractional order PI control limiters for power systems,” in *Proceedings of the 21st IFAC World Congress*, 2020, pp. 1–6. 136
- [109] M. A. A. Murad, Á. Ortega, and F. Milano, “Impact on power system dynamics of PI control limiters of VSC-based devices,” *Proceedings of the Power Systems Computation Conference*, pp. 1–7, Jun. 2018. 82
- [110] M. Netto, Y. Susuki, and L. Mili, “Data-driven participation factors for nonlinear systems based on Koopman mode decomposition,” *IEEE Control Systems Letters*, vol. 3, no. 1, pp. 198–203, Jan. 2019. 37
- [111] S. I. Niculescu, *Delay Effects on Stability: A Robust Control Approach*. Springer-Verlag, 2001. 89
- [112] R. Olfati-Saber, “Ultrafast consensus in small-world networks,” in *Proceedings of the American Control Conference*, 2005, pp. 2371–2378. 87
- [113] N. Olgac, A. F. Ergenc, and R. Sipahi, ““Delay scheduling”: A new concept for stabilization in multiple delay systems,” *Journal of Vibration and Control*, vol. 11, no. 9, pp. 1159–1172, 2005. 5, 104
- [114] G. Orosz, R. E. Wilson, and G. Stépán, “Traffic jams: dynamics and control,” *Philosophical Transactions of the Royal Society of London A*, vol. 368, no. 1928, pp. 4455–4479, 2010. 87
- [115] Á. Ortega and F. Milano, “Comparison of different PLL implementations for frequency estimation and control,” in *Proceedings of the International Conference on Harmonics and Quality of Power*, May 2018. 53
- [116] A. Oustaloup, *La commande CRONE (commande robuste d’ordre non entier)*. Hermès, Paris, 1991. 57
- [117] A. Oustaloup, F. Levron, B. Mathieu, and F. M. Nanot, “Frequency-band complex noninteger differentiator: characterization and synthesis,” *IEEE Transactions on Circuits and Systems - I: Fundamental Theory and Applications*, vol. 47, no. 1, pp. 25–39, Jan. 2000. 58, 72

- [118] A. Oustaloup, P. Melchior, P. Lanusse, O. Cois, and F. Dancla, “The CRONE toolbox for Matlab,” in *Proceedings of the IEEE International Symposium on Computer-Aided Control System Design*, Sep. 2000, pp. 190–195. 58
- [119] F. L. Pagola, I. J. Pérez-Arriaga, and G. C. Verghese, “On sensitivities, residues and participations: applications to oscillatory stability analysis and control,” *IEEE Transactions on Power Systems*, vol. 4, no. 1, pp. 278–285, Feb. 1989. 3, 39
- [120] I. Pan and S. Das, “Frequency domain design of fractional order PID controller for AVR system using chaotic multi-objective optimization,” *International Journal of Electrical Power and Energy Systems*, vol. 51, pp. 106–118, Oct. 2013. 58
- [121] S. Pandey, P. Dwivedi, and A. Junghare, “A novel 2-DOF fractional-order $PI^\lambda-D^\mu$ controller with inherent anti-windup capability for a magnetic levitation system,” *AEU - International Journal of Electronics and Communications*, vol. 79, pp. 158 – 171, 2017. 57
- [122] T. P. Peixoto, “The graph-tool Python library,” 2014. [Online]. Available: graph-tool.skewed.de 54
- [123] I. J. Pérez-Arriaga, G. C. Verghese, and F. C. Schweppe, “Selective modal analysis with applications to electric power systems, part i: heuristic introduction,” *IEEE Transactions on Power Apparatus and Systems*, vol. PAS-101, no. 9, pp. 3117–3125, Sep. 1982. 3, 4, 37, 39, 43
- [124] I. Pétras, “Stability of fractional-order systems with rational orders: A survey,” *Fractional Calculus and Applied Analysis*, vol. 12, no. 3, 2009. 65
- [125] I. Podlubny, *Fractional Differential Equations, Volume 198: An Introduction to Fractional Derivatives, Fractional Differential equations, to Methods of Their Solution and Some of Their Applications*. Academic Press, 1999. 57
- [126] I. Podlubny, “Fractional-order systems and $PI^\lambda D^\mu$ -controllers,” *IEEE Transactions on Automatic Control*, vol. 44, no. 1, pp. 208–214, Jan. 1999. 57, 59
- [127] E. Polizzi, “Density-matrix-based algorithm for solving eigenvalue problems,” *Physical Review B, American Physical Society*, vol. 79, no. 11, 2009. 21, 22

- [128] E. Polizzi, “FEAST eigenvalue solver v4.0 user guide,” 2020. 22
- [129] K. Pyragas, “Continuous control of chaos by self-controlling feedback,” *Physical Letters A*, vol. 170, no. 6, pp. 421–428, 1992. 5, 88
- [130] W. Qiao and R. Sipahi, “Consensus control under communication delay in a three-robot system: Design and experiments,” *IEEE Transactions on Control Systems Technology*, vol. 24, no. 2, pp. 687–694, 2016. 87
- [131] A. Ramírez, R. Garrido, and S. Mondié, “Velocity control of servo systems using an integral retarded algorithm,” *ISA Transactions*, vol. 58, pp. 357–366, 2015. 5, 87, 88, 90, 110
- [132] A. Ramírez, S. Mondié, R. Garrido, and R. Sipahi, “Design of proportional-integral-retarded (PIR) controllers for second-order LTI systems,” *IEEE Transactions on Automatic Control*, vol. 61, no. 6, pp. 1688–1693, 2016. 5, 88, 92
- [133] A. Ramírez and R. Sipahi, “Multiple intentional delays can facilitate fast consensus and noise reduction in a multiagent system,” *IEEE Transactions on Cybernetics*, vol. 49, no. 4, pp. 1224–1235, 2019. 88
- [134] A. Ramírez, R. Sipahi, S. Mondié, and R. Garrido, “An analytical approach to tuning of delay-based controllers for LTI-SISO systems,” *SIAM Journal Control Optim.*, vol. 55, no. 1, pp. 397–412, 2017. 5, 88
- [135] S. Roy, A. Patel, and I. N. Kar, “Analysis and design of a wide-area damping controller for inter-area oscillation with artificially induced time delay,” *IEEE Transactions on Smart Grid*, vol. 10, no. 4, pp. 3654–3663, Jul. 2019. 88
- [136] Y. Saad, *Numerical Methods for Large Eigenvalue Problems*. SIAM, 2011. 20
- [137] T. Sakurai and H. Sugiura, “A projection method for generalized eigenvalue problems using numerical integration,” *Journal of Comput. and Applied Mathematics*, vol. 159, no. 1, pp. 119–128, 2003. 21
- [138] T. Sakurai and H. Tadano, “CIRR: a Rayleigh-Ritz type method with contour integral for generalized eigenvalue problems,” *Hokkaido Mathematical Journal*, vol. 36, no. 4, pp. 745–757, 2007. 21

- [139] S. Saxena, “Load frequency control strategy via fractional-order controller and reduced-order modeling,” *International Journal of Electrical Power and Energy Systems*, vol. 104, pp. 603 – 614, Jan. 2019. 58
- [140] O. Schenk and K. Gartner, “Solving unsymmetric sparse systems of linear equations with PARDISO,” *Journal of Future Generation Computer Systems*, vol. 20, no. 3, 2004. 22
- [141] M. Shahidehpour and Y. Wang, *Communication and Control in Electric Power Systems*. Hoboken, NJ: John Wiley & Sons, 2003. 112
- [142] B. Shiri and D. Baleanu, “Numerical solution of some fractional dynamical systems in medicine involving non-singular kernel with vector order,” *Results in Nonlinear Analysis*, vol. 2, no. 4, pp. 160–168, 2019. 60
- [143] R. Sipahi, S.-I. Niculescu, C. T. Abdallah, W. Michiels, and K. Gu, “Stability and stabilization of systems with time delay,” *IEEE Control Systems Magazine*, vol. 31, no. 1, pp. 38–65, 2011. 5, 87, 90
- [144] R. Sipahi and N. Olgac, “Complete stability robustness of third-order lti multiple time-delay systems,” *Automatica*, vol. 41, no. 8, pp. 1413–1422, 2005. 5
- [145] O. J. Smith, “A controller to overcome dead time,” *ISA Journal*, vol. 6, no. 2, pp. 28–33, 1959. 88
- [146] M. Snir, S. Otto, S. Huss-Lederman, D. Walker, and J. Dongarra, *MPI-The Complete Reference, Volume 1: The MPI Core*. MIT Press, 1998. 22
- [147] D. C. Sorensen, “Implicit application of polynomial filters in a k-step Arnoldi method,” *SIAM Journal on Matrix Analysis and Applications*, vol. 13, no. 1, pp. 357–385, 1992. 20
- [148] J. W. Stahlhut, T. J. Browne, G. T. Heydt, and V. Vittal, “Latency viewed as a stochastic process and its impact on wide area power system control signals,” *IEEE Transactions on Power Systems*, vol. 23, no. 1, pp. 84–91, Feb. 2008. 5, 88
- [149] G. Stépán, *Retarded Dynamical Systems: Stability and Characteristic Function*. New York, USA: Longman Scientific & Technical, 1989. 5, 89, 90

- [150] G. W. Stewart, “A Krylov–Schur algorithm for large eigenproblems,” *SIAM Journal on Matrix Analysis and Applications*, vol. 23, no. 3, pp. 601–614, 2002. 21
- [151] B. Stott, “Power system dynamic response calculations,” *Proceedings of the IEEE*, vol. 67, no. 2, pp. 219–241, Feb. 1979. 114
- [152] G. Su, L. Lu, B. Tang, and Z. Liu, “Quasi-linearization technique for solving nonlinear Riemann-Liouville fractional-order problems,” *Applied Mathematics and Computation*, vol. 378, pp. 125–199, 2020. 60
- [153] G. Sulligoi, M. Chiandone, and V. Arcidiacono, “New SART automatic voltage and reactive power regulator for secondary voltage regulation: Design and application,” in *Proceedings of the IEEE PES General Meeting*, Jul. 2011. 120
- [154] S. A. Taher, M. H. Fini, and S. F. Aliabadi, “Fractional order PID controller design for LFC in electric power systems using imperialist competitive algorithm,” *Ain Shams Engineering Journal*, vol. 5, no. 1, pp. 121 – 135, Mar. 2014. 58
- [155] K. Takaba, N. Morihira, and T. Katayama, “A generalized Lyapunov theorem for descriptor system,” *Systems & Control Letters*, vol. 24, no. 1, pp. 49 – 51, 1995. 19
- [156] Y. Tang, M. Cui, C. Hua, L. Li, and Y. Yang, “Optimum design of fractional order $PI^\lambda D^\mu$ controller for AVR system using chaotic ant swarm,” *Expert Systems with Applications*, vol. 39, no. 8, pp. 6887–6896, 2012. 58
- [157] C. W. Taylor and R. L. Cresap, “Real-time power system simulation for automatic generation control,” *IEEE Transactions on Power Apparatus and Systems*, vol. 95, no. 1, pp. 375–384, Jan 1976. 120
- [158] A. Tepljakov, E. Petlenkov, and J. Belikov, “FOMCON: Fractional-order modeling and control toolbox for Matlab,” *Proceedings of the 18th International Conference Mixed Design of Integrated Circuits and Systems*, Jun. 2011. 58
- [159] T. Tian, X. Kestelyn, O. Thomas, H. Amano, and A. R. Messina, “An accurate third-order normal form approximation for power system nonlinear analysis,” *IEEE Transactions on Power Systems*, vol. 33, no. 2, pp. 2128–2139, Mar. 2018. 37
- [160] T. Trilinos Project Team, *The Trilinos Project Website*. 22

- [161] G. Tzounas, I. Dassios, and F. Milano, “Modal participation factors of algebraic variables,” *IEEE Transactions on Power Systems*, vol. 35, no. 1, pp. 742–750, 2020. 42, 47
- [162] G. Tzounas, I. Dassios, M. A. A. Murad, and F. Milano, “Theory and implementation of fractional order controllers for power system applications,” *IEEE Transactions on Power Systems*, vol. 35, no. 6, pp. 4622–4631, Nov. 2020. 60
- [163] G. Tzounas, M. Liu, M. A. A. Murad, and F. Milano, “Impact of realistic bus frequency measurements on wide-area power system stabilizers,” in *Proceedings of the IEEE PowerTech Conference*, 2019. 117
- [164] G. Tzounas and F. Milano, “Impact of the estimation of synchronous machine rotor speeds on wide-area damping controllers,” in *Proceedings of the IEEE PES General Meeting*, 2019, pp. 1–5. 53
- [165] G. Tzounas and F. Milano, “Delay-based decoupling of power system models for transient stability analysis,” *IEEE Transactions on Power Systems*, vol. 36, no. 1, pp. 464–473, Jan. 2021. 113
- [166] G. Tzounas, R. Sipahi, and F. Milano, “Damping power system electromechanical oscillations using time delays,” *IEEE Transactions on Circuits and Systems - I: Regular Papers*, 2021, accepted in Feb. 2021, in press. 88, 93
- [167] G. Tzounas, I. Dassios, M. Liu, and F. Milano, “Comparison of numerical methods and open-source libraries for eigenvalue analysis of large-scale power systems,” *Applied Sciences*, vol. 10, no. 21, 2020. 21
- [168] G. Tzounas, M. Liu, M. A. A. Murad, and F. Milano, “Stability analysis of wide area damping controllers with multiple time delays,” *IFAC-PapersOnLine*, vol. 51, no. 28, pp. 504 – 509, 2018, 10th IFAC Symposium on Control of Power and Energy Systems. 95
- [169] A. G. Ulsoy, “Time-delayed control of SISO systems for improved stability margins,” *Journal of Dynamic Systems, Measurement, and Control*, vol. 137, no. 4, pp. 558–563, 2015. 87

- [170] F. Uriarte, “On Kron’s diakoptics,” *Electric Power System Research*, vol. 88, pp. 146 – 150, 2012. 112
- [171] F. Uriarte, *Multicore Simulation of Power System Transients*. London, UK: The IET, 2013. 111
- [172] D. Valério and J. Costa, “Ninteger: a non-integer control toolbox for Matlab,” *Proceedings of the 1st IFAC Workshop on Fractional Differentiation and its Application*, Jan. 2004. 58
- [173] V. Venkatasubramanian, H. Schattler, and J. Zaborszky, “A time-delay differential-algebraic phasor formulation of the large power system dynamics,” in *Proceedings of IEEE International Symposium on Circuits and Systems*, vol. 6, May 1994, pp. 49–52. 111
- [174] G. C. Verghese, I. J. Pérez-Arriaga, and F. C. Schweppe, “Selective modal analysis with applications to electric power systems, part ii: the dynamic stability problem,” *IEEE Transactions on Power Apparatus and Systems*, vol. PAS-101, no. 9, pp. 3126–3134, Sep. 1982. 37, 117, 123
- [175] B. M. Vinagre, I. Podlubny, and V. Feliu, “Some approximations of fractional order operators used in control theory and applications,” *Journal of Fractional Calculus and Applied Analysis*, pp. 231–248, Jan. 2000. 58
- [176] S. Wang, X. Meng, and T. Chen, “Wide-area control of power systems through delayed network communication,” *IEEE Transactions on Control Systems Technology*, vol. 20, no. 2, pp. 495–503, Mar. 2012. 88
- [177] N. Watson and J. Arrillaga, *Power Systems Electromagnetic Transients Simulation*. London, UK: The IET, 2003. 111
- [178] Y. Wei, W. T. Peter, Z. Yao, and Y. Wang, “The output feedback control synthesis for a class of singular fractional order systems,” *ISA transactions*, vol. 69, pp. 1–9, 2017. 60
- [179] H. Wu, H. Ni, and G. T. Heydt, “The impact of time delay on robust control design in power systems,” in *Proceedings of the IEEE PES Winter Meeting*, 2002. 5, 88

- [180] H. Wu, K. S. Tsakalis, and G. T. Heydt, “Evaluation of time delay effects to wide-area power system stabilizer design,” *IEEE Transactions on Power Systems*, vol. 19, no. 4, pp. 1935–1941, Nov. 2004. 3
- [181] D. Xue, C. Zhao, and Y. Chen, “A modified approximation method of fractional order system,” in *International Conference on Mechatronics and Automation*, 2006, pp. 1043–1048. 136
- [182] D. Yang and V. Ajjarapu, “A decoupled time-domain simulation method via invariant subspace partition for power system analysis,” *IEEE Transactions on Power Systems*, vol. 21, no. 1, pp. 11–18, 2006. 3
- [183] M. Zamani, M. Karimi-Ghartemani, N. Sadati, and M. Parniani, “Design of a fractional order PID controller for an AVR using particle swarm optimization,” *Control Engineering Practice*, vol. 17, no. 12, pp. 1380 – 1387, Dec. 2009. 58
- [184] K. Zhou and J. C. Doyle, *Essentials of Robust Control*. Prentice Hall, 1998. 4